Thymol Synthesis *via* Alkylation of *m*-cresol with isopropanol

The effect of the SiO_2/Al_2O_3 ratio of H-MFI catalysts on catalyst activity and thymol selectivity

Sancha Nagooroo

Submitted in partial fulfilment of the requirements
of the degree of Master of Science in Chemical Engineering

February 2012

Centre for Catalysis Research
Department of Chemical Engineering
University of Cape Town
Cape Town
South Africa

Declaration

I know the meaning of plagiarism and declare that all the work in the document, save for that which is properly acknowledged, is my own.

..... Date .....

Sancha Nagooroo

Synopsis

This study was performed in context of a series of studies conducted investigating the use of acid zeolites for the synthesis of thymol by selective isopropylation of *m*-cresol on the 6-position.

The aim of this study was to investigate the effect of the SiO_2/Al_2O_3 ratio, i.e. the aluminium content of H-MFI (H-ZSM-5) zeolites. The results are interpreted based on a deep analysis of the reaction network.

Three commercial samples of the H-MFI zeolite were employed with high, medium and low molar SiO_2/Al_2O_3 ratios of 400, 90 and 20 respectively, whereby the first two samples consisted of agglomerates of very small crystallites, < 10 nm, while the last sample consisted of comparatively large crystallites with diameters of several 10 nm.

m-Cresol as the substrate was alkylated with isopropanol in a molar feed ratio of 1:1. Reactions were carried out in a tubular fixed-bed reactor in the gas-phase at reaction conditions of 200 - 300°C, WHSV of 0.016 – 1.03 $g_{m\text{-cresol}}/g_{cat}$.hr and 3 bar (abs) as the standard pressure. A pressure series at 275°C and WHSV of 0.25 – 1.03 $g_{m\text{-cresol}}/g_{cat}$.hr was also carried out.

The following was observed:

Isopropanol reacts in two parallel ways namely, by O-alkylation of the *m*-cresol to form isopropyl-3-tolyl ether which occurs predominantly by its dehydration to propene and secondly, by alkylation of *m*-cresol with propene with high preference on the 6-position, forming thymol with high selectivity.

The ether rearranges internally or transalkylates with *m*-cresol to form thymol, 2-isopropyl-3-methyl phenol and 4-isopropyl-3-methyl phenol with a thymol selectivity < 50%. Higher reaction temperatures were found to favour the propene route.

It appears that the major effect of the SiO_2/Al_2O_3 ratio is, as expected, a direct effect on catalyst activity and an indirect effect on thymol selectivity *via* mass transfer control. Thymol is an intermediate product in the reaction network, that is, it can react further (by isomerisation or further alkylation to higher alkylated products). Mass transfer control on such reaction sequences reduce intermediate selectivity and hence thymol selectivity. Exactly this was observed over the low SiO_2/Al_2O_3 ratio (i.e. high aluminium content), 'large' crystallite H-MFI-20 sample.

The major *conclusions and recommendations* resulting from this study are the following:

- Use propene as the alkylating agent rather than isopropanol in order to achieve high thymol selectivity
- Avoid mass transfer control.

Acknowledgements

Prof. Jack C.Q. Fletcher, my academic supervisor, for the privileged opportunity to conduct this research, his guidance in ascertaining the scope of this project and constant encouragement during the duration of my research and development of this report.

Mr. Walter Böhringer, my co-supervisor, without whom the completion of this thesis would not have been made possible. I am deeply grateful for his invaluable day-to-day supervision, vast knowledge, theoretical and practical, pertaining to the subject of this report as well as his help in the analysis of results and proofreading of this report.

Mr. Jacobus van der Merwe, a special word of thanks for the sharing of his knowledge on the subject of this thesis. I am also sincerely grateful for his approachability and willingness to dispense advice and assistance in the labs whenever needed.

Ms. Miranda Waldron, of the Electron Microscopy Unit, Physics Department, University of Cape Town, for all the help in acquiring the SEM images of the zeolite catalysts.

Prof. David Reid, of the X-Ray Fluorescence Unit, Geology Department, University of Cape Town, for the chemical composition analysis of the zeolite catalysts.

Dr. Suzanne Causemann, of the Nuclear Magnetic Resonance Unit, Chemistry and Polymer Science Department, University of Stellenbosch, for the ^{27}Al SSNMR spectra of the zeolite catalysts.

Süd-Chemie for the supply of the zeolites utilised in this research.

Merisol for the supply of the phenolic raw materials utilised in this research.

SASOL (Ltd) for their kind sponsorship, which afforded me the opportunity to experience postgraduate research.

The University of Cape Town with reference to the Department of Chemical Engineering for the use of their facilities and resources.

A word of thanks to all my **colleagues of the Centre for Catalysis Research** for their academic help and the enjoyable and friendly atmosphere they created.

And lastly, to **my family and friends**, thank you for your patience and continued words of motivation and support during this period of my studies.

Table of Contents

List of Figures

List of Tables

List of Equations

Nomenclature

^{27}Al SSNMR

^{27}Al **S**olid-**S**tate **N**uclear **M**agnetic **R**esonance spectroscopy

CV

Check **V**alve

FIC

Flow **I**ndicator and **C**ontroller

FID

Flame **I**onisation **D**etector

GC

Gas **C**hromatograph or **G**as **C**hromatogram

GCMS

Gas **C**hromatography **M**ass **S**pectrometry

H-MFI

Zeolite MFI in its acid form

HPLC

High **P**ressure **L**iquid **C**hromatography

H-ZSM-5

Zeolite ZSM-5 in its acid form

MFI

Mobil **Fi**ve, code given by the International Zeolite Association (IZA) to ZSM-5 zeolite; also product designation used by Süd-Chemie

PI

Pressure **I**ndicator

PIC

Pressure **I**ndicator and **C**ontroller

RV

Relief **V**alve

SEM

Scanning **E**lectron **M**icroscopy

SiC

Silicon **C**arbide

S_N-1

Substitution (**N**ucleophilic) reaction; involving consecutive entering and simultaneous leaving of groups

S_N-2

Substitution (**N**ucleophilic) reaction; involving entering and simultaneous leaving of groups

TI

Temperature **I**ndicator

TIC

Temperature **I**ndicator and **C**ontroller

V

Valve

VCR

A Swagelok fitting which seals by compressing a gasket between ridges on two opposing flanges

WHSV

Weight **H**ourly **S**pace **V**elocity

XRF

X-**R**ay **F**luorescence Spectrometry

ZSM-5

Zeolite **S**ocony **M**obil **5**

Variables and Dimensions

WHSV	**W**eight **H**ourly **S**pace **Velocity**	$g_{m\text{-cresol}}/g_{cat}.hr$
T	**T**emperature	°C
P	**P**ressure	bar
ΔH	Change in Enthalpy	kJ/mol
ΔG	Change in Gibbs free energy	kJ/mol
φ	Thiele Modulus	-
η	Effectiveness factor	-
k	Reaction rate constant	(dependent on order of reaction)
r_p	Radius of particle	m
D_{eff}	Effective diffusivity	-
ξ	Geometric factor of particle	-

1 Introduction

Thymol is a constituent of many natural essential oils typically extracted from plant material such as thyme, mint and eucalyptus and is also produced synthetically. It has antiseptic properties and antimicrobial activity on bacteria involved in upper respiratory tract infections (Dirdy *et al.*, 1993, Shapiro, 1996 and Botelho, 2000). It also exhibits activity as an antioxidant and is used in certain fragrances, flavourants and as an intermediate in perfumery (Teissedre and Waterhouse, 2000). Figure 1-1 shows the chemical structure of thymol.

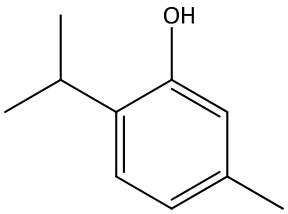

Figure 1-1: Chemical structure of thymol

Thymol may be hydrogenated to menthol and menthone and converted to chlorothymol and thymol iodide (Ashford, 1994). Approximately half of the thymol production worldwide goes into menthol manufacture (Marais, 2003), (see Figure 1-2). Menthol (specifically the L-menthol stereoisomer, see Figure 1-2), in turn, is used as a flavourant and as a raw material in the production of antiseptic, local anaesthetic, antibacterial and antifungal agents and preservatives.

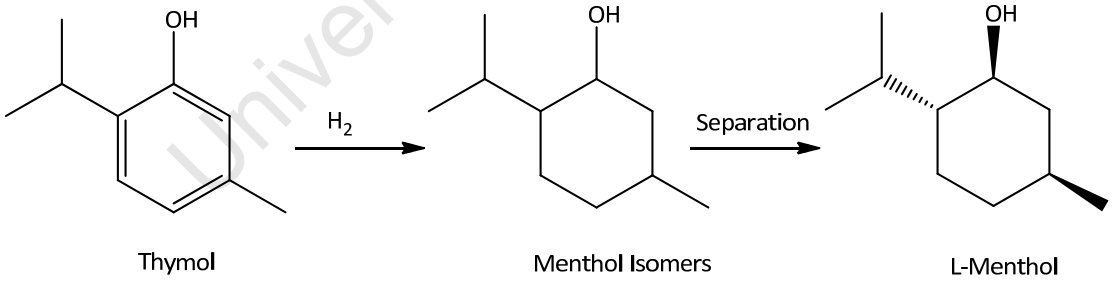

Figure 1-2: Hydrogenation of thymol to menthol (Ashford, 1994)

According to BASF, the world's largest chemical company, menthol has been deemed the world's top-selling aroma chemical by volume with a global demand that is in excess of 20 000 metric tons per year. With a selling price of approximately $19/kg, the world menthol market is currently worth approximately $380 million and according to Symrise, a synthetic menthol manufacturer in Holzminden, Germany; the demand for menthol has been rising at a double digit rate for years (McCoy, 2010).

The major producers of menthol are India and China. Currently, India has the capacity to produce 16 000 metric tons of natural menthol per year, typically derived from *mentha arvensis*, a mint plant, which is enough to supply 80% of the current world demand. However, the growing demand for synthetic menthol stems from fluctuations in the market of natural menthol which is subject to the vagaries of India's monsoons and the speculation of commodity traders. Synthetic menthol manufacturers therefore offer major international corporations supply security in the face of dependence on such a volatile natural product (McCoy, 2010).

In menthol production, thymol is an essential intermediate in one of the three different technically applied synthetic routes. Symrise, in Germany, produces menthol from *m*-cresol *via* the thymol intermediate and has a production capacity of between 3 000 and 3 600 metric tons. Symrise was formed in 2002 by the merger of the Bayer subsidiary Haarmann & Reimer with the flavour and fragrance maker Dragoco. Symrise now produces menthol in cooperation with Lanxess, a German company that was spun off from Bayer in 2005. Symrise has recently announced that it would double its menthol capacity.

Japanese company Takasago synthetically produces menthol from myrcene. Takasago has announced its production capacity would be rising to 3 000 metric tons per year.

BASF, the other German company, an age-old expert in the citral business with a 40 000-metric-ton-per-year citral plant at their Ludwigshafen facilities, plans to initiate manufacture of menthol from citral at this plant with an estimated capacity of between 3 000 to 5 000 metric tons per year (McCoy, 2010).

In the early 2000's, the thymol world market was estimated at around 4 500 tons per annum of which about half went into menthol production (Marais, 2003). Total thymol production costs and sales price were estimated at around $3.4/kg and $9/kg respectively, indicating its considerable market value (Fiege, 2003). Menthol, on the other hand, sells currently for about $19/kg (McCoy, 2010).

Industrially, synthetic thymol is produced by the liquid phase alkylation of *m*-cresol with propene over an activated alumina catalyst, known as the Bayer process, at operating conditions of 350 - 365°C and ca. 50 bar (Biedermann *et al*., 1978 and Fiege, 2003). Despite the fact that the Bayer process achieves a thymol selectivity of 80% at ca. 75% per pass conversion of *m*-cresol, the severe reaction conditions required are less favourable.

South Africa is one of the world's largest producers of 'phenolics' (aromatic compounds consisting of a benzene ring substituted with a hydroxyl group). The phenolics currently produced in South Africa are 'natural' phenolics in the sense that they are high temperature pyrolysis and cracking products derived from 'natural' materials such as coal (as is the case in South Africa), petroleum or wood.

The gasification of coal by Lurgi gasifiers (by the Sasol synfuel refineries situated in Secunda) is the major source of phenolics in South Africa. In the Lurgi gasifier the phenolics are driven off, together with some aromatic hydrocarbons and tars, by pyrolysis of the coal at 500 - 650^{o}C. The total yield of phenolics is about 3.2 kg per ton of coal (Fiege, 2003). The incentive for the extraction and work-up of the liquid gasifier product towards phenolic compounds, cresols in particular, is their comparatively high economic value. Of the cresol isomers, the market for *m*-cresol, in particular, is growing rapidly due to its extensive use in the production of vitamin E, thermally sensitive papers, thymol and derivatives such as menthol, antioxidants, agrochemicals, fragrances etc. (Fiege, 2003).

Sasol plans to build another Fischer-Tropsch technology coal-to-liquids based plant in South Africa (in the Free State or in the Waterberg, in Limpopo), in the near future, with a forecasted additional 80 000 bbl/d to the already 150 000 bbl/d refining capacity of the coal-to-liquids plant in Secunda (Webb, 2007). This translates to a raise in South Africa's production capacity of phenolic compounds (including *m*-cresol) by approximately 50%.

As outlined above, about half of the current production of thymol worldwide goes into menthol manufacture (Marais, 2003). For this purpose, thymol is hydrogenated to form a mixture of the menthol stereoisomers. In 2002, a patent was granted to AECI South Africa to separate (-)-menthol from its stereoisomers using a stereospecific enzyme (Chaplin *et al*., 2002).

Propene and isopropanol (products in Sasol's Fischer-Tropsch process) (Sasol, 2000) may be used to alkylate *m*-cresol to thymol thereby adding value to these local base chemicals. Adding value to locally produced raw materials in the country has become a primary focus in South Africa in an attempt to increase employment opportunities, import replacements, exports and foreign investment. Research aimed at value addition to locally produced raw materials (in a process such as thymol synthesis), therefore supports this objective.

2 Literature Review

2.1 Thymol synthesis by alkylation of *m*-cresol

Thymol is synthesised by isopropylating *m*-cresol on the *ortho*-position, opposite the methyl group, with an alkylating agent such as, for instance, propene (see Figure 2-1).

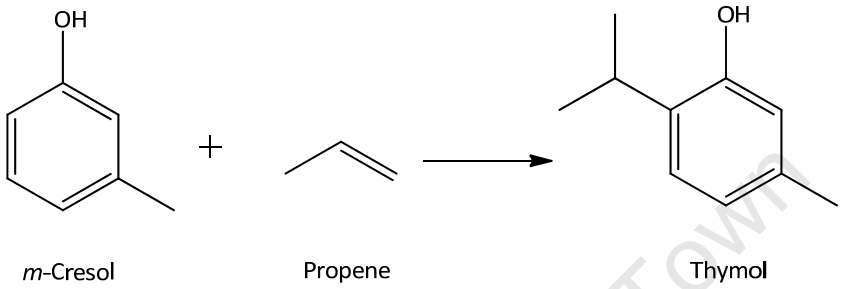

Figure 2-1: Isopropylation of *m*-cresol in the synthesis of thymol

2.1.1 Industrial synthesis of thymol

The industrial manufacture of thymol is currently performed by the Bayer process (Biedermann *et al.*, 1978) which involves the liquid phase alkylation of *m*-cresol with propene as an alkylating agent at a reaction temperature and pressure of 350 - 365°C and 50 bar, respectively (Fiege, 2003).

According to the original patent (Biedermann *et al.,* 1978), the catalyst utilised in this synthesis is an "activated aluminium oxide catalyst", which typically contains 40 wt% γ-alumina (X-ray) and 35 wt% boehmite. The acid alumina catalyst is charged with around 400 ppm of basic nitrogen (generally added to the *m*-cresol feedstock) in the form of compounds such as ammonia, urea or organic amines such as ethanolamine. The product spectrum achieved in this synthesis comprises 60% thymol, 25% unconverted *m*-cresol and 15% other products (Fiege, 2003) thus corresponding to a thymol selectivity of 80% and per pass conversion of approximately 75%.

Even though the thymol selectivity of 80% and conversion per pass of 75% of the Bayer process is considered acceptable, several technical shortcomings are inherent in the process. Operating conditions are severe (high reaction temperatures and pressures) and the addition of basic nitrogen compounds to the feed results in contamination of the product. In order to negate the addition of catalyst contaminants (nitrogen bases) and elevated temperatures and pressures, Wimmer *et al.* (1991) developed an alternative process for the preparation of thymol by reaction of *m*-cresol and propene in the gas phase at reaction temperatures between 230°C and 250°C and at atmospheric pressure over medium and wide pore zeolites. This process was, however, apparently never carried out on a commercial scale.

The use of propene as an alkylating agent, as in the Bayer process, also presents several technical limitations. Firstly, the use of propene is associated with coke formation due to its oligomerisation in secondary reactions, which consequently results in deactivation of the catalyst and depletion of the propene alkylating agent (Yadav and Pathre, 2005). Secondly, propene is gaseous at ambient conditions and highly flammable and is therefore difficult to store, transport and handle if not delivered "over the fence".

Propene is, for such reasons, not readily available everywhere in South Africa. Propene may, however, be employed commercially for thymol synthesis in South Africa by plants situated sufficiently close to South Africa's propene production site, the Sasol coal-to-liquid production facilities in Secunda, to allow this gaseous feedstock to be transported *via* pipeline. However, for industrial facilities which are located at distances which do not allow transportation by pipeline, in particular, for small and medium enterprises (SME), an alternative alkylating agent in the synthesis of thymol may be advantageous.

2.1.2 Use of alternative heterogeneous catalyst systems and alkylating agents for thymol synthesis

A variety of Friedel-Crafts and mineral acid catalysts have been investigated in the synthesis of thymol namely: $AlCl_3$, BF_3, $TiCl_4$, H_2SO_4 and HF or combinations such as $Al(OC_6H_5)_3$ and $ZnCl_2$-HCl. However, these catalysts present serious disadvantages in the form of corrosion of equipment, enhanced tar formation, generation of environmentally harmful and expensive to dispose off waste salts etc. and are, hence, no longer considered viable catalyst options for a commercial process (Olah, 1963, Olah *et al.,* 1991 and Clark and Macquarrie, 1997). A number of heterogeneous acid catalysts have been studied, such as those listed in Table 2-1 and Table 2-2, which are considered to be more environmentally friendly and have greater economic incentive, to determine whether thymol yields may be achieved which are comparable to the industrial Bayer process but at milder conditions. Studies by, for instance, Nitta *et al.* (1974) using γ-Al_2O_3 and Wimmer *et al.* (1991) using H-ZSM-5 zeolites reported lower thymol yields whilst a comparable yield to the industrial process was obtained by Grabowska and Wrzyszcz (2001) using $ZnAl_2O_4$ but at a very low rate of reaction due to the very low reaction temperature applied.

Due to the molecular structure of thymol, studies were conducted to determine whether or not shape-selective zeolites were better catalysts for synthesis, since thymol is the slimmest of the various possible position isomers of isopropylated *m*-cresol and maybe favoured through product-shape selectivity.

Preliminary studies have been performed at the Catalysis Research Unit of the University of Cape Town, testing various acid zeolite catalysts using propene as an alkylating agent (Fletcher *et al.,* 2001a). Optimum results are indicated in Table 2-1.

Isopropanol was also investigated as an alternative alkylating agent (van der Merwe, 2012 and Nagooroo and Truter, 2008) over an H-ZSM-5 catalyst with a molar SiO_2/Al_2O_3 ratio of 90 at various operating conditions. Optimum results are indicated in Table 2-1.

2.1.2.1 Use of heterogeneous catalyst systems with propene as the alkylating agent

Table 2-1 summarises the catalyst systems used as well as the key findings obtained in the synthesis of thymol with propene as an alkylating agent.

Table 2-1: Summary of results from various catalysts used in previous studies in the synthesis of thymol by alkylation of *m*-cresol with propene

Reference	**Catalyst**	**T(°C)**	**WHSV (h^{-1})**	***m*-Cresol conversion (%)**	**Thymol selectivity (%)**
Fiege, 2003*	Activated alumina	350-365	0.25	75	80
Biedermann *et al.,* 1978*	Activated alumina	360	0.25	75	75
Nitta *et al.,* 1974	γ-Al_2O_3	250	0.15	63	80
Wimmer *et al.,* 1991	H-ZSM-5	250	3.5	34	75
Fletcher *et al.,* 2001b**	H-ZSM-5	250	0.2	80	75***
Amandi *et al.,* 2005	γ-Al_2O_3****	275	N/A	47.5*****	84.5

* Industrial Bayer Process

** Only optimum reaction conditions reported here

*** It should be noted that Fletcher *et al*., strangely, did not report the formation of the 2-isopropyl-3-methyl phenol isomer. This is in contrast to other studies using propene as the alkylating agent (Biedermann *et al*, 1978) and those using isopropanol (van der Merwe, 2012 and Nagooroo and Truter, 2008) where several percent of this isomer was found in the isopropyl-2-methyl phenol isomers fraction. It may be speculated that thymol and its 2-isopropylated analogue could not be separated by the gas chromatographic column and method applied

**** In supercritical CO_2

***** Derived from data given by Amandi *et al*. (1:0.8 molar excess of *m*-cresol)

In the study conducted by Fletcher *et al.* (2001a), various acid zeolite catalysts of the Beta, Mordenite and ZSM-5 type with different SiO_2/Al_2O_3 ratios were investigated with respect to their performance as catalysts for the selective alkylation of *m*-cresol with propene in the synthesis of thymol. At operating conditions of typically 250°C and 1 bar (abs), the sample of medium-pore zeolite H-ZSM-5 with the lowest density of acid sites i.e. a high molar SiO_2/Al_2O_3 ratio of 400 (indicated as HMFI-2 in Figure 2-2), was found to be superior with respect to catalyst activity, stability and selectivity toward thymol and under milder reaction conditions compared to the alumina catalyst employed for the industrial Bayer process. The results reported 75% thymol selectivity at ca. 80% *m*-cresol conversion when feeding a 1:1 molar mixture of *m*-cresol and propene (see Table 2-1).

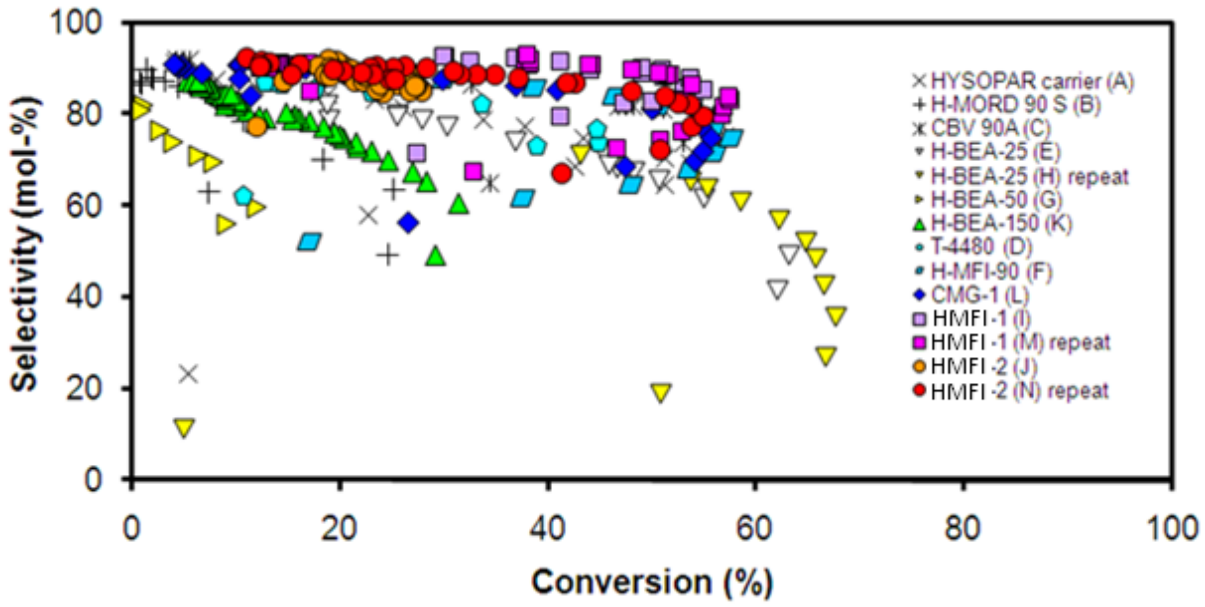

Figure 2-2: Thymol selectivity* versus conversion over H-Mordenite, H-Beta and H-ZSM-5 catalysts in the alkylation of *m*-cresol with propene at 250°C and 1 bar (abs) (Fletcher *et al.,* 2001a). All catalysts indicated were commercial zeolite catalysts or laboratory specimen manufactured by Süd-Chemie.

* It should be noted (see footnote *** to Table 2-1) that 'thymol' in the study by Fletcher et al. may also have comprised several percentages of the 2-isopropyl-3-methyl phenol isomer

The high activity, stability and thymol selectivity achieved over the H-ZSM-5 catalyst with SiO_2/Al_2O_3 of 400 was firstly regarded as a consequence of the greater resistance of the zeolite to coking since this catalyst displayed minimum formation of oligomeric, polyisopropylated and polyaromatic compounds at higher reaction temperatures, resulting in slower deactivation of the catalyst and thus prolonged catalyst lifetime. Secondly, shape-selective properties of the

H-ZSM-5 catalyst were regarded to favour, under kinetic control, the thymol isomer, since it is less bulky than the other isomers (Fletcher *et al*., 2001a).

Although the above result appears extremely favourable since conversions and thymol selectivities similar to the industrial process were achieved, but at milder conditions, the process still makes use of propene as an alkylating agent which, as mentioned in Section 2.1.1, could be problematic under certain circumstances.

2.1.2.2 Use of heterogeneous catalyst systems with C_3-alcohols and C_3-ethers as alkylating agents

The use of C_3-alcohols and C_3-ethers as alternative alkylating agents was studied over various catalysts. The use of isopropanol as an alkylating agent either enables isopropanol to react by an S_N-2 mechanism with simultaneous alkylation and elimination of water or to react by in-situ dehydration of the isopropanol to, at first, form propene (and water) that then alkylates the *m*-cresol (see Section 2.1.3.2.2). Table 2-2 summarises the catalyst systems used in previous studies in the synthesis of thymol with isopropanol as an alkylating agent as well as some of the key findings.

Table 2-2: Summary of results from various catalysts used in previous studies in the synthesis of thymol by alkylation of *m*-cresol with isopropanol

Reference	**Catalyst**	**T (°C)**	**WHSV (h^{-1})**	***m*-Cresol conversion (%)**	**Thymol selectivity (%)**
Grabowska and Wrzyszcz, 2001	$ZnAl_2O_4$	528	0.5	78.2	88.4
Umamaheswari *et al.,* 2002	Al-MCM-41	375	1.4	34.2	100
Velu *et al.,* 1998	Mg-Al hydrotalcites	400	1	40	80
Nagooroo and Truter, 2008	H-ZSM-5	250	0.125	60	60
van der Merwe, 2012	H-ZSM-5	275	0.38	68	56
Amandi *et al.,* 2005	γ-Al_2O_3*	275	N/A	22.6**	78.6
	Nafion® SAC-13*	275	N/A	28.9**	61.2

* In supercritical CO_2

** Derived from data given by Amandi *et al.* (3:1 molar excess of *m*-cresol)

The studies conducted by van der Merwe (2012) and Nagooroo and Truter (2008) were performed over an H-ZSM-5 catalyst with a molar SiO_2/Al_2O_3 ratio of 90 at significantly milder reaction conditions of 275°C and 15 bar (abs) compared to the industrial Bayer process (see Table 2-1). 56% thymol selectivity at ca. 68% *m*-cresol conversion or 60% thymol selectivity at 60% *m*-cresol conversion, respectively, were achieved when feeding a 1:1 molar mixture of *m*-cresol and propene (see Table 2-2). This was lower than the conversions and selectivities observed using propene at 250°C and 5 bar (abs).

However, while the high conversions and thymol selectivities observed from using propene (Fletcher *et al.,* 2001b) resulted from reaction temperatures of 250°C and less, experiments using isopropanol were carried out at 275°C. The difference in the operating temperatures of the two experiments may be suspected as being, at least in part, responsible for the difference in selectivities and conversion due to the different extents of consumption of alkylating agents in side reactions and proximity to thermodynamic equilibrium limitations.

The studies made by van der Merwe (2012) and Nagooroo and Truter (2008) merely investigated the effect of parameter variation on thymol selectivity and conversion.

A study which entails the investigation of the stability, activity and selectivity of H-ZSM-5 catalysts of various SiO_2/Al_2O_3 ratios using isopropanol as the alkylating agent had yet to be done. The aim of this study was therefore to firstly identify the optimal H-ZSM-5 catalyst in the alkylation of *m*-cresol with isopropanol by varying the SiO_2/Al_2O_3 ratio, secondly, by variation of operating conditions over the selected catalyst to ascertain optimal reaction conditions and, thirdly, by an investigation of the reaction mechanism and condition effects, to find the reasons behind the expected SiO_2/Al_2O_3 ratio effect.

2.1.3 Reaction chemistry

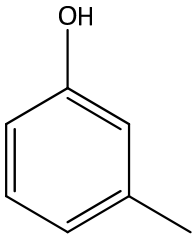

Figure 2-3: Chemical structure of *m*-cresol

m-Cresol is a compound comprised of a phenol molecule (a benzene ring with one of the ring's hydrogen's replaced with a hydroxyl group) and with a methyl group substituted in the *meta*-position of the aromatic ring (see Figure 2-3).

The presence of a substituent on the benzene ring generally influences the degree and orientation of its reactivity. $–CH_3$, $–OCH_3$ and –OH substituents are all electron-donating species and this activates the ring for electrophilic substitution. Hence, in general, toluene, anisole and phenol molecules will react faster than benzene in electrophilic substitution reactions due to an increasing activating effect from $–CH_3$ (weak) to $–OCH_3$ (moderate) to –OH (strong) (Sykes, 1986). The strong activating effect of the –OH substituent during electrophilic aromatic substitution can be accounted for by taking into consideration that the oxygen atom can share more than one pair of electrons with the aromatic ring (i.e. it can form a bond of higher order than a single bond) and thus has the effect of producing a partial negative charge on the ring. This mesomeric effect by which lone electron pairs of the oxygen atom in the –OH substituent are partly delocalised into the aromatic nucleus *via* delocalised π-orbitals activates *m*-cresol in the *ortho*- and *para*-positions relative to the hydroxyl group for electrophilic attack by, for instance, a carbenium ion (see Figure 2-4) (Sykes, 1986).

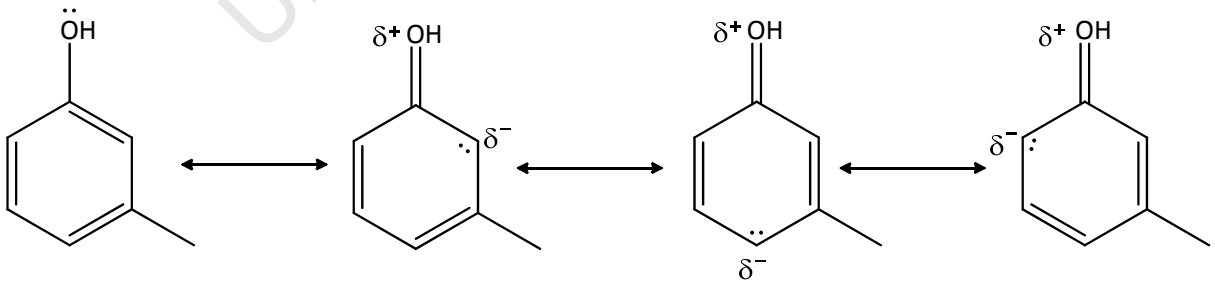

Figure 2-4: Stabilisation of *m*-cresol by resonance (Sykes, 1986)

2.1.3.1 Electrophilic substitution

2.1.3.1.1 C-Alkylation

The carbocations formed by attack by an electrophile X^+ on the aromatic ring of the cresol molecule (C-alkylation) are stabilised by delocalisation of the positive charge over the molecule resulting in the formation of several resonance structures. The extent to which these carbocations are stabilised depends on the position of the attack.

After attack on the *meta*-position of the ring, the positive charge is delocalised over the ring for which three resonance structures can be drawn (see Figure 2-5).

The *ortho*- and *para*-substituted rings have an extra resonance structure, in which the positive charge is carried by the oxygen atom (see Figure 2-6 and Figure 2-7). These additional resonance structures are specifically favoured since in these structures every atom (except for hydrogen) has a complete octet of electrons (Morrison and Boyd, 1987) and, therefore, contribute significantly to the stabilisation of the said carbocations. Hence, from a chemical kinetic point of view, the –OH group on the cresol molecule activates the ring for electrophilic substitution particularly in the *ortho*- and *para*-positions.

The *meta*-positions are to some extent deactivated by the inductive effect of the –OH group, withdrawing charge, therefore making the *meta*-positions not only the least reactive positions on the phenolic ring but even less reactive than the individual carbon atoms of a benzene ring or the *meta*-positions on a toluene molecule (Sykes, 1986).

The effect of the –OH group decreases from the *ortho*- to the *para*-positions (Sykes, 1986). In addition to this, there are two *ortho*-positions. Substitution of the *ortho*-positions will therefore be statistically favoured over substitution of the *para*-position (in the absence of steric constraints) (Venuto, 1994). Chemical kinetics therefore predicts the product isomer distribution from electrophilic substitution to be as follows: *ortho* > *para* > *meta*.

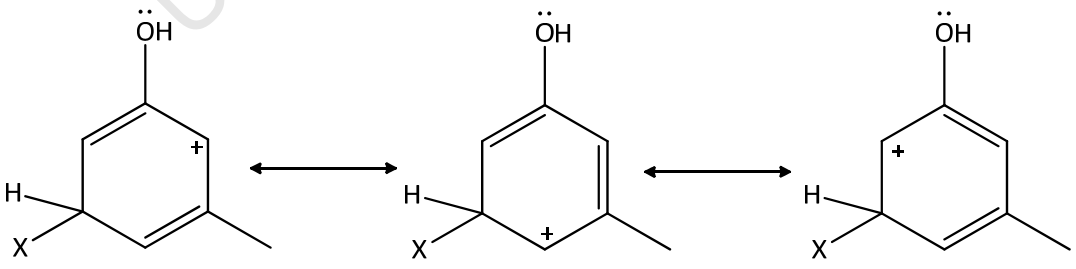

Figure 2-5: *Meta*-substitution resonance structures (Sykes, 1986)

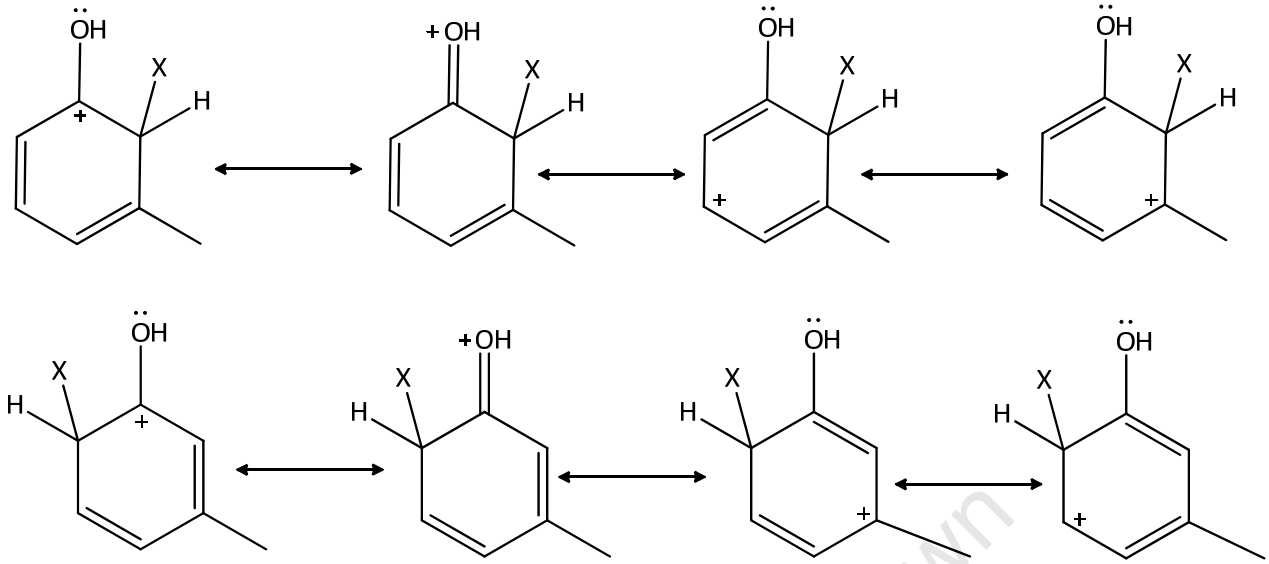

Figure 2-6: *Ortho*-substitution resonance structures (Sykes, 1986)

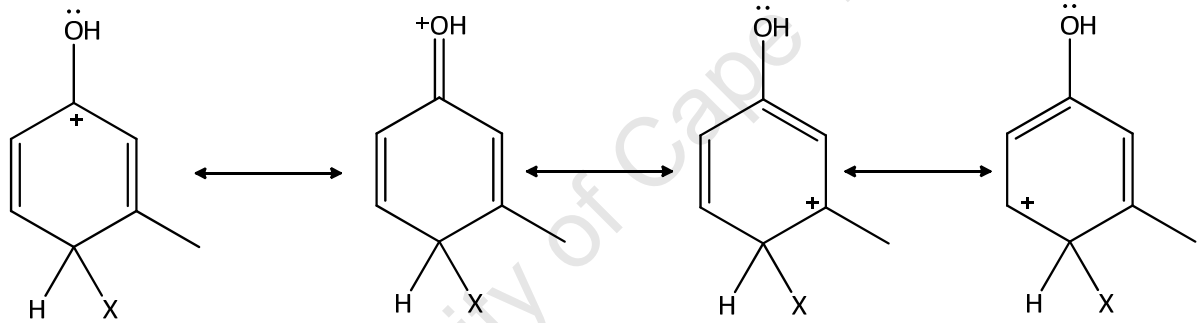

Figure 2-7: *Para*-substitution resonance structures (Sykes, 1986)

Steric hindrance may impose an additional effect. Depending on the size of the electrophile, the effect is such that the bulkier the incoming electrophile, the greater is the steric hindrance between the electrophile and adjacent groups on the ring (Sykes, 1986).

As can be seen from Figure 2-6, one of the *ortho*-positions in *m*-cresol is located between the hydroxyl and the methyl group. Under these circumstances, the electrophile will attack with less preference onto the *ortho*-position between the hydroxyl and methyl group than onto the other *ortho*-position or the *para*-position.

The H-atom that is still bonded to the attacked carbon atom is finally released as a proton.

2.1.3.1.2 O-Alkylation

Electrophilic attack by X^+ can also target the hydroxyl group of the *m*-cresol molecule and result in the formation of an intermediate comprising of an *m*-methyl phenoxy group and the electrophile attached to the oxygen atom (see Figure 2-8). This will eventually lead to the formation of an ether.

In a phenol alkylation reaction with methanol conducted over acid sites of different types and strengths *viz.* γ-Al_2O_3 (strong Lewis acid and basis sites), Nafion-H (strong Brønsted acid sites), silica-alumina (strong Brønsted acid sites as well as strong Lewis acid and basic sites) and Kieselguhr-supported phosphoric acid (medium to weak Brønsted acid sites), it was observed that at lower temperatures (200-230°C) anisole was the major product (Santacesaria *et al.,* 1990a). However, anisole selectivity appeared to decline with increasing reaction temperature. According to Balasubramanian *et al.* (2000) this apparent decrease in anisole selectivity with increasing temperature could be attributed to its conversion to *o*-cresol (see Section 2.1.3.1.3). Santacesaria *et al.* (1990a), however, suggested that this phenomenon could be ascribed to the fact that C-alkylation has a higher activation energy (134 kJ/mol over γ-Al_2O_3) compared to O-alkylation (67 kJ/mol over γ-Al_2O_3) thereby suggesting that C-alkylation will be favoured at higher reaction temperatures.

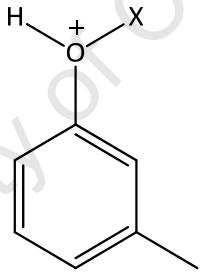

Figure 2-8: Cationic intermediate of ether formation by electrophilic attack onto hydroxyl group of *m*-cresol

2.1.3.1.3 Transformation of O-alkylated products

The products which form *via* O-alkylation, *viz.* ethers, are typically unstable species (see Section 2.1.6.5) and generally behave as intermediates in the reaction process. In this mechanism, ethers formed *via* O-alkylation (see Figure 2-13) undergo an internal rearrangement to form a C-alkylated species (see Figure 2-9). *Ortho*-substitution is preferred as the shifting alkyl group is closest to the *ortho*-positions. In *m*-cresol alkylation, taking into account the steric hindrance that the existing methyl group offers (see Section 2.1.3.1.1 and Figure 2-14), the 6-alkylated species (thymol, if the shifting alkyl group was an isopropyl group) is the favoured product. This phenomenon of internal rearrangement of unstable ether intermediates has been reported extensively in literature in the formation of *o*-cresol from phenol methylation *via* an anisole

intermediate (Marczewski *et al*., 1988, Moon, 2003, Santacesaria *et al.*, 1990a and 1990b, Venuto, 1994, Wang *et al.,* 2004, Xu *et al*., 1997).

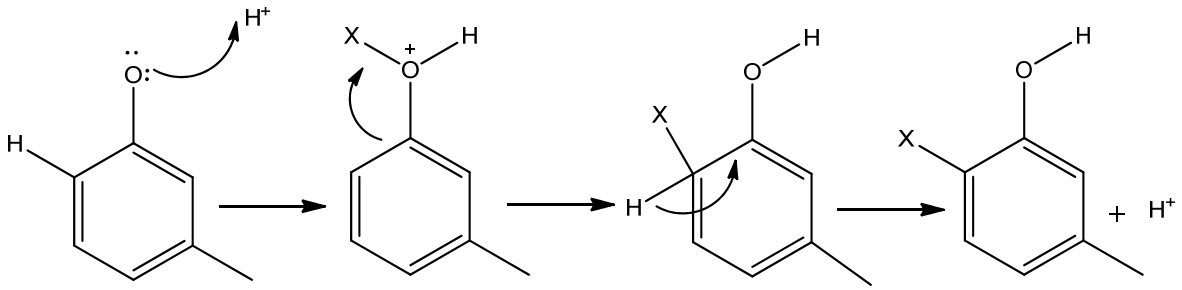

Figure 2-9: Mechanism of acid catalysed formation of 6-alkylated 3-methyl phenol (thymol) from alkyl-*m*-tolyl ether over an acid catalyst (adapted from Moon, 2003)

In the alkylation of phenol with methanol over H-Y zeolite, Marczewski *et al.* (1988) proposed a different mechanism incorporating the intermediary role of anisole. In order to explain the comparatively high *p*-selectivity obtained, it was suggested that the methyl group on the anisole intermediate was subjected to a transalkylation with phenol in the formation of a cresol by which the reaction would also produce *p*-cresol. In contrast, however, the smaller channel size of the H-ZSM-5 zeolite, compared to the H-Y zeolite, inhibited the formation of the bulky bicyclic intermediate required in this transalkylation reaction and thus the formation of cresols from anisole over H-ZSM-5 with comparatively high *o*-selectivity can only be explained by an internal *o*-selective rearrangement mechanism (Parton *et al*., 1989).

2.1.3.2 Alkylation with isopropanol

Two reactions may occur in the acid catalyzed alkylation of *m*-cresol with isopropanol to synthesize thymol *viz.* (i) the dehydration of isopropanol to form a secondary carbenium ion (and subsequently propene) followed by the alkylation of *m*-cresol with this carbenium ion intermediate (or the readsorbed propene, respectively) in an S_N-1 reaction and (ii) the direct alkylation of *m*-cresol with isopropanol in an S_N-2 reaction.

2.1.3.2.1 Dehydration of isopropanol

Alcohols are known to dehydrate to the corresponding alkene and water in the presence of an acid catalyst. The dehydration reaction of isopropanol to propene is depicted in Figure 2-10.

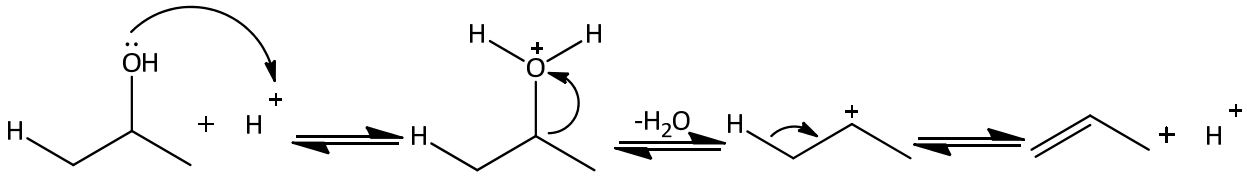

Figure 2-10: Acid catalysed dehydration reaction of isopropanol to propene

For the thermodynamics of isopropanol dehydration see Section 2.1.6.1.

Nagooroo and Truter (2008) and van der Merwe (2012) determined the extent of dehydration of the isopropanol alkylating agent over H-ZSM-5 in the presence of an equimolar percentage of *m*-cresol experimentally at various temperatures in the range 200-300°C, 1 bar (abs) and WHSV = 1.03 $g_{m\text{-cresol}}/g_{cat}$.hr. Complete dehydration of isopropanol was observed already at low conversions of *m*-cresol.

At temperatures below 250°C, selective formation of propene was observed in the dehydration reaction. At around 250°C, when dehydration of isopropanol to propene was complete, some formation of higher olefins, alkanes and aromatics was observed. At temperatures greater than 250°C, a 'pool' of olefins that are constantly isomerising, oligomerising and cracking, as well as other hydrocarbons was formed.

2.1.3.2.2 Isopropylation of m-cresol

Figure 2-11 and Figure 2-12 illustrate the possible mechanisms of isopropylation of *m*-cresol by C-alkylation in the 6-position to thymol. Three reaction pathways of ring isopropylation of *m*-cresol with isopropanol may yield thymol, namely the following:

- Dehydration of the isopropanol and formation of an adsorbed isopropyl cation that then attacks the ring (Figure 2-11)
- Dehydration of the isopropanol to propene which then readsorbs as an isopropyl cation that attacks the ring (Figure 2-11)
- Direct alkylation of the ring with isopropanol (Figure 2-12)

It should be noted that during propylation of aromatic rings with propene (or, analogously, isopropanol) under kinetic control, n-propyl substituents hardly form, since the reaction proceeds *via* the secondary carbenium ion that forms on the central carbon atom. For instance, in acid catalysed alkylation of benzene with propene to form cumene (the first stage of the cumene process of phenol synthesis) selectivity of n-propyl benzene is only around 0.01% (Hwang and Chen, 2007).

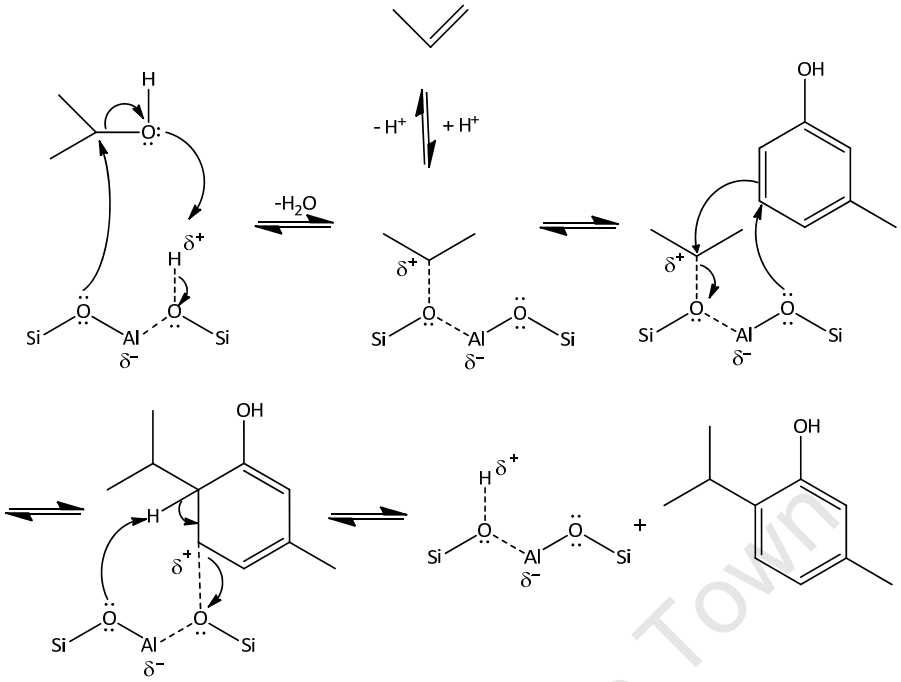

Figure 2-11: Reaction mechanism depicting the acid catalysed isopropylation of *m*-cresol with isopropanol *via* dehydration of isopropanol and the simultaneous formation of an adsorbed secondary (isopropyl) carbenium ion together with water followed by either immediate isopropylation of *m*-cresol with this intermediate or desorption/readsorption of propene (corresponding to an S_N-1 mechanism)

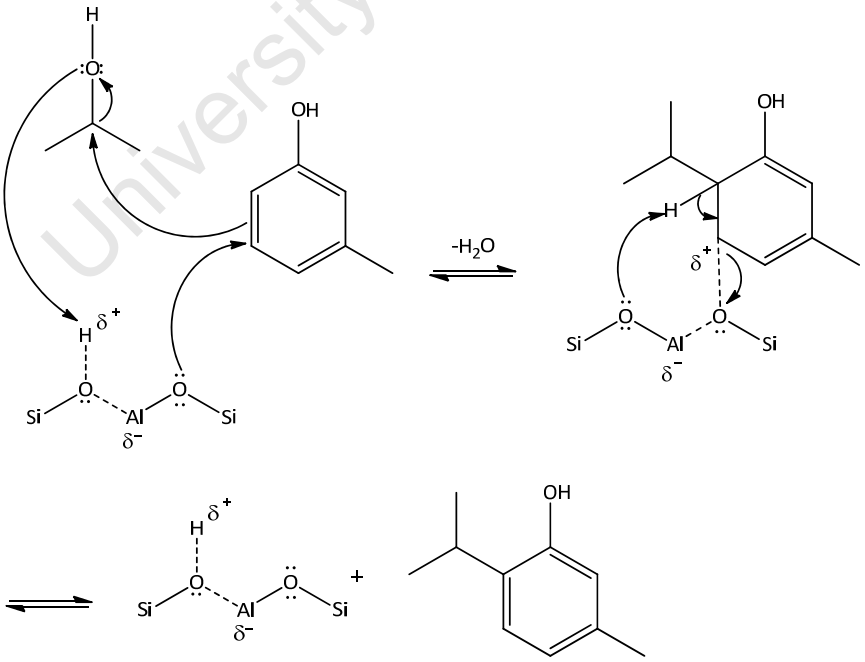

Figure 2-12: Simultaneous ring alkylation of *m*-cresol with isopropanol and release of water by S_N-2 mechanism

2.1.3.2.3 Formation of isopropyl-3-tolyl ether by condensation of m-cresol and isopropanol

As aforementioned (Section 2.1.3.1.2), ether formation is a relatively easy reaction that is favoured at low temperatures. Figure 2-13 illustrates the direct condensation of *m*-cresol and isopropanol to form the ether.

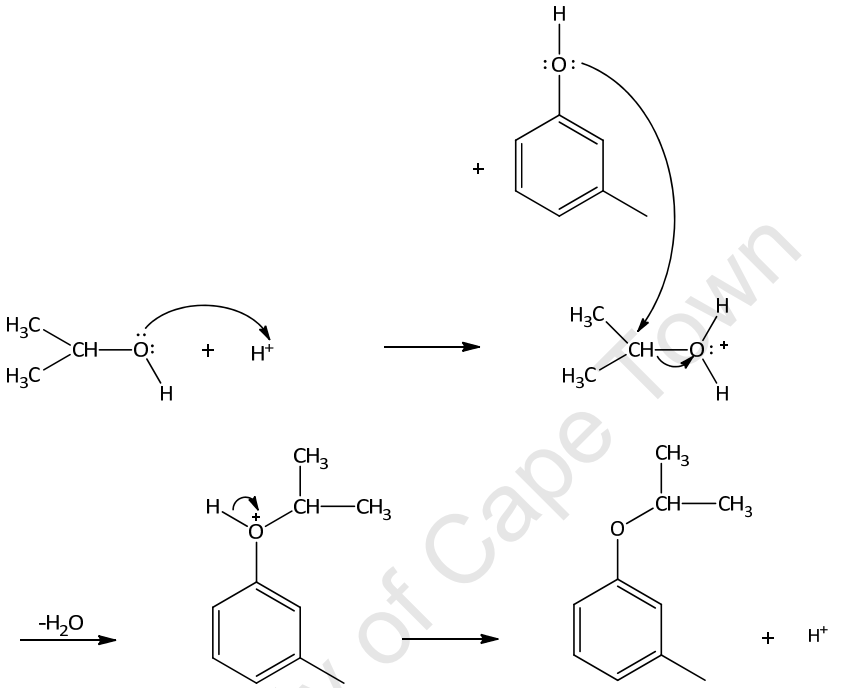

Figure 2-13: Mechanism for the formation of isopropyl-3-tolyl ether from isopropylation of the hydroxyl group of *m*-cresol over an acid catalyst (corresponding to an S_N-2 mechanism)

2.1.4 Kinetics of thymol synthesis

2.1.4.1 Order of reaction

Hardly anything in literature has been reported regarding the order of reaction in the synthesis of thymol from *m*-cresol and isopropanol. Yadav and Pathre (2005) converted the two reactants over zirconia based catalysts at 160 – 200°C in the liquid phase. It was found that second order kinetics fitted the experimental data best. The same order of reaction was found for the reaction of *m*-cresol with *tert*-butanol, also over zirconia based catalysts (Yadav and Pathre, 2006).

A reaction system similar to the isopropylation of *m*-cresol, namely the methylation of phenol with methanol over acid zeolite catalysts was studied more intensively. Over H-ZSM-5 (at 300°C) and γ-Al_2O_3 (at 200°C) and low conversion, first order of reaction was observed with respect to each of the reactants phenol and methanol (Santacesaria *et al.,* 1990b, and

Marczewski *et al.,* 1996, respectively). However, at 200°C, over all the zeolites that were investigated, first order was obtained for methanol but zero order for phenol (Marczewski *et al.,* 1996). This was ascribed to capillary condensation of phenol in the zeolite pores so that all the pores were filled with phenol. Hence, in the vicinity of the acid sites, phenol was in high excess and phenol concentration was constant, irrespective of its concentration in the gas phase.

The effect of the reactants partial pressures on anisole and cresols distribution was studied by Moon (2003). It was found that partial pressures did not directly affect product selectivities but only indirectly *via* changes in phenol conversion, meaning that the individual reactions were of the same reaction order.

2.1.4.2 Thymol selectivity

The selectivity of thymol in *m*-cresol isopropylation is high by nature compared to the other isomers (see Table 2-1, Table 2-2 and Figure 2-3). The major by-products are the position isomers where the isopropyl group is in a different position on the phenol ring; thymol is the kinetically preferred isomer in the reaction even in a non-shape selective environment. This is due to several reasons:

1. The hydroxyl group on the phenol molecule is very strongly *ortho*- and *para*-directing in electrophilic aromatic substitution (see Section 2.1.3.1.1).
2. The route *via* the initial formation of the ether yields the *o*-substituted isomers with preference (see Section 2.1.3.1.2 and Section 2.1.3.1.3).
3. The isopropyl group in the 2-position, in close vicinity to both the methyl and the hydroxyl substituents (see Figure 2-14), is strongly sterically hindered, when compared to the opposite *ortho*-position. This is reflected in the low prevalence of the 2-isopropyl-3-methyl phenol isomer (see Section 2.1.3.1.1), although substituted in the *ortho*-position.
4. The *para*-position is also sterically hindered but to a lesser extent.

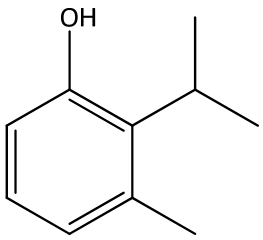

Figure 2-14: Chemical structure of 2-isopropyl-3-methyl phenol

2.1.4.3 Thymol isomerisation

"Thymol isomerisation" in this context refers only to the position of the isopropyl group on the ring and not to the isomerisation of the isopropyl group to an n-propyl group. The latter is dealt with in Section 2.1.4.5.

The delayed formation of 5-isopropyl-3-methyl phenol from the kinetically preferred position isomers generated in the alkylation reaction (*viz.* 6-isopropyl-3-methyl phenol (thymol) and 4-isopropyl-3-methyl phenol) occurs *via* isomerisation (Klein and Wedemeyer, 1976). Thymol isomerises *via* a 1,2-shift of the isopropyl group (see Figure 2-15). This occurs since in equilibrium the 5-isopropyl-3-methyl phenol position isomer is thermodynamically favoured over thymol and 4-isopropyl-3-methyl phenol (refer to Section 2.1.6.3, Figure 2-21 and Figure 2-22).

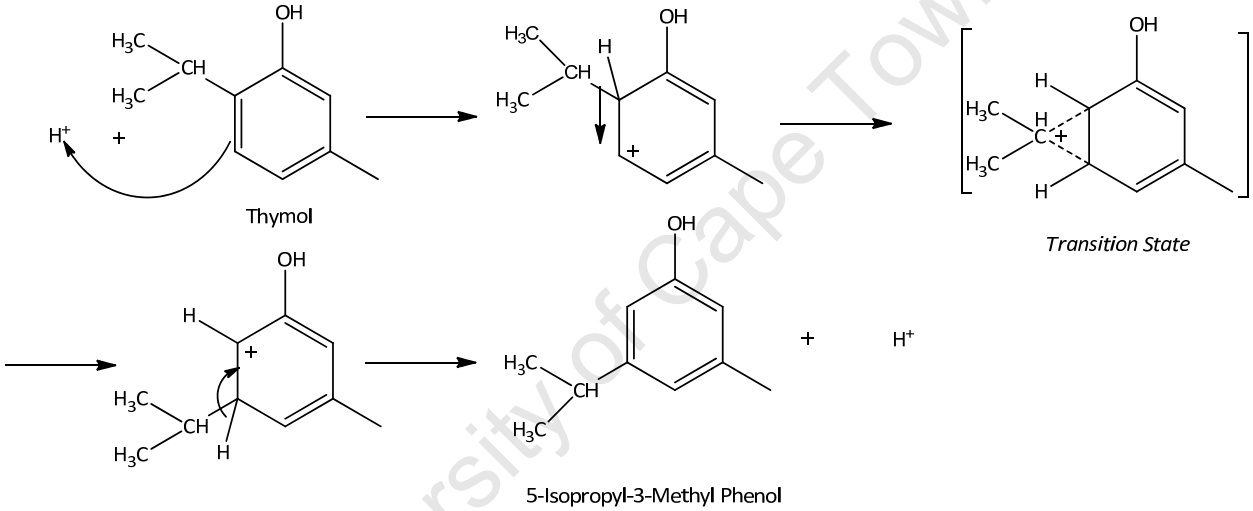

Figure 2-15: 1,2-Isopropyl shift isomerisation mechanism of 6-isopropyl-3-methyl phenol (thymol) to 5-isopropyl-3-methyl phenol (adapted from Böhringer, 2009b)

2.1.4.4 Reactivity and reactions of the existing methyl substituent on *m*-cresol

The isopropyl group, be it in the form of isopropanol or propene or in the form of a substituent on the phenolic oxygen atom or on a carbon atom of the ring, is much more reactive than the existing methyl group. This is (i) because the existing methyl group is located on the *m*-position of the phenolic ring that is both least reactive and thermodynamically most stable and (ii) because the 1,2-shift isomerisation (or the transalkylation) of a methyl substituent involves a primary carbenium ion that is less stabilised (so that the isomerisation reaction proceeds *via* a less favourable intermediate and transition state), whereas the positive charge on the binding central carbon atom of the isopropyl group is stabilised by the two methyl substituents.

Consequently, isomerisation or transalkylation of methyl substituents is insignificant under the conditions of *m*-cresol isopropylation and therefore the existing methyl group on the *m*-cresol molecule remains essentially untouched during the isopropylation of *m*-cresol.

2.1.4.5 Formation of n-propyl alkylated compounds during isopropylation

n-Propyl substituents would be thermodynamically favoured over iso-propyl substituents (see Section 2.1.6.4) but hardly form during isopropylation.

- The direct alkylation with isopropanol *via* an S_N2-mechanism (see Figure 2-12) would lead to an isopropylated product immediately.
- The indirect alkylation *via* carbenium ions (e.g. *via* a propene intermediate) would also lead to, preferentially, the isopropylated product (see Figure 2-11) since the secondary carbenium ion intermediate is much more stable than the primary carbenium ion intermediate. In the acid catalysed alkylation of benzene with propene to form cumene (the first stage of the cumene process of phenol synthesis) selectivity of n-propyl benzene is only around 0.01% (Hwang and Chen, 2007).
- Isomerisation of the iso-propyl substituent to the more stable n-propyl substituent is very unfavourable and slow, since this step would involve both unfavourable hydride abstraction from the substituent and an unfavourable primary carbenium ion intermediate.

From the aforementioned, it may be inferred that, kinetically, isopropylation is significantly favoured over n-propylation when using isopropanol or propene as the alkylating agent.

2.1.5 Reaction network of thymol synthesis by alkylation of *m*-cresol with isopropanol or propene

A scheme of the reaction sequence was suggested by Amandi *et al.* (2005). The synthesis of thymol by alkylation of *m*-cresol with isopropanol and propene was conducted in a fixed-bed reactor in supercritical CO_2. The investigations employed both a solid Lewis acid catalyst (γ-Al_2O_3) and a solid Brønsted acid catalyst (Nafion® SAC-13) which were applied over a range of reaction conditions to optimise thymol yield and selectivity. Over both catalysts the product comprised mostly thymol and position isomers, some dialkylated derivatives and a small amount of isopropyl-3-methyl-benzylether (isopropyl-3-tolyl ether). Some of the results are given in Table 2-1 and Table 2-2. The proposed mechanism is shown in Figure 2-16**.**

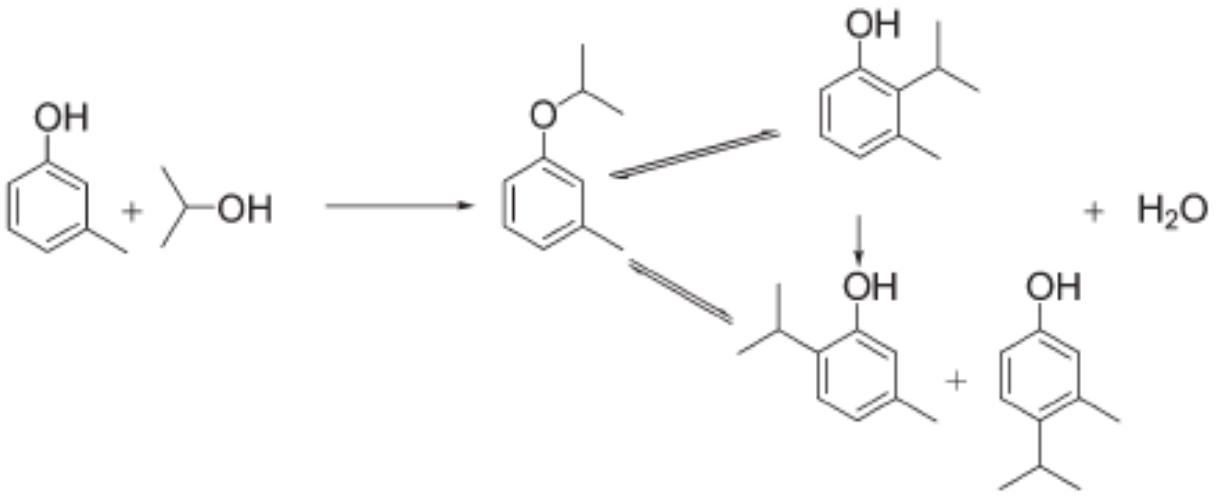

Figure 2-16: The mechanism proposed by Amandi *et al*. (2005) for the alkylation of *m*-cresol with isopropanol over γ–Al_2O_3

However, whilst the selectivity and yield data given by Amandi *et al*., (2005) maybe taken as correct, the analysis of results with respect to the observation and interpretation of trends and the development of the reaction mechanism is comparatively weak and partially incorrect. This is evident, for instance, in the following questionable suggestions proposed by the authors:

- The phenomenon of a "Fries rearrangement" of the isopropyl-3-methyl-benzylether to ring isopropylated *m*-cresol species, as proposed by the authors, is impossible since a Fries rearrangement reaction occurs with phenyl esters, not phenyl ethers, and produces hydroxyl aryl ketones, not alkyl phenols (March, 1985).
- The data indicates the disappearance of the 2-isopropyl-3-methyl phenol isomer from the reaction mixture with increasing conversion but the analysis fails to provide a reasonable explanation for this decline. The proposed mechanism suggests a direct, single step conversion of the 2-isopropyl-3-methyl phenol isomer to the 4-isopropyl-3-methyl phenol and 6-isopropyl-3-ethyl phenol isomers. However, the 2-isopropyl-3-methyl phenol isomer cannot react directly, namely by 1,2-shift isomerisation, but only by dealkylation back to *m*-cresol or transalkylation with another phenolic species, or a second alkylation of the species. However, none of these explanations are proposed for the trends observed. The phenomenon is especially confusing since no corresponding increase in the formation of dialkylated compounds was observed which could have provided an explanation for this trend.
- It is further claimed that the formation of the 5-isopropy-3-methyl phenol isomer is "believed to occur *via* an isomerisation process from the more stable species generated in the reaction, namely the other isopropyl position isomers". In fact, the 5-isopropyl-3-methyl phenol isomer itself is, thermodynamically, the most stable isomer (see Section 2.1.6.2 and Figure 2-21).

- Another study was performed by Selvaraj and Kawi (2008) in the synthesis of thymol by vapour phase isopropylation of *m*-cresol. The authors proposed the mechanistic scheme shown in Figure 2-17.

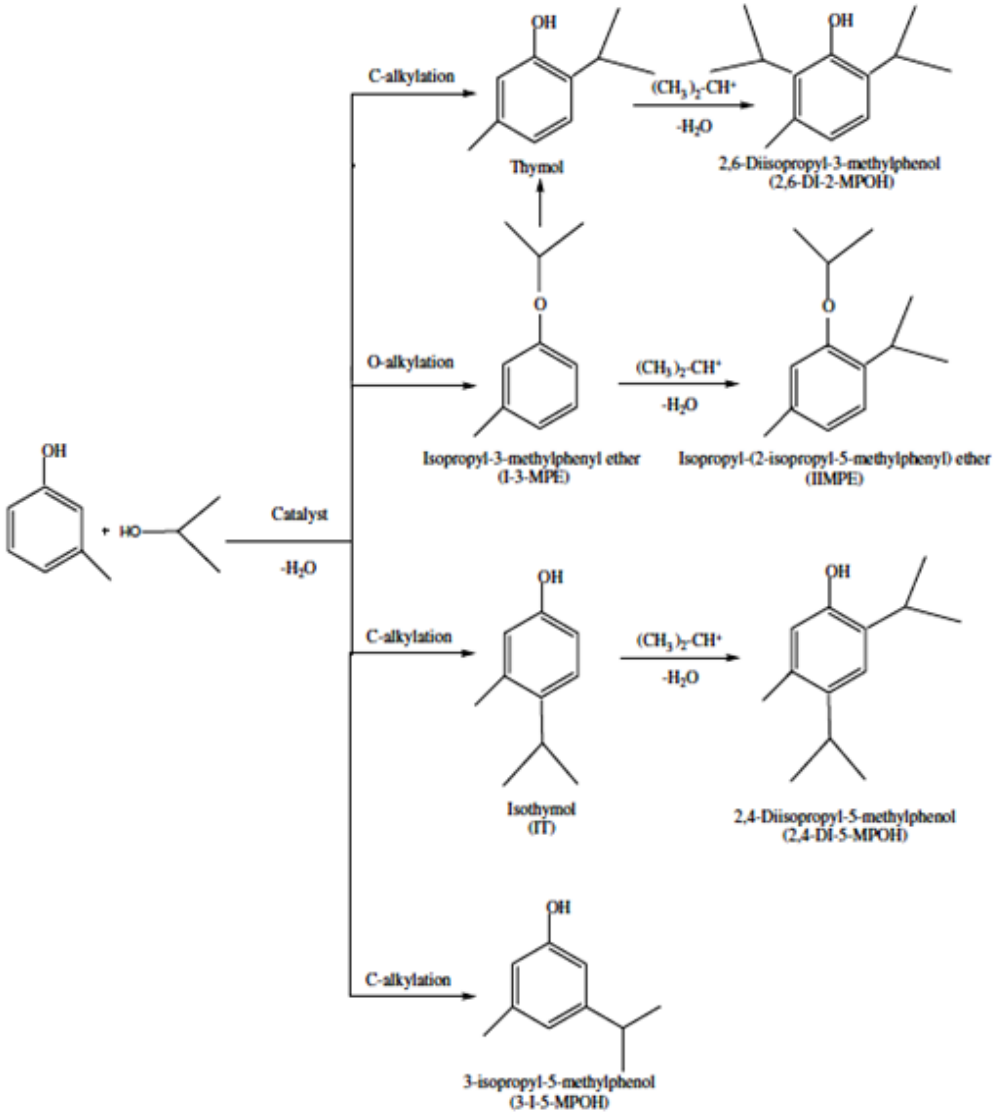

Figure 2-17: Mechanistic scheme proposed by Selvaraj and Kawi (2008) in the isopropylation of *m*-cresol to synthesise thymol

From the proposed mechanism, the following can be derived:

- Direct alkylation occurs with isopropanol. No dehydration of isopropanol to propene is considered
- O-alkylation and C-alkylation occur in parallel
- No formation of the sterically hindered isomer 2-isopropyl-3-methyl phenol is considered
- Diisopropylation of all the primary products is included
- No dealkylation or rearrangement of the ether formed is considered

In the study performed by Moon (2003) in the methylation of phenol over acidic zeolite catalysts, the following was observed as indicated by Figure 2-18.

- O- and C-alkylation occur as parallel reactions
- Internal rearrangement of the ether is observed
- The primary products formed undergo a second alkylation reaction to form diisopropylated products
- Dealkylation is observed

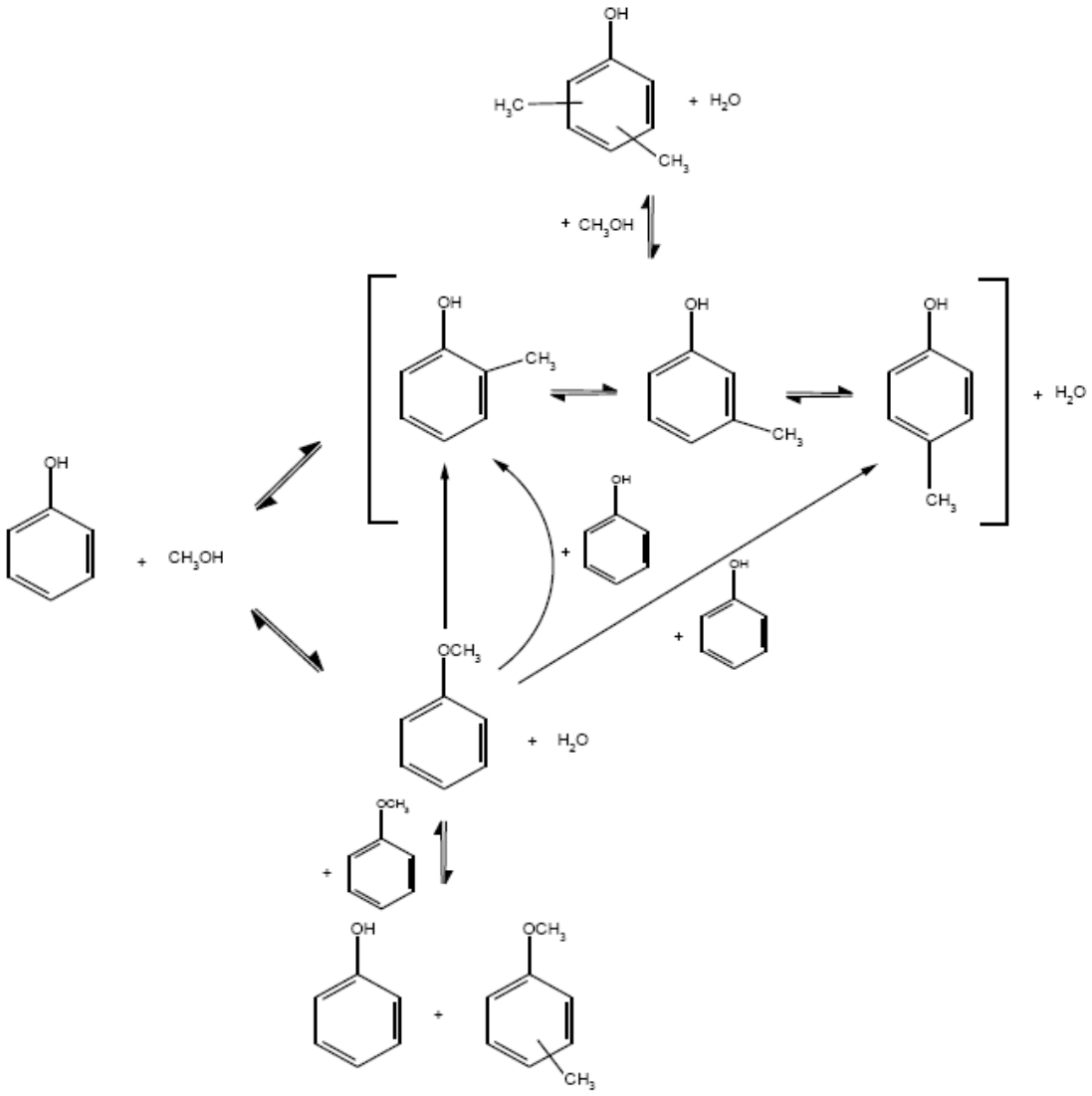

Figure 2-18: Mechanism proposed by Moon (2003) in the methylation of phenol over acidic zeolite catalysts

2.1.5.1 Decline of conversion at very low space velocity

A seemingly strange behaviour was observed at high temperature when lowering space velocity, namely, a decline of *m*-cresol conversion with declining space velocity i.e. increasing residence time (Nagooroo and Truter, 2008 and van der Merwe, 2012). The phenomenon was found to be caused by a kind of 'molar depletion' of the alkylating co-reactant due to two effects that effectively reduce the alkylating agent to *m*-cresol ratio. The effects are as follows (van der Merwe, 2012):

- Di-isopropylation: This secondary reaction consumes two isopropanol or propene molecules per *m*-cresol molecule so that the alkyl side chain carbon to ring ratio becomes >3.
- Oligomerisation of the propene molecules, followed by cracking of the higher oligiomers. This results in a 'pool' of olefins, that is alkylating species, with an average carbon number larger than that of propene, so that the alkyl side chain carbon to ring ratio also becomes >3.

Consequently, the effective molar ratio of alkylating agent to *m*-cresol (originally 1:1) declines so that less *m*-cresol can be alkylated. At the higher reaction temperatures this is reinforced by the thermodynamic equilibrium limitations of thymol formation (see Section 2.1.6.2). This means that, in the extreme, when the alkylating species to *m*-cresol ratio becomes too low, even dealkylation of primarily isopropylated *m*-cresol (e.g. thymol) which formed in the upper part of the catalyst bed, becomes dealkylated so that conversion effectively declines with increasing space velocity (van der Merwe, 2012).

2.1.6 Thermodynamics of thymol synthesis

2.1.6.1 Thermodynamics of isopropanol dehydration

The dehydration of isopropanol is an endothermic reaction which proceeds as follows:

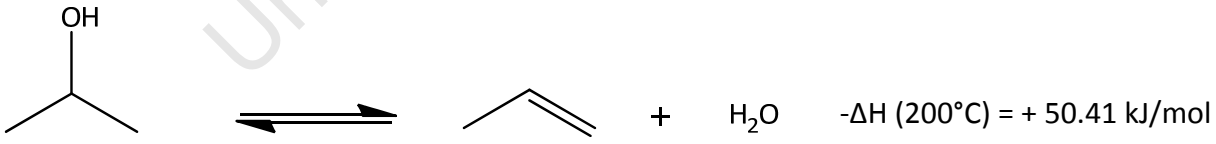

The dehydration reaction of isopropanol was modelled using Aspen Plus User Interface, Aspen Technology, Inc. (2006) under conditions of 200 - 300°C and 1.5 - 10 bar. A validation of the results of the reaction model was established by comparing the results of the Peng-Robinson Equation of State, UNIFAC and the Ideal Gas Law. All three equations of state displayed a close correlation and indicated that the dehydration of isopropanol to propene can proceed to 'completion' in the temperature and pressure range of interest for thymol synthesis in this study as can be seen in Figure 2-19.

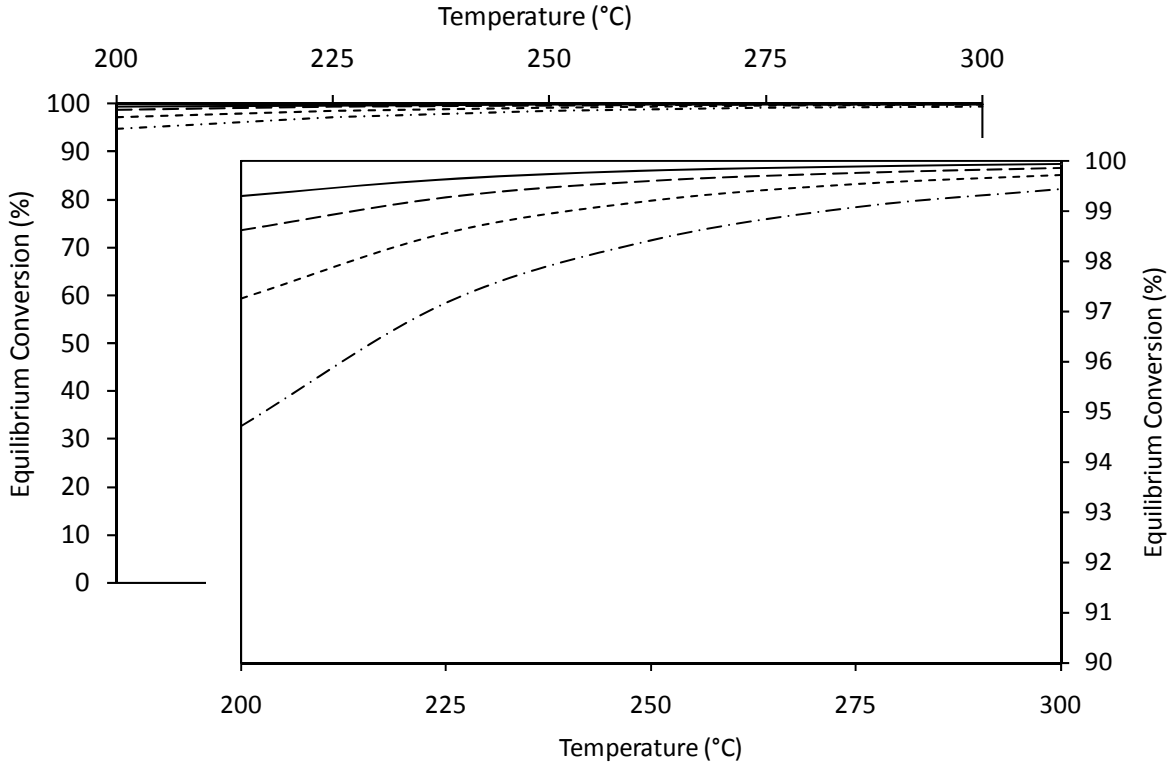

Figure 2-19: Equilibrium conversion of isopropanol to propene and water as a function of temperature as modelled by Aspen Plus User Interface, Aspen Technology, Inc. (2006) for pressures —1.5 bar – –3 bar ----6 bar -·--12 bar. A pressure of 3 bar was typically applied in this study. (The second graph is a zoom-in of the 90 – 100% conversion range of the first graph.)

2.1.6.2 Thermodynamics of *m*-cresol isopropylation

In the study conducted by Fletcher *et al.* (2001b), thermodynamic constraints were found to limit conversion of *m*-cresol and propene and, consequently, thymol yield, particularly in the upper temperature range (see Figure 2-20). Under the conditions applied, thymol yields increased with increasing reaction temperature as long as the reaction temperature was below 250°C. This is indicated by the upper edge of the array of data points shown in Figure 2-20, which represents the thymol yields attained at the lowermost space velocities applied.

The decline of the upper edge of the array with further increasing temperature that followed the yield maximum as shown in Figure 2-20 was interpreted as an indication of thermodynamic equilibrium limitations as depicted by the dashed line. At reaction conditions of 1 bar (abs), 250°C and a molar propene: *m*-cresol feed ratio of 1:1, the equilibrium yield of thymol in the aforementioned reaction was estimated to be around 75%. In the study by Fletcher *et al*. (2001b) the presence of thermodynamic equilibrium limitations at elevated temperatures of the reaction involved was deduced from the experimental data shown in Figure 2-20 as suitable thermodynamic data was unavailable.

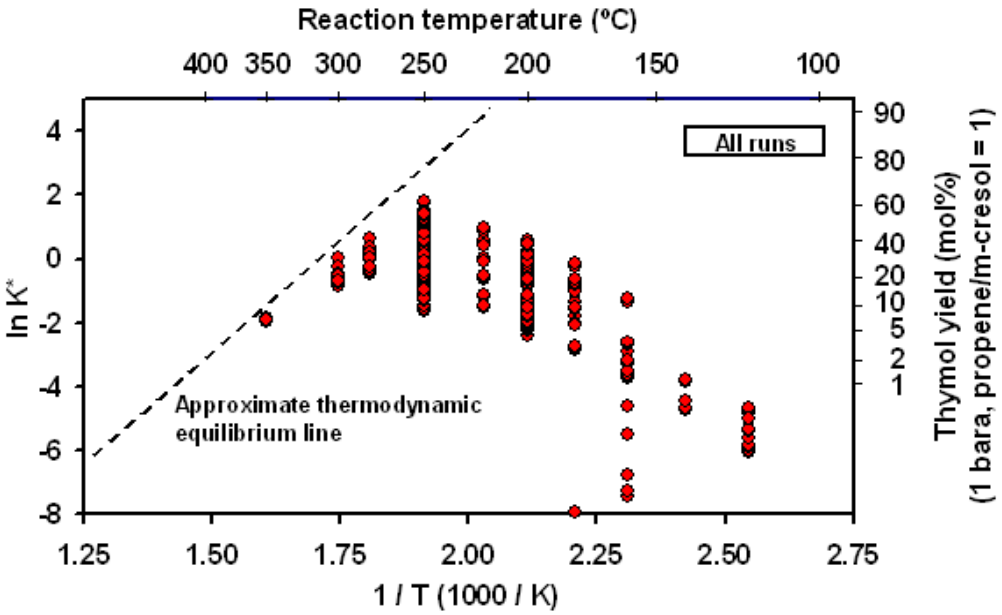

Figure 2-20: Experimental estimation of thermodynamic equilibrium approach in the alkylation of *m*-cresol with propene to thymol (1:1 molar feed ratio) over H-ZSM-5 catalyst at various reaction conditions (Fletcher *et al.,* 2001b). It should be noted that selectivity to position isomers and other by-products was small.

2.1.6.3 Thermodynamics of isopropyl group position isomers distribution

Fletcher *et al.* (2002) also investigated the isomerisation of thymol and its 4-isopropyl-3-methyl phenol and 5-isopropyl-3-methyl phenol position isomers over acid zeolite catalysts H-ZSM-5 at reaction temperatures between 200 and 300°C. Starting from an equimolar mixture of 4-isopropyl-3-methyl phenol and 5-isopropyl-3-methyl phenol (Feed 1, represented by the white circle in the middle of the bottom edge of the ternary diagram in Figure 2-21), the distribution obtained converged toward a region which represented mostly 5-isopropyl-3-methyl phenol, some thymol and a small amount of 4-isopropyl-3-methyl phenol. The same region was approached when starting from an equimolar mixture of thymol and the 5-isopropyl-3-methyl phenol isomer (Feed 2, white circle in the middle of the right edge of the ternary diagram in Figure 2-21).

The approximate equilibrium distribution of the three position isomers in the temperature range of 200-300°C was estimated from the experimental results to be around 75% 5-isopropyl-3-methyl phenol, 20% thymol and 5% 4-isopropyl-3-methyl phenol as shown in Figure 2-22.

Alkyl groups are electron donating groups. Therefore, alkyl groups on a benzene ring that carries another substituent would prefer to sit on the most electron deficient or least electron enriched

position(s) of the aromatic ring. In the case of a phenolic compound, the strongly electron donating mesomeric effect of the hydroxyl group raises electron density selectively on the *ortho*- and *para*-positions, see Figure 2-4. The lowest electron density is thus on the *meta*-positions which makes these the thermodynamically preferred positions for alkyl substituents.

Consequently, the most stable and thermodynamically preferred position isomer in *m*-cresol isopropylation should be the 5-isopropyl-3-methyl phenol isomer, followed by thymol and then the more sterically hindered 4-isopropyl-3-methyl phenol and 2-isopropyl-3-methyl phenol position isomers. This is as observed in the study by Fletcher *et al*. (2002).

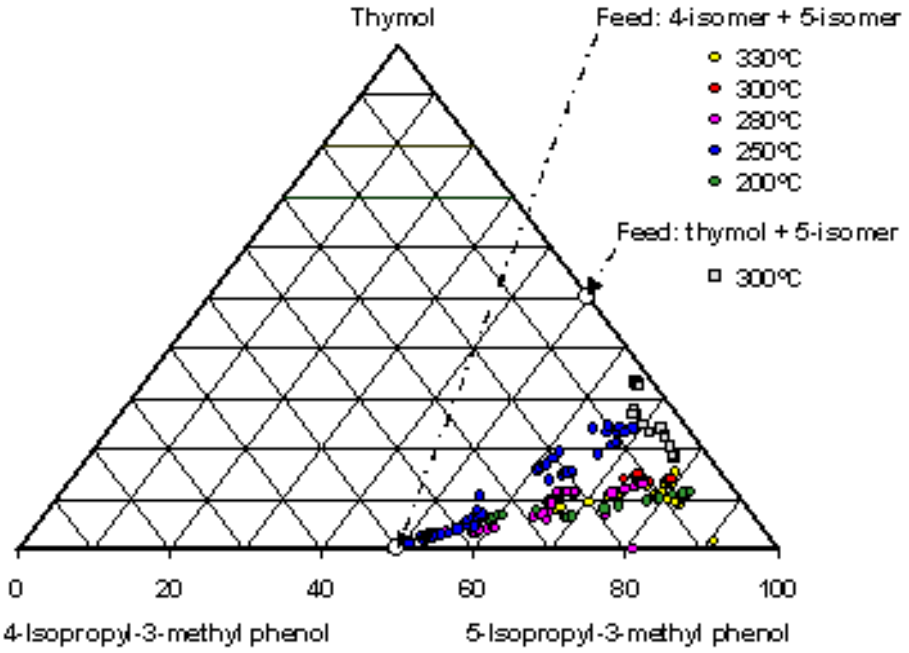

Figure 2-21: Isomerisation of thymol and its two major isomers over H-ZSM-5. Percentages are normalised to the total isopropyl-3-methyl phenol fraction except for the 2-isopropyl-3-methyl phenol isomer (Fletcher *et al*., 2002)

It should be noted that, given the starting compounds and the isomerisation mechanism, essentially by a 1,2-shift of the isopropyl group, none of the 2-isopropyl-3 methyl phenol isomer could form *via* 1,2-shift from the feed mixture applied by Fletcher *et al*. (2002) in their isomerisation study. On the other hand, given the low equilibrium percentage of 5% of the 4-isopropyl-3-methyl phenol isomer, which is to some extent sterically hindered due to the vicinity of the isopropyl group and the methyl group, it can be assumed that the equilibrium percentage of the 2-isopropyl-3-methyl phenol isomer, which is even more severely sterically hindered compared to the 4-isopropyl-3-methyl phenol isomer, is even lower and effectively insignificant.

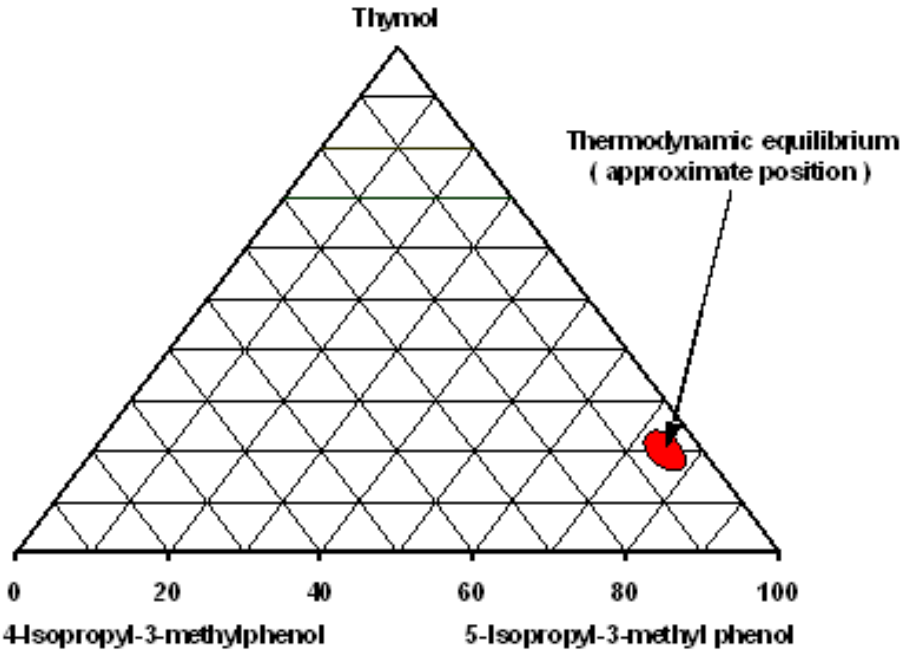

Figure 2-22: Thermodynamic equilibrium distribution of thymol and its two major isomers in the 200 - 300°C range observed from isomerisation experiments. Percentages are normalised to the total isopropyl-3-methyl phenol fraction (note that the fourth isomer, 2-isopropyl-3-methyl phenol, is not present in thermodynamic equilibrium in relevant amounts due to severe steric hindrance) (Fletcher *et al*., 2002).

2.1.6.4 Thermodynamics of iso-/n-substitution

Donating additional electrons or transferring additional negative charge onto an already electron-rich structure such as an aromatic structure does not improve its stability and is not thermodynamically favourable. Since alkyl substituents are such electron donating groups, the weakest electron donors amongst them, that is those with the least substituted α-carbon atom; therefore produce the most stable and thermodynamically favourable structures. Consequently, n-alkyl substituents on an aromatic ring are thermodynamically favoured (slightly) over iso-alkyl substituents. No respective thermodynamic data was available for n- and iso-propylated phenols. However, the above is indicated, for instance, in the Gibbs free energy of formation, ΔG_f, of cumene and of n-propyl benzene that is reported as 55.46 kcal/mol at 500 K (227°C) for the former but slightly lower, 54.5 kcal/mol, for the latter (Stull *et al.,* 1969).

2.1.6.5 Thermodynamics of O-alkylation

In the methylation of phenol with methanol, Moon (2003) deduced from literature that in the temperature range of interest i.e. 200 - 400°C, the equilibrium conversion to anisole and water

i.e. the methylation of the oxygen atom of the phenol molecule was around 90% (Daubert and Danner, 1989), and remained virtually constant.

However, in the methylation of phenol onto the ring, it was established that for temperatures between 200 and 400°C, the thermodynamic equilibrium lies far to the product (cresols and water) side with an equilibrium conversion > 99.9% to the cresols. From this it may be inferred that, thermodynamically, cresols formation (C-alkylation) is significantly favoured over anisole formation (O-alkylation). Pierantozzi and Nordquist (1986) found that at thermodynamic equilibrium at 300°C, cresols formation is favoured 10^4 times over anisole formation. This is as a result of the more stable C-C bond that has a higher energy of formation in comparison to the less stable O-C bond.

Although suitable thermodynamic data of the *m*-cresol isopropylation system are not available, it can be concluded that the system behaves similarly to the phenol methylation system i.e. it is, thermodynamically, completely on the ring isopropylation side.

2.2 Zeolite catalysts

Zeolites are crystalline, hydrated alumino-silicates with well-defined porous structures and carry surface acid sites (inside these pores) which arise as a result of the interactions of aluminium and silicon ions, present in the crystal lattice (Martens *et al.,* 1997). The aluminium and silicon occur as four-connected frameworks of AlO_4 and SiO_4 tetrahedra linked to each other by interconnecting oxygen atoms. The SiO_4 tetrahedra carry no charge whilst the AlO_4 tetrahedra carry a single negative charge. In order to balance the charge in the framework, some of the oxygen ions may carry a cation, for instance, a proton as a charge, thereby producing a Brønsted acid site which is responsible for the catalytic activity of a zeolite.

The physical and chemical properties are dependent on the aluminium content in the zeolite. Zeolites are classified according to silicon/aluminium atomic ratio into low silica (1<Si/Al<5), medium silica (5<Si/Al<10) and high silica zeolites (Si/Al>10) (Weitkamp and Puppe, 1999), which corresponds to molar SiO_2/Al_2O_3 ratios of 2 - 10, 10 - 20 and >20.

The size of the zeolite pore is determined by (Chen *et al.,* 1994):

1. The number of tetrahedral units, or alternatively oxygen atoms required to form the pore
2. The degree of puckering of the pore structure
3. The shape of the pore (circular, elliptical etc.)

The well-defined crystal structure and pore channels of a zeolite, with pore diameters comparable to the sizes of small to medium size molecules such as mono-aromatics, place physical restrictions on molecules that may enter, react inside and exit the channels and thus impose a “shape-selective” effect (see Section 2.2.2) on reactions that may occur within the channels.

The importance of zeolites to industrial catalysis can be attributed to them possessing a unique combination of the following properties (Chen *et al.*, 1994):

- High internal surface areas (>600 m2/g)
- Uniform pores with one or more discrete sizes
- The presence of ion exchangeability which produces highly dispersed catalytically active sites such as highly acidic sites when the exchangeable cations are replaced by protons
- Good thermal stability to withstand the harsh industrial environment
- The ability to sorb and concentrate hydrocarbons

2.2.1 Zeolite acidity

The acidity of zeolites arises from H^+ ions that act as counter-ions to the negatively charged AlO_4 in the zeolite framework. The acid sites may be either Brønsted or Lewis acid sites in nature. The acid site is able to either transfer a proton to the adsorbed molecule (Brønsted acidity) or accept an electron pair from the adsorbed molecule (Lewis acidity), (Nagy *et al.*, 1998).

The interaction of the oxygen atom of the hydroxyl group on the AlO_4 tetrahedron with the aluminium atom has two effects. The first effect is the weakening of the hydroxyl group's O-H bond thereby increasing the Brønsted acidity of that hydrogen atom and the second is the weakening of the Al-O bond thereby increasing the Lewis basicity of the respective oxygen atom (Martens *et al.*, 1997).

2.2.1.1 Brønsted acidity

Typically, acidity arises by the ion-exchange of the synthesized zeolite in the sodium form with ammonium followed by removal of ammonia *via* thermal treatment of the ammonium zeolite. This leaves a proton and results in the formation of a Brønsted acid site shown in Figure 2-23. Each aluminium atom in the zeolite framework is therefore responsible for the generation of a Brønsted acid site.

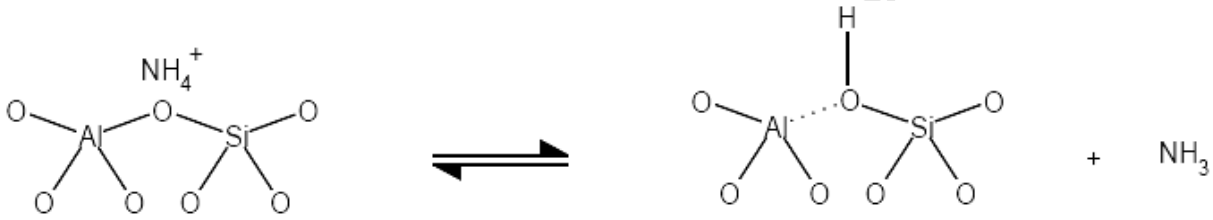

Figure 2-23: Formation of Brønsted acid sites upon thermal treatment of an Ammonium exchanged zeolite (Nagy *et al.*, 1998).

The acidity of a zeolite is directly related to the SiO_2/Al_2O_3 ratio of the zeolite framework and is consequently a function of the nature, strength and density of the acid sites on the surface (Martens and Jacobs, 1997). Thus, lower SiO_2/Al_2O_3 ratios result in an increase in the number of acid sites due to the greater occurrence of Al which is able to generate a surface hydroxyl group.

On the other hand, lower SiO_2/Al_2O_3 ratios also result in lower acid strength of the individual sites. According to Csicsery (Csicsery, 1986), the individual strength of the acid sites is inversely proportional to the concentration of framework aluminium up to about a molar SiO_2/Al_2O_3 ratio of 10. At higher ratios than 20 the acid strength of the individual sites is at its maximum and the aluminium level does not affect the acid strength of the individual sites anymore.

The increase in the individual strength of the acid sites with increasing SiO_2/Al_2O_3 ratio is observed which can be attributed to a decrease in the interactions between the individual AlO_4 tetrahedra, which decreases the force constant k of the hydroxyl groups considered as a "harmonic oscillator". It may be inferred that at low alumina contents ($SiO_2/Al_2O_3 > 20$) the AlO_4 tetrahedra in the framework are far enough from each other for no interactions to occur anymore. The maximum of proton "freedom" is then reached (Jacobs *et al*., 1978).

Indeed, according to Figure 2-24, top curve, the chemical shift (δ_H) of the H of the O-H bond in the ^{1}H MAS NMR spectra of acid zeolites of the same structure (MFI) but of varying aluminium content increases with increasing Si/Al ratio. This corresponds to a weaker O-H bond i.e. a higher acidity of the H (Freude *et al.,* 1986). However, the increase of δ_H levels out when approaching a Si/Al ratio of 10 (molar SiO_2/Al_2O_3 = 20) and is constant for higher SiO_2/Al_2O_3 ratios, indicating constant acid strength of the sites.

Correspondingly, the vibrational frequency (ν_{OH}) of the O-H group in the infrared spectrum decreases with increasing Si/Al ratio (bottom curve in Figure 2-24), also corresponding to a weaker O-H bond/higher acidity and the decrease is observed to also level out at molar SiO_2/Al_2O_3 ratios of about 20.

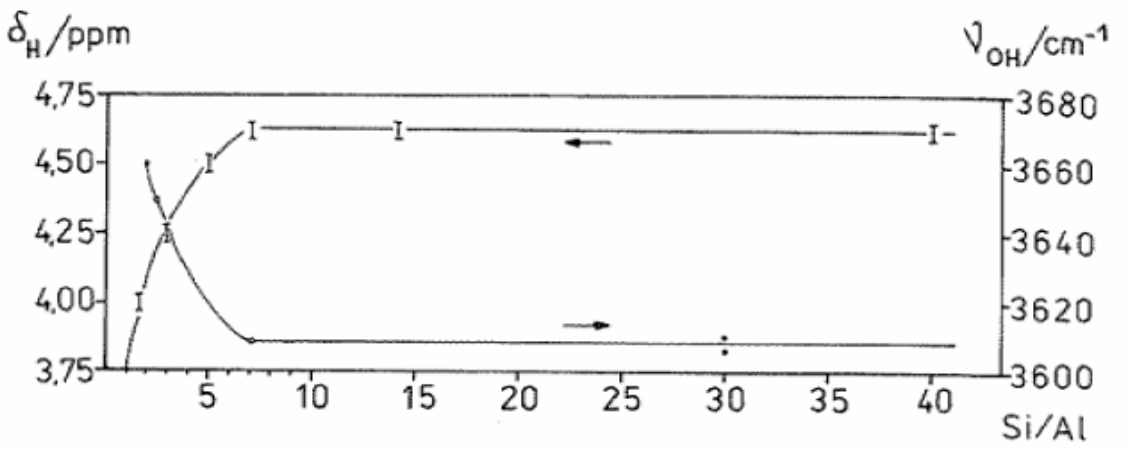

Figure 2-24: Chemical shift δ_H of hydroxyl H in the ^{1}H MAS NMR spectra of H-MFI zeolites as a function of the Si/Al atom ratio and stretching frequency ν_{OH} of the hydroxyl group in the infrared spectra (taken from Jacobs and Mortier, 1982 and Freude *et al.,* 1986)

The consequence of a steady increase in the SiO_2/Al_2O_3 ratio, i.e. a steady decrease in the number of acid sites but an initial increase of their individual strength is a maximum in total acid catalytic activity at medium SiO_2/Al_2O_3 ratios. For high SiO_2/Al_2O_3 ratios > 20, the total activity is then proportional to the concentration of acid sites as can be seen from Figure 2-25.

In the methylation of phenol an analogous phenomenon was observed with reported activities of H-ZSM-5 and H-Y decreasing with increasing SiO_2/Al_2O_3 ratio (Landau *et al*., 1997). This phenomenon, according to the authors, could be attributed to the decreasing number of acid sites, outbalancing the increase in the individual acid site strength.

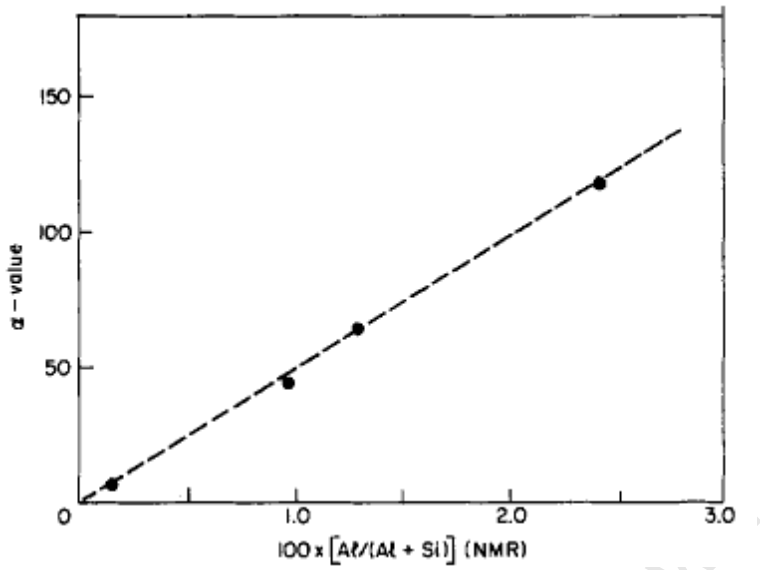

Figure 2-25: Relative hexane cracking activity (α-value) at 538°C as a function of the atomic fraction of structural aluminium measured by ^{27}Al MAS NMR for BCl_3 treated NH_4-ZSM-5 (Derouane *et al.*, 1985)

2.2.1.2 Lewis acidity

Strong heat treatment (> 500°C) of acidic zeolites causes a dehydroxylation of the Brønsted acid sites and water is split off with the concomitant formation of Lewis acid sites as shown in Figure 2-26.

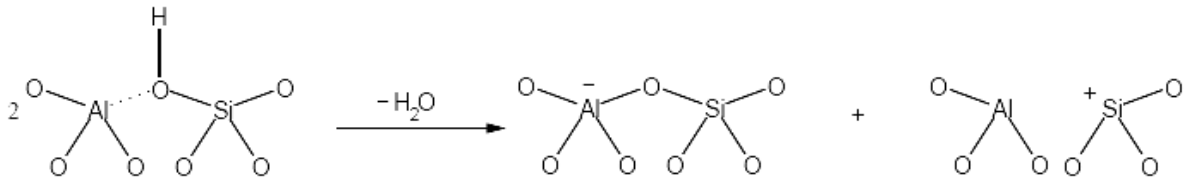

Figure 2-26: Formation of a Lewis acid site from two Brønsted acid sites (Nagy *et al.,* 1998)

In the case of framework dealumination, e.g. by high temperature steaming or acid leaching, Lewis acid sites also form, which can be attributed to extra-framework aluminium species and framework defects. Framework Lewis acid sites may act as strong electron withdrawing centres for neighbouring bridging OH groups and create Brønsted acid sites with very high strength (Weitkamp and Puppe, 1999).

2.2.1.3 External acid sites

The oxygen bridges next to the Al tetrahedra on the external surface of the zeolite crystals (or in mesopores) form Brønsted acid sites as well. The presence of external acid sites on the zeolite crystallites, since there are no spatial constraints as in micropores (see Section 2.2.2), promotes the formation of bulkier products in non-shape selective reactions although these products may form with impunity. Typically, for crystallites of about 1 µm, the external surface area will represent 1-2% of the total zeolite BET surface area (Venuto and Landis, 1968) but this is a much higher percentage with sub microcrystalline material. Hence, by external to internal surface ratio, the size of the zeolite crystallites has a direct effect on the degree of selectivity of a reaction.

A second type of hydroxyl group which is located on the external surface of the zeolite crystals or at framework defects in zeolites are silanol groups (SiOH), also known as the terminal O-H groups. Dealumination of the zeolite framework, for example by calcination, hydrothermal treatment, or treatment with strong acids is the most important reason for the formation of framework defects, silanol groups and the formation of hydroxyl groups at extra-framework species. However, silanol groups are very weak acids and irrelevant for reactions that require strong acid sites (Weitkamp and Puppe, 1999).

2.2.1.4 Effect of strength of acid sites in alkylation reactions

Studies have shown that the selective formation of *para*-cresol (in the methylation of phenol with methanol) and *para*-xylene (in the methylation of toluene with methanol) (Namba *et al*., 1984) is not only dependent on the spatial constraints of the zeolite channels (shape-selectivity, see Section 2.2.2.2) but also on the strength of the Brønsted acid sites. In the study by Namba *et al.*, the effect of the acid strength of a H-Y zeolite was investigated. It was found that the weak acid sites favoured O-alkylation and thus the formation of anisole. C-alkylation was favoured over the stronger acid sites and in the secondary alkylation of cresols to xylenols and some isomerisation of *para*-cresol to *meta*-cresol. This finding was validated by another study performed by Xu *et al.* (1997).

The trend was further confirmed in a study by Garcia *et al.* (1996) whereby the exchange of protons of the zeolite catalyst with Na or the poisoning with NH_3 led to an increased anisole/cresols ratio indicating that anisole formation requires sites with lower acid strength compared with those needed for cresol formation.

2.2.2 Shape-selective properties of zeolites

Shape selective catalysis may occur in microporous solids such as zeolites, if their pore width and the dimensions of the reactant molecules, transition states, intermediates and/or product molecules, which take part in the catalytic reaction, are similar (Weitkamp and Ernst, 1994).

The unique shape-selective properties of the MFI catalyst arise from the conjunction of four different but structurally interrelated features.

1. *With a channel/pore opening* consisting of 10-membered oxygen rings, MFI accepts, by decreasing order of preference, normal paraffins, isoparaffins, other methyl-substituted hydrocarbons, monocyclic aromatic hydrocarbons (substituted by no more than three methyl groups) and to a much smaller extent dimethyl-substituted paraffins (Chen and Garwood, 1978).
2. *The presence of channel intersections* offers a space of larger dimensions (about 9 Å) and may play a distinct role in the ordering of simple molecules and the locus of catalytic activity (Derouane and Vedrine, 1980). Valyon *et al.* (1979) have shown that two n-C_3 to n-C_5 aliphatic molecules can be adsorbed together at each intersecting element compared to only one of the isoparaffins or longer molecules such as n-hexane.
3. *The absence of cages* along the channels. Cages offer a larger available space and this may be detrimental to catalytic activity due to it being the preferential locus for the formation of carbonaceous residues in these larger cages (Rollmann, 1977).
4. *The occurrence of slightly differentiated channel networks.* Aromatics and branched paraffins were found to preferentially adsorb in the linear channels. This may lead to preferential diffusion paths and eventually prevent major counter diffusional effects (Derouane and Gabelica, 1980).

Shape-selectivity can be classified into three major groups' *viz.* reactant, product and restricted transition state shape-selectivity. Both reactant and product shape-selectivity have their origins in mass transfer control effects whilst restricted transition state shape-selectivity has its origin in intrinsic spatial and chemical effects (Csicsery, 1967).

2.2.2.1 Reactant shape-selectivity

Reactant shape-selectivity occurs when some of the reactant molecules are too bulky to enter the channels of the zeolite. These molecules are, therefore, hindered from reaching the catalytically active Brønsted acid sites located inside the pores limiting them to access only those few sites located on the external surface of the zeolite crystallites, so that they may leave without being converted (Csicsery, 1986). The resultant reactor effluent is therefore a selective conversion product of the slim reactant molecules. This phenomenon is illustrated in Figure 2-27 by the competitive cracking of n-heptane and 2-methyl hexane over a zeolite with rather

narrow pores. 2-methyl hexane is too bulky to enter the pores of this zeolite and is, therefore, hindered from reaching the catalytically active sites located inside the pores. However, n-heptane can enter the pores and so has easy access to the acid sites where it is catalytically converted.

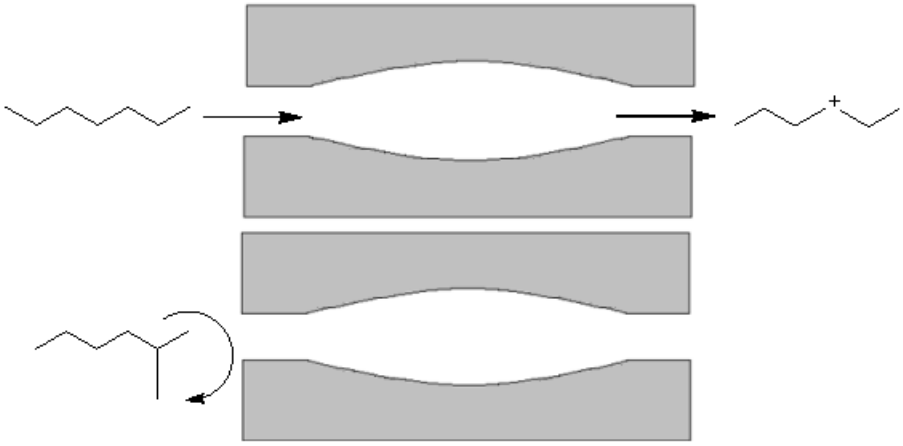

Figure 2-27: Example of reactant shape-selectivity indicating the exclusion of the bulky 2-methyl hexane whilst the slimmer n-heptane may enter and have access to the active acid sites inside the pore (redrawn from Schmidt, 2009)

2.2.2.2 Product shape-selectivity

Product shape-selectivity is essentially the reverse phenomenon of *reactant shape-selectivity.* In product shape-selectivity, the reactant molecules are small enough to enter the zeolite pores but only some of the product species (those with the shape and/or dimensions matching the diameter of the pores of the intracrystalline volume of the zeolite) may diffuse out. The bulkier product molecules which may have formed in relatively spacious intracrystalline cages or at channel intersections cannot escape the pore system of the zeolite due to physical restrictions and are either converted to less bulky molecules (e.g. by equilibration) that are able to diffuse out or eventually deactivate the catalyst by blocking the pores (Csicsery, 1986).

This phenomenon is illustrated in Figure 2-28 in the reaction of toluene with methanol in the formation of xylenes (Csicsery, 1984). The kinetic diameter of *p*-xylene is 5.85 Å and the kinetic diameter of the *meta*- and *ortho*-isomers is 6.8 Å (Szostak, 1992). Mirth *et al.* (1993) determined the diffusion coefficients of *p*-xylene : *m*-xylene : *o*-xylene in ZSM-5 to be 1000 : 1 : 10. The diffusion of the *para*-isomer out of the zeolite pore system is therefore favored due to the smaller kinetic diameter of *p*-xylene and the resulting high diffusivity. Higher *para*-selectivity is observed for large crystals where mass transfer control is more important.

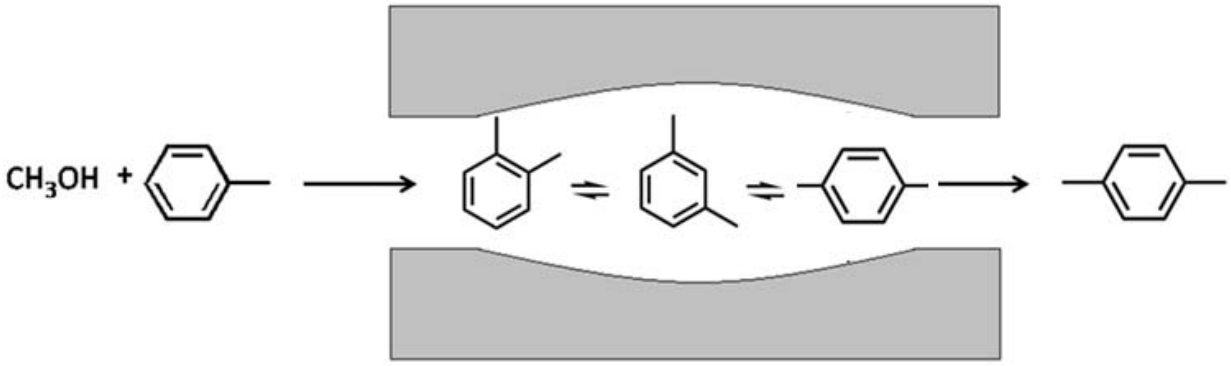

Figure 2-28: Example of product shape-selectivity in the reaction of toluene with methanol in the formation of xylenes. The restrictions placed by the narrow channels of the zeolite pore network promote isomerisation of the bulkier product molecules to the slimmer isomer which is able to easily and preferentially diffuse out of the pore network (Csicsery, 1984).

Analogously, in the case of thymol and position isomers formation by isopropylation of *m*-cresol inside a shape-selective zeolite pore system, severe transport control would restrict diffusion of the bulky isomers out of the zeolite pore network and thus favour thymol formation, see Figure 2-29.

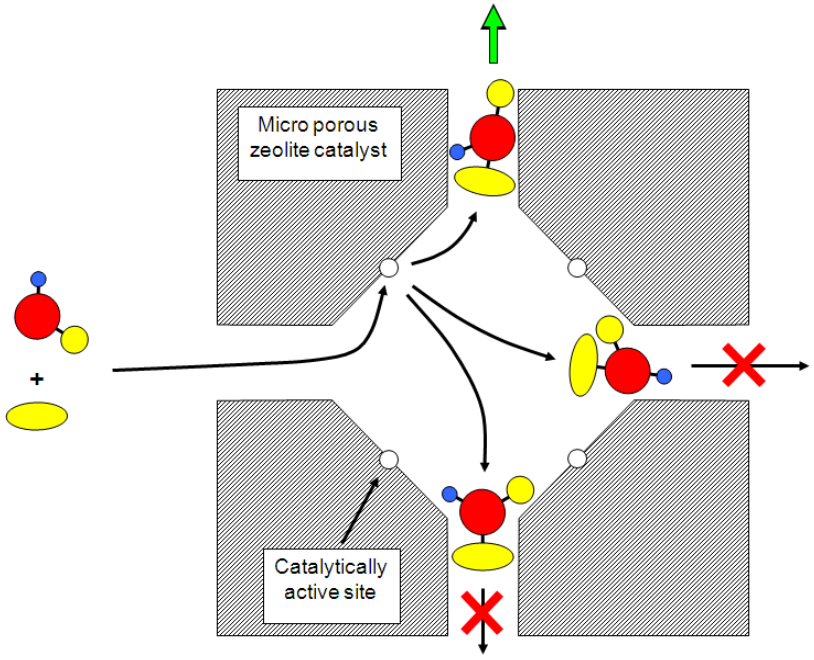

Figure 2-29: Schematic depicting product shape-selectivity in isopropylation of *m*-cresol in zeolite pores favouring the slimmest of the position isomers (Böhringer, 2010)

2.2.2.3 Restricted transition state shape-selectivity

Restricted transition state shape-selectivity occurs when certain reactions are prevented from occurring as the transition state required for them to proceed cannot form due to steric or spatial restrictions. This phenomenon is illustrated in Figure 2-30 in the acid-catalyzed transalkylation reaction of *m*-xylene in the pore system of a zeolite. In this reaction one of the alkyl groups is transferred from one molecule to another in a bimolecular reaction involving a diphenylmethane transition state. The transition state leading to the 1,2,4-trialkylbenzene isomer has enough space to form within the zeolite catalyst pores whilst the transition state leading to the 1,3,5-trialkylbenzene isomer cannot form due to the presence of spatial restrictions (Csicsery, 1967).

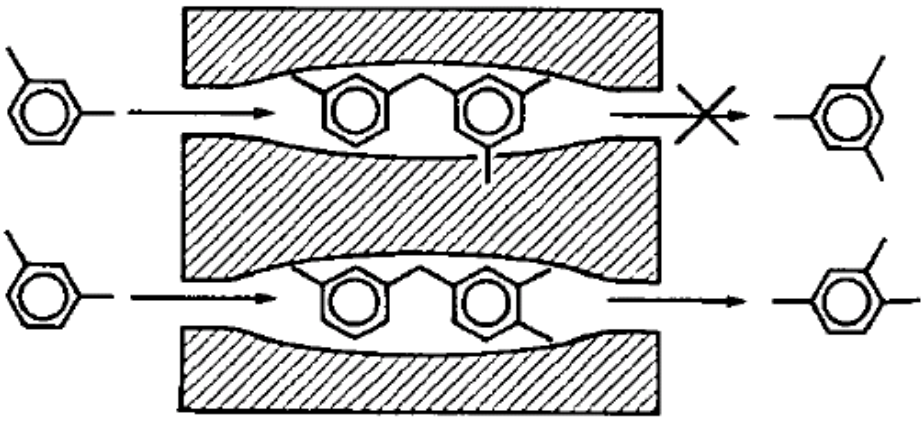

Figure 2-30: Example of restricted transition state shape-selectivity illustrating the exclusion of the bulky 1,3,5-trialkylbenzene isomer due to spatial restrictions imposed by the zeolite pore (taken from Csicsery, 1967).

Restricted transition-state shape-selectivity is perhaps one of the most important properties of the MFI zeolite, making it superior to other catalysts; in that it is sterically difficult to form the large polynuclear hydrocarbons inside the zeolite pore system, which are responsible for coking (Csicsery, 1986) and deactivation (see Section 2.2.2.4).

2.2.2.4 Shape-selective effects in carbon formation in zeolites

Coking (i.e. the lay down of carbonaceous residues) of a zeolite is a reaction intimately controlled by the pore size(s) and pore geometry of the zeolite. Coke, which is considered to be a mixture of hydrogen deficient residues, originates mainly from aromatics (Appleby *et al.,* 1962) and/or olefins (Venuto, 1977). Aromatic-ring alkylation and hydrogen-transfer reactions are highly important contributors to coke deposition.

Coking is less severe with medium pore zeolites such as the H-MFI zeolite compared to most other acid catalysts, due to the restrictive zeolite pores which impose physical restrictions, that is, the pores lack space for the polymerization of coke precursors. It is, therefore, sterically difficult to form bulky coke precursors (such as polyaromatics), so that coke formation is reduced and catalyst on-stream life is prolonged. Coke is, thus, typically deposited on the outside surface of the zeolite crystals therefore barely affecting activity (see Figure 2-31(a)). In contrast, with large-pore zeolites, most of the coke forms within the pores causing a rapid decline in catalytic activity (Csicsery, 1986 and Dejaifve *et al.*, 1981) (refer to Figure 2-31(b)).

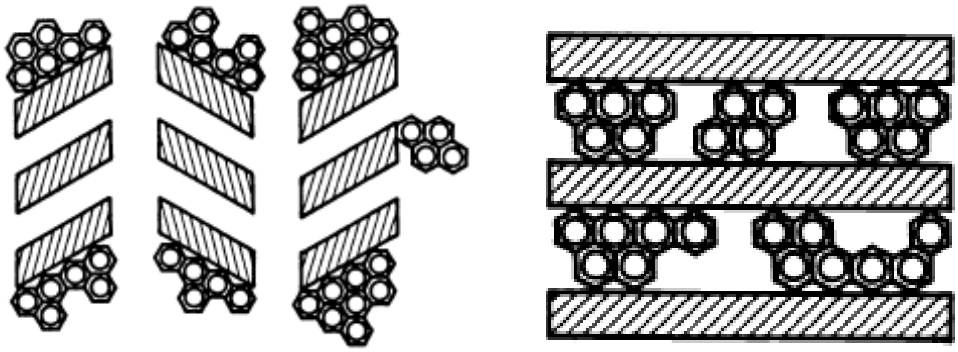

(a) (b)

Figure 2-31: (a) External deposition of carbonaceous residues on Pentasil zeolites (e.g. H-MFI), (b) Internal coke deposition in Mordenite and other large pore zeolites (Csicsery, 1986)

A distinct correlation was observed between the reactant shape-selectivity of a zeolite and its coking tendency (Rollmann and Walsh, 1979).

2.2.2.5 Influence of external acid sites on shape-selectivity

In all of the aforementioned shape-selective reaction types, the unreacted reagents as well as the product molecules can (further) react on the external surface acid sites (see Section 2.2.1.3) thereby reducing the concentration of the shape-selective product in the reactor effluent. Smaller crystallites with larger outer surfaces therefore produce a less shape-selective reactor effluent than larger crystals (Pelrine, 1978) (see Section 2.2.1.3).

Shape-selectivity may be improved by reducing the number of active sites on the external surface of the zeolite crystallites. This may be achieved by poisoning the “outside” sites with strongly adsorbing large molecules which cannot enter the pores (Derouane, 1985) or by reducing the aluminium content of the crystal surface (Rollmann and Walsh, 1979).

2.2.3 Mass transfer limitations in zeolite catalysts

The channel dimensions of a zeolite have a significant influence on the diffusivity of molecules. The widest diameter of the almost round straight channel of the MFI zeolite (5.6Å, Meier and Olson, 1978) is similar to the kinetic diameter of benzene of 5.8 Å (Breck, 1974). Thus, whilst benzene has high mobility in the MFI zeolite, diffusion of highly branched molecules such as *meta*- and *ortho*-disubstituted and polysubstituted aromatics is substantially slower (Olson *et al*., 1981) (see Table 2-3).

Table 2-3: Diffusivity of aromatics in MFI zeolite (315°C) (Olson *et al.,* 1981)

Molecule	**Size (Å)***	**Diffusivity (cm^2/s)**
Benzene	5.8	~ 10^{-7}
p-Xylene	5.8	~ 10^{-7}
o-Xylene	6.8	~ 10^{-10}
1,3,5-Trimethylbenzene	7.5	~ 10^{-12}
Pentamethylbenzene	~ 7.8	~ 10^{-12}

*The size indicated in the table does not represent the 'actual' kinetic diameter of the molecules diffusing but rather the minimum diameters measured from Courtauld molecular models for hydrocarbon molecule sizes (Olson *et al.,* 1981)

It has been demonstrated by Wu *et al.* (1986) that not only the kinetic diameter of a molecule determines whether it is adsorbed into a zeolite or not (and then may react or not), but also the shape of the molecule in relation to the shape of the zeolite pore openings. Although cyclohexane and 2,2-dimethylbutane have almost the same kinetic diameter, the former is adsorbed much faster (higher diffusion coefficient) than the latter in medium pore zeolites ZSM-5, ZSM-11 and ZSM-48. Under the adsorption conditions, the pore openings of these zeolites appeared more or less elliptical in shape matching that of the cyclohexane molecule better than that of the 2,2-dimethylbutane molecule and hence explaining the faster uptake of the former.

Upon temperature increase, the zeolite framework undergoes more intense thermal vibrations, which fractionally enlarges the effective pore size and also causes the diffusing molecules to have a higher kinetic energy thereby overcoming the repulsion forces at the pore entrance easier and allowing molecules with kinetic diameters similar to the pore diameter to pass through the pore. Therefore, in zeolite catalysed reactions, the selectivity (and reactivity) of molecules whose kinetic diameters are similar to that of the zeolite pore is dependent on the reaction temperature (Roland *et al*., 2003).

2.2.3.1 Thiele Modulus (φ) and effectiveness factor (η)

In order to fully understand the dynamics of a reaction system, all the factors influencing the activity and selectivity of the system must be investigated. In this study, mass transfer controlled zeolite intracrystalline transport is considered to play an important role. This transport is influenced by the following physicochemical characteristics of the zeolite catalyst:

- Chemical composition of framework, i.e. the SiO_2/Al_2O_3 ratio of the zeolite which determines the zeolite acidity and activity which is a function of density and strength of acid sites
- Zeolite crystal size
- Morphology of the zeolite crystals (geometry of pore system)

The extent to which diffusional transport limits the rate of conversion of a reactant can be quantified using the Thiele Modulus. The Thiele Modulus is an expression which relates the variations in a catalyst particle's (e.g. a zeolite crystal's) physicochemical characteristics to observed trends in the activity and selectivity of the system. A large value of the Thiele Modulus indicates that internal diffusion control limits the reaction or that the external surface reaction is rapid. Consequently, reactants are consumed very close to the surface of the catalyst particles and very little reactant is able to penetrate to the interior of the catalyst. Conversely, small values of the Thiele Modulus indicate that the chemical reaction rate controls and the reactants are able to penetrate easily to the interior of the catalyst (Fogler, 1999).

The Thiele Modulus for a first order reaction is given by Equation 2-1.

Equation 2-1: The Thiele Modulus for a first order reaction (Fogler, 1999)

$$\varphi \approx \varepsilon \sqrt{\frac{k \cdot r_p^{\,2}}{D_{eff}}}$$

Where:

- φ Thiele Modulus
- ε Geometric factor for particle
- k Reaction rate constant
- r_p Critical dimension (e.g. radius of spherical particle)
- D_{eff} Diffusivity of compound

The Thiele Modulus is a dimensionless expression, which relates k, the reaction rate constant, with D_{eff}, the effective diffusivity and r_p, the critical dimension of the catalyst particle. In the case of a zeolite catalyst, the effective diffusivity reflects the relationship between the pore

size, the channel geometry and the critical dimensions of the molecules. The reaction rate constant reflects the intrinsic activity of the active acid sites (a function of the aluminium content of the zeolite). The critical dimension reflects the maximum distance for the molecules to travel inside the particle (Fogler, 1999).

The Thiele Modulus determines the effectiveness factor (η) which accounts for the observed reaction rate of a component as a factor of its intrinsic rate and is defined by the ratio between observed and intrinsic rate constants. The relationship between the Thiele Modulus and the effectiveness factor therefore depends on the reaction order and geometry of the catalyst (Fogler, 1999), in this case, the morphology of the catalyst crystallites

Assuming a first order reaction and spherical catalyst particles, e.g. spherical zeolite crystallites, the effectiveness factor can be expressed as shown in Equation 2-2:

Equation 2-2: Effectiveness factor for first order reaction with catalyst of spherical geometry (Weisz and Prater, 1954)

$$\eta_A = \frac{3}{\phi_A}\left(\frac{1}{\tanh\phi_A} - \frac{1}{\phi_A}\right)$$

From this it maybe inferred that the catalytic activity of a given type of zeolite, that is, with a given effective diffusivity D_{eff} of the respective compound, is still strongly dependent on the other parameters of the Thiele Modulus i.e. the intrinsic activity of the active acid sites, the crystallite size and the shape.

As can be inferred from Figure 2-32, for low Thiele Moduli (large zeolite channels and/or low aluminium content and/or small crystallites) the effectiveness factor in the rate of formation of the product, will be close to unity, indicating that the observed rate of formation of the product is equivalent to the intrinsic rate, and hence the system is kinetically controlled. However, with an increase in the Thiele Modulus (smaller zeolite channels i.e. lower effective diffusivity D_{eff} and/or higher aluminium content and/or larger zeolite crystals) the reaction system reaches a threshold whereupon any further increase in the Thiele Modulus' value would result in a rapid decline in the effectiveness factor away from unity. The system, at this point, deviates from a region of kinetic control to that of diffusion control (Ruthven and Post, 2001)

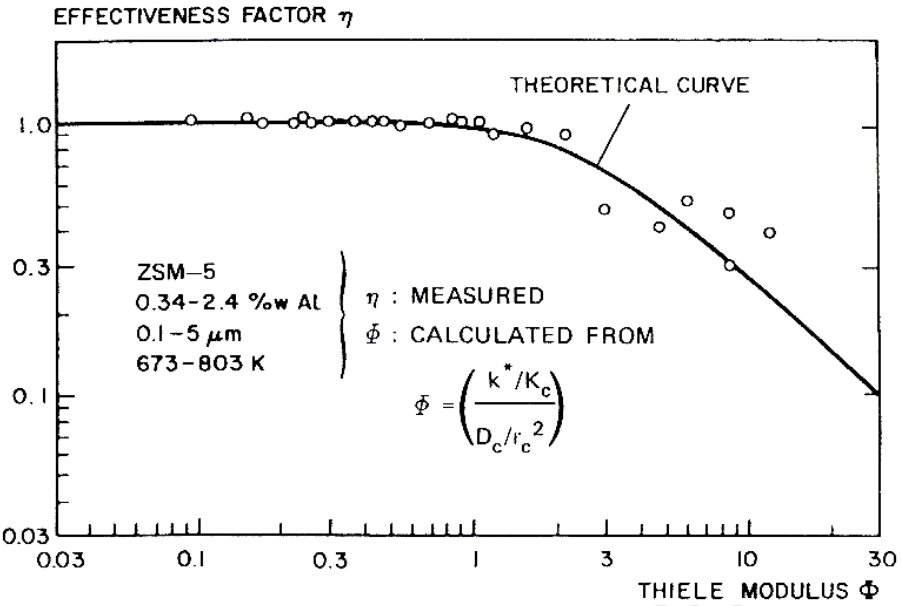

Figure 2-32: Experimental verification of the Thiele Modulus model for zeolite catalysis by conversion of 2,2-dimethyl butane over H-ZSM-5 (adapted from Ruthven and Post, 2001). k* represents the intrinsic reaction rate constant and K_c represents the equilibrium constant.

2.2.3.2 Effect of mass transfer limitations on intermediate selectivity

There exists the possibility that, if diffusion of the primary products formed out of the catalyst particles, e.g. the zeolite crystallites, is inhibited, these products can undergo further reaction before diffusing out.

With amplified mass transfer limitations, the probability of primary products B undergoing secondary reactions increases, hence resulting in a shift toward the consecutive, secondary product C as depicted in Figure 2-33 (a). In terms of reactor selectivity, the secondary reaction may appear as either a consecutive reaction or, under strong mass transfer control, as a pseudo-parallel reaction as depicted in Figure 2-33 (b):

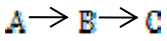

(a) Secondary reaction depicted as consecutive reaction

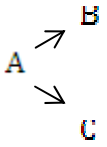

(b) Secondary reaction depicted as a pseudo-parallel reaction

Figure 2-33: Secondary reactions represented as either consecutive or pseudo-parallel (adapted from Wheeler, 1951)

In the isopropylation of *m*-cresol, thymol appears as a primary product (B) but there are a number of consecutive reactions in place, such as isomerisation or dialkylation that may consume the thymol, hence forming secondary products (C). With significant differences in the ratio of rate constants (i.e. if $k_1 > k_2$, $k_1 \approx k_2$ or if $k_1 < k_2$) in the consecutive reaction sequence:

$$A \xrightarrow{k_1} B \xrightarrow{k_2} C$$

the reaction forming the final product C will also have a Thiele Modulus significantly different to the reaction forming the intermediate product B and, consequently, a different effectiveness factor will result for the formation of each of the two products. It should be noted that the formation of product B (in terms of yield) is a function of the rate constants k_1 and k_2 whereas the formation of product C is solely a function of the rate constant k_2. The Thiele Modulus for the formation of intermediate product B is then defined by Equation 2-3.

Equation 2-3: Thiele Modulus for formation of intermediate product B in a consecutive reaction (Wheeler, 1951)

$$\Phi_B = R\left(\frac{k_2 - k_1}{D_{eff}}\right)$$

The variation of the effectiveness factor in relation to the formation of the intermediate product B as a function of the Thiele Modulus is shown in Figure 2-34.

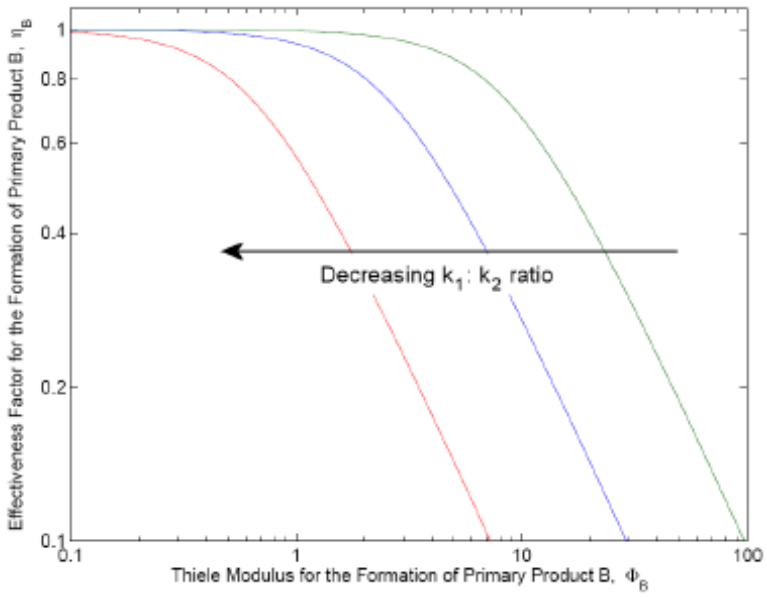

Figure 2-34: Effectiveness factor for the formation of intermediate product B with variation of the Thiele Modulus of primary product B formation in the consecutive reaction $A \xrightarrow{k_1} B \xrightarrow{k_2} C$ (Kukard, 2008, redrawn and modified from Ruthven and Post, 2001)

The yield and selectivity of the intermediate product B, when consumed *via* a consecutive or pseudo-parallel reaction in a diffusion controlled reaction system was examined extensively by Wheeler (1951) and is expressed by the relationship given in Equation 2-4.

Equation 2-4: Expression for yield of intermediate product B (Wheeler, 1951)

$$Y_B = \frac{Q}{Q-1}(1-X_A)\left[\left((1-X_A)^{-\left(1-\frac{1}{\sqrt{Q}}\right)}-1\right)\right]$$

Where:

X_A = Conversion of feed species A

Y_B = Yield of intermediate product B

Q = Ratio of primary and secondary reaction rate constants (k_1/k_2)

Figure 2-35 shows a graphical representation of this relationship.

In a mass controlled reaction system, at large Q values (i.e. $k_1 > k_2$), the yield and selectivity of the intermediate product B is high (the rate of formation of primary product B is significantly higher than its rate of consumption). Conversely, with a decline in Q values, a corresponding decline in yield of the intermediate product B is observed as a consequence of the more rapid re-adsorption and reaction of the intermediate product B inside the particle where it was formed and the formation of the secondary product C.

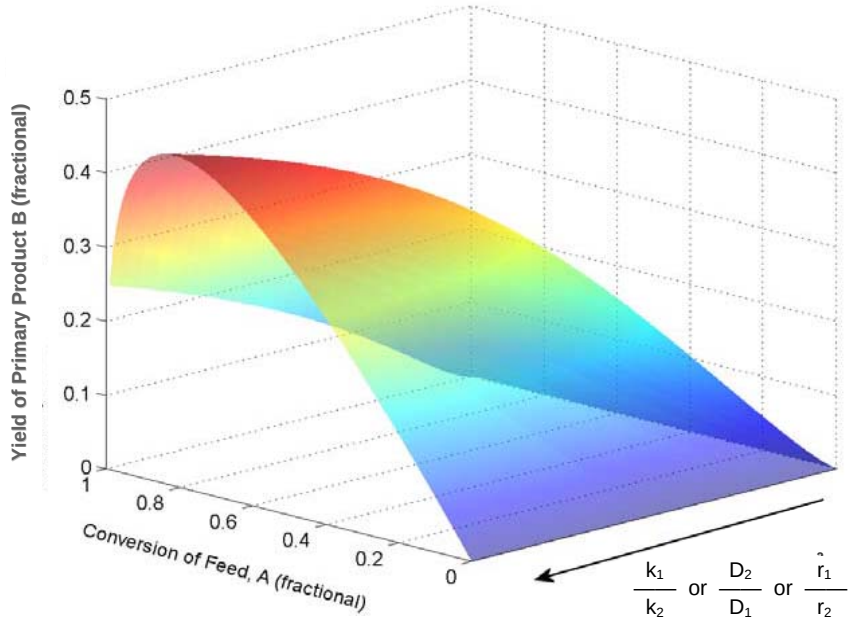

Figure 2-35: Observed yield of primary (intermediate) product B, as influenced by the ratios of reaction rate constants (k), diffusivities (D) and particle dimensions (r), (modified from Kukard, 2009)

Different diffusivities D of the reactant (D_1) and the intermediate (D_2) e.g. in zeolite pores, can also effect different Thiele Moduli for the two reactions and, consequently, different yields. At large D_2/D_1 ratios i.e. when the intermediate is diffusing out faster than the reactant is diffusing in ($D_2>D_1$), and under conditions of mass transfer control, the yield of the intermediate B is high (see Figure 2-35) and vice versa.

Similarly, an increase in particle size, i.e. $r_2>r_1$ reduces the yield and selectivity of the intermediate under mass transfer control (see Figure 2-35).

Experimental results reflect the said relationship. For instance, Möller *et al.* (1999), investigated H-ZSM-5 zeolite catalysts of different crystallite sizes but very similar SiO_2/Al_2O_3 ratios in the conversion of methanol to olefins *via* intermediate formation of dimethyl ether (DME), in a jet loop reactor (an ideally back mixed reaction system), (see Figure 2-36).

A kinetic model for the methanol-to-olefins reaction was developed to interpret the influence of crystal size on the rates of the individual reaction steps. The kinetic rate equations were derived assuming that they are elementary. Using an ideally back mixed reactor model for the specified reaction pathway, the global rate constants were obtained by fitting the experimental data. The study found that an increase in crystallite size resulted in a corresponding increase in the formation of the secondary products *viz.* olefins and a decrease in the formation of the intermediate DME.

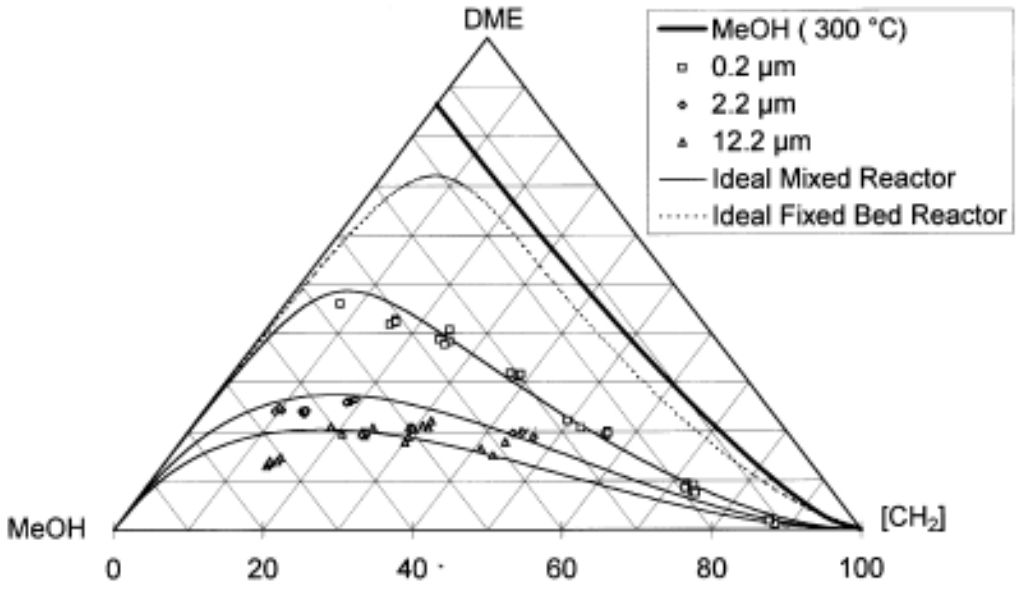

Figure 2-36: The conversion of methanol (MeOH) to hydrocarbons [CH_2] *via* dimethyl ether (DME) over H-ZSM-5 zeolite catalysts with different average crystal sizes of 0,2 µm, 2,2 µm and 12,2 µm (Möller *et al.,* 1999) but equal SiO_2/Al_2O_3 molar ratios (measured between 95 and 105) at 300°C: model prediction (curves) of experimental data with "MeOH (300°C)" depicts MeOH ⇔ DME equilibrium conversion

According to Möller *et al.,* this phenomenon can be attributed to the intrusion of increased diffusional resistances with an increase in H-ZSM-5 crystallite size, which increases the residence time of the DME intermediate inside the H-ZSM-5 crystal thereby providing further opportunity for the DME to be converted to olefins in the secondary reaction (see Figure 2-36).

2.2.4 Properties of MFI zeolite

In this study, the high silica medium-pore MFI structure type zeolite (ZSM-5), in its acid form H-MFI, was selected as the catalyst of choice due to its high catalytic activity, stability, acid strength and most importantly low coking tendency (Rollmann and Walsh, 1979) compared with other zeolites. The MFI, also ZSM-5, zeolite is a medium-pore zeolite with pores of uniform dimension.

The MFI framework (see Figure 2-37) contains two types of three-dimensionally interconnected perpendicularly intersecting channels formed by rings of 10 oxygen atoms. One is straight and has near circular openings (5.3 x 5.6 Å) whilst the other is sinusoidal and has elliptical openings (5.1 x 5.5 Å) (Meier and Olson, 1978). Diffusion in the third direction occurs by constant altering between channel systems. The channel intersections offer a space of larger dimensions (9 Å) (Derouane and Vedrine, 1980). The acid sites in the H-MFI zeolite are located at the pore intersections (Csicsery, 1986).

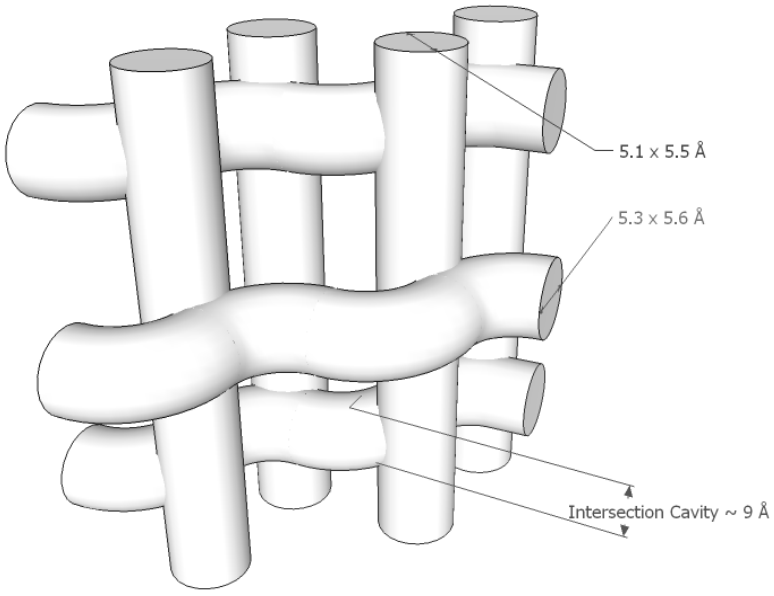

Figure 2-37: Three-dimensional representation of MFI pore structure with pore dimensions (Kukard, 2008)

2.3 Physico-chemical zeolite catalyst characterisation

The zeolite catalysts employed in this study were characterised using the following techniques:

2.3.1 Scanning Electron Microscopy (SEM)

Scanning Electron Microscopy is used to generate high resolution images of a sample by using electrons instead of light to produce the image. A beam of electrons is produced by an electron gun. The beam travels through electromagnetic fields that act as lenses, which focus the beam toward the sample. Once the beam hits the sample, electrons and X-Rays are ejected. Detectors collect these X-Rays, backscattered electrons and secondary electrons and convert them into a signal that is used to produce an image (Purdue University, 2010). In this study, SEM images were used to determine the morphology and critical dimensions of the zeolite crystallites.

2.3.2 X-Ray Fluorescence Spectroscopy (XRF)

X-Ray Fluorescence Spectroscopy is used to determine the composition of a sample by analysing the fluorescence of atoms within the sample when they interact with radiation provided by an X-Ray beam. The photons from the X-Ray tube eject electrons out of the innermost orbitals of the atoms in the sample. A more energetic electron moves from an outer orbital to the inner vacant orbital. The excess energy is given off as a photon which can be detected by an X-Ray detector. The emitted energy is equal to the difference in the energies between the two orbitals (i.e. outer and inner) and is characteristic of the element fluorescing (Innov-X Systems, 2010). The percentage of each element is derived by comparison to standards whose composition is known from analyses by other techniques. XRF spectroscopy was used in this study to determine the contents of silicon and aluminium in the zeolite samples.

2.3.3 ^{27}Aluminium Solid-State Nuclear Magnetic Resonance Spectroscopy (^{27}Al SSNMR)

XRF spectroscopy only determines the total aluminium content of a zeolite sample and does not provide information regarding the environment of the atoms quantified. ^{27}Al SSNMR is able to distinguish between zeolite framework (tetrahedral) aluminium which forms the active acid sites and extra-framework (pentahedral and octahedral) aluminium which does not contribute toward the acidity of the zeolite and exists as bulk Al_2O_3 on the surface (Causemann, 2010). ^{27}Al SSNMR was used in this study to determine the percentage of active tetrahedrally and non-active pentahedrally and octahedrally co-ordinated aluminium present in the sample.

3 Research Aims and Objectives

3.1 Aims and objectives of study

The aims and objectives of this study were firstly to investigate and understand the effect of the SiO_2/Al_2O_3 ratio on the activity, selectivity and stability of MFI zeolite catalysts in the synthesis of thymol by isopropylation of *m*-cresol with isopropanol. Secondly, to determine operating conditions suitable for the optimum performance of the most suitable catalyst with respect to this reaction.

3.2 Hypotheses

Over small crystallites of zeolite H-MFI:

1. The SiO_2/Al_2O_3 ratio has a direct effect on the catalytic performance of the zeolite with respect to **activity and conversion**.
2. The SiO_2/Al_2O_3 ratio has a direct effect on the catalytic performance of the zeolite with respect to **thymol selectivity at equal conversion**.

Over comparatively large crystallites of zeolite H-MFI:

3. An **optimum SiO_2/Al_2O_3 ratio** exists for stable catalyst performance at high activity and selectivity for thymol.
4. The SiO_2/Al_2O_3 ratio has also an indirect effect on the catalytic performance of the zeolite through its influence on **transport control** induced by the **pore system** of the MFI zeolite crystals (in combination with crystal size and shape).
5. Transport control plays a role in increasing the primary product selectivity towards the slimmest isopropyl-3-methyl phenol isomer i.e. thymol.
6. Since thymol is an **intermediate** in the reaction, that is, it may be consumed by consecutive reactions; too much transport control is not beneficial with regard to maximising thymol yield.

In general:

7. Optimum reaction conditions exist for stable catalyst performance at high activity and selectivity for thymol.

3.3 Key questions

In achieving the above-mentioned aims, the following key questions arose:

1. Does variation of the SiO_2/Al_2O_3 ratio of the MFI zeolite catalysts have an effect on the stability and activity of the catalyst?
2. Does variation of the SiO_2/Al_2O_3 ratio of the MFI zeolite catalysts have an effect on the selectivity toward thymol?
3. To what extent do commercially available, acid MFI zeolites with typically small crystallite sizes effect transport control of thymol and thymol isomers formation and a shape-selective product?
4. Is increased transport control indeed beneficial towards thymol selectivity and yield, given that thymol maybe consumed by consecutive reactions?
5. How do thymol yield and selectivity, achieved over the optimum MFI zeolite catalyst under optimum conditions, compare to the thymol selectivity achieved in the industrial synthesis over activated alumina?

4 Experimental

4.1 Experimental objectives

The principal objective of this study was to evaluate the performance of H-MFI zeolite catalysts of different SiO_2/Al_2O_3 ratios in terms of catalytic activity and selectivity toward thymol synthesised from *m*-cresol and isopropanol. Taking into account that the basis of comparison between catalysts should include the effects of the various physical properties of each catalyst, such as in the case of zeolite catalysts, the SiO_2/Al_2O_3 ratio, crystallite size and shape, experiments were to be conducted in a way so as to ensure that the physical properties of the respective zeolite catalysts were effectively the only varying parameters.

In order to make an apt comparison in terms of catalyst activity and thymol selectivity, most experiments were conducted at constant reaction pressure and constant feed ratio but at various reaction temperatures. At each reaction temperature a range of conversions had to be achieved by varying the space velocity i.e. by changing the feed flow rate. This was done in order to build a data base that allowed for a quantitative comparison between H-MFI zeolite catalysts of different SiO_2/Al_2O_3 ratios at different temperatures by observing the degree of catalytic activity and comparing the selectivity toward the desired product, thymol, at equal conversions. Finally, the pressure was varied at the optimum reaction temperature over the most suitable H-MFI zeolite catalyst.

4.2 Catalysts

This study made use of commercial MFI catalysts (Süd-Chemie) in their acidic form. The H-MFI catalysts employed, of different SiO_2/Al_2O_3 ratios, and their associated properties are provided in Table 4-1.

Table 4-1: H-MFI catalysts tested and their properties (manufacturer Süd-Chemie)

Sample code	Material form	Size	SiO_2/Al_2O_3 molar ratio*	Channel size (Å)**	Channel shape**
H-MFI-20	Powder***	---	20	5.1 x 5.5 5.3 x 5.6	Straight Sinusoidal
H-MFI-90	Extrudates****	1/16"	90		
H-MFI-400	Extrudates****	1/16"	400		

* As reported by manufacturer (general product designation/sample code)
** Baerlocher *et al.,* 2001
*** In crystallite agglomerate form
**** With alumina binder, the extrudate form assumes a binder weight of 20 mass% when calculating the mass of zeolite charged

The comparison of alumina bound, extruded catalysts with alumina-free, non-extruded catalysts in this work appeared to be possible. Alumina binders are considered to be rather

inert with respect to the performance of acid zeolite catalysts (Fletcher, 2009). Alumina binders were, nevertheless, reported to bring about some increase in zeolite acidity and activity, in particular external crystallite surface acidity and activity, and therefore possible reverse effects on product shape selectivity, but to, overall, little to moderate extent only (Truter, 2011, Lee et al., 2010, Choudhary et al., 1999 and Choudhary et al., 1997).

In this work, activities of extruded catalysts H-MFI-90 and H-MFI-400 were found to differ by about a factor 3 (see Figure 5-5), reflecting the different contents of the zeolites of tetrahedrally coordinated aluminium close enough (see Table 5-7).

4.3 Physico-chemical catalyst characterisation

In order to account for the differences in catalytic behaviour observed for the H-MFI catalysts tested, certain physical properties, namely composition and geometrical crystal properties had to be confirmed or determined. Zeolite crystals were analysed for total aluminium and silicon content (SiO_2/Al_2O_3 ratio) using XRF (X-Ray Fluorescence Spectroscopy), percentage of aluminium in the tetrahedrally co-ordinated environment zeolite crystal framework using ^{27}Al SSNMR (^{27}Al Solid-State NMR Spectroscopy) and crystal size and morphology using SEM (Scanning Electron Microscopy).

4.3.1 XRF (X-Ray Fluorescence Spectroscopy)

The percentages of the two relevant elements, Al and Si, were determined using fusion discs prepared with LiT-LiM flux in the mass proportion 57:43 (Sigma Chemicals) and LiBr as the releasing agent. All discs were analysed on a Philips PW1480 wavelength dispersive XRF spectrometer[1] with a dual target Mo/Sc X-ray tube. Measurements were made with the tube at 50kV, 50mA.

Fusion discs made up with 100% Johnson Matthey Specpure SiO_2 were used as blanks for the analysis of all elements except Si. Fusion disks made up from mixtures of Johnson Matthey Specpure Fe_2O_3 and $CaCO_3$ were used as blanks for the determination of Si. The intensity data was collected and evaluated using the Philips X40 software.

4.3.2 SEM (Scanning Electron Microscopy)

Scanning Electron Microscopy (SEM) was used to identify crystal size and shape using a Nova Nanosem 230 electron microscope[2] to take images of the H-MFI zeolite samples. The samples were mounted on aluminium stubs which were coated with a mixture of water-based glue and carbon. The H-MFI zeolite samples were then coated with a layer of Au/Pd.

[1] X-Ray Fluorescence Unit, Geology Department, University of Cape Town

[2] Electron Microscopy Unit, Physics Department, University of Cape Town

4.3.3 ^{27}Al SSNMR (^{27}Al Solid-State Nuclear Magnetic Resonance Spectroscopy)

The solid-state NMR spectra were acquired on a Varian VNMRS 500 MHz two-channel spectrometer[3] using 4 mm Zirconia rotors and a 4 mm Chemagnetics™ T3 HX MAS probe. At the field strength applied of 11.74 T the resonance frequency of ^{27}Al was 132.3 MHz. The ^{27}Al One Pulse MAS (Magic Angle Spinning) NMR spectra obtained were referenced externally to a 1 M aqueous $Al(NO_3)_3$ solution and measured at a spinning speed of 17 kHz to avoid an overlapping of the isotropic signals of the central transition with spinning sidebands. The nutation behaviour of the samples was carefully characterized. For all measurements 30° pulse lengths of the solid sample were used, typically in a range of 0.35 to 0.60 µs corresponding to a nutation frequency (1/(2*180°)) of 89 kHz of a liquid sample. Using a relaxation delay of 0.5 to 1.0 s, 50000 to 200000 FIDs were accumulated.

4.4 Feedstocks

The feedstocks and auxiliary chemicals used in this study as well as details thereof are provided in Table 4-2.

Table 4-2: Feedstocks and auxiliary chemicals used and their properties

Material/chemical	Purity (%)*	Manufacturer	Use
m-Cresol	>99	Merisol	Feedstock
Isopropanol	99.8	Merck	Feedstock
Nitrogen	>99.999	Messer Fedgas	Catalyst drying and activation, pressurisation of system
Hydrogen	>99.999	Messer Fedgas	To pressurise for leak testing
Silicon carbide (930-1035 µm)	--	Colbern	Packing in the preheater/evaporator zone of the reactor, diluent in the catalyst bed and as support packing

* Purity as reported by industrial manufacturer

Prior to experimentation, both *m*-cresol and isopropanol feed stocks were analysed by Gas Chromatography (GC) to test for impurities. Details of the GC analysis are described in Section 4.7. The isopropanol feedstock did not contain amounts of organic impurities to merit mention. The GC analyses of the *m*-cresol (see Figure 4-1 and Figure 4-2) indicated that the *m*-cresol contained trace amounts (approximately 0.83%) of impurities, predominantly *p*-cresol (see Table 4-3). The impurities in the *m*-cresol feedstock have been taken into account when calculating the total *m*-cresol conversion.

[3] Nuclear Magnetic Resonance Unit, Chemistry and Polymer Science Department, University of Stellenbosch

No further purification of the *m*-cresol with respect to gums, which may have formed in the *m*-cresol during storage, was required since reactions were conducted in the gas phase. In effect, the *m*-cresol was "distilled" upstream of the catalyst bed in the vaporiser section of the reactor packing so that gums were left in the packing, upstream of the catalyst bed.

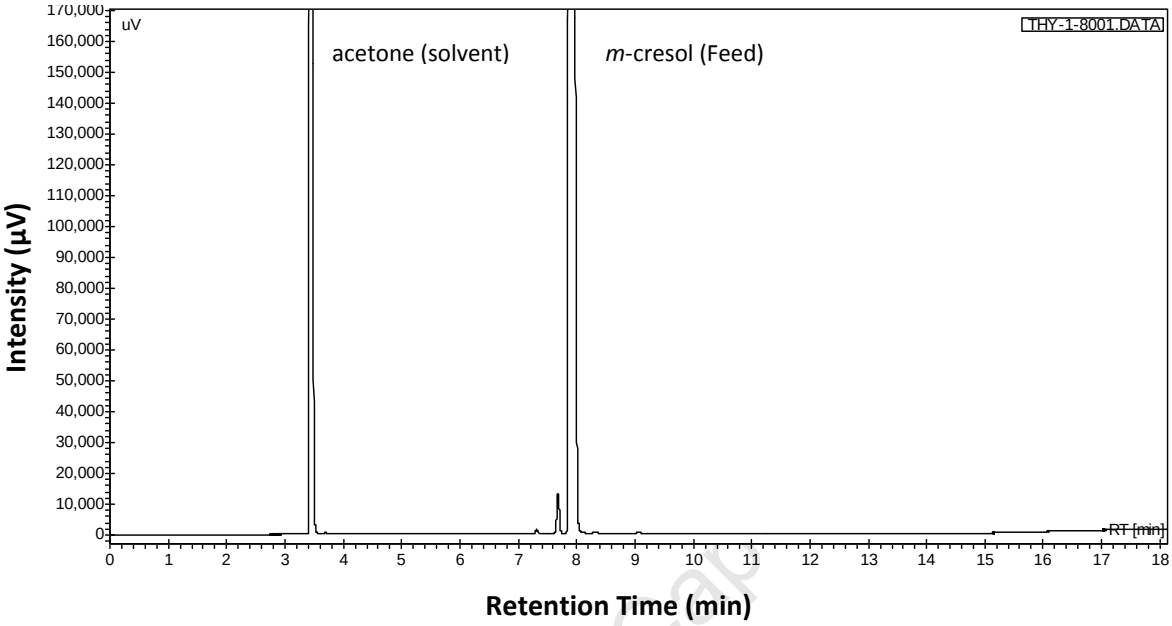

Figure 4-1: Typical gas chromatogram of the *m*-cresol feedstock

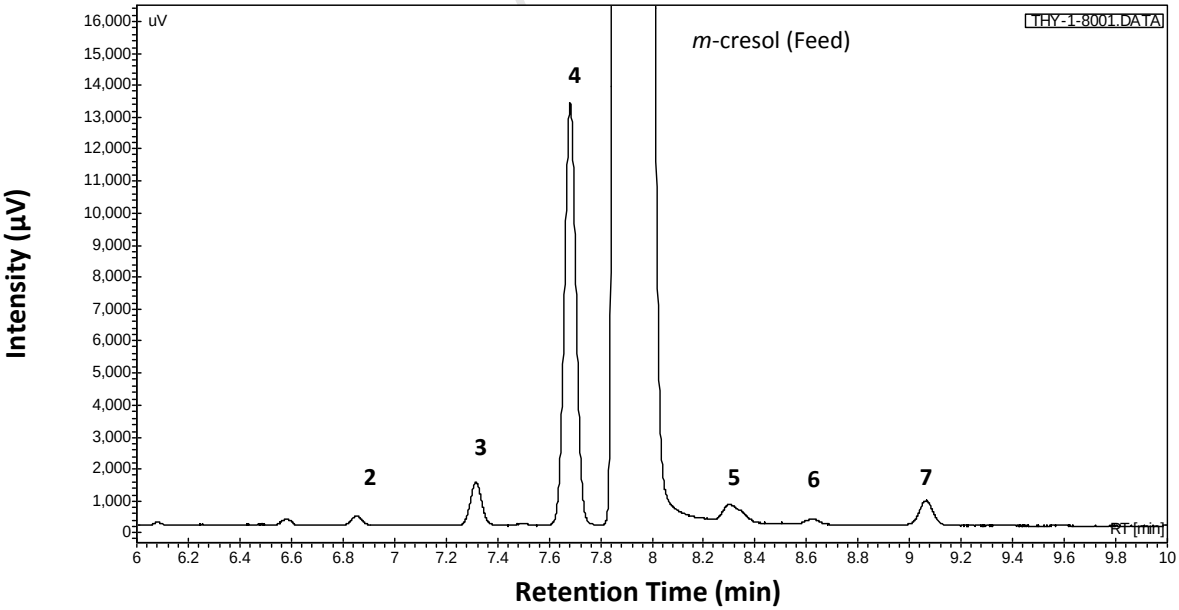

Figure 4-2: Enlargement of section of gas chromatogram around *m*-cresol showing peaks of *m*-cresol (Feed) and feed impurities *viz.* (2) phenol, (3) *o*-cresol, (4) *p*-cresol, (5) 2,4-xylenol, (6) 2,5-xylenol and (7) 2,3-xylenol

Table 4-3: Impurities in feed component *m*-cresol

Component	Molar composition (%)
m-Cresol	99.17
p-Cresol	0.64
o-Cresol	0.06
Others (mostly xylenols)	0.13
Total	100.00

4.5 Experimental apparatus

A schematic of the experimental apparatus used in this study is shown in Figure 4-3. All parts of the experimental apparatus were made from stainless steel, SS 316. Reactions were carried out in the gas phase, typically at 3 bar (abs) reaction pressure.

4.5.1 Hydrogen and nitrogen feeds

Hydrogen gas was used in the pressure testing of the system for leaks. Nitrogen gas was used to dry and activate the catalyst as well as to inertise and pressurise the system. Gaseous hydrogen and nitrogen were supplied from pressurized cylinders *via* the main house line. Filters (0.5 µm) were installed on the connections to the H_2 and N_2 house lines to remove any solid particulate matter possibly entrained in the gaseous stream. Valve V-1.1 allowed altering between H_2 and N_2. The supply pressure from the house line was reduced by pressure controllers PIC-1.1 and PIC-2.1.

Flow of the gases to the system was controlled by a Brooks thermal mass flow controller, FIC-1.1. A check valve (CV-1.1) as well as a guard catch pot were installed after the mass flow controller to protect it in the event of any liquid backflow from the reactor due to improper reactor functioning or downstream line blockages.

4.5.2 Liquid feed (*m*-cresol and isopropanol)

The 2 L glass feed pot containing a liquid mixture of *m*-cresol and isopropanol feedstock in a molar ratio of 1:1 was heated to approximately 55°C in order to ensure that the feed mixture, which was partially solid at room temperature, was in the liquid phase but still sufficiently low in temperature to prevent evaporation of the isopropanol. The liquid feed contained in the pot was stirred by a radial flow impeller attached to an overhead Heidolph stirrer drive to prevent separation of the feed components into two distinct layers (as observed with the, initially, unstirred feed) and to keep the feed homogenously mixed.

The feed pot was placed on a balance which was used to check the weight hourly space velocity (WHSV) set by the pump flow rate, that is, to check the correct functioning of the pump by recording the mass of the feed pumped after certain time periods.

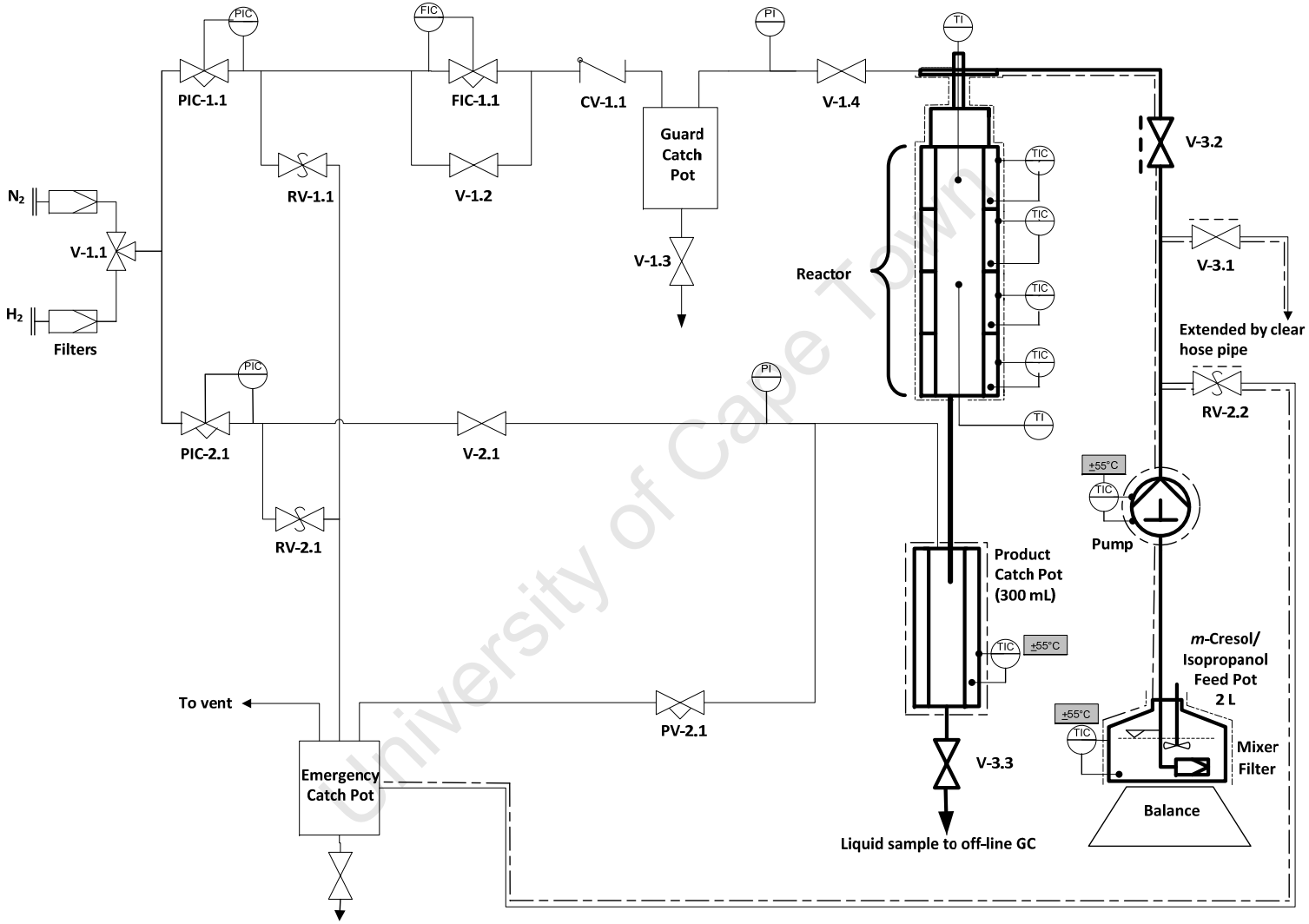

Figure 4-3: Schematic of experimental apparatus (=·=·=heated lines and devices)

An HPLC metering pump (LabAlliance, Series I; flow range 0.01–10 ml/min; adjustable in intervals of 0.01 ml/min) was used to transport the liquid feed from the feed pot to the reactor. A filter was fitted at the beginning of the suction line to prevent solid impurities entering the line which could cause damage to the pump. The pump head and the line from the feed pot to the reactor inlet were also heated to about 55°C at all times to prevent the feed from solidifying.

4.5.3 Reactor

4.5.3.1 Reactor body

The reaction was carried out in a bench scale, tubular fixed bed plug flow reactor. A schematic representation of the reactor is provided in Figure 4-4.

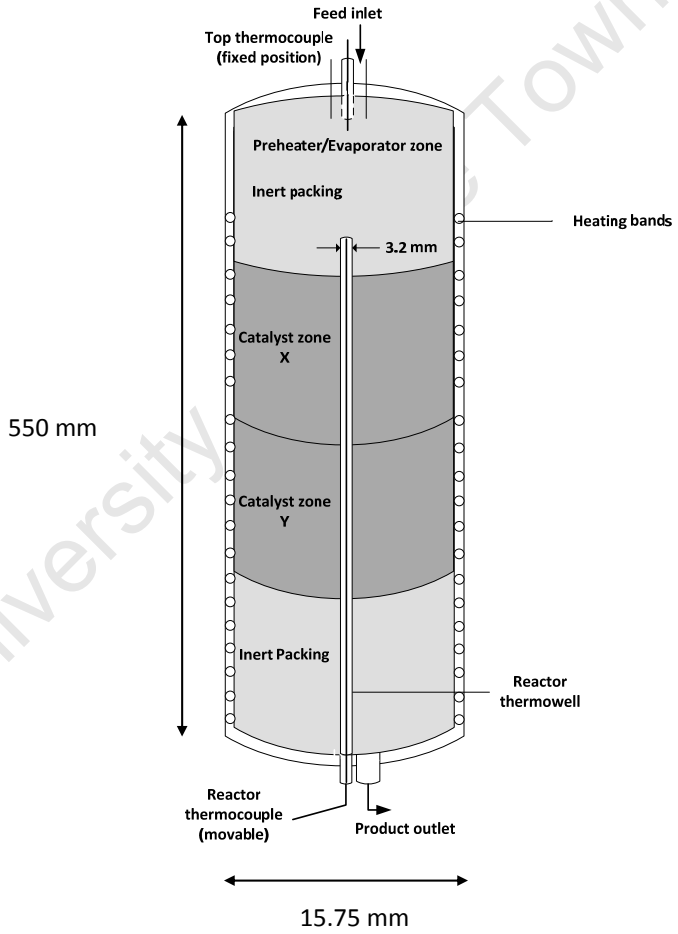

Figure 4-4: Schematic representation of reactor and reactor oven (not to scale)

The body of the reactor consisted of an approximately 550 mm stainless steel tube (¾") with an internal diameter of 15.75 mm. The reactor had a cross-sectional area of 187 mm^2. The top end was extended by a kind of flange (a Swagelok VCR fitting) connected to the gas and liquid feed lines and the top thermocouple. A central thermowell, with an external diameter of ⅛", rising

from the bottom of the reactor, was located in the reactor. The thermocouple located inside the thermowell could be moved up and down to measure the temperature profile of the reactor. During experimentation, the reaction temperature was measured with the tip of the thermocouple positioned in the middle of the catalyst bed (see Section 4.5.3.3 and Figure 4-5).

The thermocouple which was situated at the top of the reactor ranged slightly into the top packing and was used to ensure the temperature of the entering feed was below the boiling point of the feed mixture at the specified reaction pressure. The feed inlet line was also positioned slightly into the top packing. These measures were necessary to ensure constant feed flow from the feed line into the packing and constant evaporation rates which translated to a constant space velocity and composition of the feed vapour entering the catalyst bed.

4.5.3.2 Reactor catalyst packing

The schematic shown in Figure 4-4 illustrates the different zones that made up the reactor length. The catalyst bed was arranged in the isothermal zone of the reactor between layers of inert SiC packing.

The upper packing of inert material (SiC, with a particle size of 930-1035 µm) acted as a preheater and evaporator zone for the feed. A temperature gradient was established in the upper packing ranging from an inlet temperature below the boiling point of the feed mixture at the beginning up to reaction temperature at the end of the zone. The low inlet temperature was not only necessary to keep the feed in the liquid form at the inlet but also to avoid possible coking in the outlet of the feed line as experienced earlier (Böhringer, 2009).

The liquid isopropanol component of the feed mixture evaporated first in the upper SiC zone of the reactor whilst the liquid *m*-cresol feed travelled further down before it evaporated. The lowermost section of the preheater/evaporator zone served to homogenise the feed vapour mixture, to preheat it to reaction temperature and to secure a uniform flow pattern before, finally, the feed vapour mixture reached the catalyst bed of the reactor. The bottom SiC zone of the reactor was actually a spacer and allowed for the position of the catalyst bed to be adjusted according to the isothermal zone when loading. The positioning of the isothermal zone and the catalyst bed far down along the reactor allowed for the maintenance of the reactor inlet temperature to be sufficiently low.

The catalyst bed of the reactor was divided into two zones *viz.* catalyst zone X and catalyst zone Y (refer to Figure 4-4). The catalyst was mixed with inert SiC (with a particle size of 930-1035 µm) in a volume ratio of 1:8 in the top catalyst zone X and a volume ratio of 1:1 in the bottom catalyst zone Y (reasons for this are discussed below). Table 4-4 summarises the catalyst loadings for each of the zeolites tested and Appendix 10.1 gives an example of the catalyst loading calculations for the H-MFI-90 zeolite catalyst.

Table 4-4: Catalyst mass and SiC diluent loadings

Catalyst	Total catalyst (g)	Total zeolite (g)	Top catalyst zone		Bottom catalyst zone	
			Catalyst (g)	SiC (g)	Catalyst (g)	SiC (g)
H-MFI-20*	4.69	4.69	2.35	86.40	2.35	12.80
H-MFI-20	18.77	18.77**	2.35	56.80	16.42	49.70
H-MFI-90	5.87***	4.70	2.93	71.03	2.93	8.87
H-MFI-400	5.87***	4.70	2.93	71.03	2.93	8.87

* Catalyst loadings of abandoned run (see Section 4.5.5)

** Experimental run was conducted over 18.7 g of H-MFI-20, fourfold the usual mass of zeolite (see Section 4.5.5).

*** Extrudates assuming 20 wt% γ-Al_2O_3 binder (see Table 4-1)

The reasons for the dilution of the catalyst bed with SiC were as follows:

- To reduce the effective particle size within the catalyst bed in the case of the catalyst extrudates and thus to improve the hydrodynamic flow properties in the bed
- To reduce channelling along the walls of the reactor in the case of the catalyst extrudates
- To promote increased contact between the catalyst extrudates and the reactants
- To improve radial mixing and to improve radial heat exchange and heat exchange through the reactor wall by extension of the catalyst bed, given the non-thermoneutral nature of the main reactions (dehydration of isopropanol and alkylation of *m*-cresol)
- Catalyst zone X of the reactor bed was diluted to a greater extent due to the occurrence of a rapid endothermic reaction (dehydration of isopropanol to propene) in the first layers of catalyst (van der Merwe, 2012).

The catalyst bed was supported by a 120 mm layer of SiC packing in the testing of the H-MFI-90 and H-MFI-400 catalysts and adjusted less high to accommodate a longer catalyst bed in the testing of the H-MFI-20 catalyst. A plug of glass wool was located at the bottom of the reactor to prevent any of the packing from falling out.

4.5.3.3 Reactor heating zones and temperature profiles

The reactor was fitted with an 80 mm x 80 mm x 500 mm brass heating block to ensure axial levelling of the temperature profile and by this means to create a long isothermal zone.

Four heating zones ranged down the length of the heating block. These zones consisted of individually controlled heating bands which were tightly attached to the outside of the heating block. The temperature settings of the heating bands were adjusted accordingly in order to obtain an isothermal zone in the reactor wherein the catalyst bed was placed, which ranged over different heating zones. The reactor heating system was covered with an insulation jacket to minimise heat loss to the surroundings. The top end of the reactor tube extended out of the

heating block, allowing for the temperature at the inlet to be lower than the boiling temperature of the feed mixture at the given reaction pressure.

The temperature profile did change marginally when changing reaction conditions (reaction temperature and feed rate) and was therefore continually monitored and adjusted to ensure that the reactor bed remained isothermal and at constant temperature. Figure 4-5 shows examples of the temperature profiles obtained over the H-MFI-90 catalyst at a feed pump rate of 0.16 ml/min and at temperatures of 225°C and 250°C, respectively, in the middle of the catalyst bed.

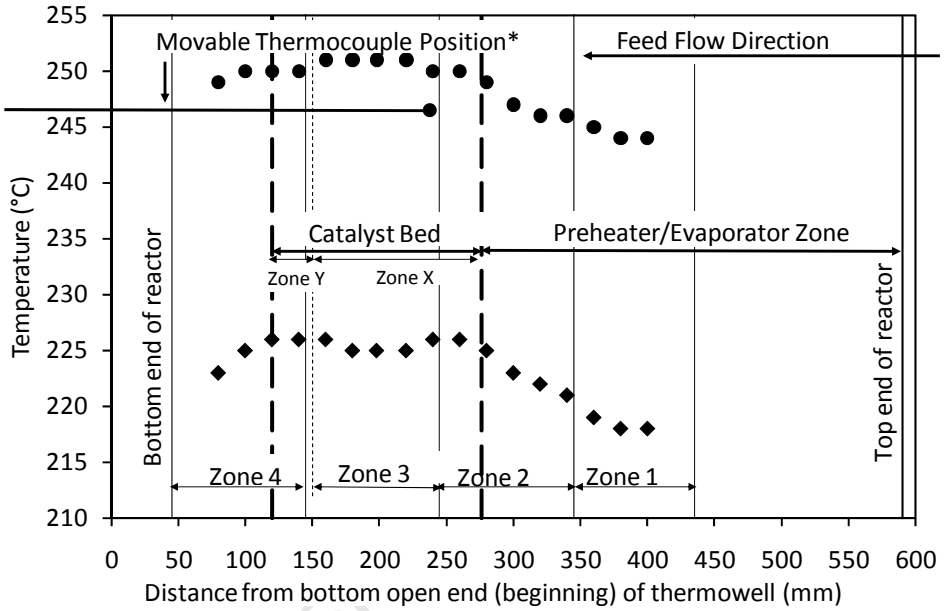

Figure 4-5: Temperature profiles of reactor packing and catalyst bed at 225°C and 250°C and WHSV = 1.03 $g_{m\text{-cresol}}/g_{cat}$.hr (feed pump rate of 0.16 ml/min) over H-MFI-90 catalyst. The entry temperature of the feed mixture was approximately 140°C. It should be noted that flow direction is from the right to the left.

As can be seen from the figure, a decrease in temperature was observed as soon as the feed came into contact with the catalyst bed. This temperature decrease could be attributed to the rapid initial dehydration reaction of the Isopropanol alkylating agent to propene, which is endothermic in nature, when reaching the catalyst bed (van der Merwe, 2012). It should be noted that this drop in temperature was much more pronounced when the first part of the catalyst bed (catalyst zone X) was less diluted (van der Merwe, 2012). It is recommended for future experimentation that further dilution of the top section of the catalyst bed will promote a further reduction in this observed endothermic effect.

4.5.3.4 Sample catch pot

Product and any unconverted reactant, after leaving the catalyst zone, continued to travel through the support packing in the reactor and upon exiting the reactor were cooled by air cooling. The heavy constituents condensed (all the phenolic compounds) before being collected in a 300 ml sample catch pot while the light products (such as the dehydration product propene) were vented *via* an outlet line from the sample catch pot to the emergency catch pot (see Figure 4-3). The pressure in the sample catch pot was maintained at the reaction pressure and the pot was heated to approximately 55°C to, on the one hand, prevent possible solidification of unconverted *m*-cresol and/or heavier products with higher melting temperatures but, on the other hand, to also prevent flashing of the lighter phenolic products which could occur at higher temperatures. The sample catch pot could be emptied *via* valve V-3.3.

4.5.3.5 Control of reaction pressure

Control of the reaction pressure within the system was achieved by feeding a pressure controlled nitrogen stream *via* PIC-2.1 and valve V-2.1 to throttle valve PV-2.1 (refer to Figure 4-3). Throttle valve PV-2.1 was opened just enough to maintain a sufficient flow of this pressure controlled nitrogen stream through PV-2.1. The outlet line of the product catch pot led into this pressurised line to the throttle valve. Thus the nitrogen pressure determined the pressure in the product catch pot and thus in the reactor. Pressure indication was achieved *via* the pressure indicator (PI) connected to the pressure control gas line.

4.5.4 Safety features of experimental apparatus

Safety features were built into the experimental apparatus *viz.* the inclusion of pressure relief valves (RV-1.1, RV-2.1 and RV-2.2), a check valve (CV-1.1) and a guard catch pot. The pressure relief valves eliminated the possibility of the system building up pressure to beyond the relief valves' set points, while the check valve CV-1.1 and guard catch pot (as mentioned before) prevented any form of backflow of either reactants or products into the gas lines to prevent the mass flow controller from being contaminated or damaged in the event of downstream line blockages or erroneous system operation.

4.5.5 Troubleshooting of experimental problems

1. At the commencement of experimentation, separation of the feed mixture into two distinct layers comprising an *m*-cresol rich and an isopropanol rich layer occurred in the feed pot that lead to an observed decline in conversion since only the *m*-cresol rich fraction from the bottom of the feed pot was being pumped and fed into the reactor. To eradicate this problem, the use of a radial flow impeller attached to an overhead Heidolph stirrer drive was implemented to ensure complete mixing of the two feed constituents.

2. Initially, in the catalytic testing of the H-MFI-20 catalyst, the usual amount of catalyst was loaded (see H-MFI-20* in Table 4-4). However, this catalyst loading correlated to low conversions that fell outside the desired range for comparison with the other H-MFI catalysts tested and for which compensation by decreasing the WHSV (by reducing the feed flow rate) was not possible due to the technical limitations of the feed pump and its lowest possible settings. Consequently a fourfold increased amount of zeolite was loaded (see H-MFI-20 in Table 4-4). However, this fourfold zeolite loading lead to significantly higher conversions. Only increasing the pump rate significantly to achieve weight hourly space velocities equal to the other experiments resulted in conversions of a comparable nature to the other H-MFI zeolites tested. It was deduced that the low conversions obtained in the initial experiment were probably due to initial incomplete activation of the catalyst.

4.6 Experimental operation

4.6.1 Catalyst loading

Catalysts tested were packed in the catalyst zones of the reactor with inert SiC diluent (in a volume ratio of ca. 1:8 in catalyst zone X and a volume ratio of ca. 1:1 in catalyst zone Y, except for catalyst H-MFI-20 in the second experiment when volume ratios were around 1:5 and 1:0.7, respectively). The total masses of the respective catalysts and diluent loaded are provided in Table 4-4.

4.6.2 Start-up procedure

1. After the preceding experimental run had been completed, the top connector of the reactor was removed to dismount and empty the reactor. Thereafter, the reactor was rinsed several times with acetone until clean and allowed to stand until completely dry.
2. A small ball of glass wool was placed around the central thermowell and pushed downwards gently until it was positioned at the base of the reactor. This served to prevent any of the SiC packing from falling out.
3. An adequate amount of SiC was filled in to allow this inert packing to be sufficiently high (120 mm from the bottom end of the reactor) to ensure that the catalyst bed was within the isothermal zone of the reactor. The bed height was determined using a glass rod.
4. The required catalyst and SiC diluent masses, as described in Table 4-4, were weighed out.
5. For each catalyst zone (i.e. catalyst zones X and Y) of the reactor, the catalyst and SiC were mixed until visually homogenous.
6. The mixture for each catalyst zone was then poured into the reactor (catalyst bed Y first, followed by catalyst bed X).

7. Sufficient SiC packing was added above the catalyst bed until the packing level was less than 1 cm below the top of the reactor to ensure that the feed inlet line ranged into the packing (see Section 4.5.3.1).
8. Finally the loaded reactor was tapped to allow the catalyst loading to settle. Additional SiC was filled in, if required.
9. A sealing washer was positioned on the top VCR fitting and the top connector of the reactor was fitted and tightened.
10. The reactor was then mounted in the experimental apparatus, together with position washers on the feed and gas lines as well as the connect line from the reactor bottom to the sample catch pot.

4.6.3 Pressure leak test

Once the reactor had been mounted, the experimental apparatus was pressurised with hydrogen by setting valve V-1.1 to H_2 supply, setting the pressure controller PIC-1.1 to a pressure of 15 bar (abs), opening the mass flow controller bypass valve V-1.2 and also opening valves V-1.4, V-2.1 and V-3.2 while valves V-1.3, V-3.1, V-3.3 and PV-2.1 were closed (refer to Figure 4-3). The pump was equipped with check valves to prevent any backflow (malfunctioning would have been detected by the appearance of bubbles leaving the filter at the beginning of the suction line in the glass feed pot).

A gas leak detector was applied to all the joints of the experimental apparatus. Where a leak was detected, the joint on the apparatus was tightened and the leak sealed. If this did not stop the leak, the respective part of the apparatus was replaced. Finally, valve V-1.4 was closed and the pressure of the apparatus was monitored *via* the pressure indicator, PI, in the pressure control gas supply line for an hour in order to detect any pressure drop in the system.

If after an hour no pressure drop was observed and consequently no leaks were present anymore, the experimental apparatus was deemed “pressure tight”. Valve V-1.1 was closed. Valves V-1.4 and valve PV-2.1, but only slightly, were opened to depressurise the system.

4.6.4 Catalyst activation

Prior to the introduction of the *m*-cresol/isopropanol feed mixture, the catalyst was dried and activated under nitrogen flow fed at atmospheric pressure by setting valve V-1.1 to N_2 supply, setting the pressure controller PIC-1.1 to 5 bar (abs), setting the mass flow controller FIC-1.1 (with valve V-1.2 closed) to a flow rate of 50 ml/min and leaving valve V-1.4 open (refer to Figure 4-3). The nitrogen gas left the apparatus *via* valve PV-2.1 which was completely opened for this purpose.

Figure 4-6 illustrates the drying and activation temperature ramp-up procedure (at atmospheric pressure). Each temperature increase was performed at a rate of 1°C/min with intermediate holding periods. During the drying phase, the catalyst was heated to 90°C, held for an hour, heated to 100°C, held for an hour, heated to 110°C and held for an hour to slowly remove the moisture.

During the activation phase (i.e. the removal of other adsorbed compounds from the catalyst), the catalyst was heated to 350°C, held for approximately 4 hours and then cooled to 225°C, where it was held since this was the start up temperature for the first experimental series carried out. The activation temperature was measured by the central thermocouple that was pushed through the thermowell and positioned in the middle of the catalyst bed (as indicated in Figure 4-6).

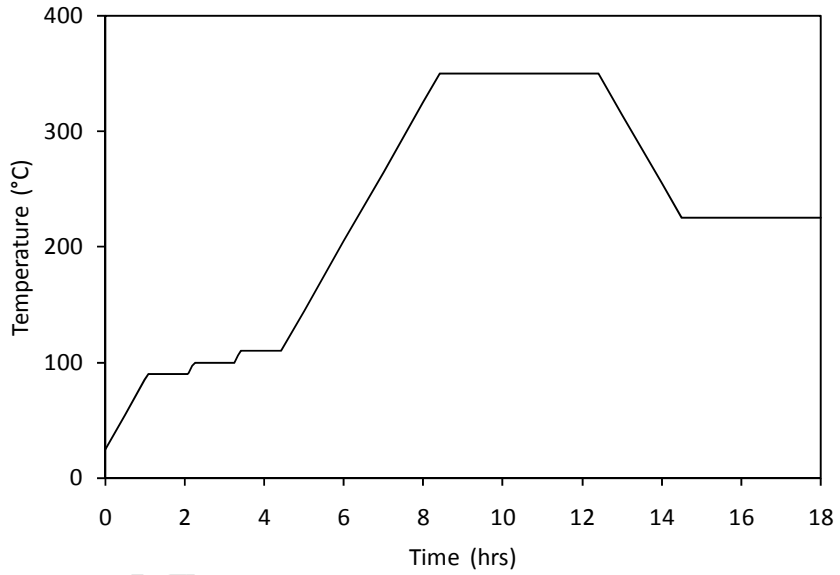

Figure 4-6: Temperature program for the catalyst drying and activation procedure

4.6.5 On-line procedure

After the drying and activation of the catalyst, catalyst testing began (refer to Figure 4-3).

1. The upstream pressure regulator PIC-1.1 was closed
2. FIC-1.1 was turned off and the reactor gas feed valve V-1.4 was closed
3. The valve in the pressure control gas supply line, V-2.1 was opened and throttle valve PV-2.1 was also kept fully open to ensure no pressure build-up in the system
4. Sufficient nitrogen was allowed to flow through the downstream pressure regulator PIC-2.1 (set to approximately 5 bar (abs))
5. The product sample catch pot was emptied of any remaining product and flushed with N_2 by temporarily opening valve V-3.3

6. The heating band for the product catch pot was switched on (the heating of the feed supply system was never switched off)
7. In order to prime the pump, valve V-3.2 to the reactor was closed and valve V-3.1 was opened
8. The pump was set to prime mode until no bubbles appeared anymore in the clear hose pipe extending from valve V-3.1, meaning that no bubbles were present in the feed line as well as no leaks in the suction line
9. The pump was turned off
10. The valves were then set to feed flow to the reactor by closing V-3.1 and opening valve V-3.2
11. The pump was then set again to prime mode until the temperature in the middle of the catalyst bed, indicated by the reactor thermocouple (see Figure 4-5) decreased significantly. This indicated that the cold liquid feed had reached, and partially filled, the catalyst bed
12. The pump was then turned off
13. The product sample catch pot was drained again *via* valve V-3.3
14. Valve PV-2.1 was partially closed (this did not cause a backflow of N_2 up the reactor since most of the reactor was filled with liquid)
15. PIC-2.1 was set to the reaction pressure of, usually, 3 bar (abs)
16. The pump was set to the required flow rate
17. The pump and stopwatch (for the recording of time-on-stream) were then switched on.

It should be noted that the catalyst bed was at reaction temperature after catalyst activation (see Section 4.6.4).

Experimentation was initiated with each catalyst at the standard or reference conditions of 225^{o}C, 3 bar (abs), WHSV = 1.03 $g_{m\text{-cresol}}/g_{cat}$.hr and a molar feed ratio (*m*-cresol: isopropanol) of 1:1. After start-up the catalyst was allowed to settle and reach quasi-steady state performance (usually within approximately 72 hours). On alteration of a reaction condition (reaction temperature or WHSV), the system required time to stabilise because of the hold-up and back mixing in the product carrying sections of the experimental apparatus with the time needed to approach steady-state and constant composition of the samples drawn being dependant on the WHSV of the system (pump rate).

At times and on completion of an experiment, the reaction conditions were changed back to the standard or reference conditions, mentioned above, in order to establish a quantitative measure of the extent of catalyst deactivation.

4.6.6 Sampling procedure

The liquid product mixture collected in the sample catch pot was transferred through valve V-3.3 (refer to Figure 4-3) into 50 or 100 ml glass sample bottles with rubber sealed screw lids at regular intervals, depending on the pump rate (WHSV).

For WHSVs lower than 1 $g_{m\text{-cresol}}/g_{cat}$.hr, samples were collected every 3-4 hours whilst at a space velocity of 1.03 $g_{m\text{-cresol}}/g_{cat}$.hr, hourly samples were collected. When drawing samples, care was taken to ensure that the reaction pressure did not drop and that the sample catch pot was completely drained of the liquid product to minimise back-mixing.

For each experiment, each of the batch-wise collected samples was analysed. At each experimental condition, a number of samples were drawn. Samples were analysed immediately, *via* offline gas chromatography, for constancy. Once constancy was confirmed, several steady-state data points were sampled at the actual operating condition. Thereafter the next change in reaction conditions was made.

4.6.7 Experimental plan

The experimental plan comprised conducting a WHSV series for each temperature in the range of 200-300°C for each of the respective catalysts (H-MFI-20, H-MFI-90 and H-MFI-400). WHSV's ranged between 0.016 and 1.03 $g_{m\text{-cresol}}/g_{cat}$.hr depending on the activities of the individual catalysts and the reaction temperatures. The goal was to obtain a series of data points in the range of 20 to 30% conversion. Thereafter, a pressure series (1.5-12 bar (abs)) was conducted over the optimal catalyst (H-MFI-400) at the optimum reaction temperature found of 275°C and WHSV varied between 0.25 and 1.03 $g_{m\text{-cresol}}/g_{cat}$.hr to obtain data points around the 20-30% conversion range.

4.6.8 Procedure for variation of reaction conditions

Operating conditions were varied as follows:

- WHSV was altered by changing the pump setting (reported WHSV data, see Chapter 5, was derived by recording the mass of the feed mixture pumped from the feed pot after each sample drawn)
- Temperature was varied by manipulating the heating zone settings so as to achieve an isothermal catalyst bed at the set temperature
- Pressure was altered by varying the pressure of the nitrogen gas (fed *via* Valve V-2.1) using pressure controller PIC-2.1 (refer to Figure 4-3).

4.6.9 Shut-down procedure

The experimental apparatus was shut-down in the following manner:

1. The feed pump was switched off and valve V-3.2 was closed
2. All temperature controllers were switched off
3. The N_2 mains (valve V-1.1) was closed and pressure controller PIC-2.1 was set to zero
4. In order to completely depressurise and vent the system of N_2 , valve PV-2.1 was fully opened

5. Nitrogen flow to the top of the reactor was introduced by setting valve V-1.1 back to N_2 supply and pressure controller PIC-1.1 to slightly elevated pressure. The reactor was flushed with a N_2 stream of about 50 ml/min by opening the mass flow controller bypass valve V-1.2 and also opening valves V-1.4 and valve V-3.3. This was done in order to remove all volatile matter present in the system
6. The reactor was then allowed to cool overnight before being dismounted and unloaded.

4.7 Feed and product analysis

4.7.1 Gas chromatography

For analysis, about 0.4 ml of each of the liquid product samples and, initially, the individual feed constituents, *m*-cresol and isopropanol, were transferred into Autosampler vials (1.5 ml) and diluted with acetone in an approximately 1:3 volume ratio to exemplify the different compound peaks. All samples were analysed *via* Gas Chromatography using the special 'positional isomers' column described in Table 4-5. The column was mounted into a Varian 3800 GC that was equipped with a Varian CP-8400 Autosampler and a Flame Ionisation Detector (FID). Table 4-6 describes the settings of the GC program.

Table 4-5: Properties of the GC column used for the analysis of the *m*-cresol alkylation product

Type	Fused silica capillary column, wall coated
Length	30 m
Internal diameter	0.25 mm
Film thickness	0.25 µm
Stationary phase	α-DEX 120*
Manufacturer	Supelco
Product number	24310

* Special 'positional isomers' stationary phase consisting of 20% permethylated α-cyclodextrin (a crown ether) in 35% diphenyl/65% dimethyl siloxane (Supelco, 2010)

Peaks of product constituents identified in the chromatograms are listed in Table 4-7. If the pure compounds were available (see Table 4-7), identification of the peaks within chromatograms entailed spiking a product sample and then matching the corresponding peak intervals, patterns and/or retention times of the reference chromatograms to the chromatograms of all the product samples in order to identify the species present. Gas chromatography mass spectroscopy (GCMS) was used to identify the other compounds present in the liquid product sample.

Table 4-6: GC settings

Injector head pressure* (psig)	3.3		
Injector temperature (°C)	300		
Carrier gas	H_2		
Carrier gas flow (ml/min)	171		
Column flow (ml/min)	0.5		
Volume injected (µL)	5		
Split ratio	340		
Column oven program	Heating rate (°C/min)	Final temperature (°C)	Holding time (min)
	Initial	50	0
	30	170	2
	0.5	174	0
	40	220	3
Total GC analysis time (min)			18.15
Detector	FID		
Detector temperature (°C)	320		

*Operated in constant pressure mode

The library of MS patterns of the GCMS comprised all of the isopropyl 2-methyl phenol and isopropyl 3-methyl phenol isomers. This allowed identifying the isomers of the isopropylated *m*-cresol molecule. However, the MS patterns of the Isopropyl 4-methyl phenol isomers were not available in the said library.

A single, small peak, peak number 8 in Table 4-7 and in the chromatograms shown in Figure 4-9 and Figure 4-13, was left unidentified by then. Since the peaks of all the isomers of isopropylated *m*-cresol have been identified (peak numbers 9, 10, 13 and 14 in Table 4 7 and Figures 4-9 and 4-13), it was concluded, based on the MS fragmentation patterns, the low percentage of the respective compound in the product mixture and the elution of the respective compound from the GC column right before thymol, that this peak represented most likely the 2-isopropylation product of *p*-cresol, the major impurity in the *m*-cresol feed (refer to Table 4-3 and Table 5-3), since the isopropyl group would most likely have attached to one of the two reactive (identical) *ortho*-positions.

Table 4-7: Peak identification of gas chromatograms (note that compound designations do not strictly follow IUPAC rules in that the larger alkyl substituent is assigned the lowest position number but leave the methyl group in the 3-position of the *m*-cresol reactant)

Peak number	Compound eluted	Identification
1	Isopropyl-3-tolyl ether	GCMS
2	Phenol	Pure compound
3	*o*-Cresol	Pure compound
4	*p*-Cresol	Pure compound
Feed	*m*-Cresol	Pure compound
5	2,4-Xylenol	Pure compound
6	2,5-Xylenol	Pure compound
7	2,3-Xylenol	Pure compound
8	2-Isopropyl- 4-methyl phenol*	GCMS*
9	2-Isopropyl-3-methyl phenol	GCMS
10	6-Isopropyl-3-methyl phenol (thymol)	Pure compound
11	6-n-Propyl-3-methyl phenol	GCMS
12	2,6-Diisopropyl-3-methyl phenol	GCMS
13	5-Isopropyl-3-methyl phenol	Pure compound
14	4-Isopropyl-3-methyl phenol	Pure compound
15	4,6-Diisopropyl-3-methyl phenol	GCMS
16	5,6-Diisopropyl-3-methyl phenol	GCMS
17	Heavies	GCMS

* Not present in GCMS fragmentation pattern library. See text for details of peak identification.

Figure 4-7 shows the chromatogram of a typical product sample obtained at low *m*-cresol conversion of 16%. Figure 4-8 to Figure 4-10 show enlarged sections of this chromatogram.

Figure **4-11** shows the gas chromatogram of a typical sample obtained at a higher conversion of 50%. Figure 4-12 to Figure 4-14 show enlarged sections of this chromatogram.
...Figure 4-12 show the feed impurity and product peaks that appear before and around the *m*-cresol feed peak. Figure 4-13 and Figure **4-14** illustrate the product peaks that appear at higher retention times.

Figure 4 7 also shows that there was no isopropanol present in the product anymore already at low conversion.

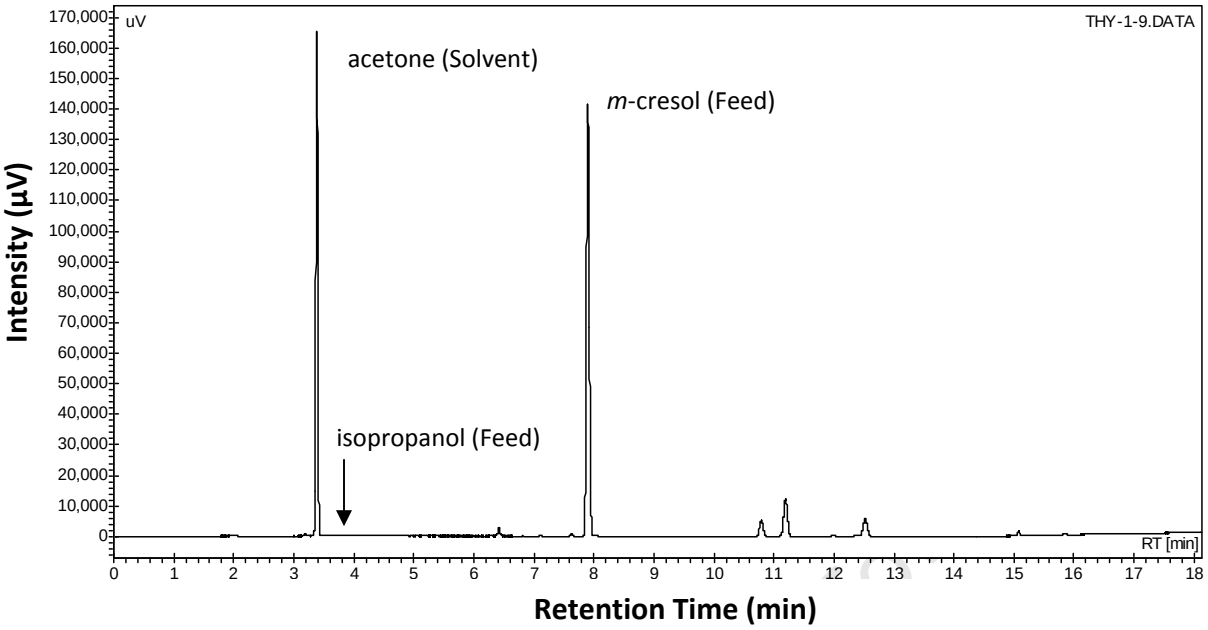

Figure 4-7: Typical gas chromatogram of the liquid *m*-cresol isopropylation product mixture obtained over H-MFI-90 at standard conditions (T = 225°C, WHSV = 1.03 $g_{m\text{-}cresol}/g_{cat}$.hr, P = 3 bar (abs) and a low *m*-cresol conversion of 16%.

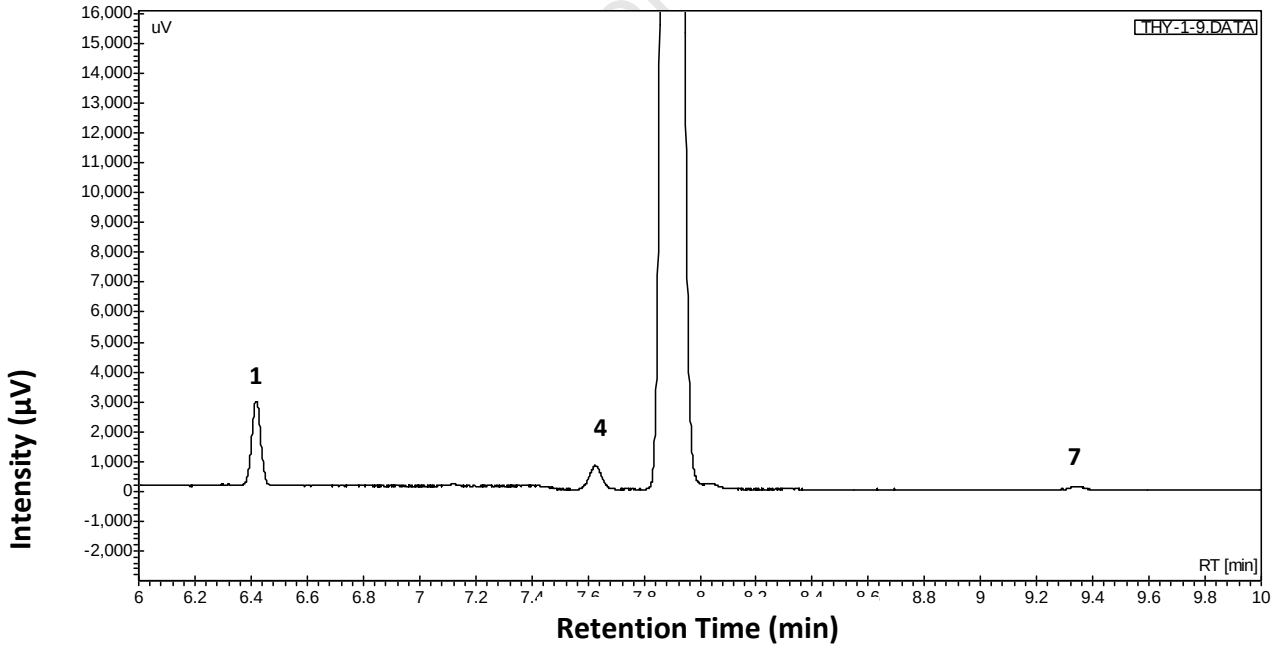

Figure 4-8: Enlargement of early section of gas chromatogram Figure 4-7 showing peaks of (1) isopropyl-3-tolyl ether, (4) *p*-cresol (Feed impurity*), *m*-cresol (Feed) and (7) 2,3-xylenol (Feed impurity*). *Refer to Figure 4-2.

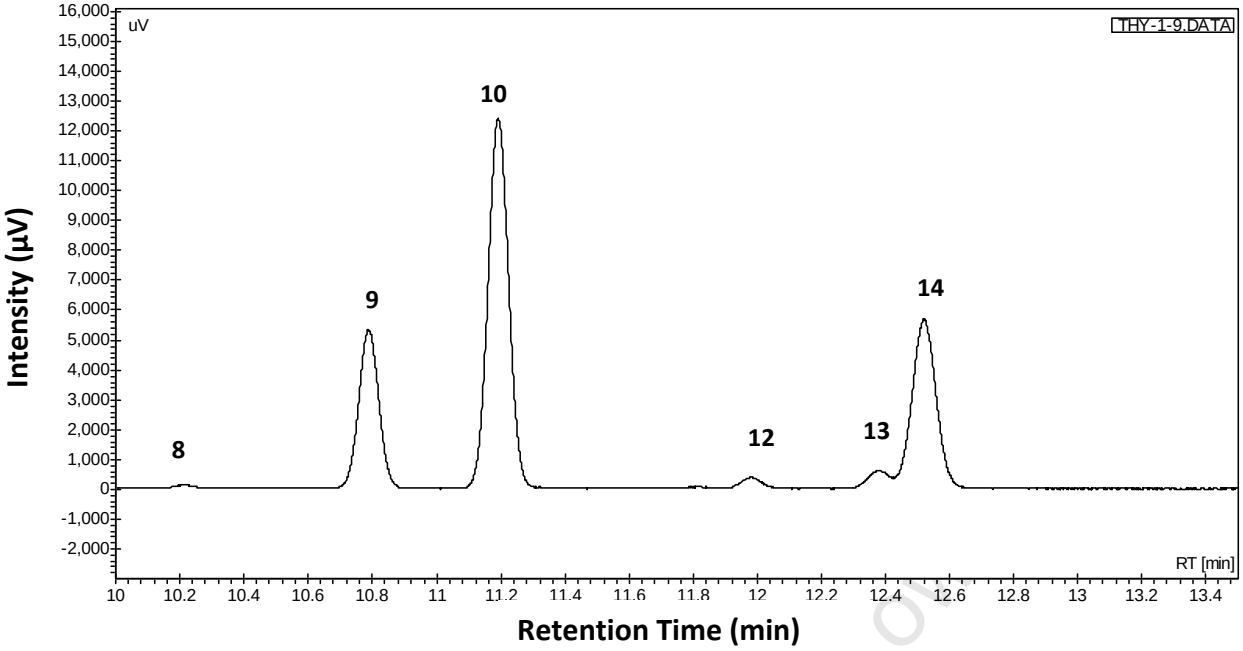

Figure 4-9: Enlargement of middle section of gas chromatogram Figure 4-7 showing peaks of (8) 2-isopropyl-4-methyl phenol, (9) 2-isopropyl-3-methyl phenol, (10) 6-isopropyl-3-methyl phenol (thymol), (12) 2,6-diisopropyl-3-methyl phenol, (13) 5-isopropyl-3-methyl phenol and (14) 4-isopropyl-3-methyl phenol

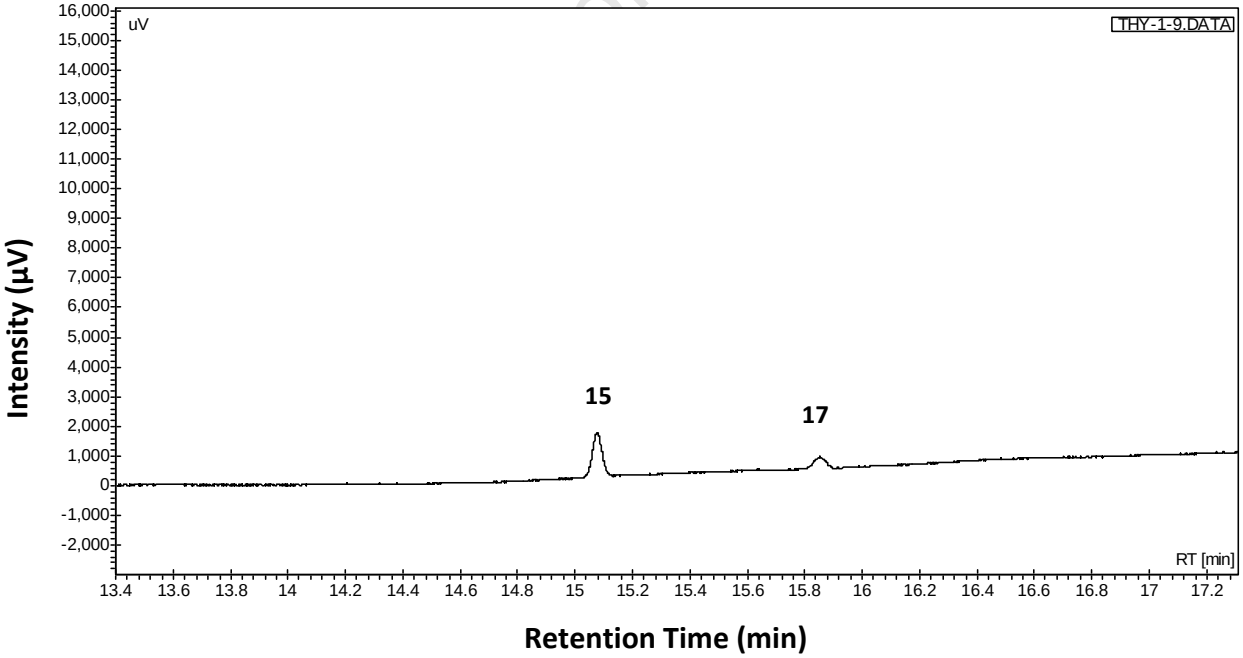

Figure 4-10: Enlargement of last section of gas chromatogram Figure 4-7 showing peaks of (15) 4,6-diisopropyl-3-methyl phenol and (17) heavies

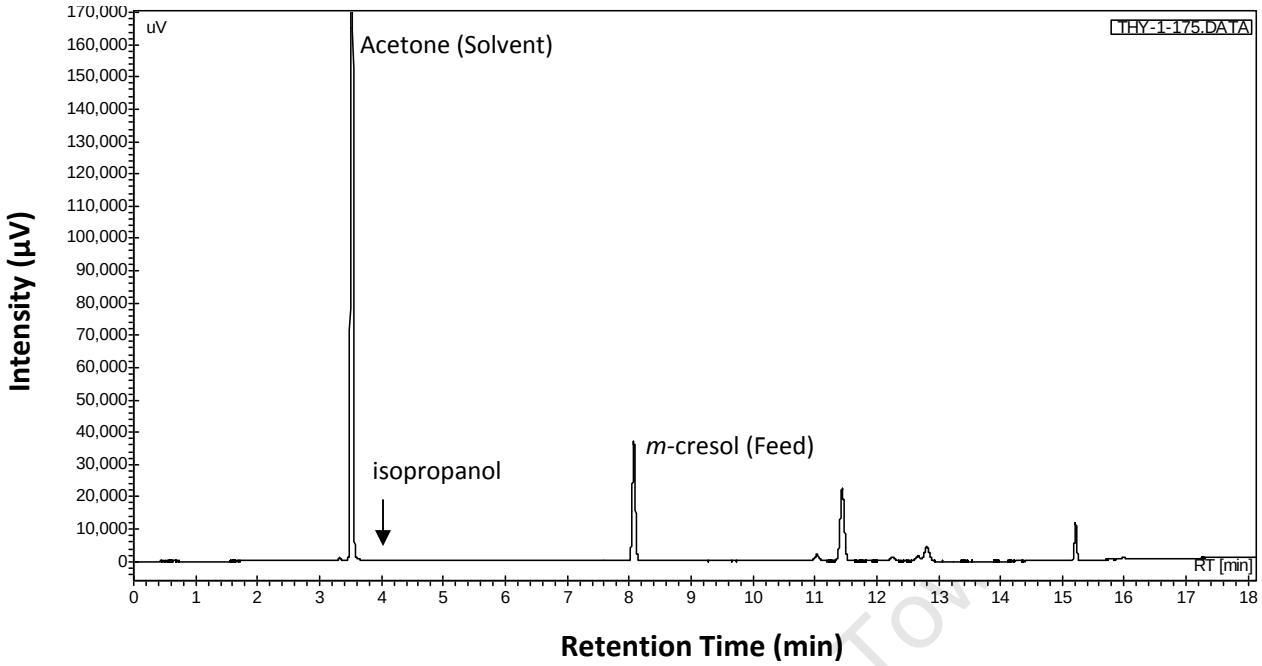

Figure 4-11: Typical gas chromatogram of the liquid *m*-cresol isopropylation product mixture obtained over H-MFI-90 at low space velocity and T = 250°C, WHSV = 0.125 $g_{m\text{-cresol}}/g_{cat}$.hr, P = 3 bar (abs) and a high *m*-cresol conversion of 50%

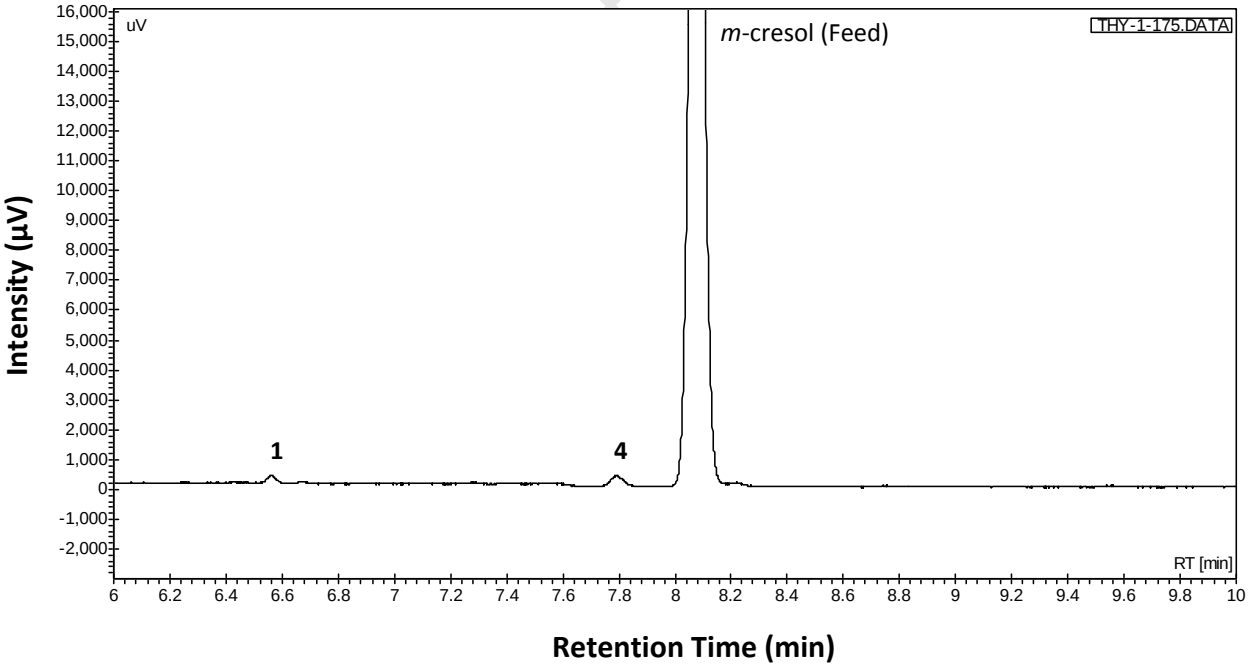

Figure 4-12: Enlargement of early section of gas chromatogram Figure 4-11 showing peaks of (1) isopropyl-3-tolyl ether, (4) *p*-cresol (Feed impurity*), *m*-cresol (Feed). *Refer to Figure 4-2.

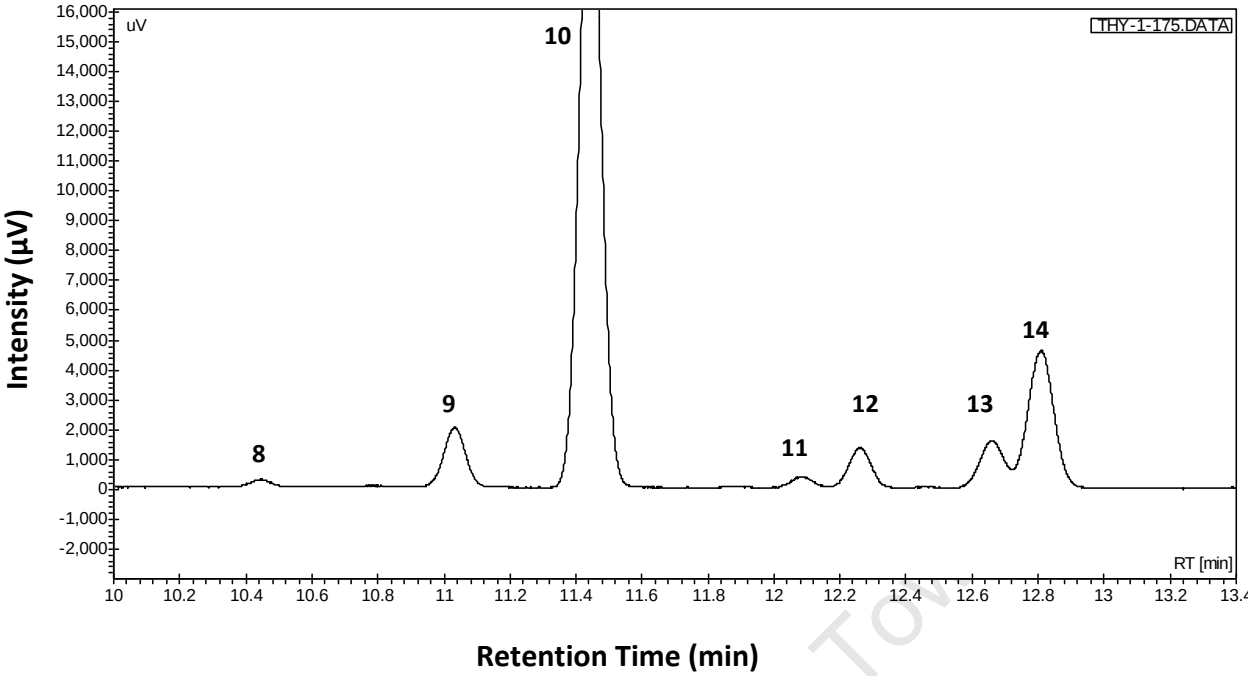

Figure 4-13: Enlargement of middle section of gas chromatogram Figure 4-11 showing peaks of (8) 2-isopropyl-4-methyl phenol, (9) 2-isopropyl-3-methyl phenol, (10) 6-isopropyl-3-methyl phenol (thymol), (11) 6-n-propyl-3-methyl phenol, (12) 2,6-diisopropyl-3-methyl phenol, (13) 5-isopropyl-3-methyl phenol and (14) 4-isopropyl-3-methyl phenol

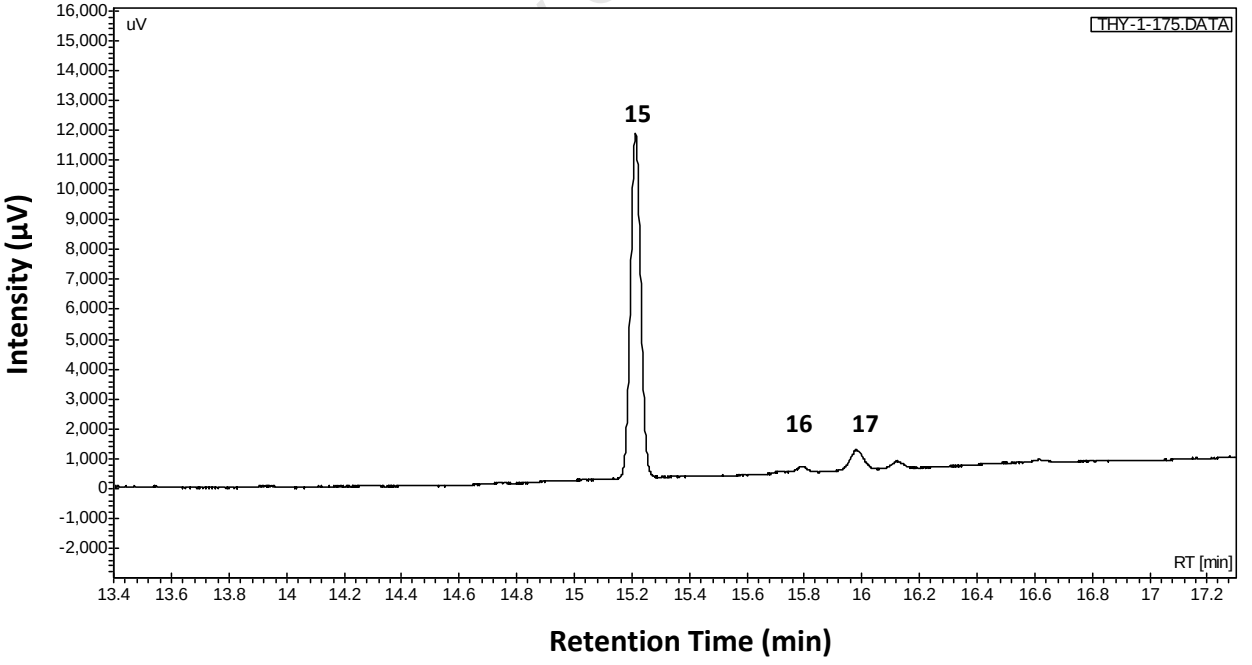

Figure 4-14: Enlargement of last section of gas chromatogram Figure 4-11 showing peaks of (15) 4,6-diisopropyl-3-methyl phenol, (16) 5,6-diisopropyl-3-methyl phenol and (17) heavies

4.7.2 Corrected Peak Areas (PAC) and response factors

The GC Flame Ionisation Detector (FID) signal integrator calculates the peak areas which are a measure of both the amount of carbon associated with a peak and the intensity of the carbon atom ionisation of the particular species. The intensity of the FID signal is strongly dependent on the nature of the atoms bonded to a carbon atom, as each carbon atom will give a different intensity due to the type of contiguous atoms. Carbon-carbon and carbon-hydrogen bonded carbon atoms give equal FID signals whilst carbon singly bonded to oxygen has been experimentally determined to only have a response of 55% (Callanan van Steen, 1999).

Thus for a specific oxygen containing species, the intensity of the FID signal needs to be corrected for the carbon atoms bound to the oxygen atom(s). The average response factor (f_i) takes this into account by considering the different response in the FID signal of a carbon atom bound or not to the oxygen atom(s) of the particular component. The measured peak area of an oxygen compound must therefore be multiplied by the respective response factor to obtain the "corrected peak area" which represents the actual amount of carbon associated with that specific peak.

4.7.3 Calculation of response factors

The response factor for a particular species was calculated by dividing the total number of carbon atoms of the compound by the relative response of these carbon atoms. The response factor for, as an example, *m*-cresol is calculated in Equation 4-1.

Equation 4-1: Calculation for response factor (f) of *m*-cresol

$$f_{m-cresol} = \frac{\text{Number of carbon atoms in } m\text{-Cresol}}{\text{Response of carbon atoms in } m\text{-Cresol}} = \frac{7}{6 \times 1 + 1 \times 0.55} = \frac{7}{6.55}$$

4.7.4 Corrected Peak Areas and Molar Corrected Peak Areas (PAC and PAM)

To obtain the corrected peak area of a compound i (PAC_i), the peak area PA_i, as obtained from the gas chromatogram, was multiplied by the response factor for the particular species. Maintaining the example of *m*-cresol, the corrected peak area ($PAC_{m\text{-cresol}}$) is calculated from the measured peak area ($PA_{m\text{-cresol}}$) as shown in Equation 4-2.

Equation 4-2: Calculation for corrected peak area (PAC) of *m*-cresol

$$PAC_{m-cresol} = PA_{m-cresol} \times f_{m-cresol} = PA_{m-cresol} \times \frac{7}{6.55}$$

For a Phenolic compound ring balance, the corrected peak areas (PAC_i) were converted to mol proportional values (PAM_i). The PAM_i is calculated by dividing the corrected peak area by the number of carbon atoms in the specific molecule. This calculation is shown in Equation 4-3.

Equation 4-3: Conversion of Corrected Peak Area (PAC) of *m*-cresol to mol proportional basis, the Molar corrected Peak Area (PAM)

$$PAM_{m-cresol} = \frac{PAC_{m-cresol}}{\text{Number of atoms in } m-\text{Cresol}} = \frac{PA_{m-cresol}}{7} \times \frac{7}{6.55} = \frac{PA_{m-cresol}}{6.55}$$

For the product compounds, calculations are analogous. For instance, the molar corrected peak area for thymol is as follows:

Equation 4-4: Calculation for Molar corrected Peak Area (PAM) of thymol

$$PAM_{Thymol} = \frac{PA_{Thymol}}{\text{Number of Carbon atoms in Thymol}} = \frac{PA_{Thymol}}{9 \times 1 + 1 \times 0.55} = \frac{PA_{Thymol}}{9.55}$$

It should be noted that in the case of the ether (isopropyl-3-tolyl ether) formed, two carbon atoms are bonded to the oxygen atom, so that the molar corrected peak area for the ether is as follows:

Equation 4-5: Calculation for the Molar corrected Peak Area (PAM) of isopropyl-3-tolyl ether

$$PAM_{IP-3-Tolyl\ Ether} = \frac{PA_{IP-3-Tolyl\ Ether}}{\text{Number of Carbon atoms in Isopropyl}-3-\text{Tolyl Ether}}$$

$$= \frac{PA_{IP-3-Tolyl\ Ether}}{8 \times 1 + 2 \times 0.55} = \frac{PA_{IP-3-Tolyl\ Ether}}{9.1}$$

4.7.5 Conversion and product yield and selectivity calculations

In order to evaluate the performance of the catalysts, conversions, yields and selectivities at the various operating conditions needed to be determined. All the calculations assume that all the feed phenolic material that had entered the rector also exited the reactor as phenolic compounds and were detected by the FID. This assumption is made on the following basis (Böhringer, 2010):

- The catalyst displays long term stability with no significant loss of material to coke formation
- Only traces, if at all, of ring fragmentation products are observed in the product
- The general experience in the group by similar reactions such as isomerisation of phenolic compounds confirms the assumption

4.7.5.1 Molar yield

Molar yield of a specific product was calculated by dividing its mol proportional corrected peak area (PAM_i) by the sum of the mol proportional corrected peak areas (ΣPAM_i) of all the phenolic components present in the reactor effluent system, i.e. the remaining phenolic reactant and all of the phenolic products. Equation 4-6 illustrates this calculation.

Equation 4-6: Calculation of thymol molar yield

$$Y_{Thymol} = \frac{PAM_{Thymol}}{\sum_i^n PAM_i}$$

4.7.5.2 Conversion

Conversion of *m*-cresol was calculated using the mol proportional corrected peak area of the remaining *m*-cresol ($PAM_{m\text{-cresol}}$) and the sum of the mol proportional corrected peak areas of the phenolic products. Equation 4-7 illustrates this calculation.

Equation 4-7: Calculation of *m*-cresol conversion

$$X_{m-Cresol} = 1 - \frac{PAM_{m-Cresol}}{\sum_i^n PAM_i}$$

4.7.5.3 Selectivity

The molar selectivity of a specific product was calculated by dividing its mol proportional corrected peak area (PAM_i) by the sum of the mol proportional corrected peak areas of all phenolic products. Equation 4-8 illustrates this calculation.

Equation 4-8: Calculation of molar selectivity of thymol

$$S_{Thymol} = \frac{PAM_{Thymol}}{(\sum_i^n PAM_i) - PAM_{m-Cresol}}$$

5 Results

5.1 Experimental programme

The key objectives of this study were to evaluate the overall activity of each catalyst tested as well as the associated selectivity toward the desired formation of Thymol in the alkylation of *m*-cresol with isopropanol. It was therefore necessary to evaluate each catalyst under a range of temperatures and space velocities with this range yielding combined conversion and selectivity data. The data obtained was then to be projected as necessary to allow for the selectivities of all the catalysts tested to be compared at the same total conversion.

Experiments conducted as well as the associated operating conditions are listed in Table 5-1.

Table 5-1: Experimental programme carried out in the alkylation of *m*-cresol with isopropanol feed ratio (molar) = 1 : 1 (amounts of catalysts loaded see Table 4-4)

Experiment	Catalyst	Temperature (°C)	WHSV ($g_{m\text{-cresol}}/g_{cat}$.hr)	Pressure (bar (abs))
1	H-MFI-90	200 - 300*	0.0625 - 1.03**	3
2	H-MFI-400	200 - 300*	0.0625 - 1.03**	3
3	H-MFI-20	200 - 300*	0.0625 - 1.03**	3
		200 , 225	0.016	3
4	H-MFI-400***	275	0.25	1.5-12****

* Incremental temperature increase by 25°C

** Incremental WHSV increase by factor 2

*** Fresh load of catalyst. Identical loading as in Experiment 2

**** Incremental pressure increase by factor 2

Based on previous experimental work (van der Merwe, 2012), appropriate standard or reference conditions as shown in Table 5-2 were determined. All experiments in this study were initiated at these standard conditions and operating conditions were varied around the standard conditions as shown in Table 5-1.

Table 5-2: Reaction standard or reference conditions

Parameter	Standard or reference condition
Temperature (°C)	225
Pressure (bar (abs))	3
WHSV ($g_{m\text{-cresol}}/g_{cat}$.hr)	1.03
m-Cresol: isopropanol feed ratio (molar)	1 : 1

5.2 Blank run

A blank run was performed in order to evaluate the extent of reaction that occurs when no catalyst is present i.e. the reaction of the feed mixture with either the reactor wall or the SiC packing. The blank experiment was conducted over a bed of SiC packing at the comparatively high temperature of 275°C, 3 bar (abs) and a feed flow rate corresponding to the comparatively low WHSV of 0.25 $g_{m\text{-cresol}}/g_{cat}$.hr that is under much more severe conditions than the standard or reference conditions.

From Table 5-3 it can be seen that an overall conversion of *m*-cresol of 0.87% was achieved in the blank run taking into consideration the impurities present in the *m*-cresol feed on analysis.

Table 5-3: Molar product composition from blank run

Component	**Molar composition (mol %)**	
	***m*-Cresol feed**	**Blank run**
m-Cresol	99.17	98.30
p-Cresol	0.64	0.64
o-Cresol	0.06	0.06
Isopropyl-3-tolyl ether	------	0.17
Thymol and Position Isomers	------	0.70
Others*	0.13	0.13
Total	100.00	100.00

*2,4-xylenol and 2,3-xylenol

5.3 Isopropanol dehydration

No isopropanol was found in any of the product samples as can be seen from the chromatograms shown in Chapter 4 (Figure 4-7 and Figure 4-11). As discussed in Section 2.1.3.2.1, the isopropanol alkylating agent undergoes rapid dehydration to propene as soon as the feed comes into contact with the catalyst bed as evidenced in the temperature decline shown in Figure 4-5. Thermodynamics of the isopropanol dehydration reaction for the reaction conditions tested indicate that isopropanol dehydration goes almost to completion (see Section 2.1.6.1).

5.4 Catalyst stability

5.4.1 Stabilisation of reactor operation

Due to the holdup of the experimental apparatus and back-mixing (in particular in the lines downstream of the reactor, where the reactor effluent had been converted to liquid, and in the product catch pot) the response on varying reaction conditions was delayed and extended.

Therefore, after a change of reaction conditions, all samples collected during the transition state prior to attainment of quasi-steady state again were disregarded in the comparison of catalyst activity and selectivity toward thymol and only analyses of samples attained during steady-state were used. On alteration of experimental conditions at least five samples attained at steady-state were collected before changing the reaction conditions again. Each data point in Figure 5-5 and subsequent figures therefore represents the average composition of at least five samples collected during the periods of quasi-steady state activity. The denotation of space velocity given in $g_{m\text{-cresol}}/g_{cat}$.hr in Figure 5-5 and subsequent figures actually denotes the mass of catalyst that is in zeolite form.

Error bars indicated on each data point reflect the standard deviation of the average data point. In fact, most of the error bars are not visible, since they lie behind the symbols in the graphs.

5.4.2 Initial catalyst deactivation

Due to significant initial catalyst deactivation, all experimental runs were started at the standard or reference condition (T = 225°C, P = 3 bar (abs), WHSV = 1.03 $g_{m\text{-cresol}}/g_{cat}$.hr) and run for 50-85 hours on stream to allow the catalysts to reach quasi-steady state. A graphical representation of the *m*-cresol conversion versus time-on-stream data obtained for the zeolite catalysts tested at the beginning of each run is presented in Figure 5-1.

Figure 5-1 shows that the conversion declined by 70-80% over the initial 30-70 hours for each of the catalysts before reaching the quasi-steady state. In the case of the H-MFI-20 catalyst, the conversion declined from 45 percentage points to 12 percentage points in the first 30 hours on stream. The H-MFI-90 catalyst also showed a considerable drop in conversion from 55 percentage points in the initial hours on stream to 16 percentage points after 72 hours. The H-MFI-400 catalyst displayed the most substantial loss in activity, but also required the most time for this, with a decline in conversion from 52 percentage points to approximately 10 percentage points after 85 hours on stream.

It should be noted that the initial increase in conversion (0-5 hours on stream) is not an induction period but an artificial effect that simply reflects the holdup and back-mixing in the experimental apparatus and the priming with the feed (see Sections 4.6.2 and 5.4.1).

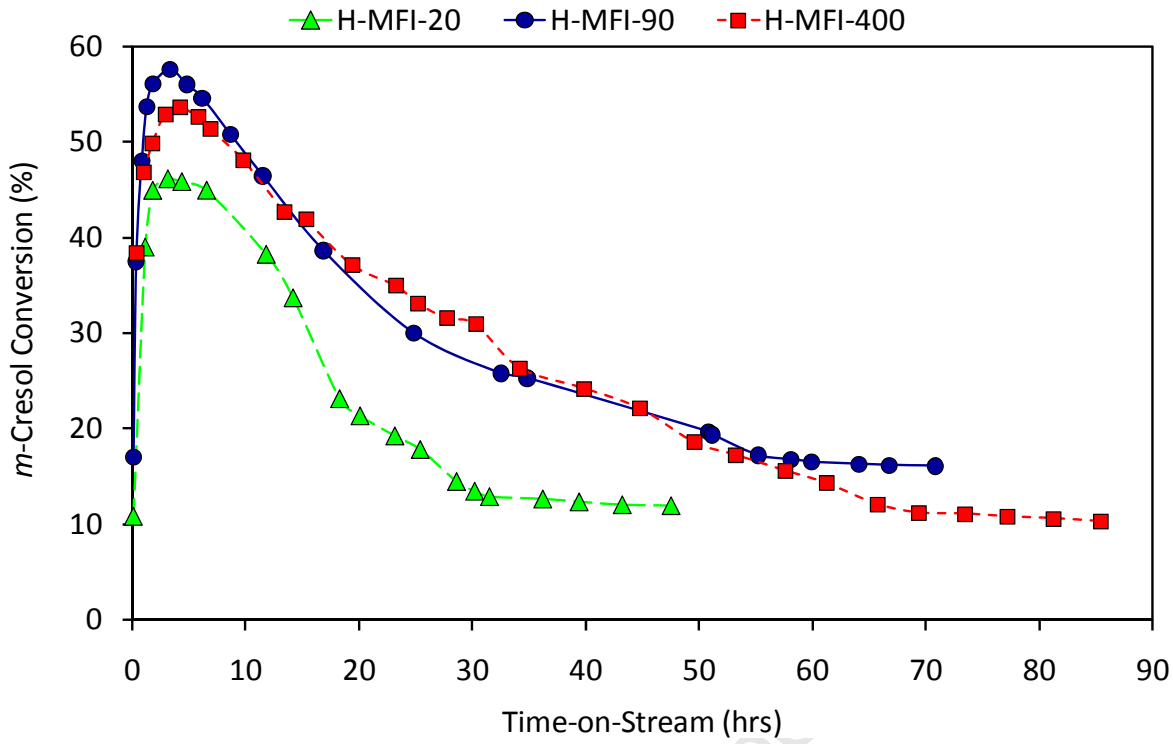

Figure 5-1: Catalyst deactivation during the first 50-85 hours of reaction over the catalysts tested (at the standard condition of T = 225°C, P = 3 bar (abs), WHSV = 1.03 $g_{m\text{-cresol}}/g_{cat}$.hr)

5.4.3 Long term catalyst deactivation

Experimental runs over each of the catalysts tested were conducted over long time periods and it was therefore necessary to also quantify the extent of catalyst deactivation in quasi-steady state. This was achieved by reverting back to the standard condition repeatedly after several reaction parameter changes and finally at the end of each experiment. It appears that catalyst activities, after the significant initial decline, were rather stable over pronounced times on stream. Graphical representations depicting the extent of long term catalyst stability for each of the catalysts tested are presented in Figure 5-2.

It was found that all catalysts still lost some activity on time-on-stream, though rather little. The magnitude of activity loss was strongly dependent on, trivially, the catalyst type and reaction conditions. The most rapid decline at quasi-steady state operation was observed at the high reaction temperature of 300°C applied between 1600 and 1800 hours on stream with the H-MFI-90 catalyst.

From Figure 5-2 it can be clearly seen that the H-MFI-90 catalyst showed the most substantial deactivation with time-on-stream, declining from 16 percentage points initially to approximately 6.5 percentage points at the end of the experimental run. Both the H-MFI-20 and H-MFI-400 catalysts displayed less of a decline in activity with time-on-stream. It should, however, be noted that the H-MFI-90 catalyst was worked the most vigorously (see above).

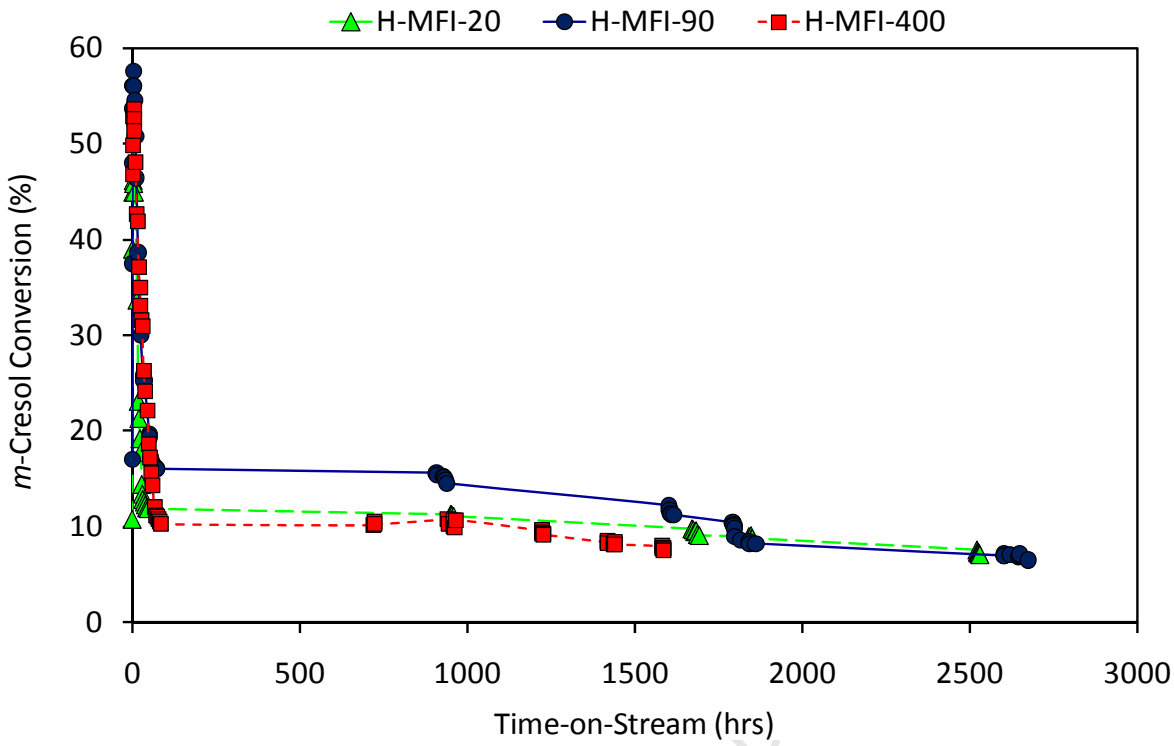

Figure 5-2: Catalyst deactivation during time-on-stream for all catalysts tested (at the standard condition of T = 225°C, P = 3 bar (abs), WHSV = 1.03 $g_{m\text{-cresol}}/g_{cat}$.hr)

The repeatability test (see Figure 5-4) shows also that quasi-steady state activity loss was still small at 275°C.

It was therefore decided, to carry out all variations of condition settings with a certain catalyst with the same charge of catalyst. Only for the reaction pressure series over the H-MFI-400, which also comprised the repeatability test, was a fresh charge of catalyst used.

5.5 Experimental repeatability

Experimental repeatability is essential in confirming the validity of observed trends from experimental procedures. In this study, experimental repeatability was tested over the H-MFI-400 catalyst by Experiment 2 and Experiment 4, each with a fresh load of catalyst. Figure 5-3 and Figure 5-4 show the results of the two experiments, obtained at identical reaction conditions and catalyst loadings. The 275°C data shown in Figure 5-4 confirm, in addition to the 225°C data shown in Figure 5-2, also the very slow progress of deactivation once the initial decline of activity is over.

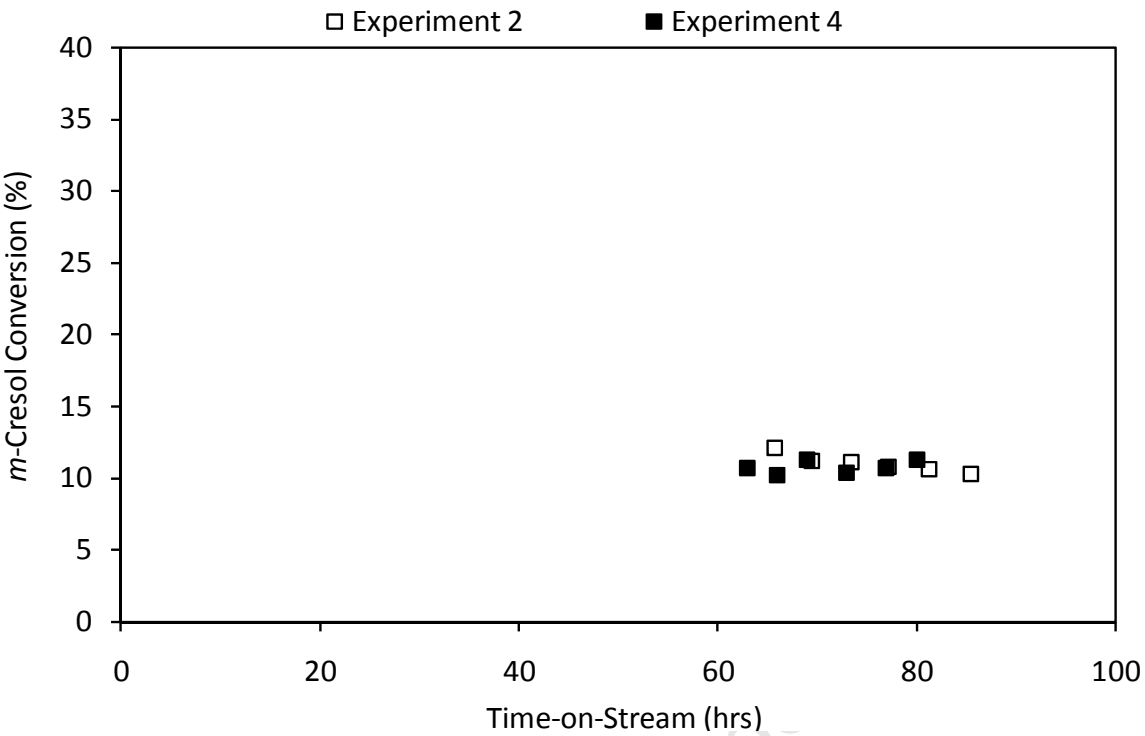

Figure 5-3: *m*-Cresol conversion vs. time-on-stream over H-MFI-400 at identical catalyst loadings (at T = 225°C, 3 bar (abs), 1.03 $g_{m\text{-cresol}}/g_{cat}$.hr) and times on stream

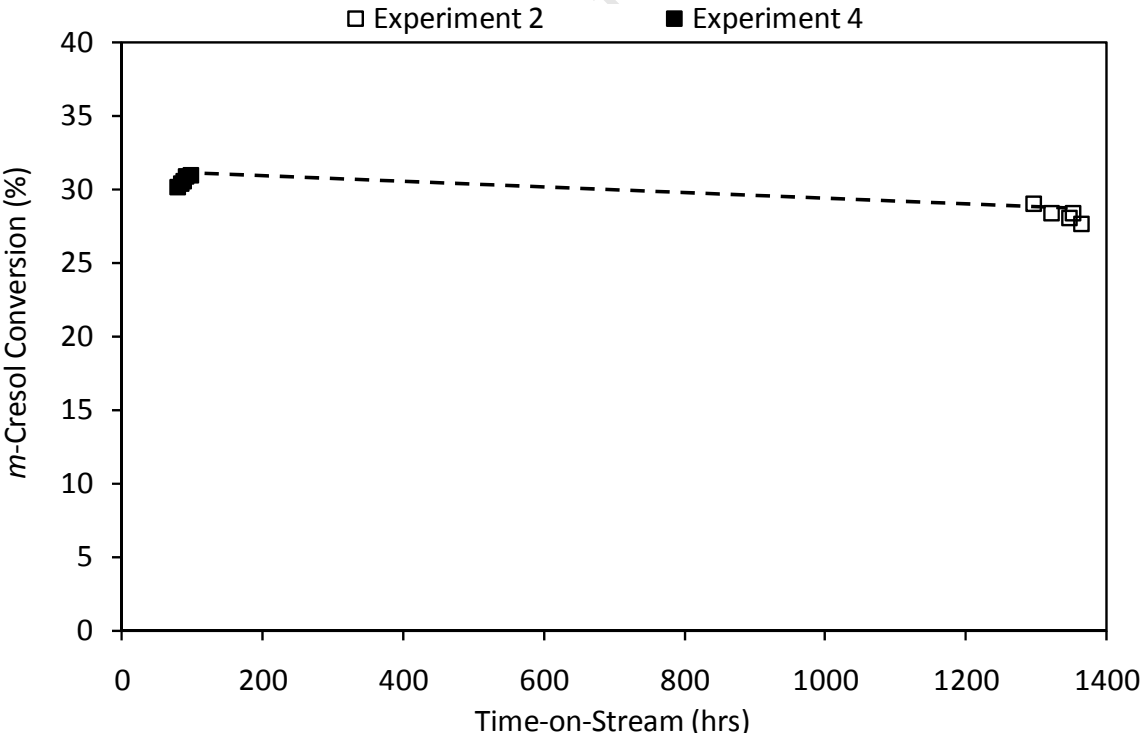

Figure 5-4: *m*-Cresol conversion vs. time-on-stream over H-MFI-400 at identical catalyst loadings (at T = 275°C, 3 bar (abs), 0.25 $g_{m\text{-cresol}}/g_{cat}$.hr) but at different times on stream

5.6 Catalyst comparison

The comparison of catalyst performance, i.e. the comparison of the effect of different SiO_2/Al_2O_3 ratios, was made at equal conversions of 20% and 30%. The aim was to establish which catalyst, if any, exhibited a higher selectivity to shape-selective products, in particular thymol, and to ascertain the differences, if any, in the product distributions from the catalysts under identical reaction temperatures and pressures and at equal conversions.

The activities of the catalysts in quasi-steady state, however, differed considerably (Figure 5-2) and hence the conversions attained varied widely. In some cases, it was impossible, due to technical limitations (i.e. the lowermost possible feed pump rate) to achieve the 20-30% conversion range over the given catalyst charge and to make a comparison of product selectivities at these conversions. Slight extrapolation of the observed trends (to conversions of 20% and 30%) was therefore implemented sometimes in obtaining an indication of the selectivities of all the products over all catalysts tested at 20% and 30% conversion (see Section 5.7).

5.6.1 Catalyst activity comparison

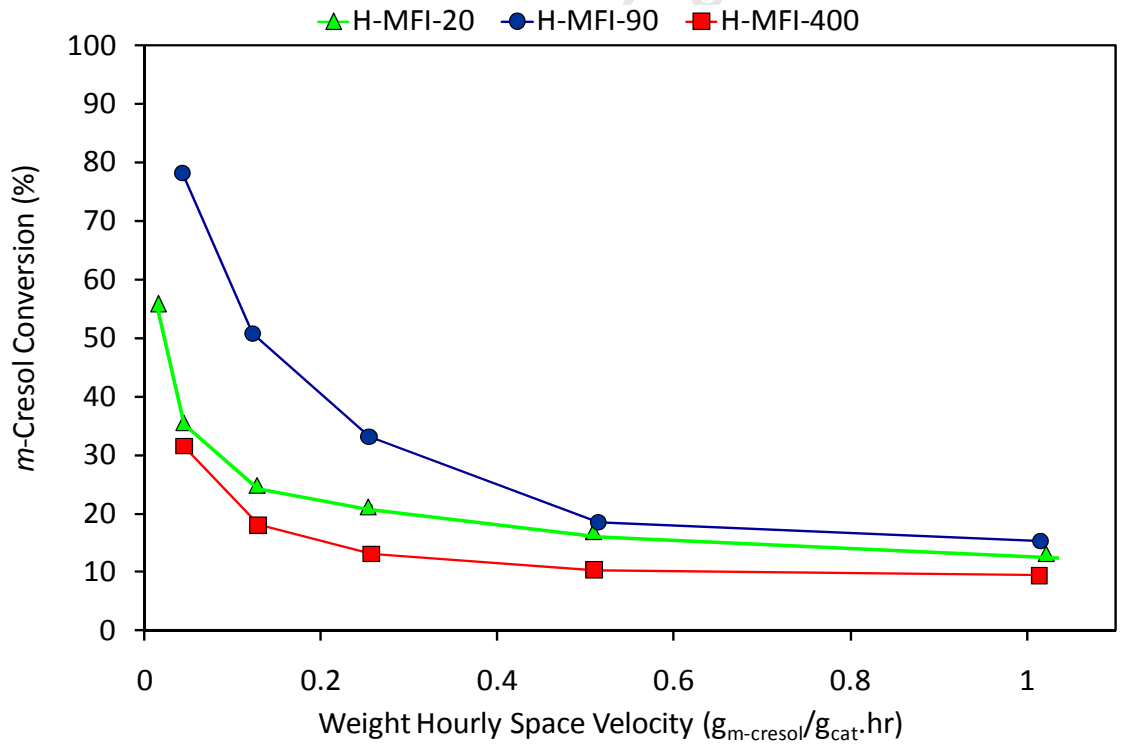

.

Figure 5-5: Comparison of activity of the catalysts tested (at T = 225°C and 3 bar (abs)) with varying WHSV

As can be seen from Figure 5-5, at the standard temperature of 225°C, all of the zeolite catalysts tested showed the expected trend of decreasing conversion with increasing space velocity. The relative activities are ranked as H-MFI-90 >> H-MFI-20 > H-MFI-400 for space velocities between 0.0625 and 0.25 $g_{m\text{-cresol}}/g_{cat}$.hr. For higher space velocities, however, the activities of the H-MFI-20 and H-MFI-90 catalysts were similar.

5.6.2 *Ortho*- and *para*-cresol

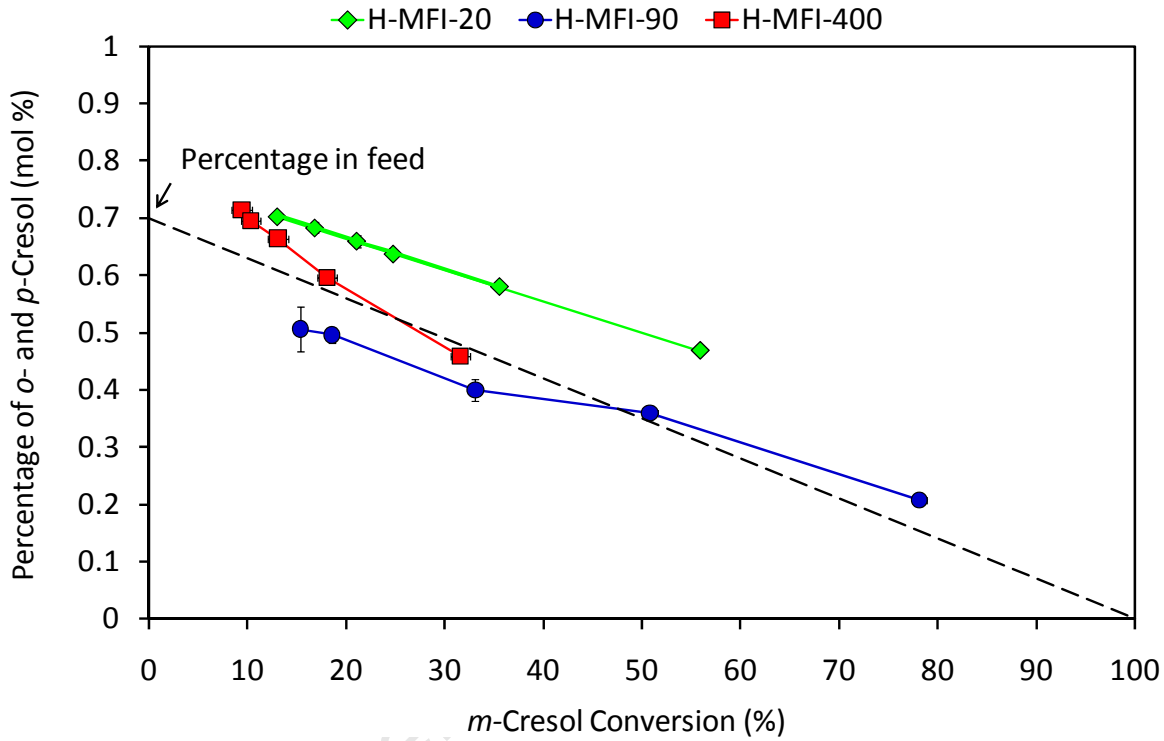

Figure 5-6: Percentage of *o*- and *p*-cresol compared to the respective impurity content of the feedstock (see Table 5-3) vs. *m*-cresol conversion for *m*-cresol isopropylation over the catalysts tested (at WHSV = 0.016 – 1.03 $g_{m\text{-cresol}}/g_{cat}$.hr, P = 3 bar (abs), T = 225°C)

As shown in Figure 5-6, the analysis of product samples indicated the presence of *p*-cresol and a trace of *o*-cresol. Comparison of the analyses of the raw *m*-cresol feed stock and the product from the blank run (Table 5-3) with that of individual product samples from the runs over the different catalysts indicates a constant decrease of the concentrations of *o*- and *p*-cresol from the initial concentration of 0.7 mol% to almost zero, thus suggesting isopropylation of the *o*- and *p*-cresol impurities present in the *m*-cresol feed stock to occur as well. Indeed, product chromatograms show a very small peak that was identified to be (most probably) 2-isopropyl-4-methyl phenol, the isopropylation product of *p*-cresol (see Table 4-7**,** Figure 4-8 and Figure 4-13). All catalysts showed a linear decrease in the percentage of *o*- and *p*-cresol with increasing *m*-cresol conversion which was proportional to conversion (the dashed line) thus indicating similar reactivity.

5.6.3 Isopropyl-3-tolyl ether

Isopropyl-3-tolyl ether is produced when isopropylation occurs on the oxygen atom of the *m*-cresol molecule (O-alkylation).

5.6.3.1 Yield of isopropyl-3-tolyl ether

Yield of isopropyl-3-tolyl ether versus conversion is shown in Figure 5-7.

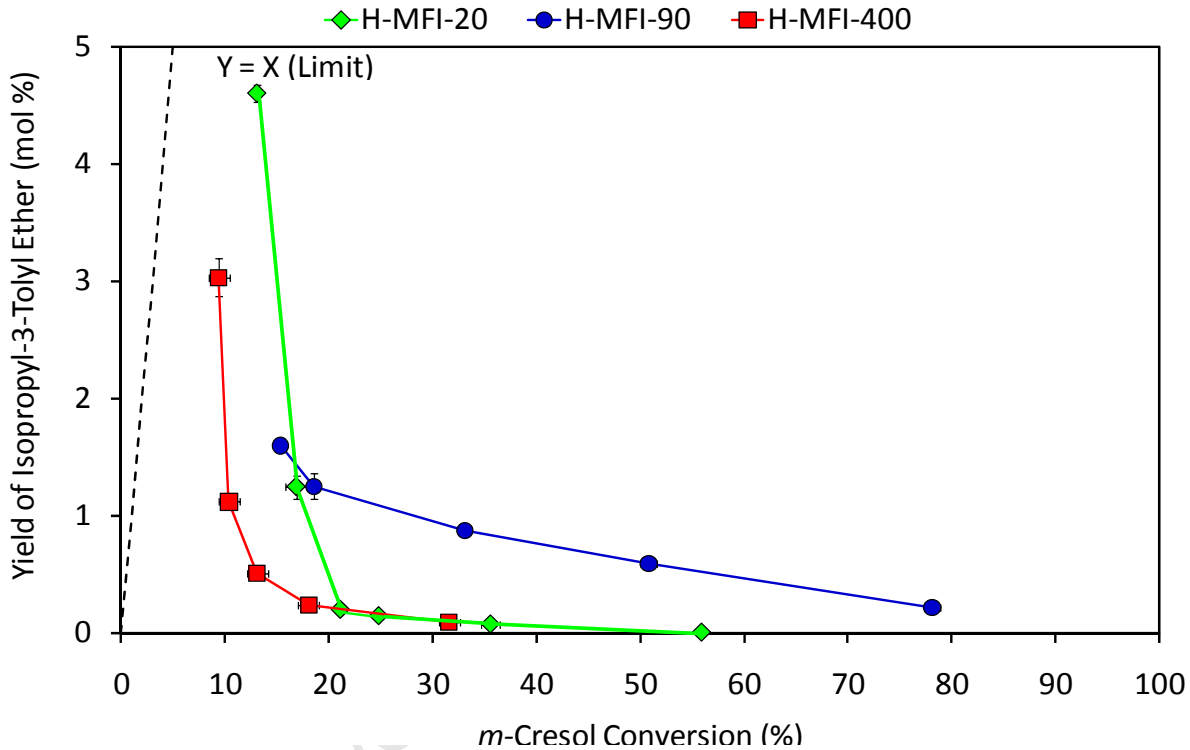

Figure 5-7: Yield of isopropyl-3-tolyl ether vs. *m*-cresol conversion for *m*-cresol isopropylation over the catalysts tested (at WHSV = 0.016 – 1.03 $g_{m\text{-cresol}}/g_{cat}$.hr, P = 3 bar (abs), T = 225°C)

Generally, the highest yields of isopropyl-3-tolyl ether were produced at low conversion and then yields declined very steeply with increasing conversion. The H-MFI-20 catalyst produced the most isopropyl-3-tolyl ether at low conversions. The H-MFI-90 and H-MFI-400 catalysts also displayed noticeable yields of isopropyl-3-tolyl ether at low conversions though to a lesser extent than the H-MFI-20 catalyst. The H-MFI-90 showed a more gradual decline in yield with increasing conversion than the other catalysts so that yields were higher at medium conversion compared to the H-MFI-20 and H-MFI-400 catalysts.

5.6.3.2 Selectivity to isopropyl-3-tolyl ether

Selectivity to isopropyl-3-tolyl ether versus conversion is shown in Figure 5-8.

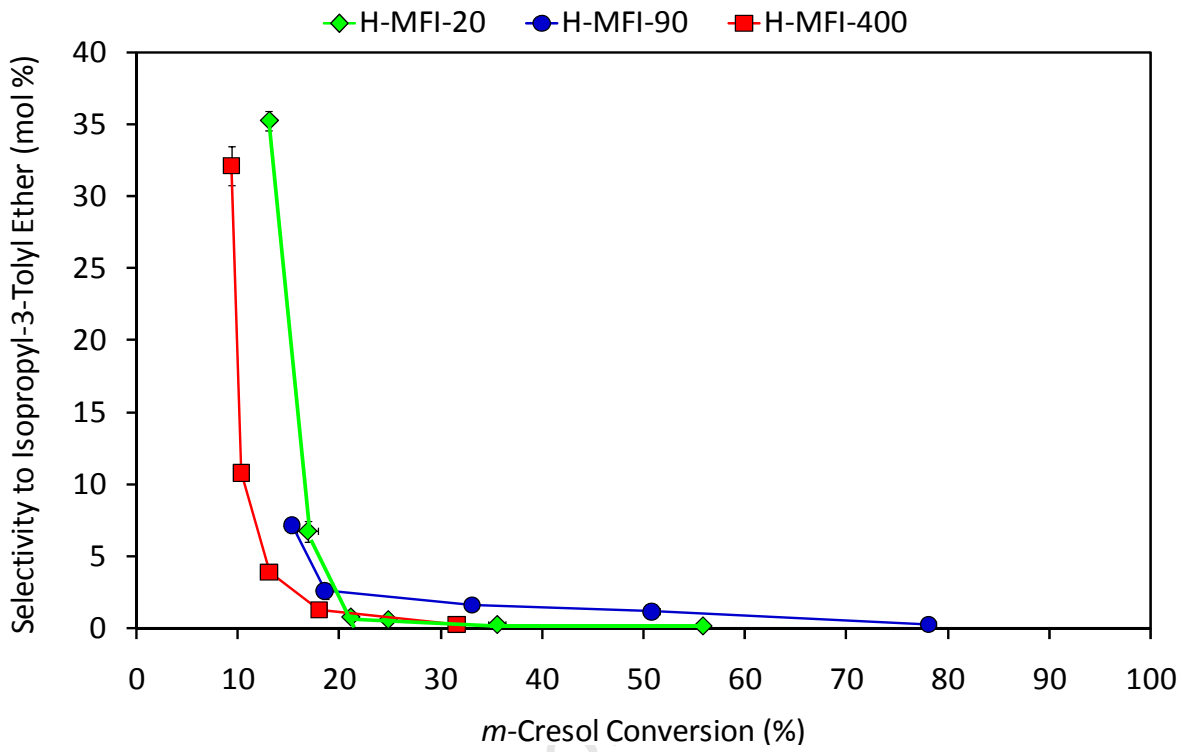

Figure 5-8: Selectivity to isopropyl-3-tolyl ether vs. *m*-cresol conversion for *m*-cresol isopropylation over catalysts tested (at WHSV = 0.016 – 1.03 $g_{m\text{-cresol}}/g_{cat}$.hr, P = 3 bar (abs), T = 225°C)

For all catalysts tested, corresponding to the yields, selectivity toward isopropyl-3-tolyl ether was high and a steep decline in the selectivity was observed with increasing conversion. At a conversion of 20%, all the catalysts showed similarly low selectivity toward isopropyl-3-tolyl ether which declined further with increasing conversion.

Corresponding to the yields, at higher conversions, the H-MFI-90 selectivity toward isopropyl-3-tolyl ether showed a more gradual decline with an increase in conversion and remained higher than the observed selectivities for the H-MFI-20 and H-MFI-400 catalysts.

5.6.4 Thymol and position isomers

Thymol and position isomers are C-alkylation products i.e. the isopropyl group is alkylated onto the aromatic ring.

5.6.4.1 Yield of thymol and position isomers

Yields of thymol and position isomers i.e. the sum of all ring mono-isopropylated (C-alkylated) *m*-cresols are shown in Figure 5-9.

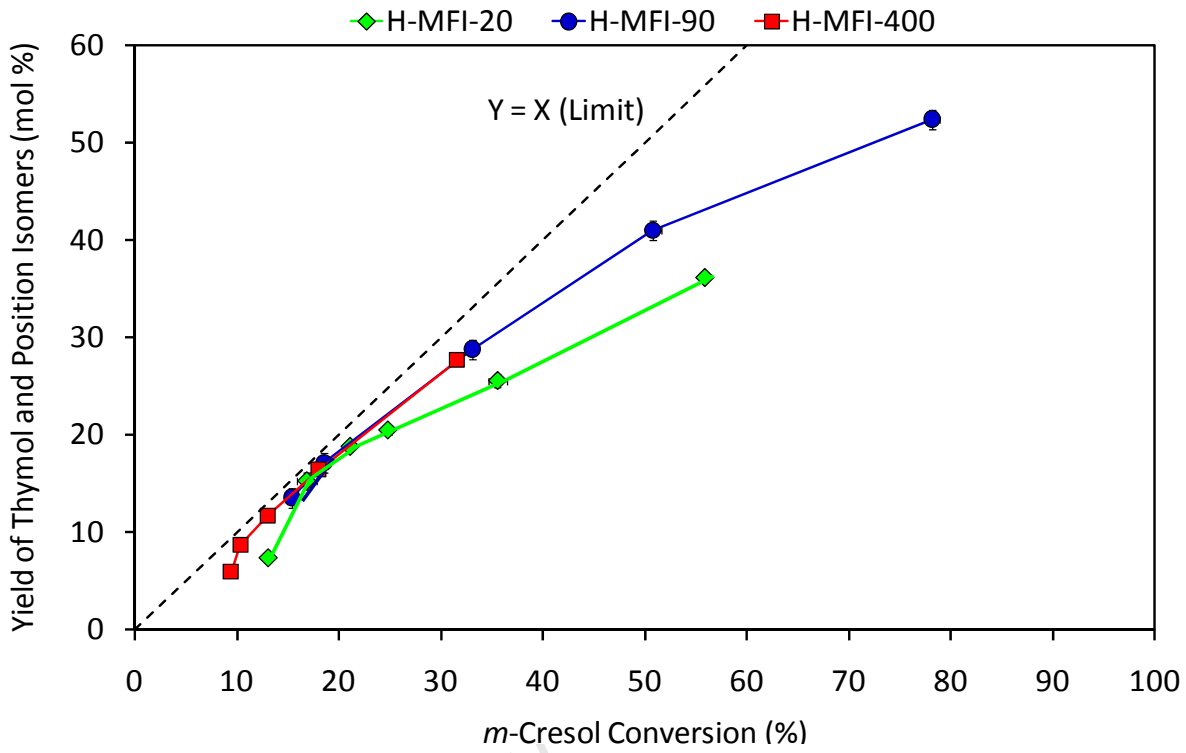

Figure 5-9: Yield of thymol and position isomers vs. *m*-cresol conversion for *m*-cresol isopropylation over the catalysts tested (at WHSV = 0.016 – 1.03 $g_{m\text{-cresol}}/g_{cat}$.hr, P = 3 bar (abs), T = 225°C)

All catalysts tested showed a similar trend of an increase in the yield of thymol and position isomers with increasing conversion. At conversions of around 20%, all catalysts showed a comparable yield, close to the theoretical maximum. At higher conversions, yields still increased but deviated significantly from the theoretical maximum. The H-MFI-90 and H-MFI-400 catalysts, which produced very similar yields at around 20% conversion, displayed higher yields of thymol and position isomers than the H-MFI-20 catalyst.

At lower conversion, at around 10%, yields of thymol and position isomers deviate again from the theoretical maximum and yields over H-MFI-20 are lower again. It appears that the trends of yields at very low conversion cannot be extended straight to the origin but take a 'dip'. This corresponds to the steep increase of the yield of isopropyl-3-tolyl ether at low conversions (≤ 20%) shown in Figure 5-7.

5.6.4.2 Selectivity to thymol and position isomers

The selectivity to thymol and position isomers (C-alkylation) is shown in Figure 5-10.

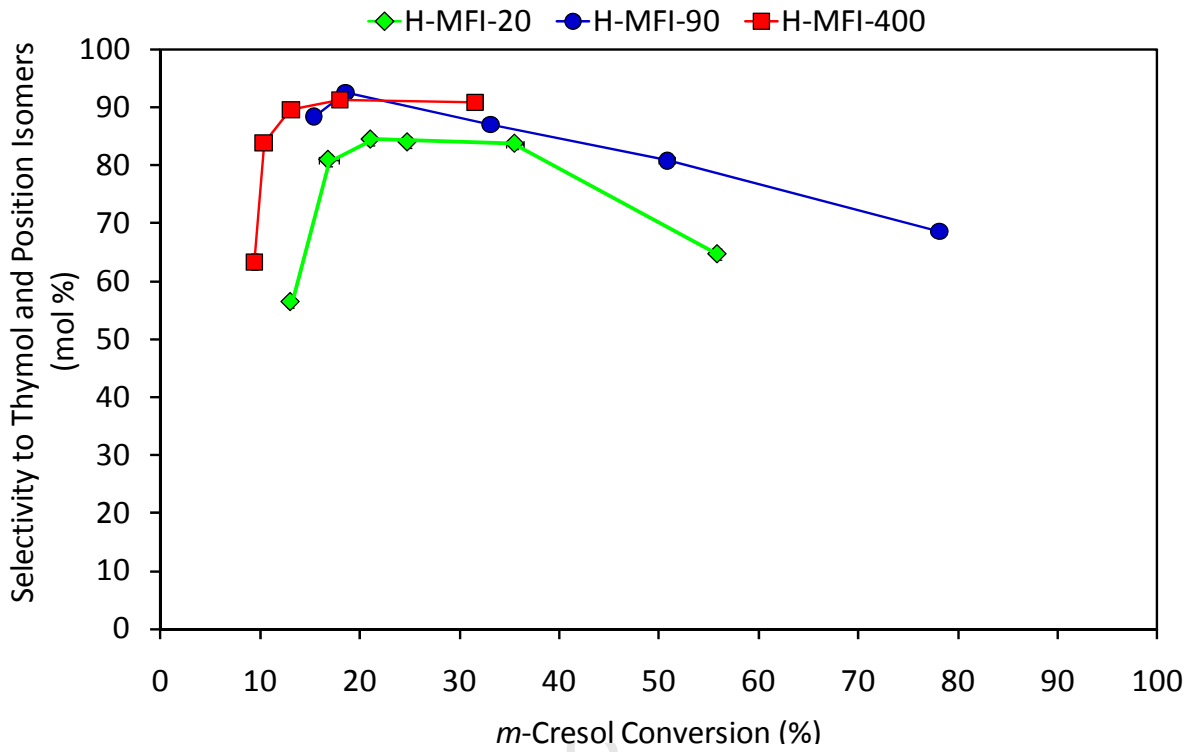

Figure 5-10: Selectivity to thymol and position isomers vs. *m*-cresol conversion for *m*-cresol isopropylation over the catalysts tested (at WHSV = 0.016 – 1.03 $g_{m\text{-cresol}}/g_{cat}$.hr, P = 3 bar (abs), T = 225°C)

The general trend appears to be selectivities passing over a maximum of 80-90% at around 20% conversion and to decline with an increase in conversion beyond 20% (showing for H-MFI-20 and H-MFI-90 catalysts whilst for the H-MFI-400 catalyst such high conversion data are unavailable). Throughout, the H-MFI-90 and H-MFI-400 catalysts showed a comparable and higher selectivity than the H-MFI-20 catalyst.

Selectivity to thymol and position isomers declines steeply at lower conversions than 20%. This corresponds to the sharp increase in the selectivity of isopropyl-3-tolyl ether at these low conversions (Figure 5-8).

5.6.5 Thymol

The target product forms at selectivities of around 50% and higher over all the catalysts tested and the range of conversions studied, but differences are significant.

5.6.5.1 Yield of thymol

Figure 5-11 indicates the yield of thymol versus conversion.

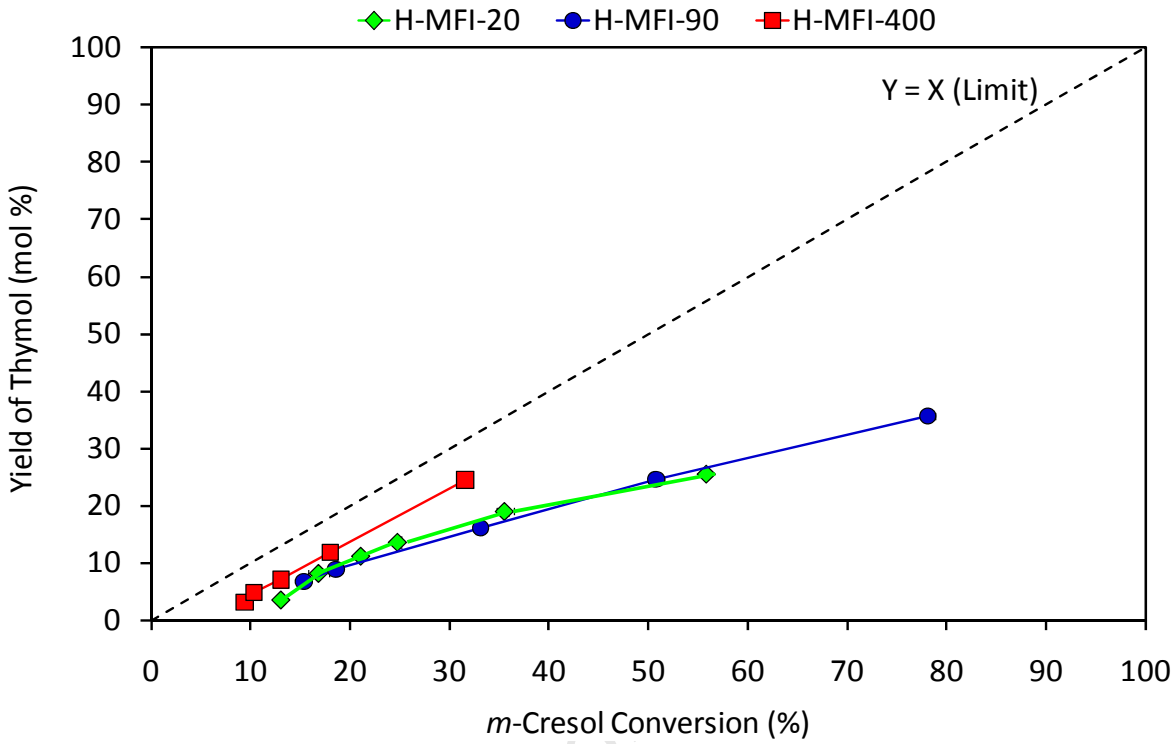

Figure 5-11: Yield of thymol vs. *m*-cresol conversion for *m*-cresol isopropylation over the catalysts tested (at WHSV = 0.016 – 1.03 $g_{m\text{-cresol}}/g_{cat}$.hr, P = 3 bar (abs), T = 225°C)

With increasing conversion, an increase in thymol yield is observed. Throughout, thymol yield is observed to be highest over the H-MFI-400 catalyst (although high conversion data are not available), with the H-MFI-20 and H-MFI-90 catalysts showing comparable, yet significantly lower yields toward thymol, in particular with increasing conversion.

It should be noted that, similar to the yields of thymol and position isomers (see Section 5.6.4.1 and Figure 5-9), yields appear to show a 'dip' at very low conversion (below 20%) and trends do not extend straight toward the origin.

5.6.5.2 Selectivity to thymol

The selectivity toward thymol versus conversion is shown in Figure 5-12.

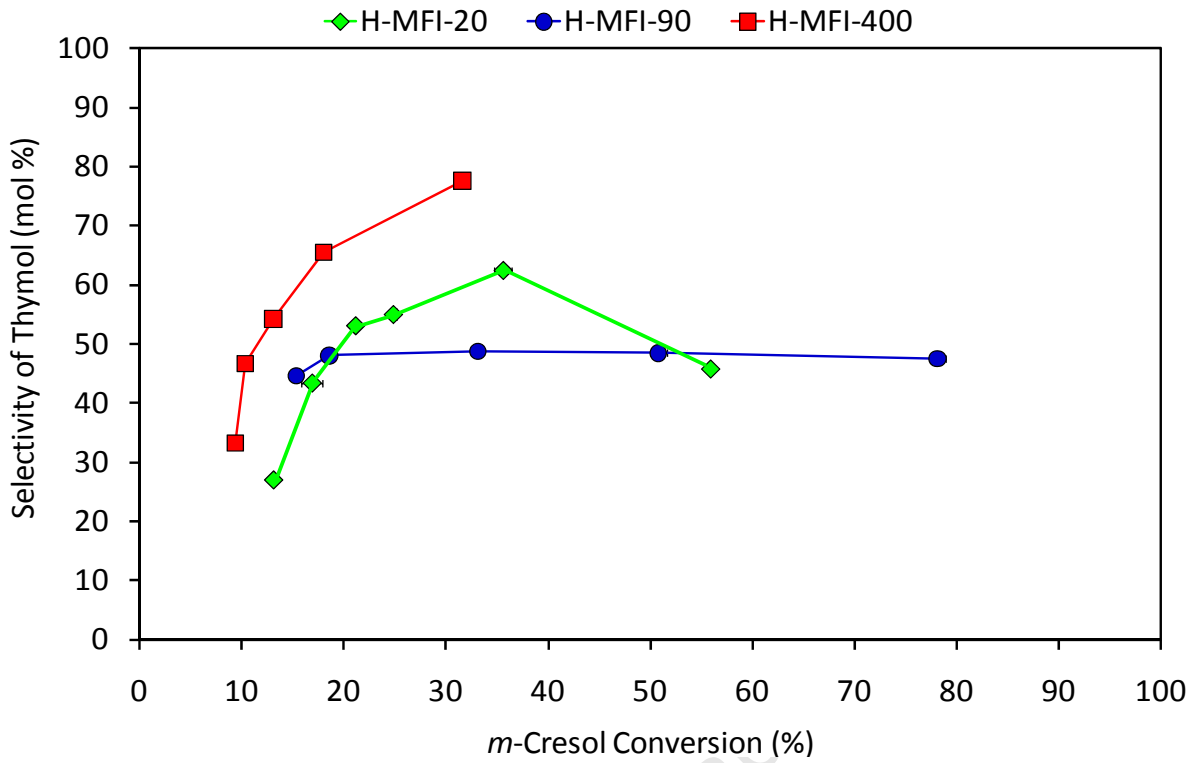

Figure 5-12: Selectivity of thymol vs. *m*-cresol conversion for *m*-cresol isopropylation over the catalysts tested (at WHSV = 0.016 - 1.03 $g_{m\text{-cresol}}/g_{cat}$.hr, P = 3 bar (abs), T = 225°C)

At equal conversion of 20%, the selectivity toward thymol was observed to be highest over the H-MFI-400 catalyst, whilst the H-MFI-20 and H-MFI-90 catalysts showed similar but lower selectivity toward thymol. At the higher conversion of 30%, the H-MFI-400 catalyst still showed the highest selectivity toward thymol, followed by the H-MFI-20 and the H-MFI-90 that showed the lowest selectivity toward thymol.

A clear trend of decreasing thymol selectivity with decreasing conversion was observed at low conversions for all of the catalysts. This reflects the increase in isopropyl-3-tolyl ether selectivity (Figure 5-8). With the H-MFI-90 catalyst, a levelling out is indicated at higher conversions. The H-MFI-20 catalyst shows thymol selectivity passing over a maximum with increasing conversions.

Selectivity curves for thymol reflect the selectivity curves for the total selectivity of the ring mono-isopropylated products (thymol and position isomers) closely (see Section 5.6.4.2 and Figure 5-10).

5.6.5.3 Percentage of thymol in thymol and position isomer fraction

The percentage of thymol in the thymol and position isomers fraction versus conversion is shown in Figure 5-13.

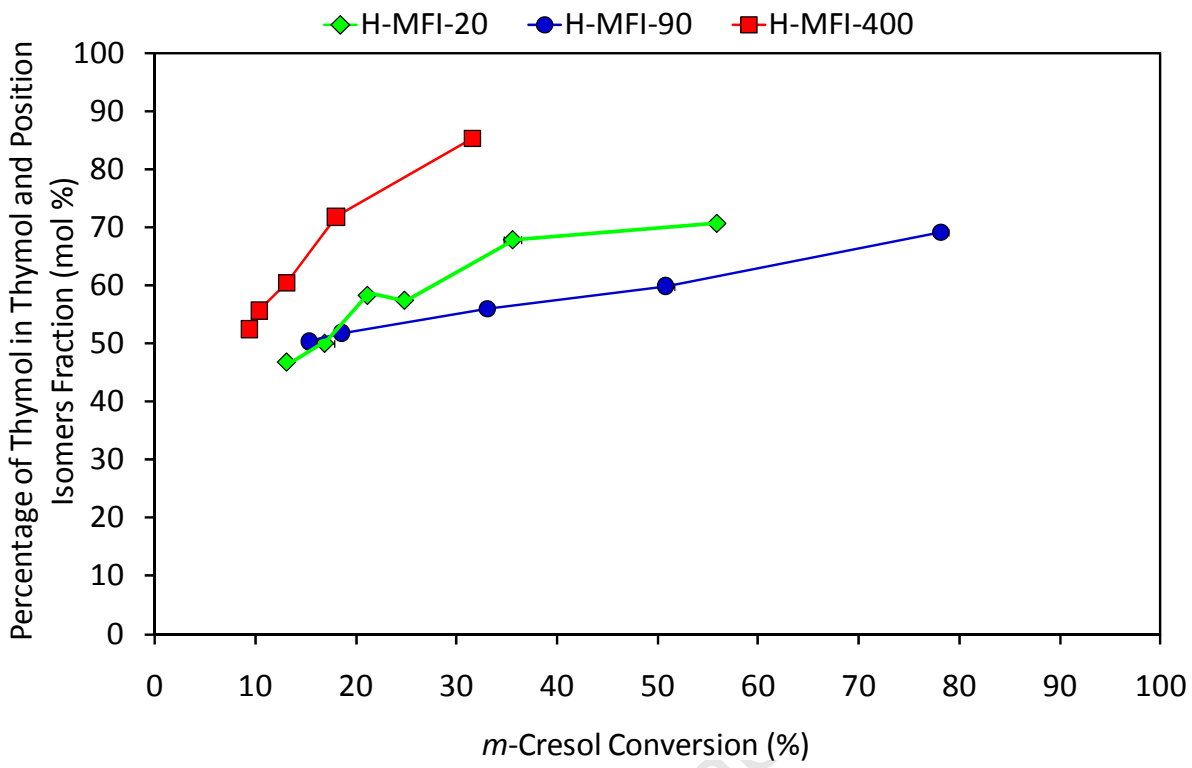

Figure 5-13: Percentage of thymol in the thymol and position isomers fraction vs. conversion for *m*-cresol isopropylation over the catalysts tested (at WHSV = 0.016 - 1.03 $g_{m\text{-cresol}}/g_{cat}$.hr, P = 3 bar (abs), T = 225°C)

The observed trends are similar to the trends observed for the selectivity of thymol (see Figure 5-12), although trends show a steeper increase in the percentage of thymol with increasing conversion and indicate, for the H-MFI-400 and H-MFI-20 catalysts, a levelling out at higher conversions.

Throughout, the H-MFI-400 catalyst showed the highest percentage of thymol in the thymol and position isomer fraction followed by the H-MFI-20 and then the H-MFI-90 catalyst.

5.6.6 Thymol and position isomers distribution

The individual position isomer yields and selectivity distributions versus conversion for each of the catalysts tested in the isopropylation of *m*-cresol are compared in subsequent figures at identical reaction temperatures and pressures of 225°C, 3 bar (abs) and varying WHSV. Figures 5-16, 5-19 and 5-22 show the isomers distribution over each of the catalysts tested. This distribution indicates the respective percentage of each position isomer making up the entire fraction of total positional isomers.

5.6.6.1 Position isomer yields and selectivities over H-MFI-20

The yield and selectivities of the position isomers as well as the position isomers distribution for the H-MFI-20 catalyst are shown in Figure 5-14 to Figure 5-16.

Of the isomers, only the yields of thymol and the 5-isopropyl-3-methyl phenol position isomer were observed to steadily increase with increasing *m*-cresol conversion, with the latter observed to form later and increase the steepest, relatively.

Yields of 4-isopropyl-3-methyl phenol and 2-isopropyl-3-methyl phenol were observed to pass over maxima already at around 20% conversion with the latter declining rapidly after passing over the maximum. The steep decline in yields towards low conversion reflects the presence of the isopropyl-3-tolyl ether in this range (see Figure 5-7).

Selectivities of all isomers except the 5-isopropyl-3-methyl phenol position isomer were observed to pass over maxima with increasing conversion. For 2-isopropyl-3-methyl phenol and 4-isopropyl-3-methyl phenol these maxima are identified at rather low conversions, typically less than 20% while the maxima of thymol selectivity is only achieved at medium conversion. The selectivity of the 5-isopropyl-3-methyl phenol isomer increases steadily. The steep decrease of selectivities of all of the position isomers at low conversion reflects the high selectivity of the isopropyl-3-tolyl ether (see Figure 5-8).

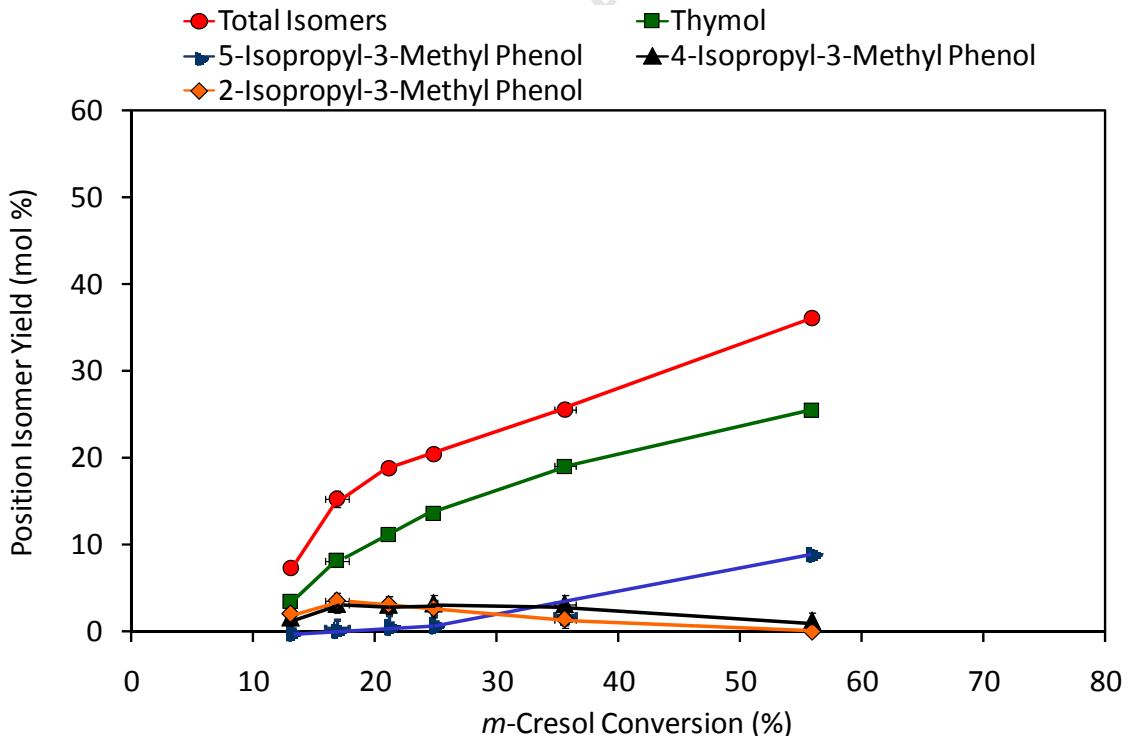

Figure 5-14: Position isomer yields vs. *m*-cresol conversion for *m*-cresol isopropylation over the H-MFI-20 catalyst (at WHSV = 0.016 – 1.03 $g_{m\text{-cresol}}/g_{cat}$.hr, P = 3 bar (abs), T = 225°C)

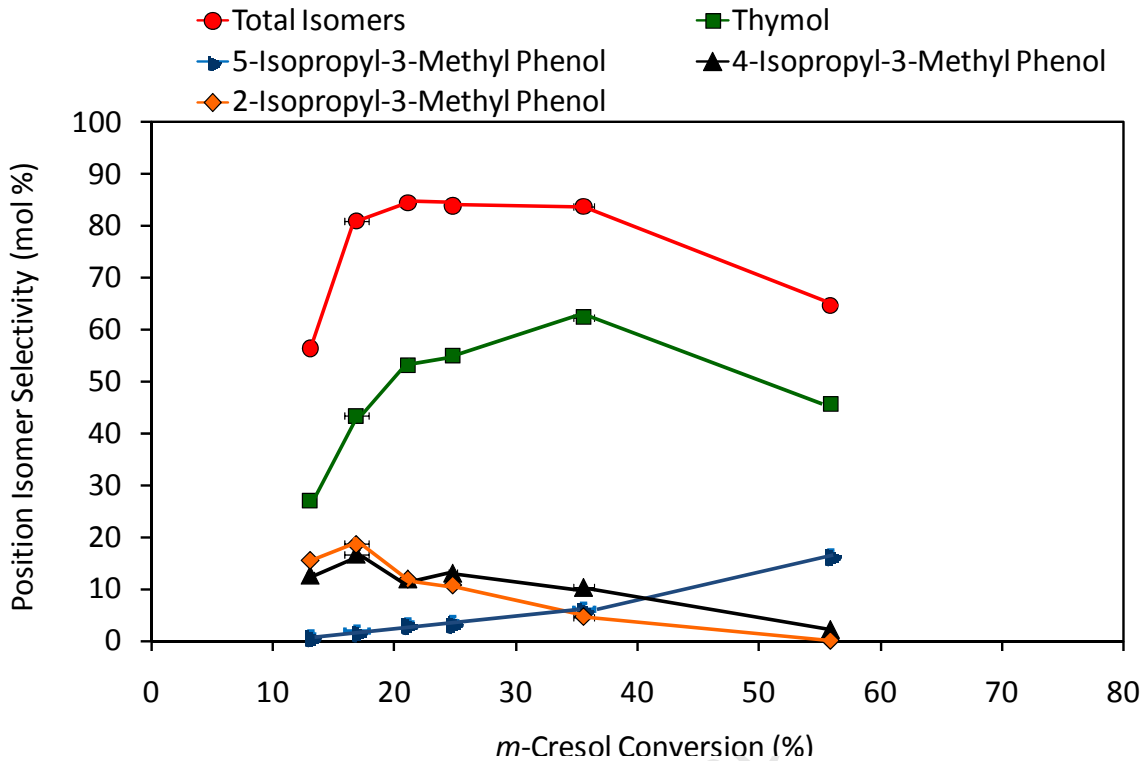

Figure 5-15: Position isomer selectivities vs. *m*-cresol conversion for *m*-cresol isopropylation over the H-MFI-20 catalyst (at WHSV = 0.016 – 1.03 $g_{m\text{-cresol}}/g_{cat}$.hr, P = 3 bar (abs), T = 225°C)

The distribution of the isomers (see Figure 5-16) shows a steady increase in the percentage of the 5-isopropyl-3-methyl phenol isomer while the 2-isopropyl-3-methyl phenol isomer and 4-isopropyl-3-methyl phenol isomer disappear rapidly from the isomer pool. At > 50% conversion only thymol and the 5-isopropyl-3-methyl phenol isomer are left with a trend of a constantly increasing percentage of the latter.

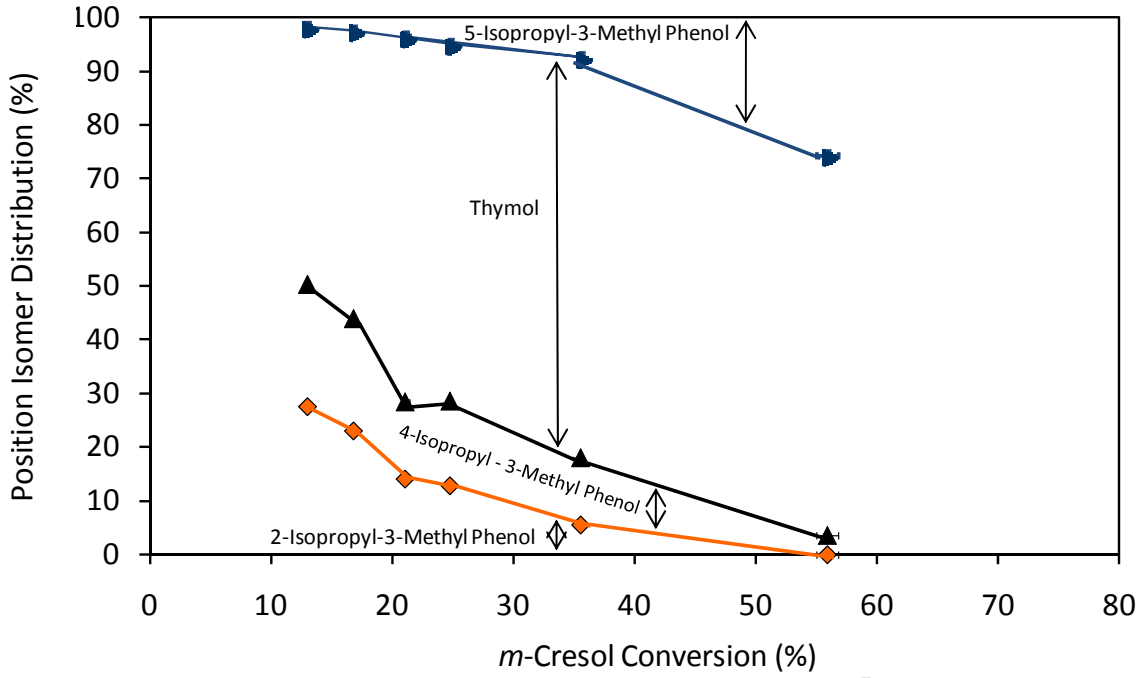

Figure 5-16: Distribution of the position isomers, successively adding up the specific percentages of the individual compounds to 100% (the total isomers) for each of the individual conversions vs. *m*-cresol conversion for *m*-cresol isopropylation over the H-MFI-20 catalyst (at WHSV = 0.016-1.03 $g_{m\text{-cresol}}/g_{cat}$.hr, P = 3 bar (abs), T = 225°C)

5.6.6.2 Position isomer yields and selectivities over H-MFI-90

The yields and selectivities of the position isomers as well as the position isomers distribution for the H-MFI-90 catalyst are shown in Figure 5-17 to Figure 5-19.

The general trends are similar to those observed over the H-MFI-20 catalyst, just less pronounced. Similarly, the selectivity of the 2-isopropyl-3-methyl phenol isomer declines rather steeply and the yield passes over a maximum (at about 50% conversion). Thymol selectivity also declines to some extent, while the 5-isopropyl-3-methyl phenol isomer is the only isomer whose yield, selectivity and percentage in the isomers fraction steadily increases though on a low level.

Over H-MFI-90, the effect of conversion on selectivity appears to be the weakest compared to the two other catalysts tested.

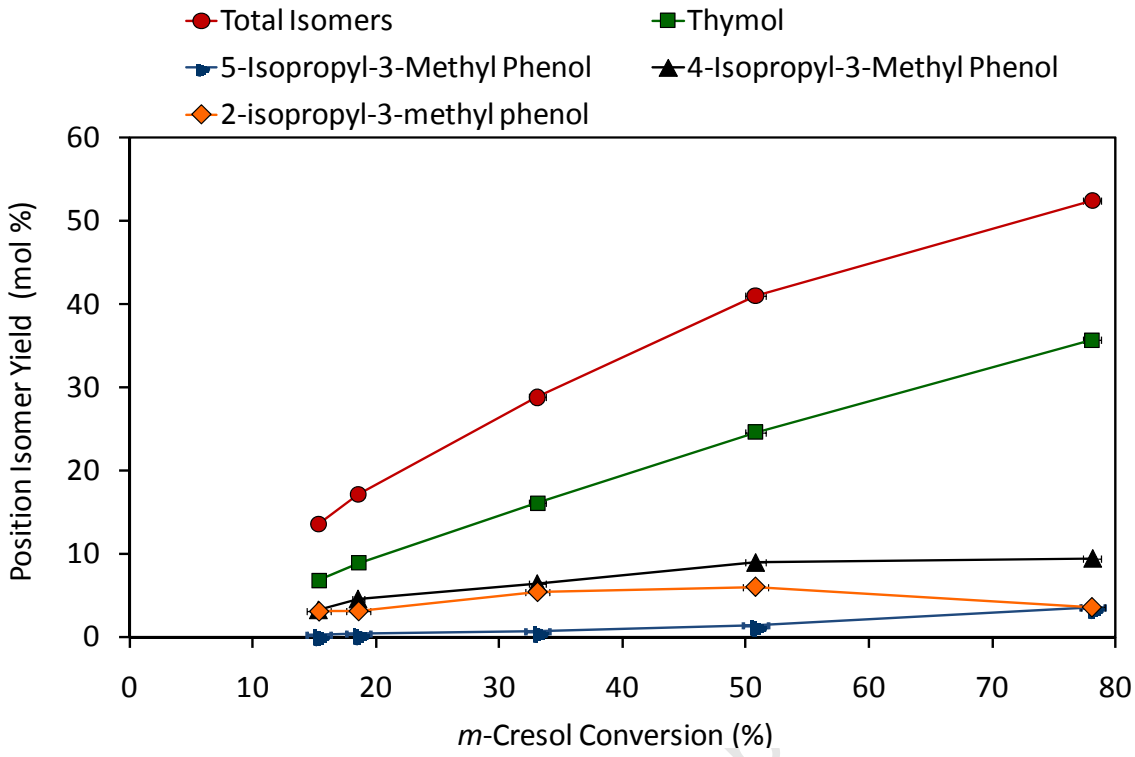

Figure 5-17: Position isomer yields vs. *m*-cresol conversion for *m*-cresol isopropylation over the H-MFI-90 catalyst (at WHSV = 0.0625 – 1.03 $g_{m\text{-cresol}}/g_{cat}$.hr, P = 3 bar (abs), T = 225°C)

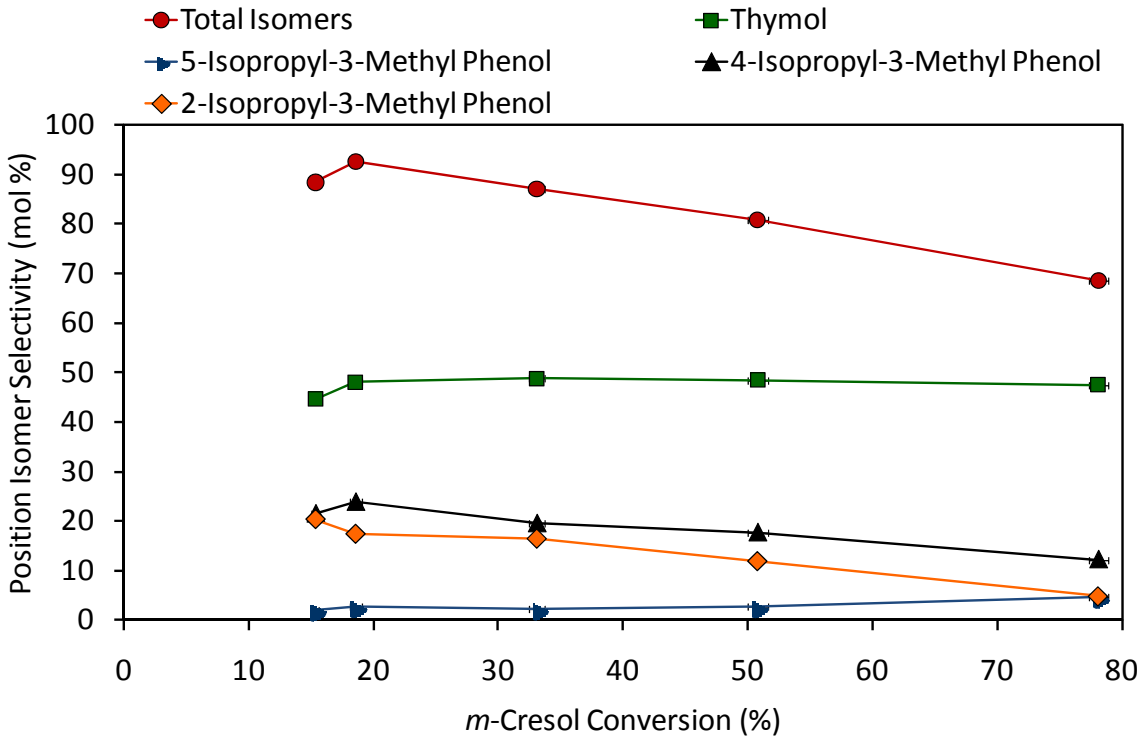

Figure 5-18: Position isomer selectivities vs. *m*-cresol conversion for *m*-cresol isopropylation over the H-MFI-90 catalyst (at WHSV = 0.0625 – 1.03 $g_{m\text{-cresol}}/g_{cat}$.hr, P = 3 bar (abs), T = 225°C)

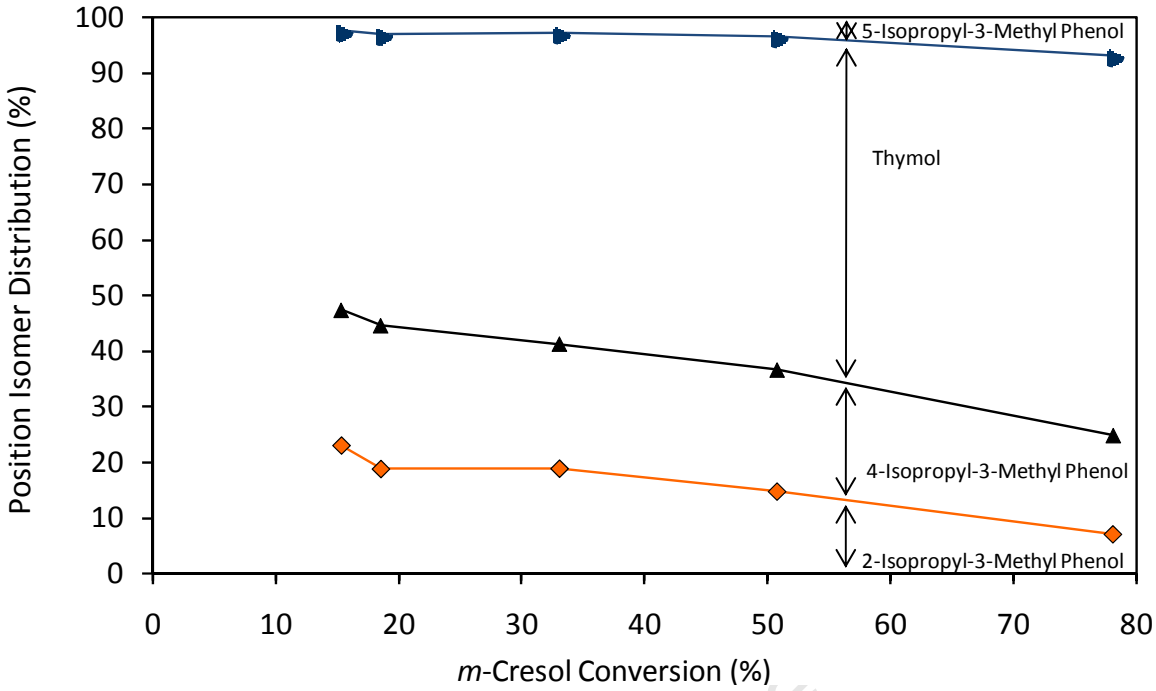

Figure 5-19: Distribution of the position isomers, successively adding up the specific percentages of the individual compounds to 100% (the total isomers) for each of the individual conversions vs. *m*-cresol conversion for *m*-cresol isopropylation over the H-MFI-90 catalyst (at WHSV = 0.0625-1.03 $g_{m\text{-cresol}}/g_{cat}$.hr, P = 3 bar (abs), T = 225°C)

5.6.6.3 Position isomer yields and selectivities over H-MFI-400

The yields and selectivities of the position isomers as well as the position isomers distribution for the H-MFI-400 catalyst are shown in Figure 5-20 to Figure 5-22.

The general trends follow the same pattern as observed for the two other catalysts, namely the pronounced decline in selectivity toward the 2-isopropyl-3-methyl phenol isomer already beginning at low conversion, and the corresponding maximum and decline in yield.

The selectivity toward thymol and the 5-isopropyl-3-methyl phenol isomer are increasing. The range of conversion covered with the H-MFI-400 catalyst is, however, too short to indicate toward a levelling out or maximum of thymol selectivity at higher conversions, as observed with the other catalysts.

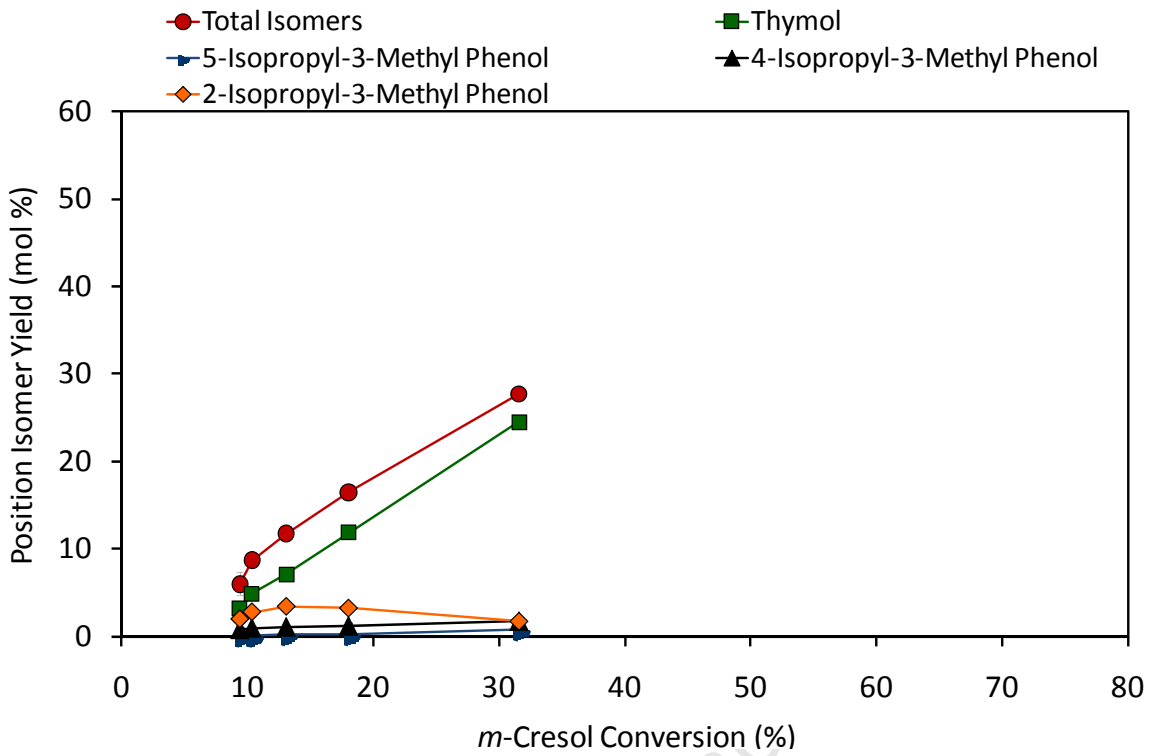

Figure 5-20: Position isomer yields vs. *m*-cresol conversion for *m*-cresol isopropylation over the H-MFI-400 catalyst (at WHSV = 0.0625 – 1.03 $g_{m\text{-cresol}}/g_{cat}$.hr, P = 3 bar (abs), T = 225°C)

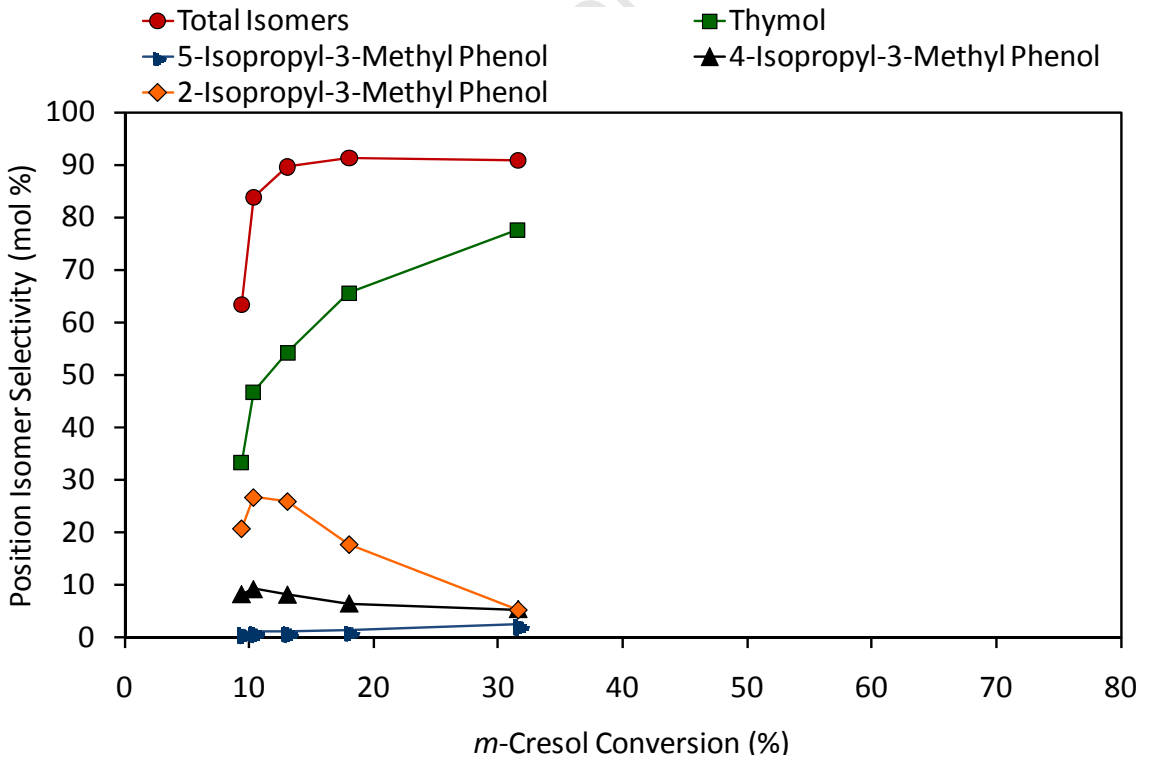

Figure 5-21: Position isomer selectivities vs. *m*-cresol conversion for *m*-cresol isopropylation over the H-MFI-400 catalyst (at WHSV = 0.0625 – 1.03 $g_{m\text{-cresol}}/g_{cat}$.hr, P = 3 bar (abs), T = 225°C)

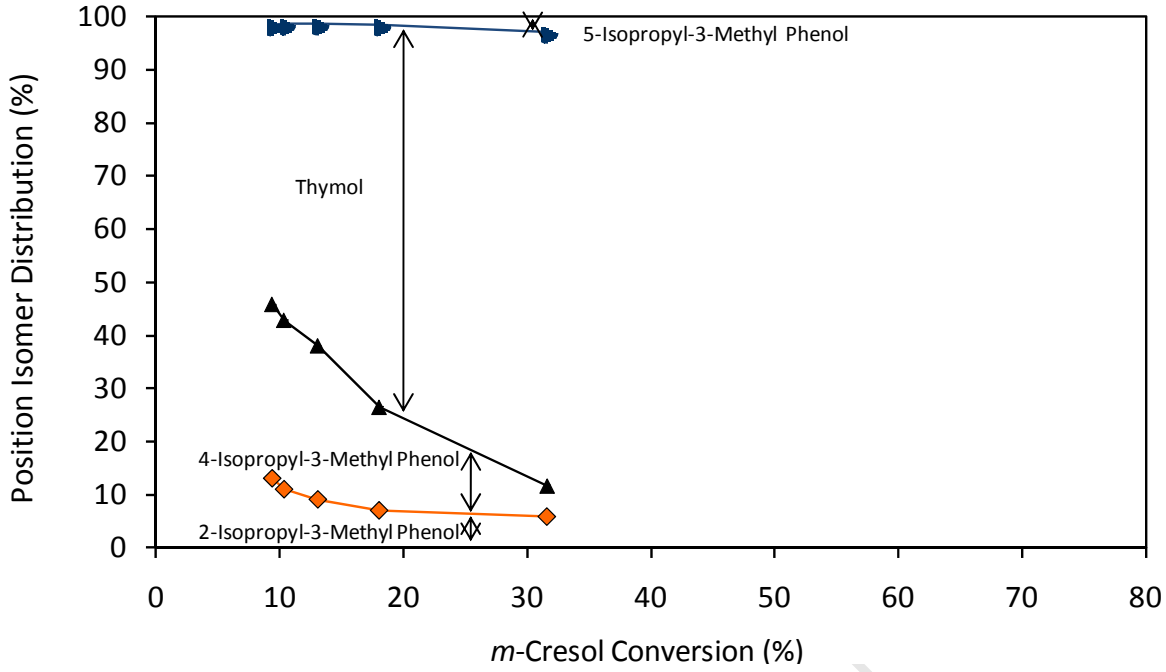

Figure 5-22: Distribution of the position isomers, successively adding up the specific percentages of the individual compounds to 100% (the total isomers) for each of the individual conversions vs. *m*-cresol conversion for *m*-cresol isopropylation over the H-MFI-400 catalyst (at WHSV = 0.0625-1.03 $g_{m\text{-cresol}}/g_{cat}$.hr, P = 3 bar (abs), T = 225°C)

5.6.6.4 General trends of positions isomers distribution

Position isomers distributions show a common trend over all the catalysts tested but the extents differ. While hardly any 5-isopropyl-3-methyl phenol forms over the entire range of conversions obtained over the H-MFI-90 and H-MFI-400 catalysts, even at high conversions, significant amounts of this isomer form over the H-MFI-20 catalyst at high conversions. In contrast, both the 2-isopropyl-3-methyl phenol and the 4-isopropyl-3-methyl phenol isomers disappear from the product spectrum over the H-MFI-20 and the H-MFI-400 catalyst at high conversion. H-MFI-90 exhibits the same trends but it is much less pronounced. It appears that the thymol isomer dominates the position isomer fraction at high conversion even more than at low conversion.

For the 5-isopropyl-3-methyl phenol isomer a steady increase of yield, selectivity and percentage in the position isomers fraction is observed with increasing conversion, which is most pronounced over the H-MFI-20 catalyst.

5.6.7 Diisopropylated *m*-cresol compounds

"Diisopropylated *m*-cresol" comprises compounds where two isopropyl groups are alkylated onto the carbon atoms of the aromatic ring of the *m*-cresol feed compound preferentially onto either or both of the *ortho*-positions or the *ortho*- and *para*-positions of the *m*-cresol molecule, see Figure 4-9, Figure 4-10, Figure 4-13 and Figure 4-14.

This group does not include compounds where one of the isopropyl groups is bonded onto the oxygen (ether). Such heavy ether compounds were not found in the product mixture (according to GC traces, see Figure 4-7 to Figure 4-14).

5.6.7.1 Yield of diisopropylated *m*-cresol compounds

The total yield of diisopropylated *m*-cresol compounds versus conversion is shown in Figure 5-23.

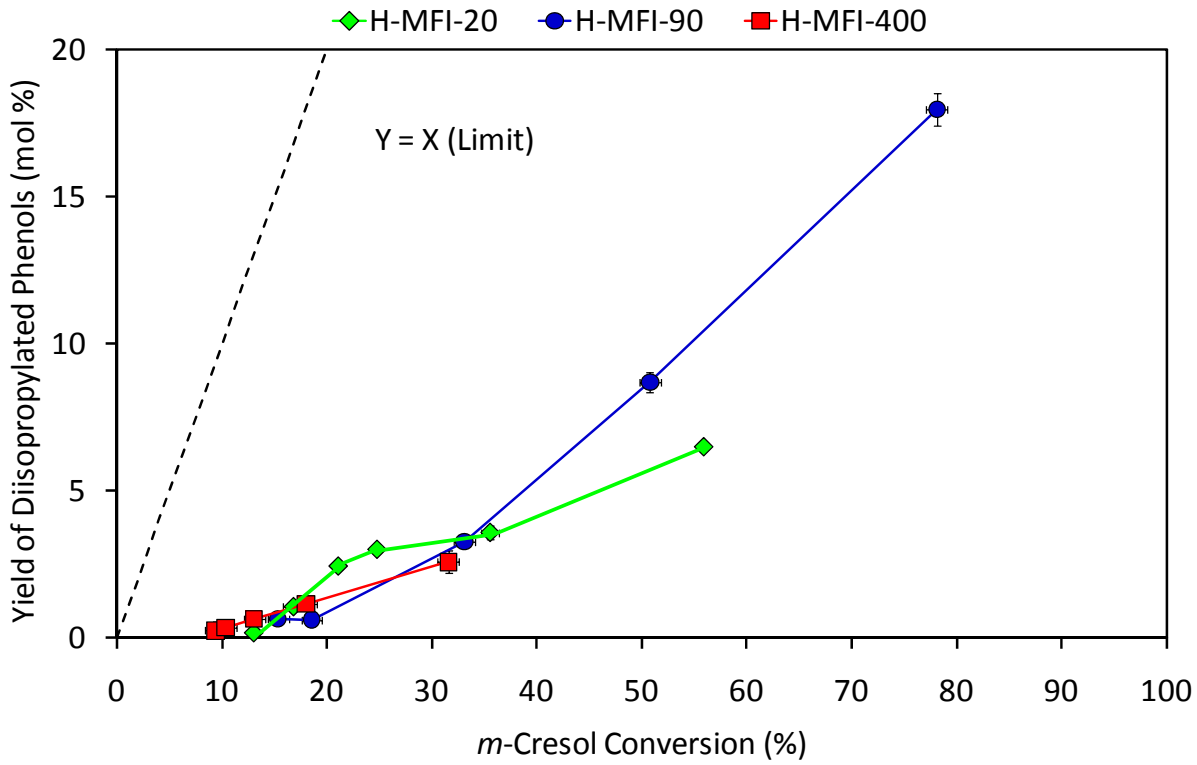

Figure 5-23: Total yield of diisopropylated *m*-cresol compounds vs. *m*-cresol conversion for *m*-cresol isopropylation over catalysts tested (at WHSV = 0.016 – 1.03 $g_{m\text{-cresol}}/g_{cat}$.hr, P = 3 bar (abs), T = 225°C)

In general, all three catalysts tested showed a similar trend of increasing yield toward diisopropylated *m*-cresol compounds with increasing conversion. However, diisopropylated *m*-cresols appear to occur with noticeable yield only from about 10% conversion onwards, and

yields appear to further increase constantly over the conversion range. The curves appear to rise exponentially from the origin.

5.6.7.2 Selectivity to diisopropylated *m*-cresol compounds

Selectivity to the total diisopropylated *m*-cresol compounds versus conversion is shown in Figure 5-24.

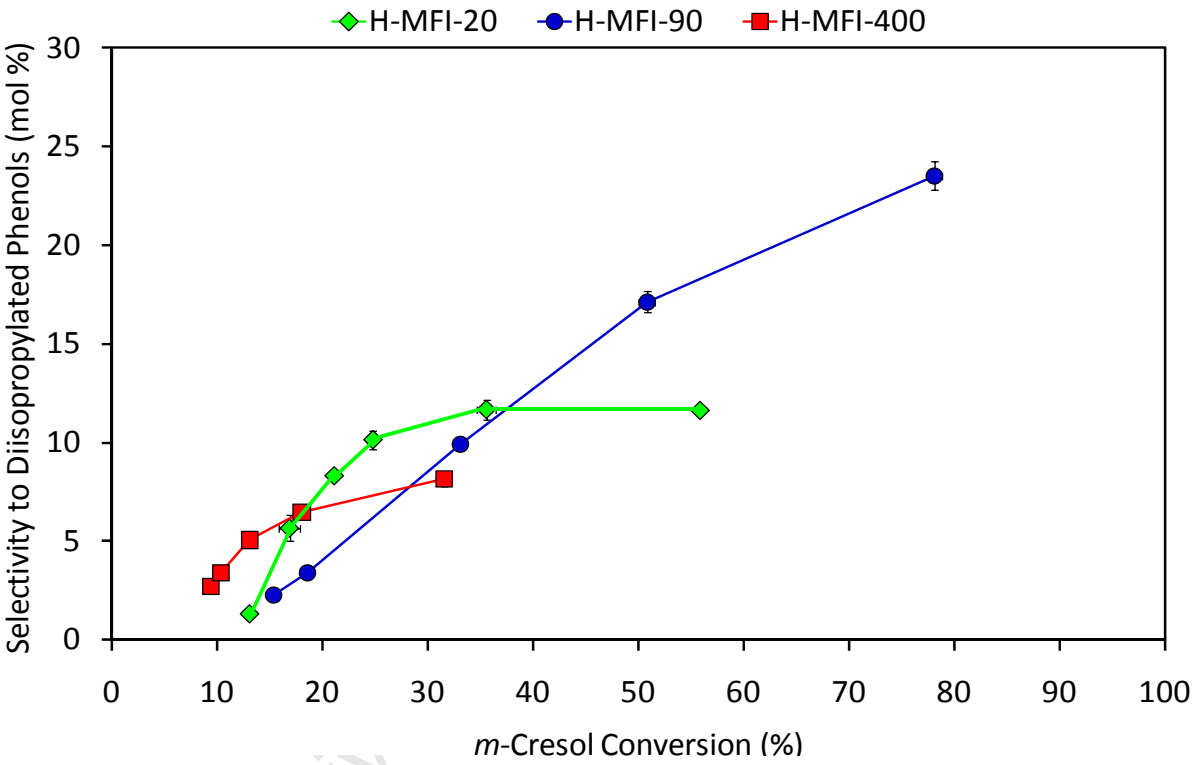

Figure 5-24: Selectivity to total diisopropylated *m*-cresol compounds versus *m*-cresol conversion for *m*-cresol isopropylation over the catalysts tested (at WHSV = 0.016 – 1.03 $g_{m\text{-cresol}}/g_{cat}$.hr, P = 3 bar (abs), T = 225°C)

Like the thymol and position isomers fraction, the selectivities of diisopropylated *m*-cresol compounds appear to approach or pass over maxima, although at higher conversions. At low conversion, the H-MFI-400 catalyst displayed the highest selectivity toward the diisopropylated *m*-cresol compounds. At a moderate conversion of 30%, the H-MFI-20 showed the highest selectivity and at very high conversions the selectivity was highest over the H-MFI-90 catalyst.

5.6.8 "Others"

All phenolic compounds, except isopropyl-3-tolyl ether, thymol and the position isomers, as well as diisopropylated *m*-cresol compounds, and also except *o*- and *p*-cresol, the xylenols and 2-isopropyl-4-methyl phenol, that are feed impurities or the isopropylation product thereof, are grouped together as "Others". "Others" therefore comprises compounds observed in the product mixture such as 6-n-propyl-3-methyl phenol and heavier compounds.

5.6.8.1 Yield of "Others"

The yield of "Others" versus conversion is shown in Figure 5-25.

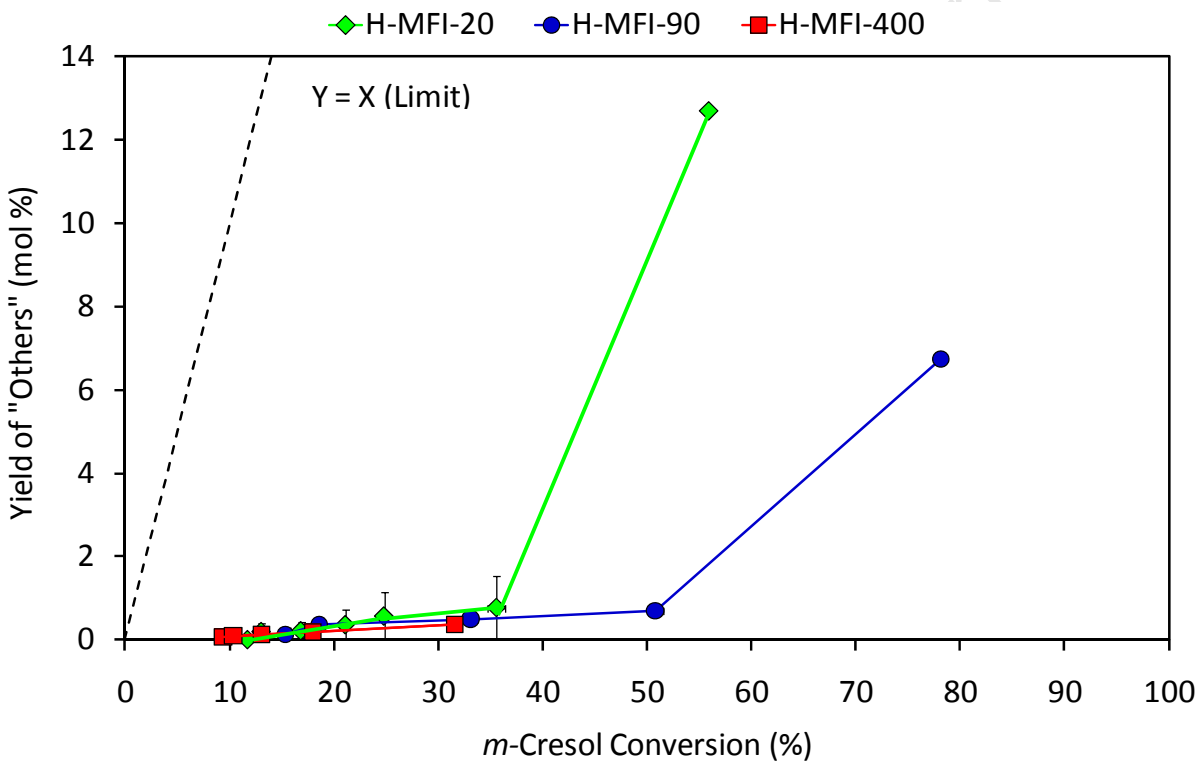

Figure 5-25: Yield of "Others" vs. *m*-cresol conversion for *m*-cresol isopropylation over catalysts tested (at WHSV = 0.016 – 1.03 $g_{m\text{-cresol}}/g_{cat}$.hr, P = 3 bar (abs), T = 225°C)

At low to medium conversion, yields of 'other' compounds were very low, although a general trend of increasing yield to "Others" with increasing conversion is observed for all catalysts tested. However, at the high conversion of 55% over H-MFI-20 and 80% over H-MFI-90, a much higher yield to "Others" was observed. This could particularly be attributed to the formation of the n-analogue of thymol, 6-n-propyl-3-methyl phenol, at the very high conversions.

5.7 Effect of reaction conditions

For each of the catalysts tested, WHSV series (0.016 or 0.0625 – 1.03 $g_{m\text{-cresol}}/g_{cat}$.hr) at different temperatures (200 – 300°C), constant reaction pressure of 3 bar (abs) and constant feed composition of 1 : 1 (molar), were carried out to ascertain the optimum catalyst and reaction conditions for isopropylation of *m*-cresol (see Table 5-1). On determination of the optimum conditions, a pressure series (1.5 – 12 bar (abs)) at 275°C, WHSV = 0.25 and 0.5 $g_{m\text{-cresol}}/g_{cat}$.hr and molar feed ratio of 1: 1 was conducted over H-MFI-400, the catalyst that was found to be the best. The results of the condition variations are presented in the subsequent sections.

Two symbols at the same condition represent a repeat setting of this condition within the same experiment. The slight differences observed in the WHSVs at different temperatures and pressures can be attributed to scatter of the records read from the weighing balance that carried the feed pot (see Figure 4-3) or irregular feed supply by the feed pump.

5.7.1 Effect of reaction temperature and space velocity

Reactions were conducted over all catalysts at 200°C, 225°C, 250°C, 275°C and 300°C respectively. For each temperature, a number of WHSV settings were tested in order to vary conversion. Several samples were collected and analysed at steady-state for each WHSV and temperature setting and average values of the results were determined, thus validating the trends observed (see Section 5.4.1).

5.7.1.1 *m*-Cresol conversion at different reaction temperatures and space velocities

Figures 5-26 through to 5-28 show *m*-cresol conversion versus WHSV at the different temperatures applied for all catalysts tested in the isopropylation of *m*-cresol.

At low reaction temperatures conversion increases with decreasing space velocity (indicated best by the 'long' WHSV series at 225°C). However, this increase is less proportional to 1/WHSV as was expected. Additionally, this trend reverses at the high reaction temperatures (most pronounced at 300°C).

It should be noted that the decline in conversion at the highest reaction temperatures when approaching the lowermost space velocities is not an artificial effect. This seemingly strange phenomenon was observed earlier (Nagooroo and Truter, 2008 and van der Merwe, 2012) and is explained in Sections 2.1.5.1 and 2.1.6.2.

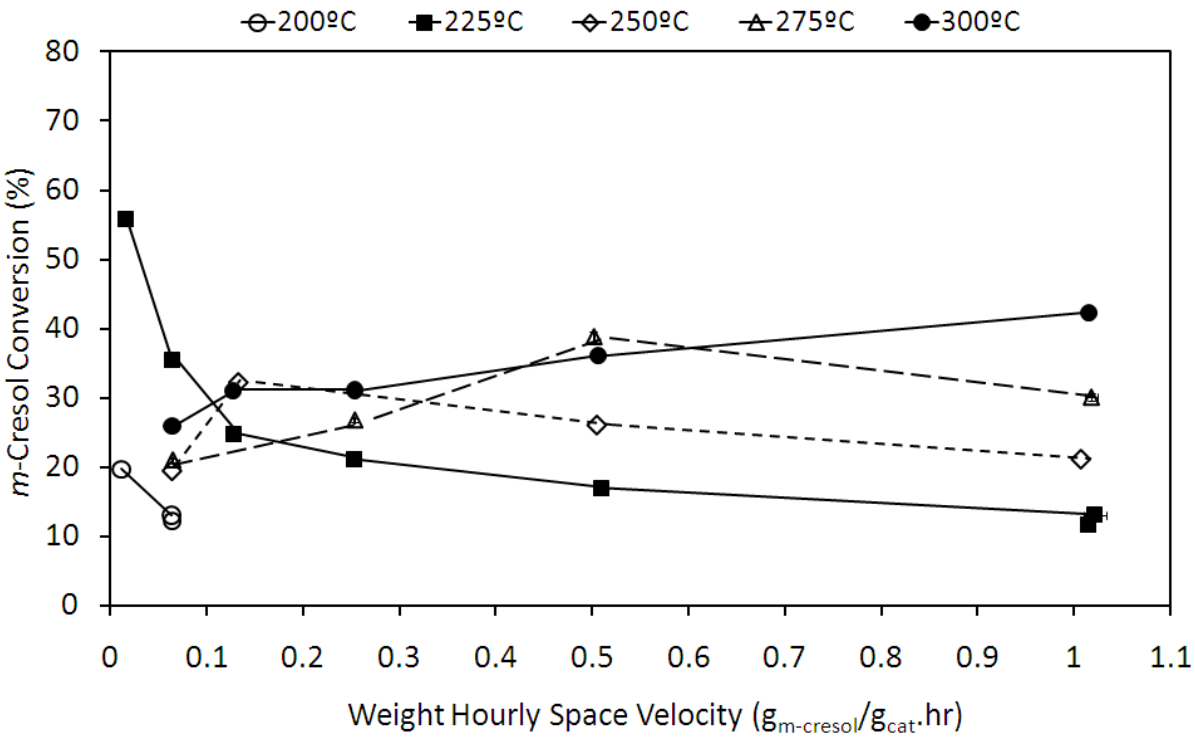

Figure 5-26: *m*-Cresol conversion vs. WHSV for isopropylation of *m*-cresol over the H-MFI-20 catalyst at different temperatures (at P = 3 bar (abs))

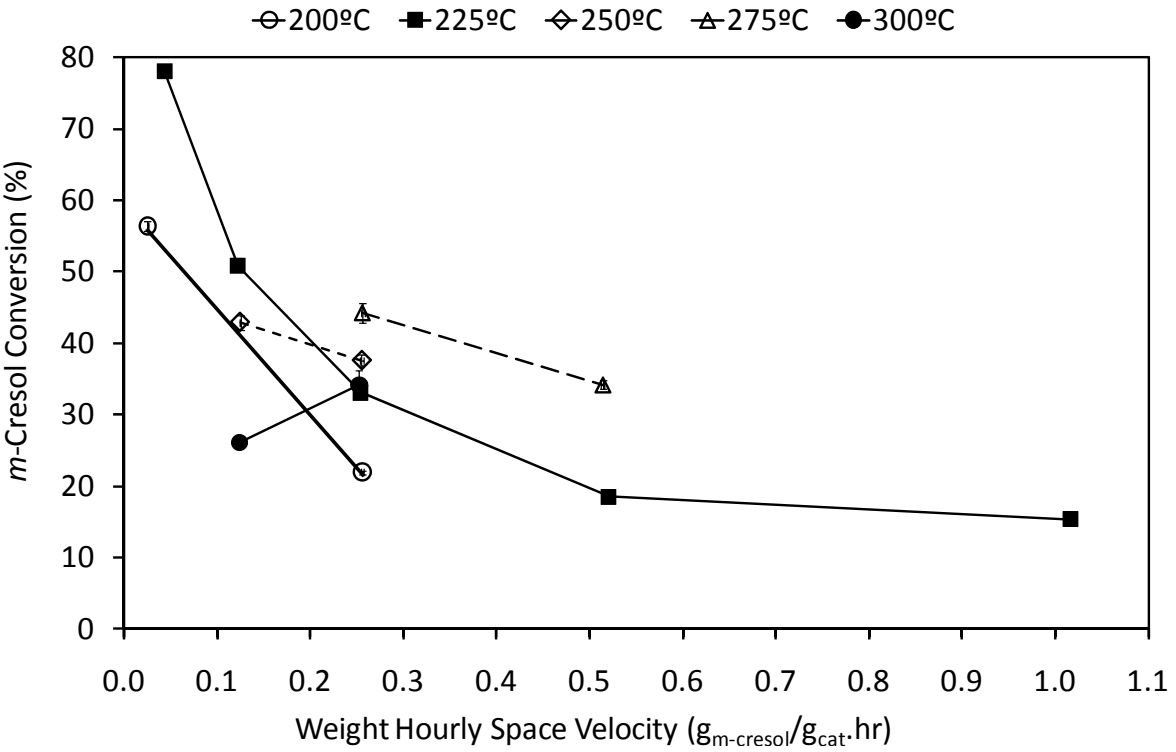

Figure 5-27: *m*-Cresol conversion vs. WHSV for isopropylation of *m*-cresol over the H-MFI-90 catalyst at different temperatures (at P = 3 bar (abs))

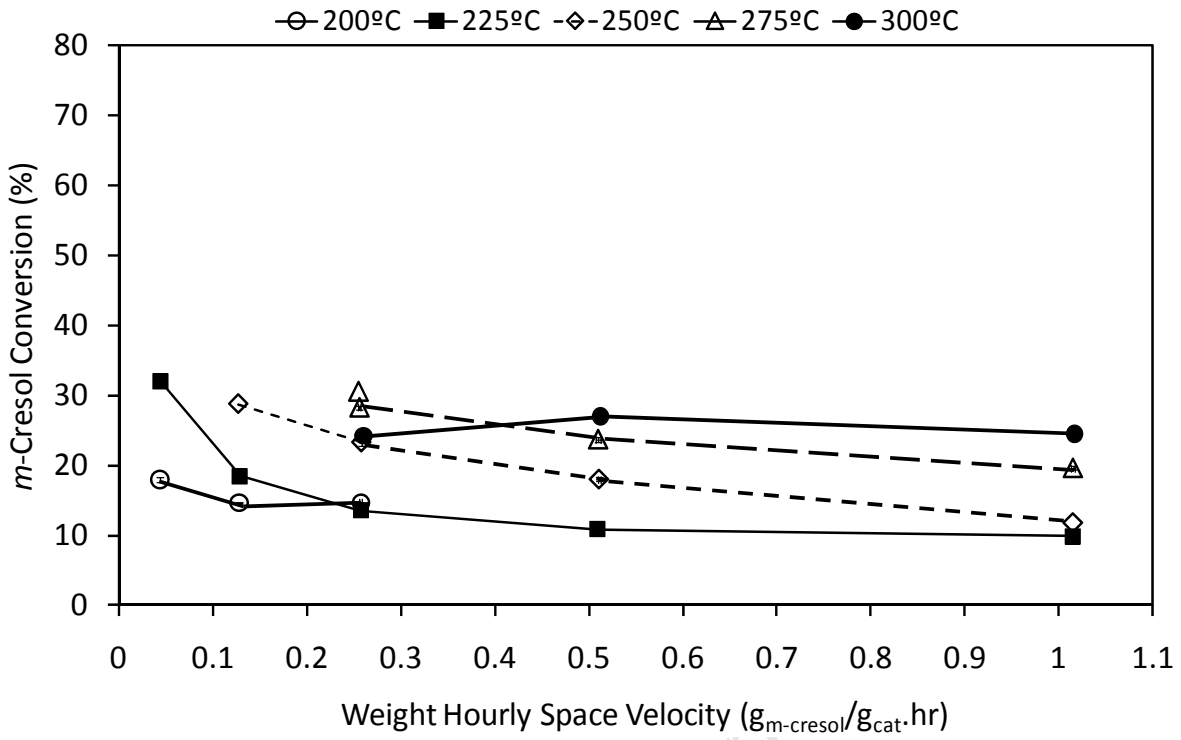

Figure 5-28: *m*-Cresol conversion vs. WHSV for isopropylation of *m*-cresol over the H-MFI-400 catalyst at different temperatures (at P = 3 bar (abs))

Catalyst activities are ranked clearly, best indicated by the 225°C series, in the following order:

H-MFI-90 > H-MFI-20 ≥ H-MFI-400.

The order is confirmed by the temperature series (see Figure 5-35**)**.

The said decline of conversion with decreasing WHSV appears most pronounced over the H-MFI-20 catalyst.

5.7.1.2 Thymol yield at different reaction temperatures

Figures 5-29 through to 5-31 show the thymol yield versus WHSV at different temperatures for all catalysts tested in the isopropylation of *m*-cresol.

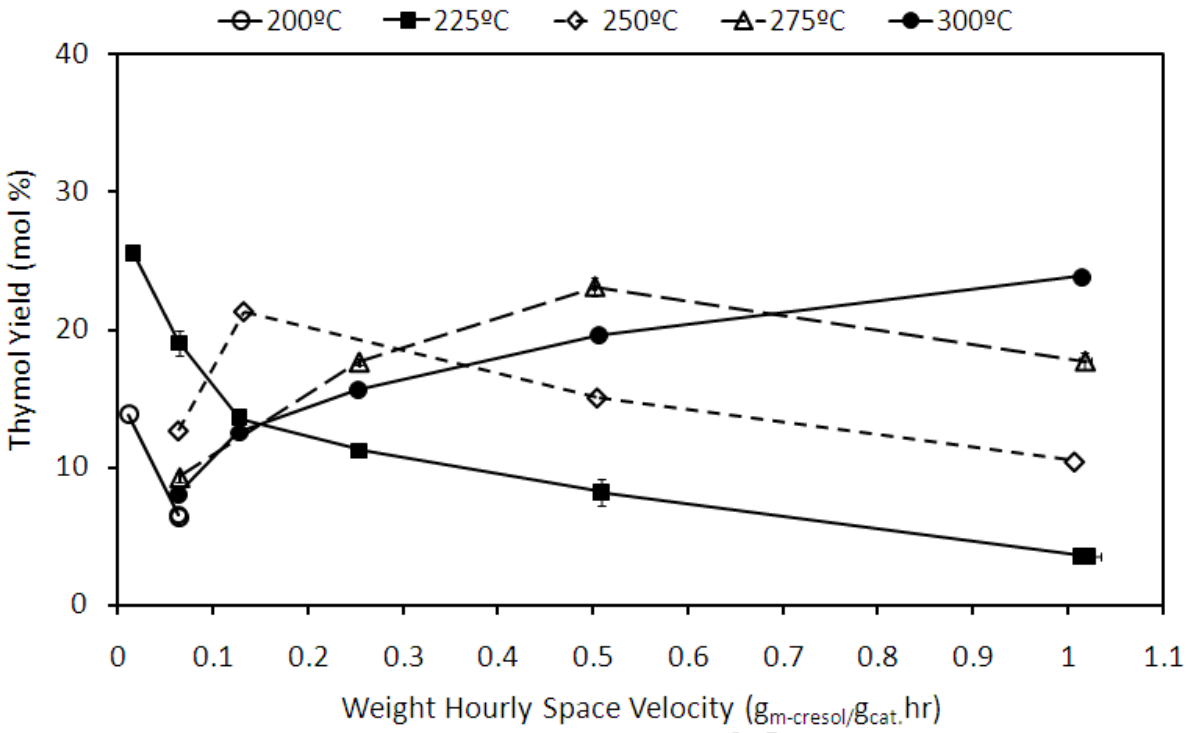

Figure 5-29: Thymol yield vs. WHSV for isopropylation of *m*-cresol over the H-MFI-20 catalyst at different temperatures (at P = 3 bar (abs))

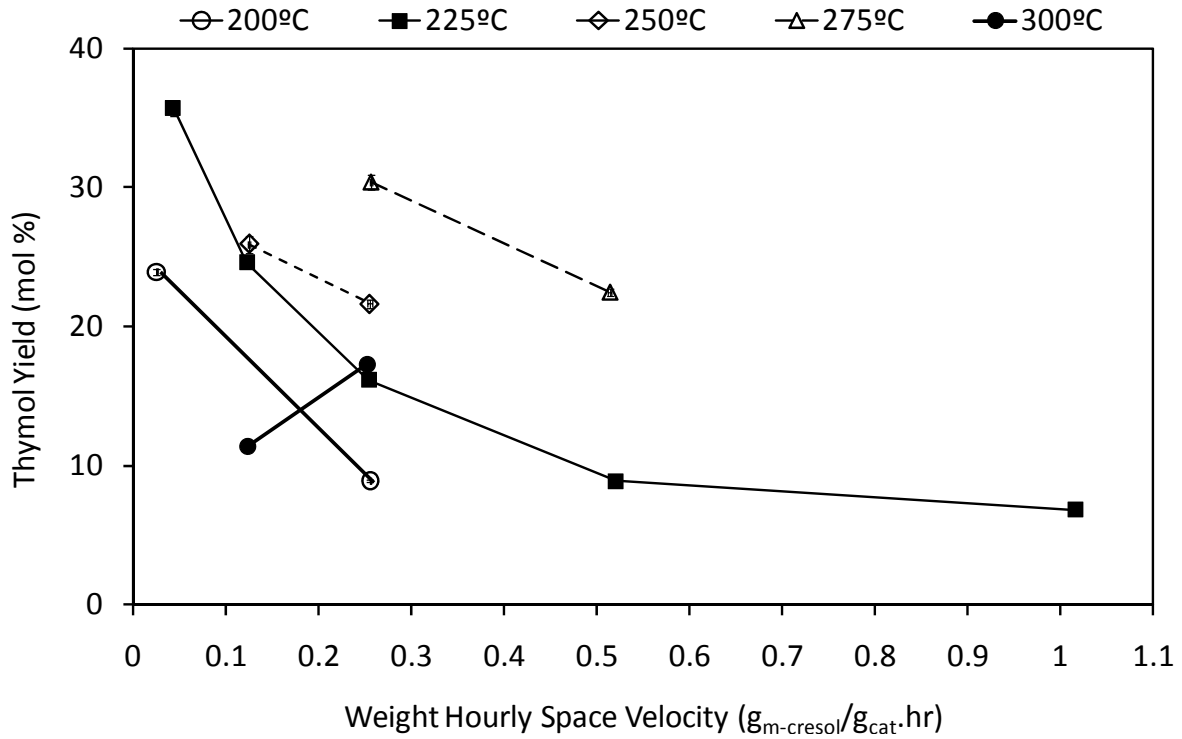

Figure 5-30: Thymol yield vs. WHSV for isopropylation of *m*-cresol over the H-MFI-90 catalyst at different temperatures (at P = 3 bar (abs))

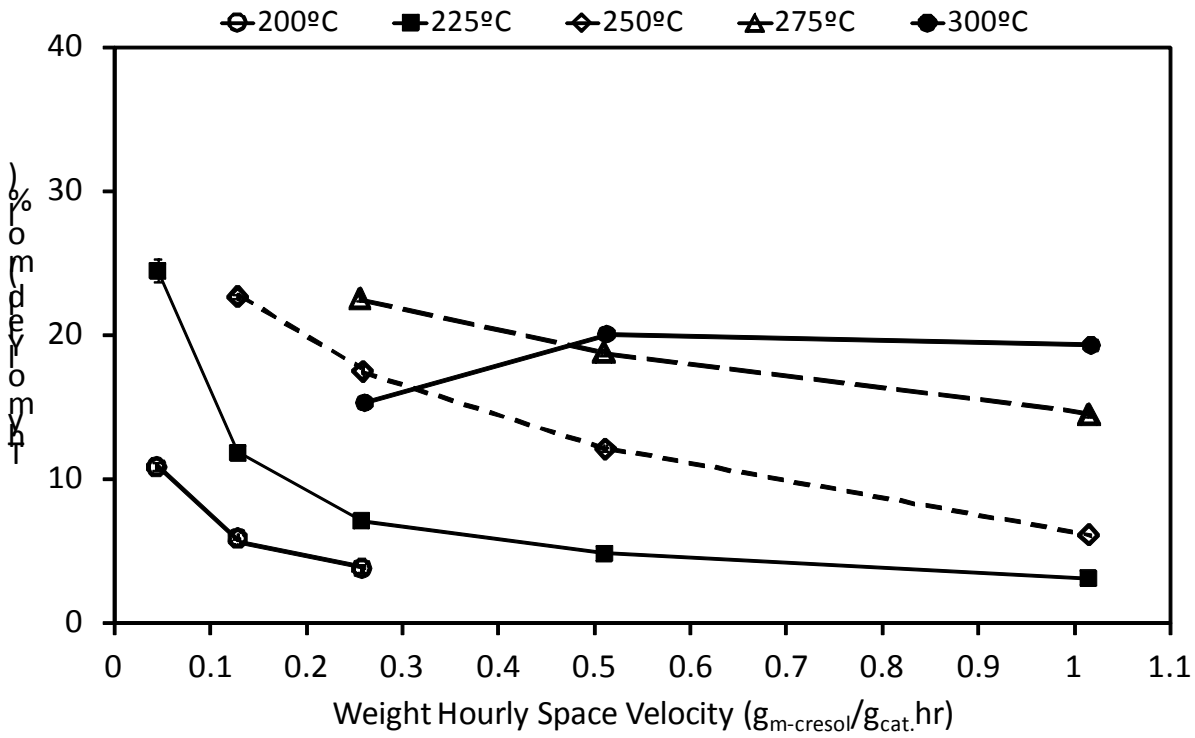

Figure 5-31: Thymol yield vs. WHSV for isopropylation of *m*-cresol over the H-MFI-400 catalyst at different temperatures (at P = 3 bar (abs))

Thymol yields show essentially the same pattern and trends on conversion with respect to reaction temperatures and catalyst. However, differences in yields appear somewhat more pronounced than differences in conversion, in particular over the least active catalyst H-MFI-400.

5.7.1.3 Thymol selectivity at different reaction temperatures

Figures 5-32 through to 5-34 show the thymol selectivity versus WHSV at different temperatures for all catalysts tested in the isopropylation of *m*-cresol.

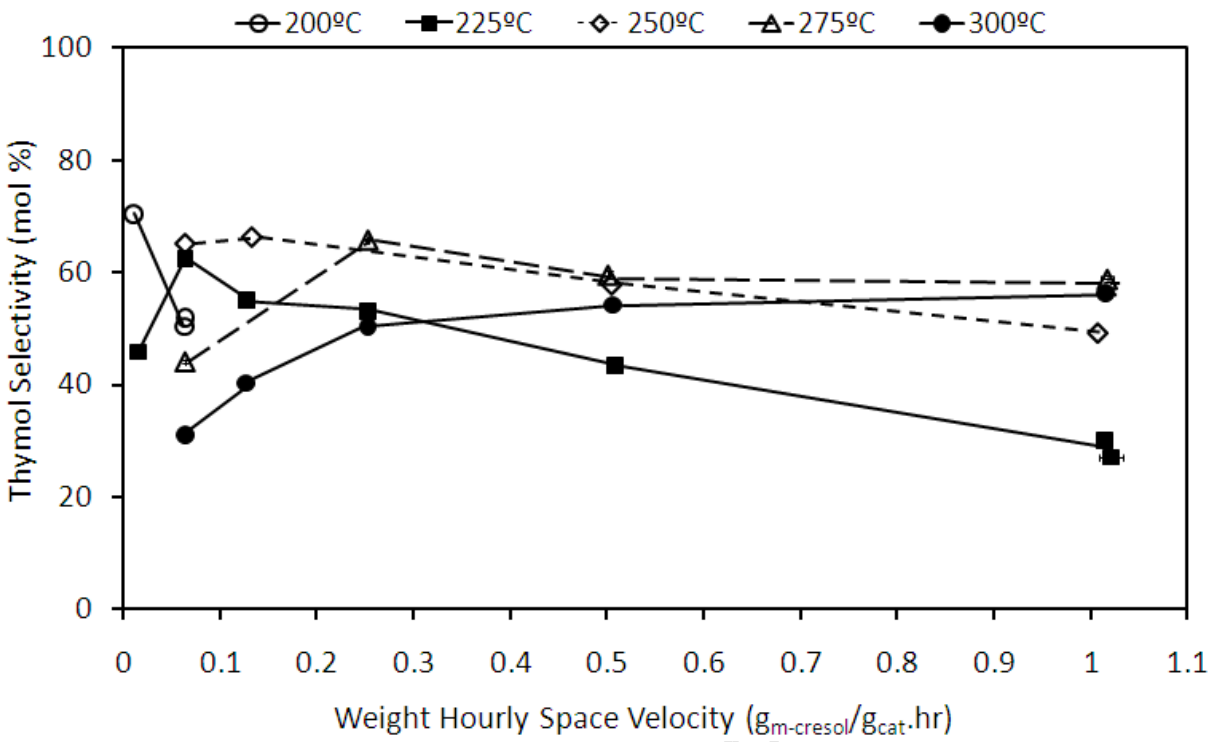

Figure 5-32: Thymol selectivity vs. WHSV for isopropylation of *m*-cresol over the H-MFI-20 catalyst at different temperatures (at P = 3 bar (abs))

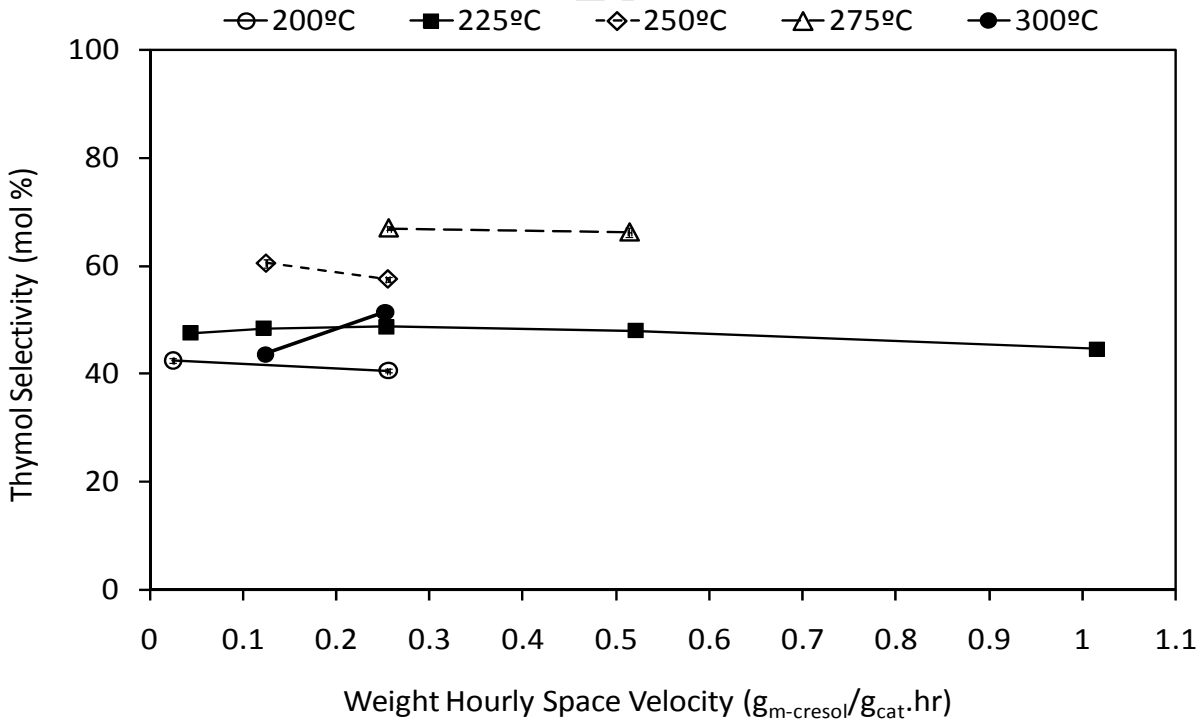

Figure 5-33: Thymol selectivity vs. WHSV for isopropylation of *m*-cresol over the H-MFI-90 catalyst at different temperatures (at P = 3 bar (abs))

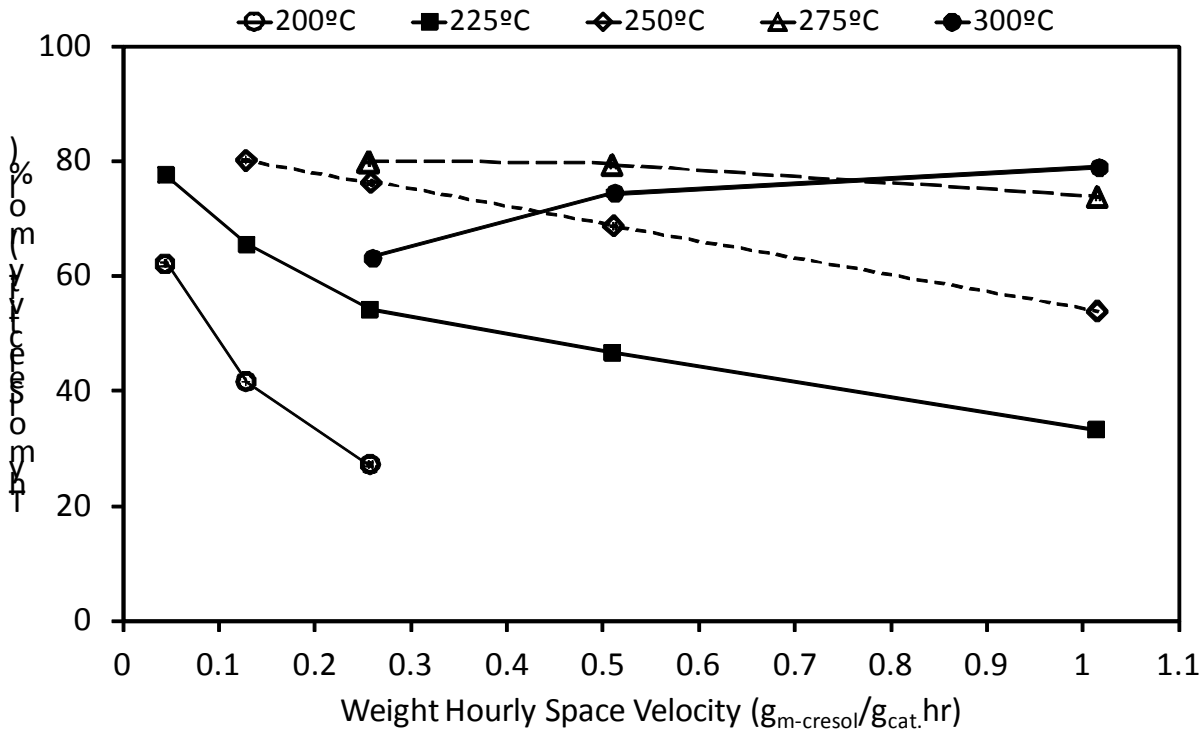

Figure 5-34: Thymol selectivity vs. WHSV for isopropylation of *m*-cresol over the H-MFI-400 catalyst at different temperatures (at P = 3 bar (abs))

Trends in thymol selectivities with variation of space velocity are similar over all three of the catalysts. However, over the more active catalysts, H-MFI-20 and H-MFI-90, and over the least active catalyst H-MFI-400 at the higher temperatures (and conversions), the effects of both temperature and space velocity are comparatively small, while this is not evident over the H-MFI-400 at the lowermost temperatures and conversions.

5.7.1.4 Effect of temperature on yields of major products

Figure 5-35 and Figure 5-36 compare the direct influence of temperature on *m*-cresol conversion, extent of C-mono-isopropylation (total isomers yield), thymol yield and the yields of the most abundant by-products over the catalysts tested.

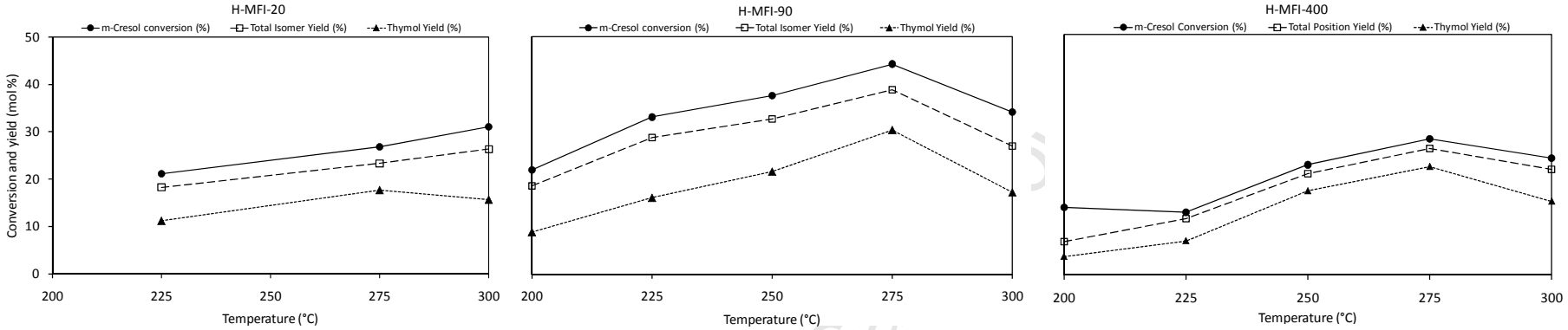

Figure 5-35: Effect of temperature on *m*-cresol conversion and yields of thymol and total ring mono-isopropylated products over zeolites tested (at WHSV = 0.25 $g_{m\text{-cresol}}/g_{cat}$.hr, P = 3 bar (abs))

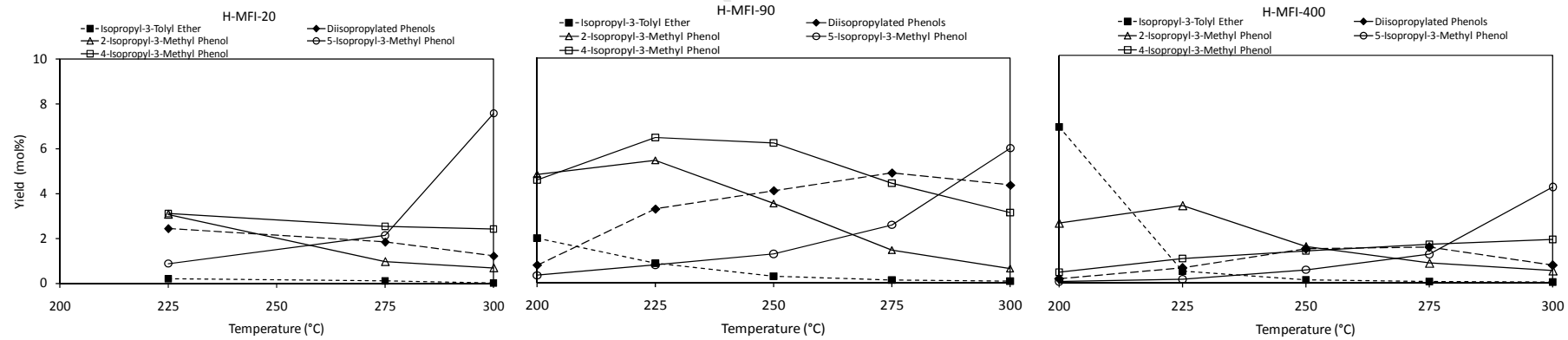

Figure 5-36: Effect of temperature on the yields of the most abundant by-products over zeolites tested (at P = 3 bar (abs), WHSV = 0.25 $g_{m\text{-cresol}}/g_{cat}$.hr))

The temperature series corresponds to the results obtained from the space velocity series, namely the following order of catalyst activity

H-MFI-90 > H-MFI-20 ≥ H-MFI-400

The previously observed decline of conversion at high temperatures, when reducing space velocity to very low values (see Section 5.7.1.1) is observed again (the temperature series was carried out at the rather low WHSV of 0.25 $g_{m\text{-cresol}}/g_{cat}$.hr.

Yields of the most abundant by-products show a constant decline of the yield of isopropyl-3-tolyl ether with increasing temperature and a constant increase in the yield of 5-isopropyl-3-methyl phenol. All other products shown appear to pass over a yield maximum with an increase in temperature. These trends are similar to those observed when reducing space velocity.

5.7.1.5 Effect of reaction pressure

In order to investigate the effect of reaction pressure, reactions were conducted over the catalyst and under the reaction conditions found optimal as determined from the reaction temperature and WHSV experiments. (It should be noted that "optimum" did not simply refer to activities but mostly to thymol and by-product selectivities). Experimental runs were thus conducted over the H-MFI-400 catalyst at T = 275°C, WHSV = 0.25-1.03 $g_{m\text{-cresol}}/g_{cat}$.hr and P = 1.5, 3, 6 and 12 bar (abs), respectively.

5.7.1.6 *m*-Cresol conversion at different reaction pressures and space velocities

Figure 5-37 and Figure 5-38 show *m*-cresol conversion versus WHSV for the isopropylation of *m*-cresol over the H-MFI-400 catalyst at different pressures and versus pressure at different WHSVs, respectively.

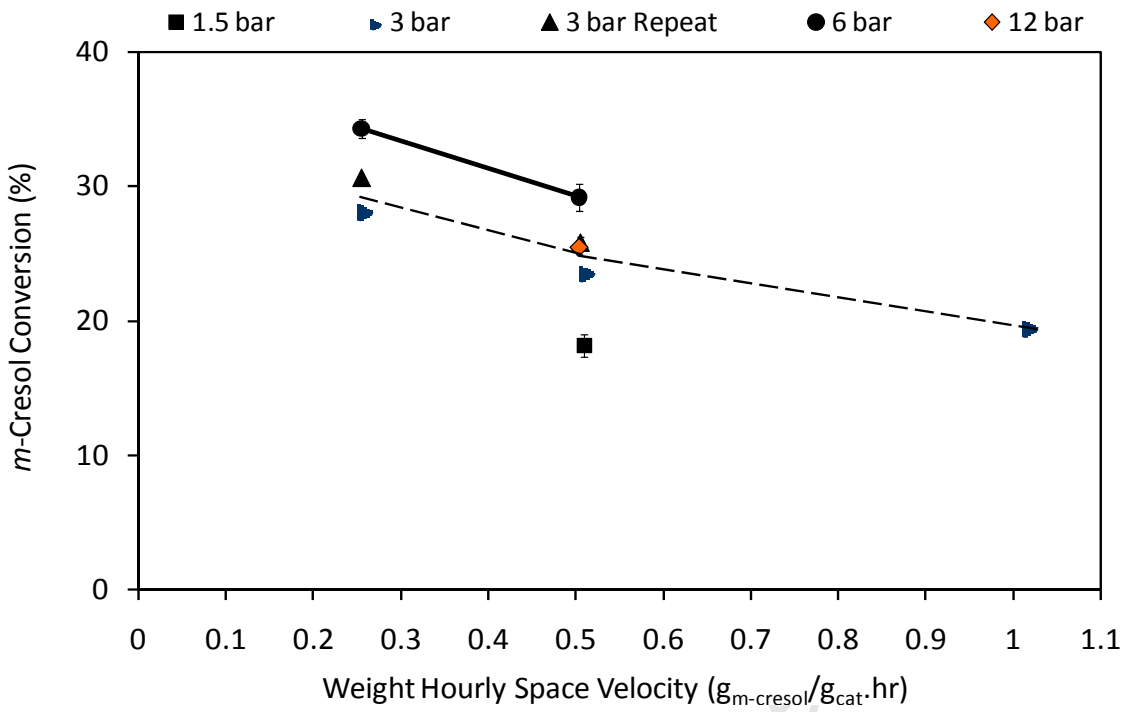

Figure 5-37: *m*-Cresol conversion vs. WHSV for isopropylation of *m*-cresol over the H-MFI-400 catalyst at different pressures (abs) (at T = 275°C)

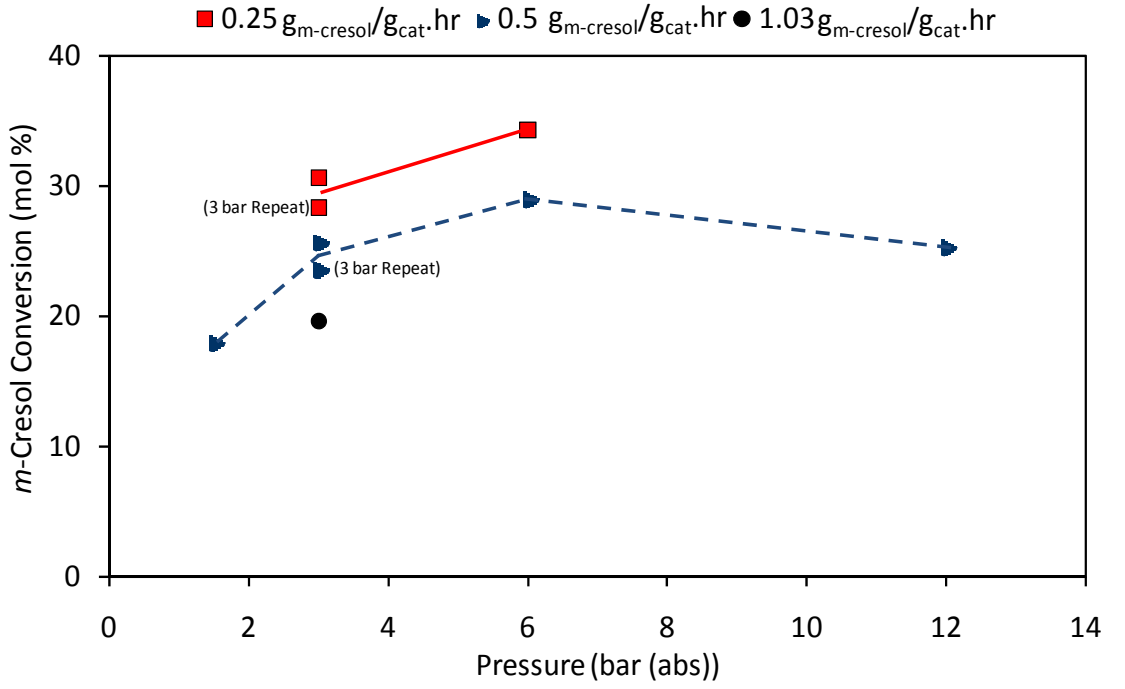

Figure 5-38: *m*-Cresol conversion versus pressure for isopropylation of *m*-cresol over the H-MFI-400 catalyst at different WHSV (at T = 275°C)

Lower space velocity, as reported earlier (see Section 5.7.1.1), results in a moderate increase in conversion at both 3 bar and 6 bar reaction pressure. In general, higher pressure increases conversion, although to a rather small extent in the pressure range studied. Conversion less than doubles after a fourfold increase in pressure (WHSV = 0.5$g_{m\text{-cresol}}/g_{cat}$.hr). The reverse in trend at 12 bar is, however, only indicated by a single data point and is therefore rather inconclusive.

5.7.1.7 Thymol yield at different reaction pressures and space velocities

Figure 5-39 and Figure 5-40 show thymol yield versus WHSV for the isopropylation of *m*-cresol over the H-MFI-400 catalyst at different pressures and versus pressure at different WHSVs, respectively. Figure 5-41 shows thymol yield versus conversion.

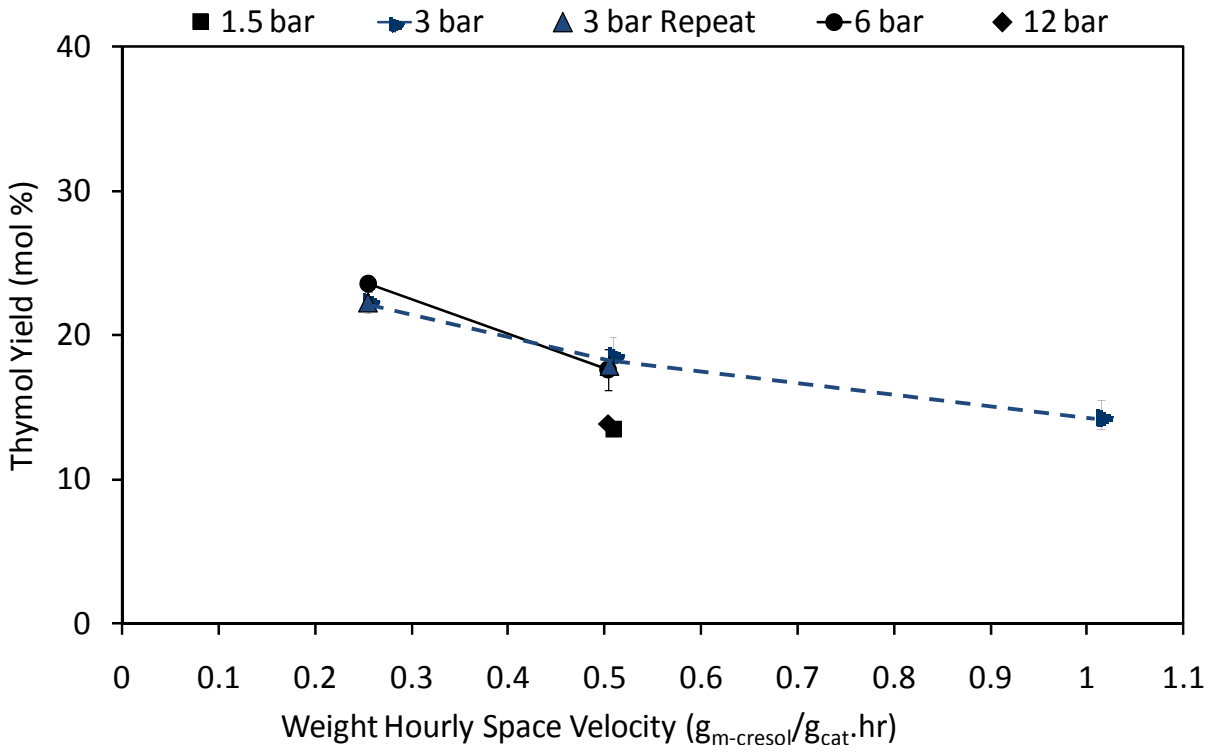

Figure 5-39: Thymol yield versus WHSV for isopropylation of *m*-cresol over the H-MFI-400 catalyst at different pressures (at T = 275°C)

Pressure has a similar effect on thymol yield as on conversion. However, as Figure 5-41 indicates, thymol yield, at constant conversion, declines with increasing pressure.

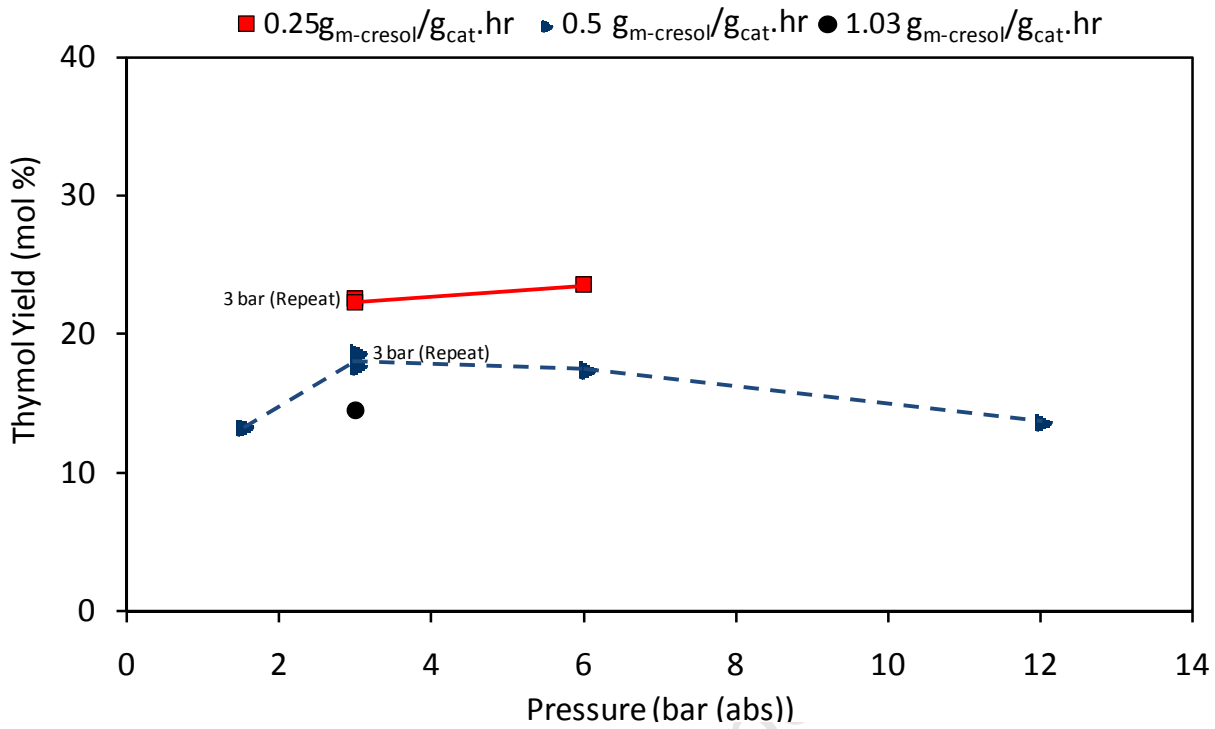

Figure 5-40: Thymol yield versus pressure for isopropylation of *m*-cresol over the H-MFI-400 catalyst at different WHSV (T = 275°C)

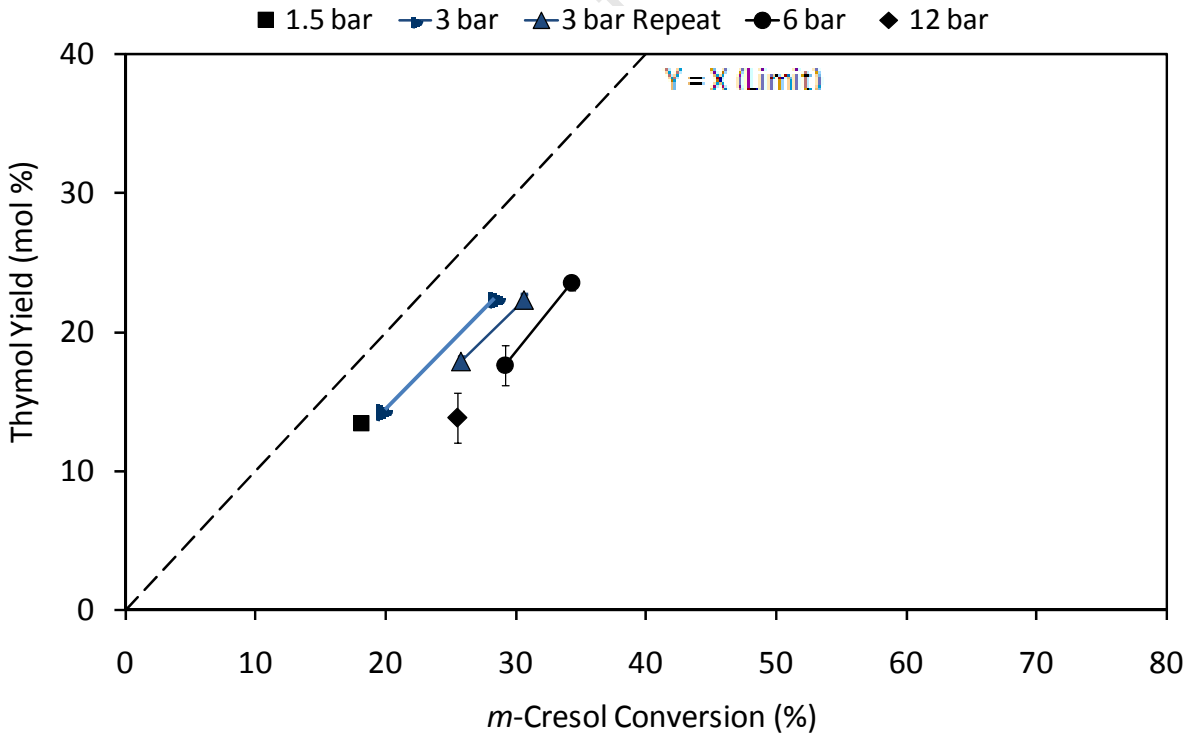

Figure 5-41: Thymol yield versus *m*-cresol conversion for isopropylation of *m*-cresol over the H-MFI-400 catalyst at different pressures (at T = 275°C)

5.7.1.8 Thymol selectivity at different reaction pressures and space velocities

Figure 5-42 to Figure 5-44 show thymol selectivity versus WHSV for the isopropylation of *m*-cresol over the H-MFI-400 catalyst at different pressures, versus pressure at different WHSVs and versus conversion respectively.

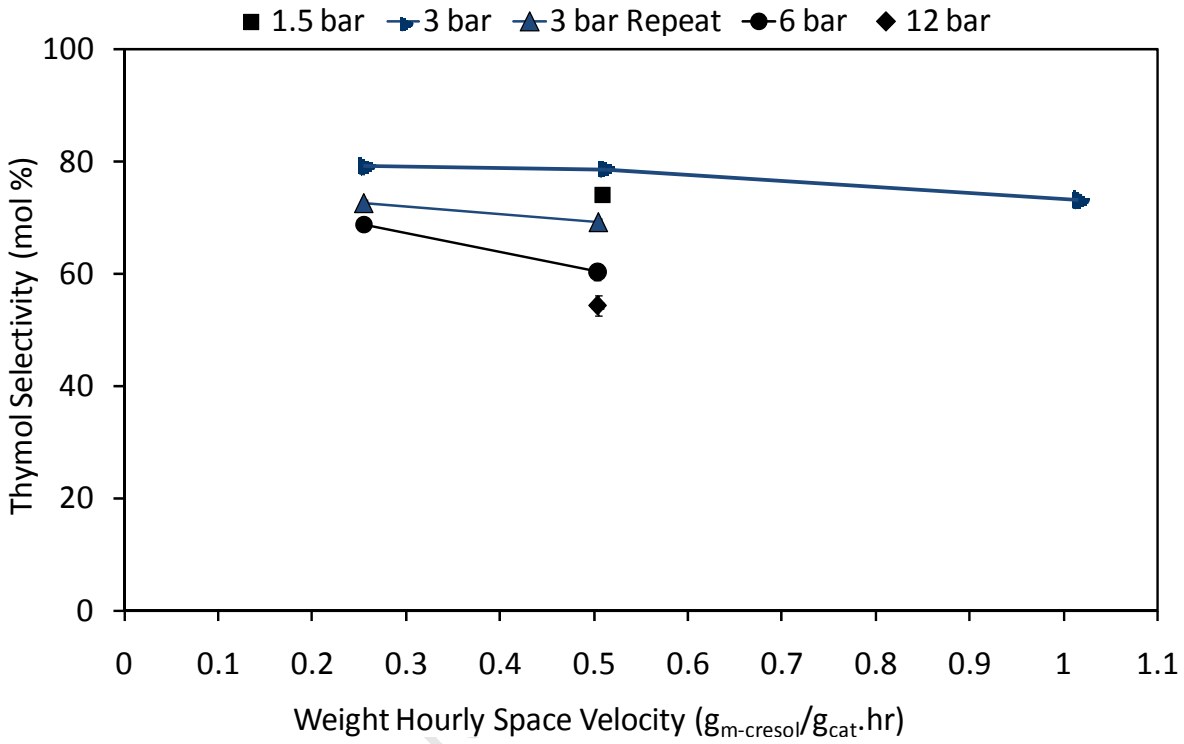

Figure 5-42: Thymol selectivity versus WHSV for isopropylation of *m*-cresol over the H-MFI-400 catalyst at different pressures (abs) (at T = 275°C)

As the figures indicate, the effect of pressure is obvious and consistent in the case of thymol selectivity. Higher pressure was found to reduce thymol selectivity.

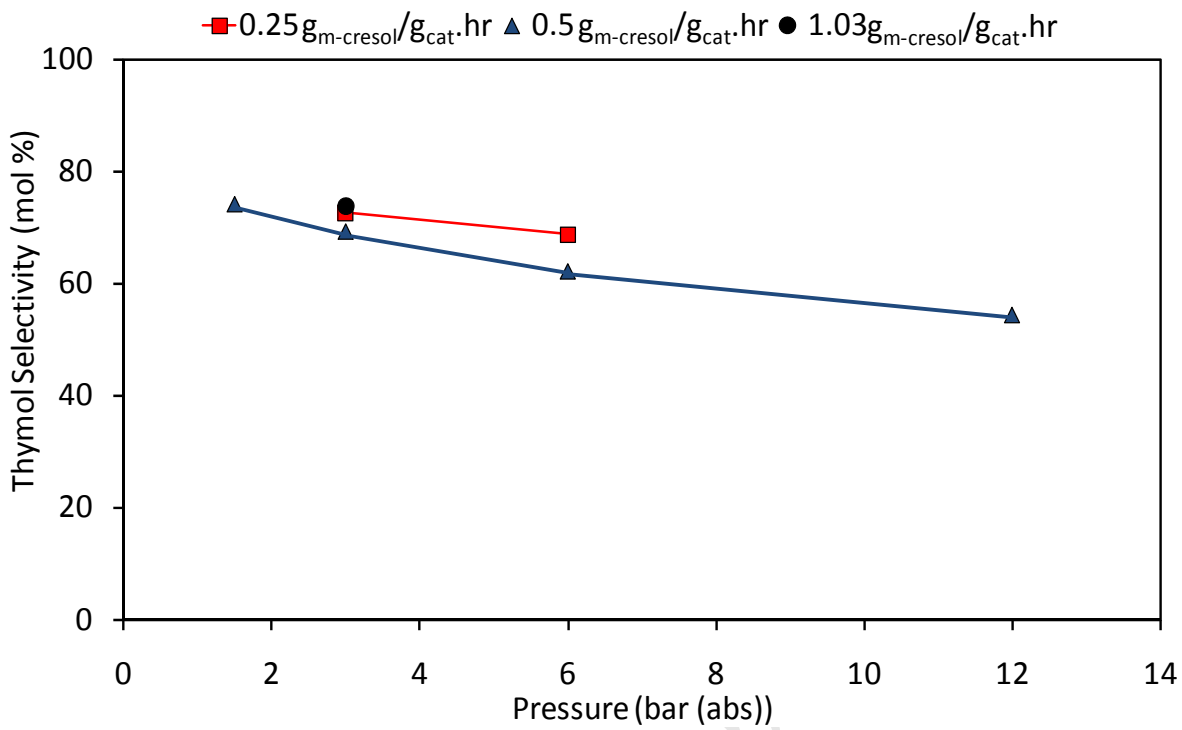

Figure 5-43: Thymol selectivity versus pressure for isopropylation of *m*-cresol over the H-MFI-400 catalyst at different WHSV (at T = 275°C)

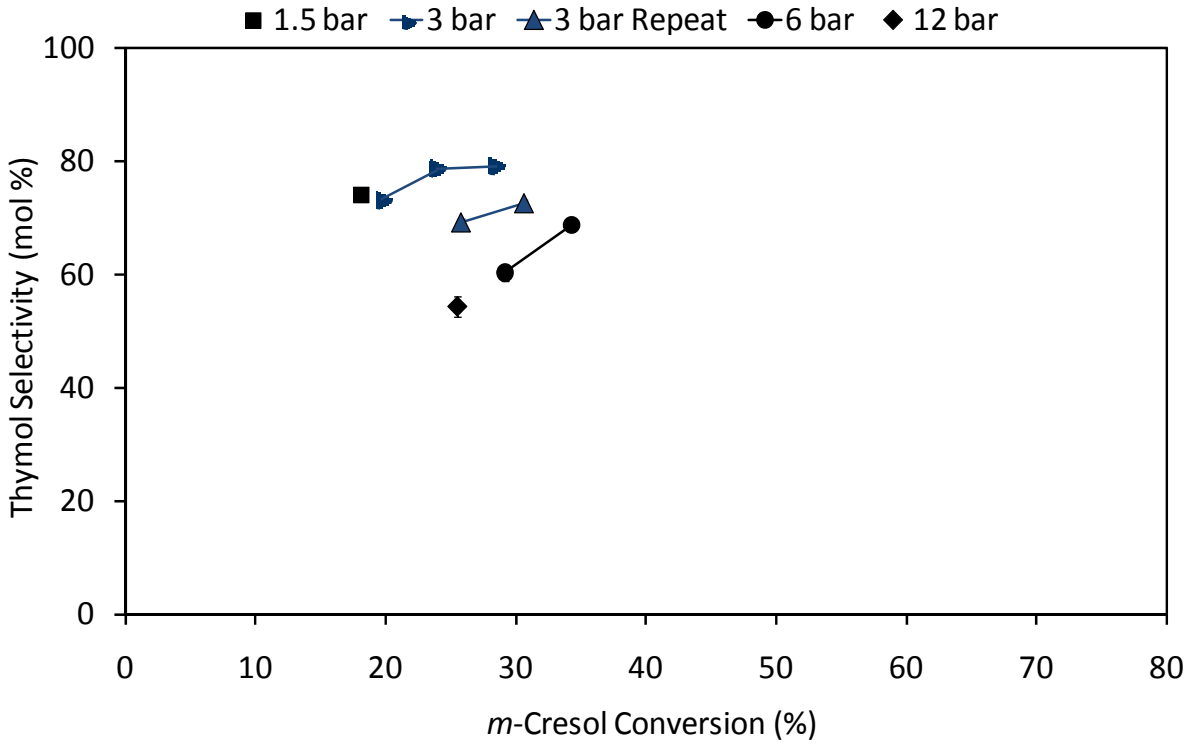

Figure 5-44: Thymol selectivity versus *m*-cresol conversion for isopropylation of *m*-cresol over the H-MFI-400 catalyst at different WHSV (at T = 275°C)

5.7.1.9 Yield of diisopropylated *m*-cresol compounds at different space velocities and reaction pressures

Figure 5-45 to Figure 5-47 show the yield of diisopropylated *m*-cresol compounds versus WHSV for the isopropylation of *m*-cresol over the H-MFI-400 catalyst at different pressures, versus pressure at different WHSVs and versus conversion respectively.

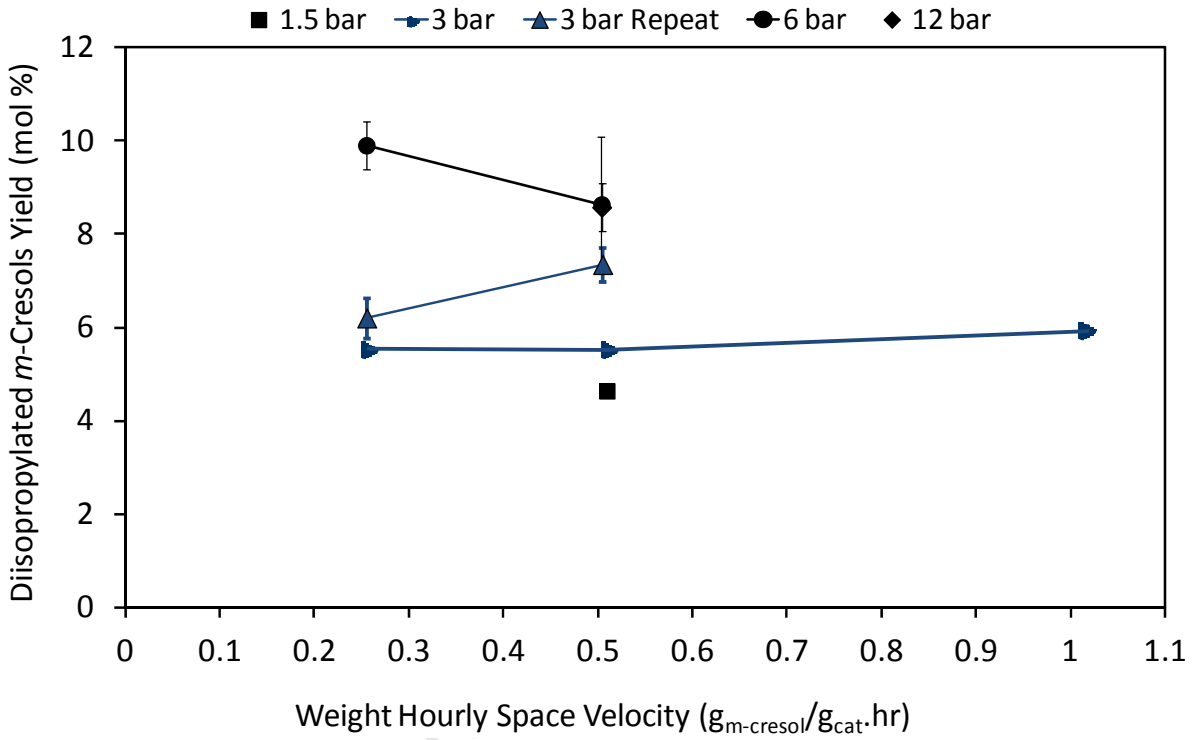

Figure 5-45: Diisopropylated *m*-cresol compounds yield versus WHSV for isopropylation of *m*-cresol over the H-MFI-400 catalyst at different pressures (abs) (at T = 275°C)

While space velocity has hardly any effect, the yields of the diisopropylated by-products increase significantly with increasing pressure, mirroring the decline in thymol selectivity.

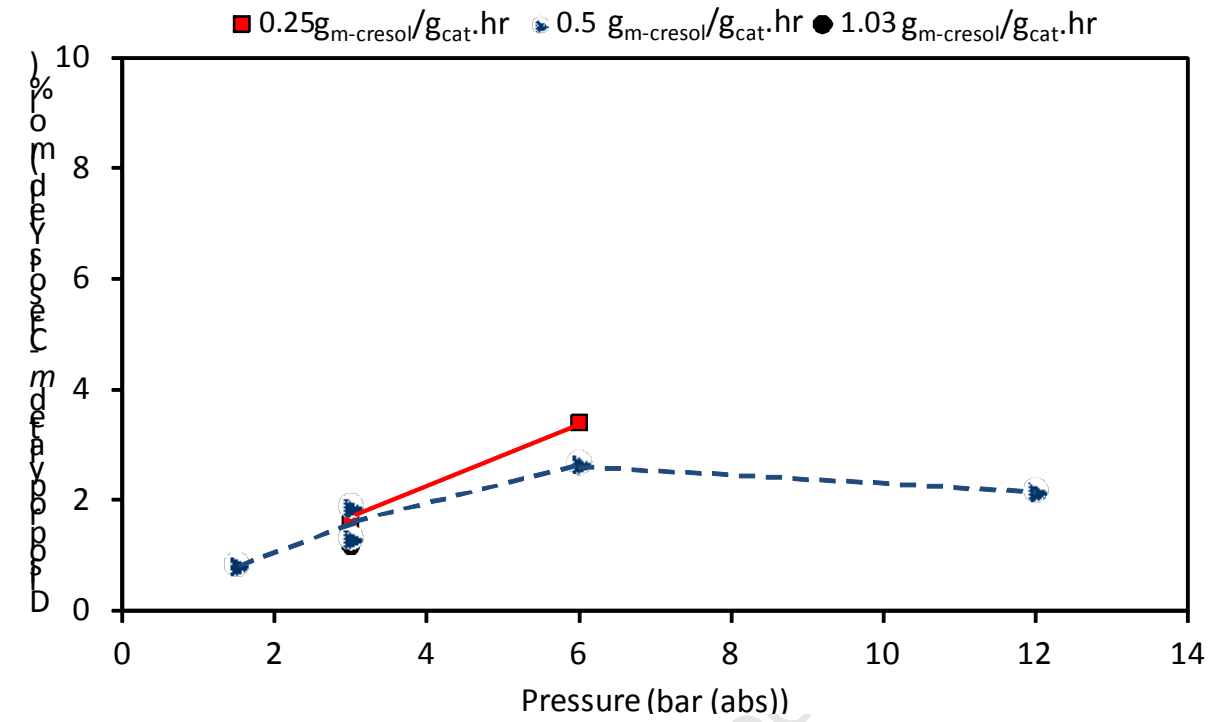

Figure 5-46: Diisopropylated *m*-cresol compounds yield versus pressure for isopropylation of *m*-cresol over H-MFI-400 catalyst at different WHSVs (at T=275°C)

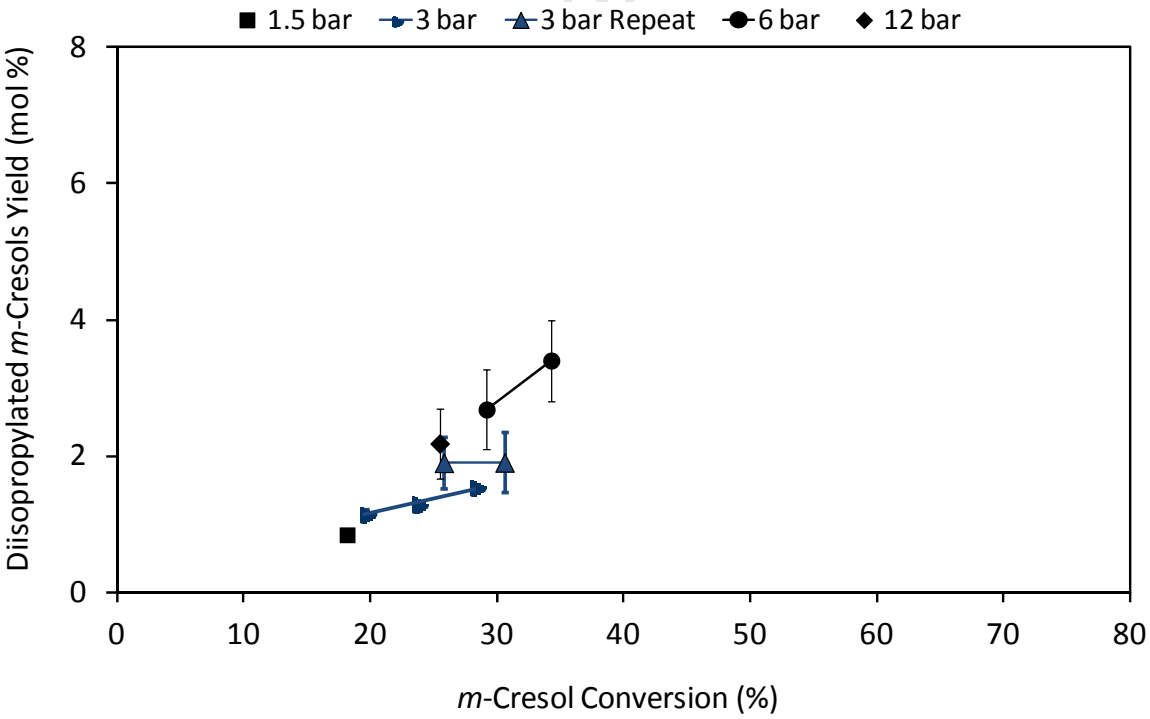

Figure 5-47: Diisopropylated *m*-cresol compounds yield versus *m*-cresol conversion for isopropylation of *m*-cresol over the H-MFI-400 catalyst at different pressures (abs) (at T = 275°C)

5.7.1.10 Selectivity of diisopropylated *m*-cresol compounds at different space velocities and reaction pressures

Figure 5-48 to Figure 5-50 show the selectivity of the diisopropylated *m*-cresol compounds selectivity versus WHSV for the isopropylation of *m*-cresol over the H-MFI-400 catalyst at different pressures, versus pressure at different WHSVs and versus conversion at different pressures, respectively.

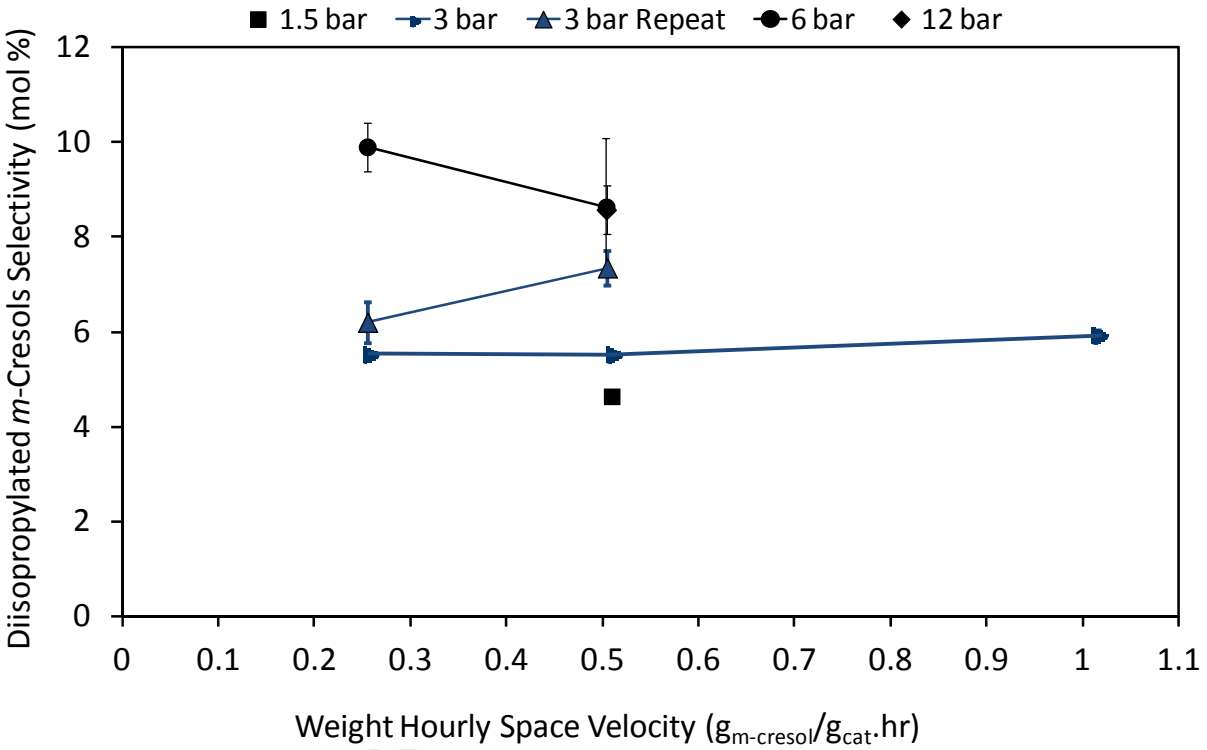

Figure 5-48: Diisopropylated *m*-cresol compounds selectivity versus WHSV for isopropylation of *m*-cresol over the H-MFI-400 catalyst at different pressures (abs) (at T = 275°C)

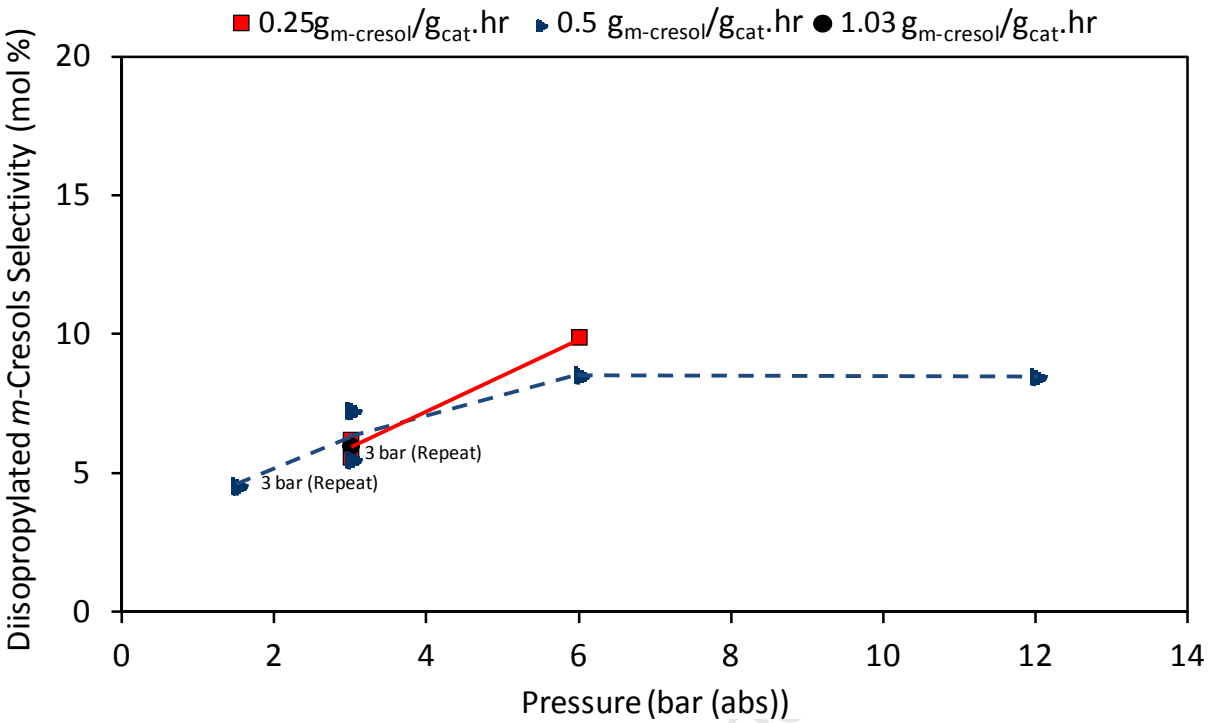

Figure 5-49: Diisopropylated *m*-cresol compounds selectivity versus pressure for isopropylation of *m*-cresol over the H-MFI-400 catalyst at different WHSV (at T = 275°C)

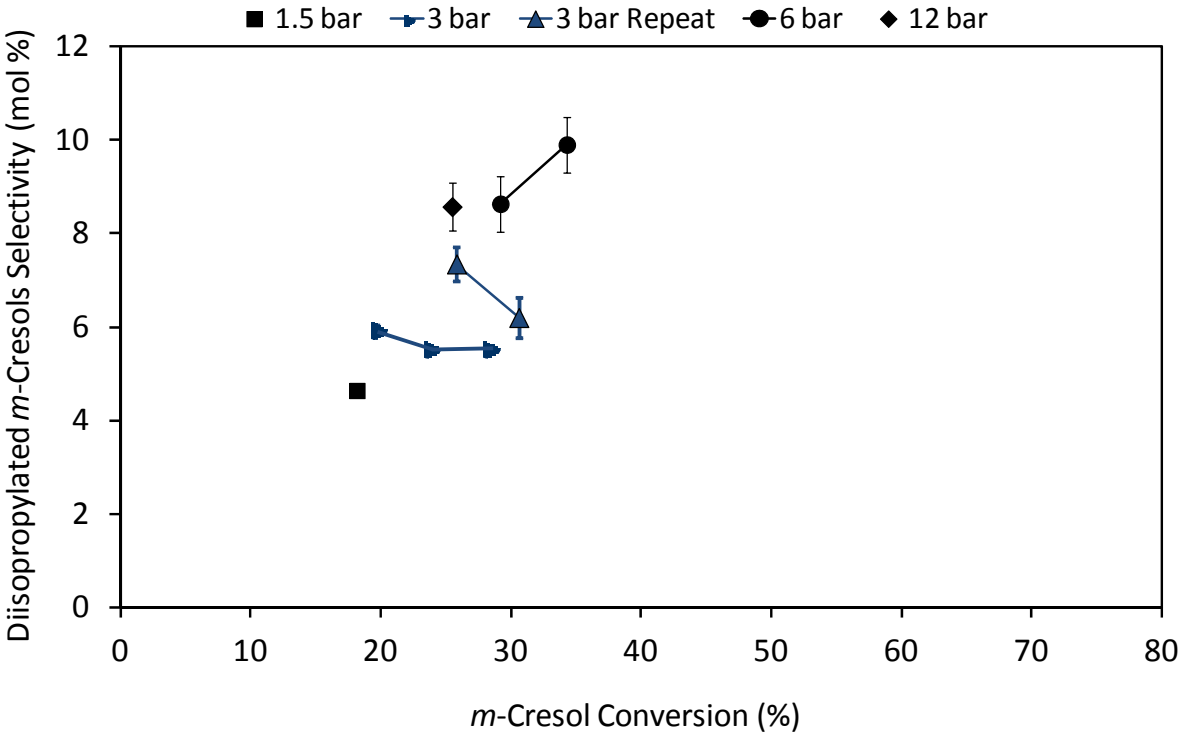

Figure 5-50: Diisopropylated *m*-cresol compounds selectivity versus *m*-cresol conversion for isopropylation of *m*-cresol over the H-MFI-400 catalyst at different pressure (at T = 275°C)

Figures indicate that pressure has a direct effect on the selectivity of diisopropylated *m*-cresol compounds, which increases significantly with an increase in pressure, but confirm, that space velocity has no effect.

It is also obvious that the trends of declining thymol selectivity with increasing pressure (see Figure 5-43 and Figure 5-44) and increasing selectivity of diisopropylated *m*-cresol compounds with increasing pressure (see Figure 5-48 and Figure 5-49) correlate qualitatively.

On the other hand, both thymol selectivity and selectivity of diisopropylated *m*-cresol compounds increase with increasing conversion (over the range of conversions covered).

5.8 Physico-chemical catalyst characterisation

5.8.1 X-Ray Fluorescence Spectroscopy (XRF)

Table 5-4 summarises the results of the elemental analysis of the MFI zeolite catalysts tested, as obtained from XRF spectroscopy (see Sections 2.3.2 and 4.3.1).

The actual molar SiO_2/Al_2O_3 ratios were determined by the conversion of the weight percentages of SiO_2 and Al_2O_3 reported by XRF into molar values. The molar values were then used to calculate the actual molar SiO_2/Al_2O_3 ratios as follows:

Equation 5-1: Calculation for actual molar SiO_2/Al_2O_3 ratio using XRF elemental analysis results

$$n_{SiO2} = \frac{m_{SiO2}(\%)}{M_{SiO2} \times 100}$$

$$n_{Al2O3} = \frac{m_{Al2O3}(\%)}{M_{Al2O3} \times 100}$$

$$\frac{n_{SiO2}}{n_{Al2O3}} = \frac{m_{SiO2}(\%) \times M_{Al2O3}}{m_{Al2O3}(\%) \times M_{SiO2}}$$

Where

n_{SiO2} and n_{Al2O3} = Molar quantities of SiO_2 and Al_2O_3

m_{SiO2} and m_{Al2O3} = Mass percentages of SiO_2 and Al_2O_3 as determined by XRF (see Table 5-4)

M_{SiO2} and M_{Al2O3} = Molecular masses of SiO_2 and Al_2O_3

Table 5-4: Chemical analysis of H-MFI crystal agglomerate powder using XRF technique

Sample code*	**HMFI-20**	**HMFI-90 (powder)****	**H-MFI-400*****
SiO_2 (wt%)****	90.49	97.07	-
Al_2O_3 (wt%)****	7.96	1.77	-
Reported SiO_2/Al_2O_3 molar ratio*****	20	90	400
Actual SiO_2/Al_2O_3 molar ratio	19.3	93.7	-

* General product designation (Süd-Chemie)

** A sample of H-MFI-90 (Süd-Chemie) in crystal agglomerates powder form (without binder) was analysed as a reference though not tested in this study

*** H-MFI-400 was only available in extrudate form (with alumina binder)

**** Actual alumina and silica content as determined by XRF

***** From general product designation, -20, -90 and -400 (Süd-Chemie)

The data in Table 5-4 for the zeolite catalysts in crystal agglomerates powder form, H-MFI-20 and H-MFI-90, confirm the close proximity of the actual compositions to the reported composition (product designation). It was assumed that this also holds for the H-MFI-400 sample.

5.8.2 Scanning Electron Microscopy (SEM)

Figures 5-51 to 5-53 show the scanning electron micrographs of the H-MFI zeolites of different SiO_2/Al_2O_3 ratios tested in this study (see Sections 2.3.1 and 4.3.2). Table 5-5 summaries the results of the analyses of the micrographs with respect to the morphology and average crystal size of the various zeolite samples.

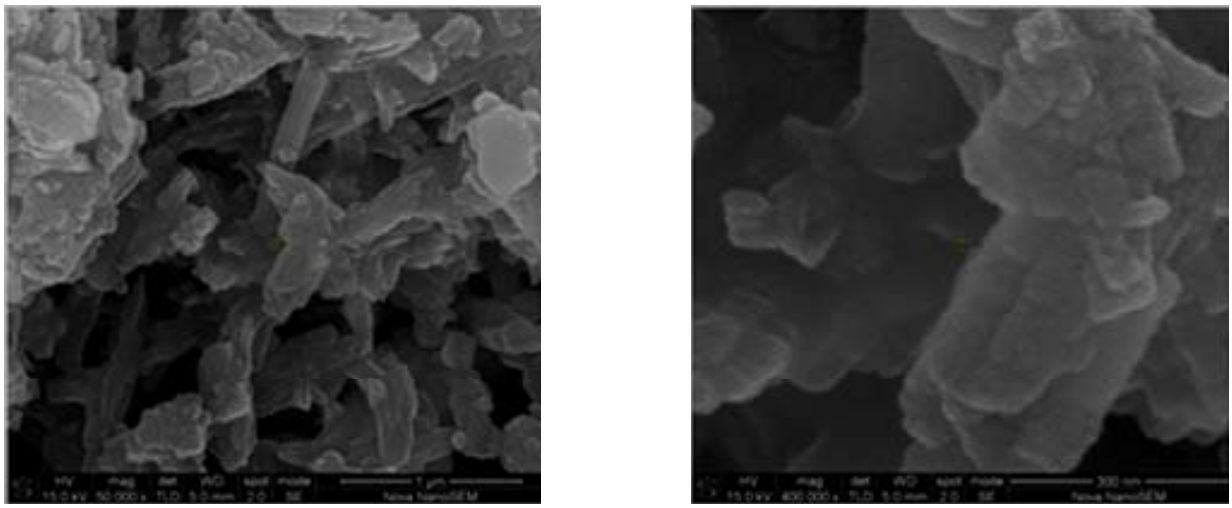

Figure 5-51: Scanning electron micrograph of H-MFI-20 (crystal agglomerates powder; size of agglomerates 0.1 – 0.5 µm)

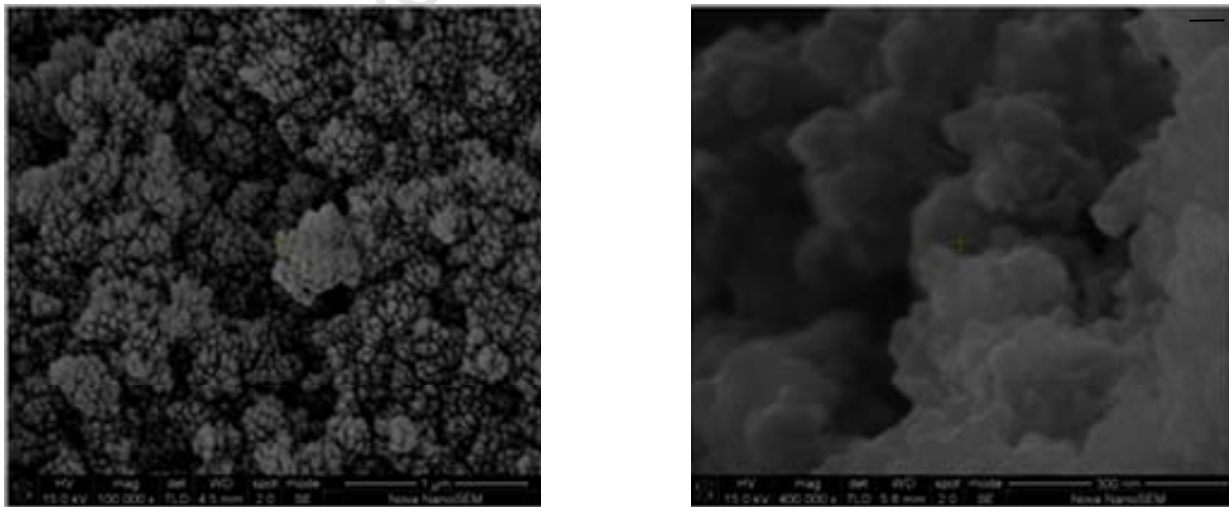

Figure 5-52: Scanning electron micrograph of H-MFI-90 (crystal agglomerates powder, size of agglomerates ≤ 1 µm)

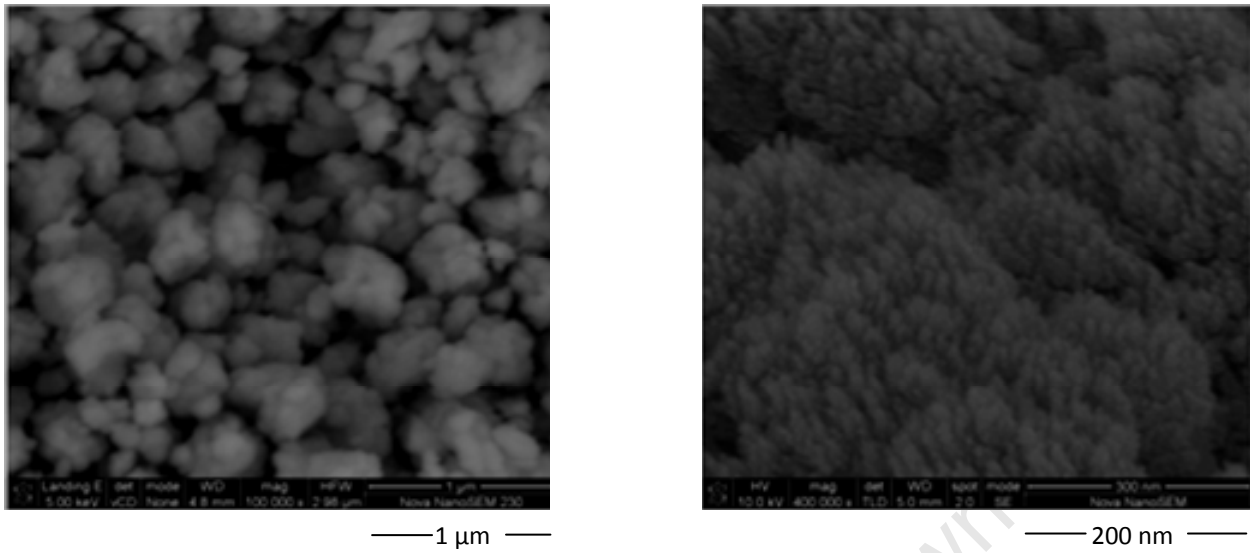

Figure 5-53: Scanning electron micrograph of H-MFI-400 (extrudates, external surface, diameter of extrudates 1/16, see Table 4-1)

Table 5-5: Morphology and crystal size of H-MFI zeolites tested

Sample code	Morphology of crystals	Critical dimension of primary zeolite crystallite
H-MFI-20	Packed Platelets	Thickness several 10 nm
H-MFI-90	Approximated as spherical	Diameter < 10 nm
H-MFI-400	Approximated as spherical	Diameter < 10 nm

5.8.3 ^{27}Al Solid-State Nuclear Magnetic Resonance Spectroscopy (SSNMR)

Figure 5-54 shows the ^{27}Al One Pulse Solid-State Nuclear Magnetic Resonance spectra (SSNMR), obtained from Magic Angle Spinning Nuclear Magnetic Resonance (MAS NMR) spectroscopy (refer to Sections 2.3.3 and 4.3.3) of the different zeolite samples tested in comparison with γ-Al_2O_3 (used as a binder for the H-MFI-90 and H-MFI-400 zeolites in extrudate form), the binder-free H-MFI-90 reference and the H-MFI-20 samples.

The top of the Figure 5-54 summarizes the assignment of the different signals and coordinate environments of the aluminium according to their typical chemical shift ranges, namely tetrahedral environment: 80-45 ppm, pentahedral environment: 40-25 ppm and octahedral environment: 20-(-20) ppm (Kentgens, 1997 and Smith, 1993).

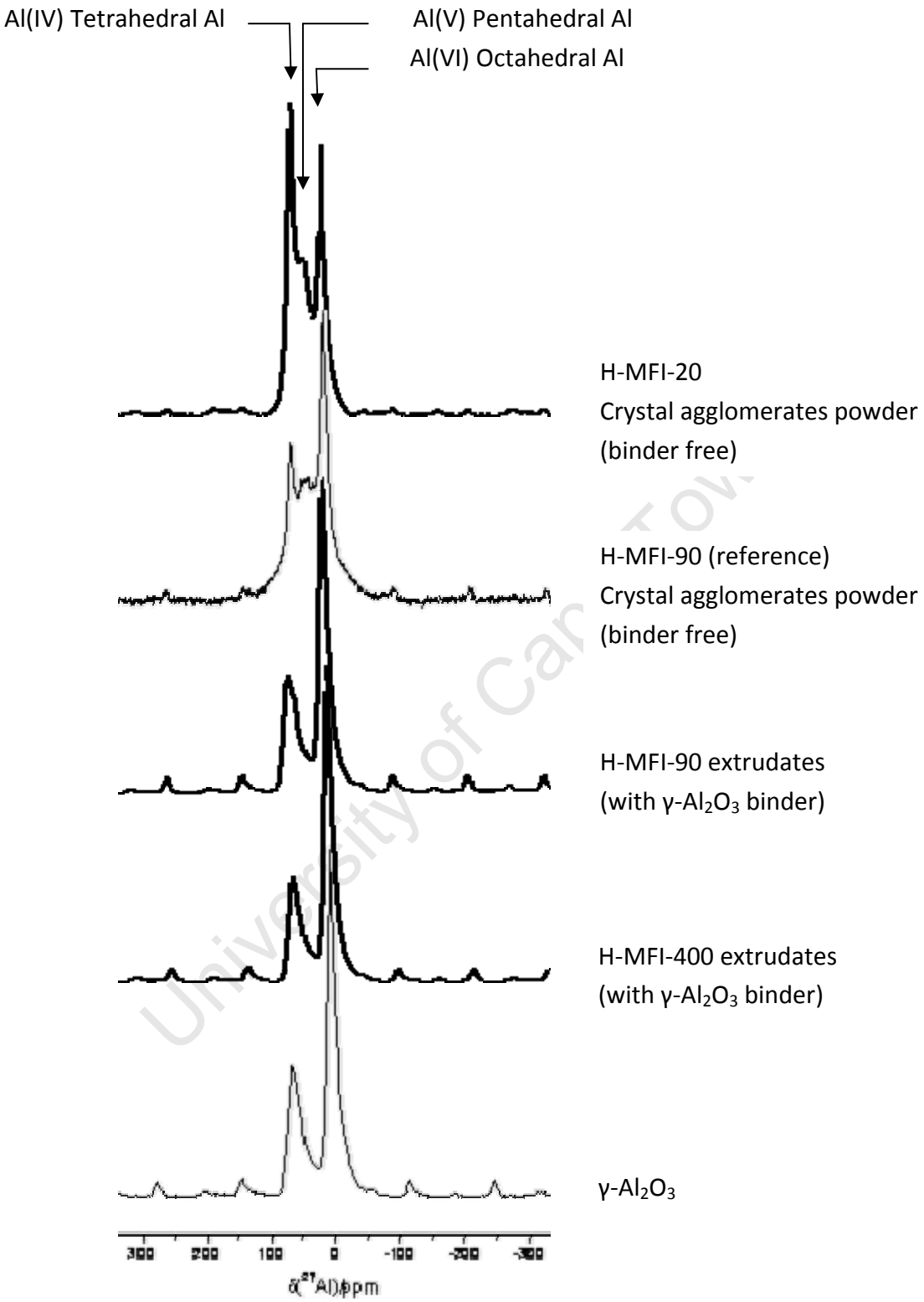

Figure 5-54: ^{27}Al One Pulse MAS NMR spectra of γ-Al_2O_3 and extruded (with about 20 wt% alumina binder) and binder-free H-MFI zeolite samples

Aluminium in the *tetrahedral* environment is associated with Brønsted acidity (Kentgens, 1997). This is the "catalytically active" aluminium.

Aluminium in *octahedral* environment is not catalytically active (Kentgens, 1997).

The *pentahedrally* coordinated aluminium, as evidenced in the binder-free H-MFI-90 reference and H-MFI-20 samples, is repeatedly reported in literature as extra-framework species that does not contribute to the acidity of the zeolite sample (Cabral de Menezes *et al.*, 2006, Motz *et al.,* 1998 and Wan *et al.*, 2008).

The γ-Al_2O_3 spectrum shows two peaks: a tetrahedral environment peak at around 80 ppm, which is at the high end of the range of 80-45 ppm of aluminium in tetrahedral environment (see above) and an octahedral environment peak at around 10 ppm.

In the spectrum of the binder free H-MFI-90 reference and H-MFI-20 zeolite samples, peaks of the tetrahedrally and octahedrally coordinated aluminium appear also, but slightly shifted to lower values of chemical shift in comparison to the corresponding peaks in the γ-Al_2O_3 spectrum. This is due to the presence of the peaks of tetrahedrally and the octahedrally coordinated aluminium within or in immediate proximity to a zeolitic environment as present in the H-MFI-20 and H-MFI-90 zeolite samples (Kentgens, 1997).

The H-MFI-90 reference sample spectrum shows that most of its aluminium is in the octahedral environment. More pentahedrally coordinated aluminium as in the H-MFI-20 sample is also observed for the H-MFI-90 reference sample.

H-MFI-90 and H-MFI-400 in the extrudate form implies the addition of alumina binder to the pure H-MFI-90 and H-MFI-400 samples as is represented by the H-MFI-90 reference sample. The addition of binder contributes to the aluminium content in the sample. This is evidenced by the fact that the spectra of both the H-MFI-90 and H-MFI-400 extrudates are very similar to the spectrum of the γ-Al_2O_3, indicating that the signals of the aluminium in the zeolites might be concealed by signals of the γ-Al_2O_3, which was used as the binder. In fact, of the total aluminium in the extrudated H-MFI-90 catalyst only about 8% was zeolitic aluminium and even less for the extrudated H-MFI-400. The shoulder on the low shift side of the signal of the tetrahedrally coordinated aluminium in the H-MFI-90 extrudate spectrum may indicate the presence of the zeolitic tetrahedral aluminium

Table 5-6 summarizes the details of integration of the centerband line and the resulting values of the integrals for tetrahedrally plus pentahedrally and octahedrally coordinated Al sites. Table 5-6 does not distinguish between tetrahedrally and pentahedrally coordinated sites, since the latter appeared just on the shoulders of the signals of the former. An attempt to resolve the overlaying peaks with the software available was not undertaken since this was not possible due to the significant tailing of the peaks (Causemann, 2010).

Table 5-6: Integrals of bands of tetrahedrally and octahedrally coordinated aluminium sites

Sample	Coordinative environment	Range of integral	Integral
H-MFI-90 reference	Octahedral	-85 - 10	1477950
	Tetrahedral +Pentahedral	10 - 100	1232728
H-MFI-90 extrudates	Octahedral	-45 - 25	6924566
	Tetrahedral	25 - 90	3512390
H-MFI-400 extrudates	Octahedral	-45 - 25	5499860
	Tetrahedral	25 - 90	2471408
H-MFI-20	Octahedral	-80 - 10	1281713
	Tetrahedral + pentahedral	10 - 90	2304410
γ-Al_2O_3	Octahedral	-45 - 25	14831
	Tetrahedral	25 - 90	7920

The said tangent method assumes the peak of the pentahedrally coordinated aluminium to "sit" on the slope of the tailing of the peak of the tetrahedrally coordinated aluminium and to be separated by a tangent (H-MFI-20) or to "sit" in the valley between the peaks of the tetrahedrally and octahedrally coordinated aluminium.

Table 5-7 gives the results of a graphical approach (tangent method) to the percentages of the different aluminium environments for the binder-free zeolite samples.

The said tangent method assumes the peak of the pentahedrally coordinated aluminium to "sit" on the slope of the tailing of the peak of the tetrahedrally coordinated aluminium and to be separated by a tangent (H-MFI-20) or to "sit" in the valley between the peaks of the tetrahedrally and octahedrally coordinated aluminium.

Table 5-7: Approximate percentages of aluminium in the different coordinative environments of the binder-free zeolite samples

Sample	Coordinative environment	Aluminium distribution (%) (approximation)	Tetrahedral Al in zeolite (wt%)
H-MFI-90 reference	Octahedral	55	0.67
	Tetrahedral	38	
	Pentahedral	7	
H-MFI-400	Tetrahedral		0.15
H-MFI-20	Octahedral	36	4.90
	Tetrahedral	62	
	Pentahedral	2	

Obviously, a significant percentage of the aluminium present in the zeolites is extra framework, non-active aluminium, while only about 60% (in H-MFI-20) and 40% (in H-MFI-90) are tetrahedrally coordinated and catalytically active.

This translates into 4.9 wt% of active, tetrahedrally coordinated aluminium in zeolite H-MFI-20 and 0.67 wt% in zeolite H-MFI-90.

Similar aluminium distributions as for the H-MFI-90 reference sample maybe assumed for the zeolitic component of the H-MFI-400 extrudates. This would translate into about 0.15 wt% of active aluminium in this zeolite.

6 Discussion

6.1 Experimental repeatability and catalyst stability

Figure 5-3 and Figure 5-4 show the results obtained from the repeated runs performed to validate the experimental integrity of this study. The results of the repeated runs conducted over the H-MFI-400 catalyst (Experiment 2 and Experiment 4) clearly show very similar activity, with only a slightly higher activity observed for Experiment 4 which can be attributed to the rather fresh load of catalyst on a shorter time-on-stream. The results of the various runs performed over the catalysts can thus be assumed to be of a reasonable level of accuracy and repeatability.

Figure 5-1, 5-2 and 5-4 show that after a steep initial decline, catalyst activity was rather constant and could be considered 'quasi-steady' compared to the little loss of activity during a parameter variation series. The decision (see Section 5.4) to carry out all variations of condition settings with a certain catalyst over the same charge of catalyst, in 'quasi-steady' state, was therefore justified.

6.2 Catalyst activity

Figure 5-5 clearly shows that the catalytic activity of the zeolites differed. Tested over a range of space velocities (in the 'quasi-steady' state regime), activities can be ranked as H-MFI-90 > H-MFI-20 > H-MFI-400. In particular, for the low space velocities between 0.0625 – 0.25 $g_{m\text{-cresol}}/g_{cat}$.hr, it was observed that the catalytic activity of the H-MFI-90 catalyst was substantially higher than that of the H-MFI-20 and H-MFI-400 catalysts.

The observed differences in catalytic activity could be attributed to various factors, the most important in this study being the acidity of the zeolite samples. Zeolite acidity is primarily a function of the density and strength of the individual acid sites. Taking into account that this study incorporates only the use of high SiO_2/Al_2O_3 ratio H-MFI zeolites (of molar SiO_2/Al_2O_3 ratios equal to or greater than 20) the only factor therefore affecting the zeolite acidity was the density of acid sites (see Section 2.2.1.1).

From XRF analyses (see Section 5.8.1) of the two catalysts that were available in the form of crystallite agglomerate powders, namely H-MFI-20 and H-MFI-90 (reference), it followed that the actual aluminium content was very close to the reported aluminium content (the molar SiO_2/Al_2O_3 ratio given in the sample code), as can be derived from Table 5-4. The same can, therefore, be assumed for the H-MFI-400 catalyst.

However, ^{27}Al MAS NMR spectra (see Section 5.8.3 and Figure 5-54) revealed that only about half of the total aluminium present appears in catalytically active form, that is, in a tetrahedral

environment, while the rest of the aluminium appears in octahedral or pentahedral environments (see Table 5-6) that are catalytically not active.

Table 5-6 also gives the percentages of active (tetrahedrally coordinated) aluminium in the different zeolites and the effective molar SiO_2/Al_2O_3 ratios (with respect to active aluminium).

Figures 5-5 and 6-1 show that the zeolite catalyst H-MFI-90 is much more active (per unit mass of catalyst i.e. at equal WHSV) than the H-MFI-400 zeolite catalyst. This is expected given its higher content of active, tetrahedrally coordinated aluminium. However, the H-MFI-20 zeolite catalyst despite its much higher content of active, tetrahedrally coordinated aluminium (about sevenfold) is about 1.5 times less active.

When plotting conversion versus WHSV related to the mass of active, tetrahedrally coordinated aluminium (see Figure 6-2) the curves for the H-MFI-90 and H-MFI-400 zeolite catalysts coincide but not the curve for the H-MFI-20 zeolite catalyst which is significantly lower.

It follows from Figures 6-1 and 6-2 that the activities of the tetrahedrally coordinated aluminium in zeolite catalysts H-MFI-90 and H-MFI-400 correspond to each other, that is, conversions are approximately proportional to the content of tetrahedrally coordinated aluminium, while the tetrahedrally coordinated aluminium in the H-MFI-20 catalyst seems to be much less active as suggested by the observed low conversions.

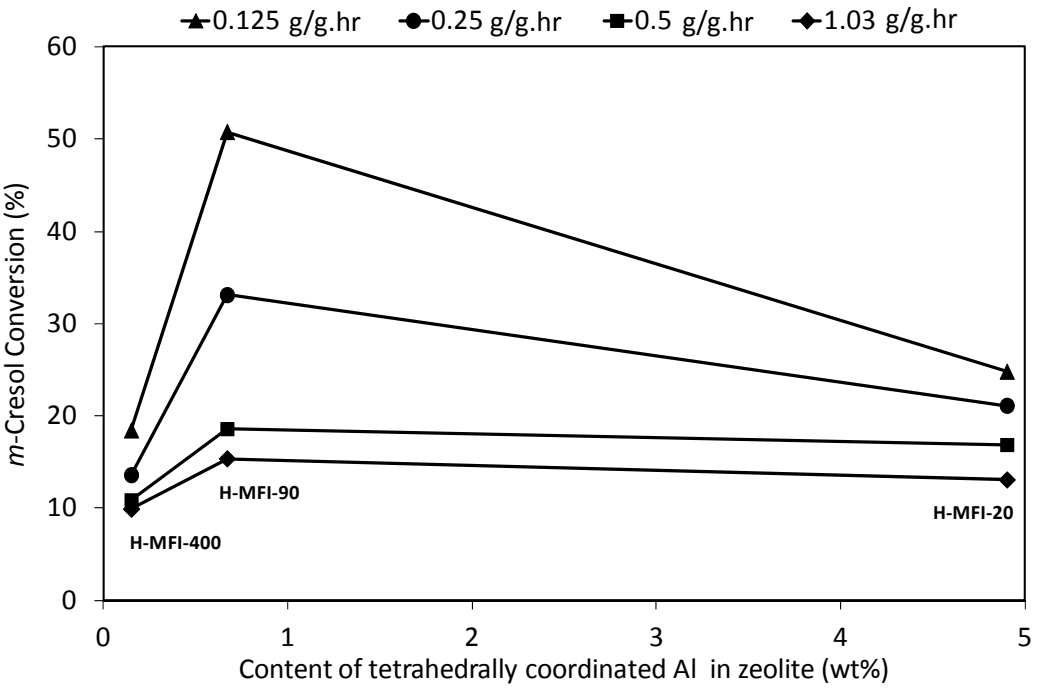

Figure 6-1: Comparison of the activities of the catalysts tested with respect to their content of active, tetrahedrally coordinated zeolitic aluminium (at T = 275°C, 3 bar (abs) and different WHSV)

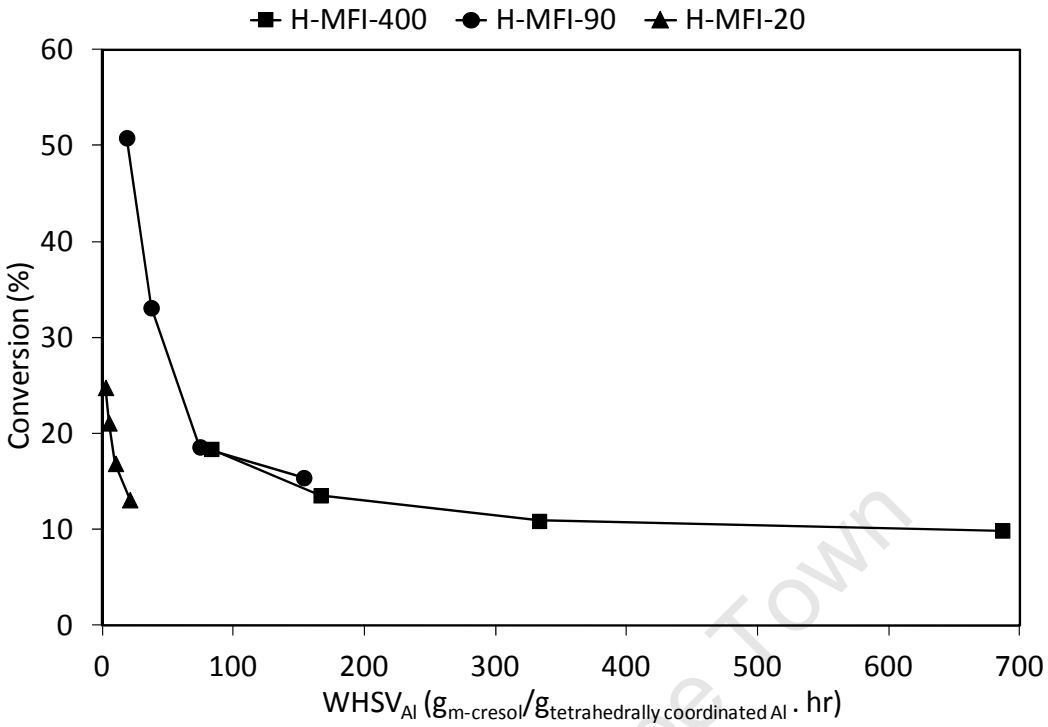

Figure 6-2: Comparison of the effective activities of the tetrahedrally coordinated zeolitic aluminium in the catalysts tested as a function of WHSV (Al relative to the amount of tetrahedrally coordinated zeolitic aluminium charged)

A possible reason for the deviation and unexpectedly low apparent activity of the total and tetrahedrally coordinated aluminium in the aluminium-rich H-MFI-20 zeolite maybe derived from the SEM micrographs of the catalysts (see Section 5.8.2 and Figures 5-51 to 5-53). Zeolite crystallites in the H-MFI-90 and H-MFI-400 catalysts are very small and irregularly shaped, measuring < 10 nm in size on average (see Figures 5-52 and 5-53 and Table 5-5) while crystallites of the H-MFI-20 catalyst are comparatively well shaped and much larger, appearing as platelets with a thickness of several 10 nm (see Figure 5-51 and Table 5-5).

The large size of the H-MFI-20 crystallites, in contrast to the crystallites of the H-MFI-90 and H-MFI-400 catalysts suggest that mass transfer control may reduce the effectiveness of the crystallites of the former. Thus the 'effective' content of tetrahedral aluminium appears lower resulting in lower conversion.

A simple data fit supports this conclusion assuming the following:

- Spherical zeolite crystallites for the H-MFI-90 and H-MFI-400 catalysts (see Table 5-5)
- Platelet-shaped zeolite crystallites for the H-MFI-20 catalyst (see Table 5-5)
- Average characteristic dimensions of the H-MFI-90 and H-MFI-400 crystallites of approximately 7 nm (based on data given in Table 5-5)

- An average characteristic dimension of the H-MFI-20 crystallites of approximately 30 nm (based on data given in Table 5-5)
- Intrinsic rate constants (k) proportional to the contents of tetrahedrally coordinated aluminium
- Equal diffusivities

Fitting the Thiele Modulus φ for the reaction over H-MFI-90 to a value of 1.0, results in the following (see Figure 6-3):

- H-MFI-400: $\varphi = 0.48$ $\eta = 0.98$
- H-MFI-90: $\varphi = 1.00$ $\eta = 0.94$
- H-MFI-20: $\varphi = 35$ $\eta = 0.083$

Figure 6-3 gives the ratio of effectiveness factors between H-MFI-90 and H-MFI-20 as:

$$\eta_{H\text{-}MFI\text{-}90} / \eta_{H\text{-}MFI\text{-}20} = 12$$

It can be derived from Figure 6-1 that this ratio corresponds to the ratio of the conversions over the two catalysts, related to their content of tetrahedrally coordinated Al:

$$(\text{Conversion/Content Al}_{tetr})_{H\text{-}MFI\text{-}90} / (\text{Conversion/Content Al}_{tetr})_{H\text{-}MFI\text{-}20} = 8 \text{ to } 15$$

The differences in product selectivities (see Sections 5.6.3 – 5.6.8), in context with the detailed reaction network derived (see section 6.4), support the above conclusion.

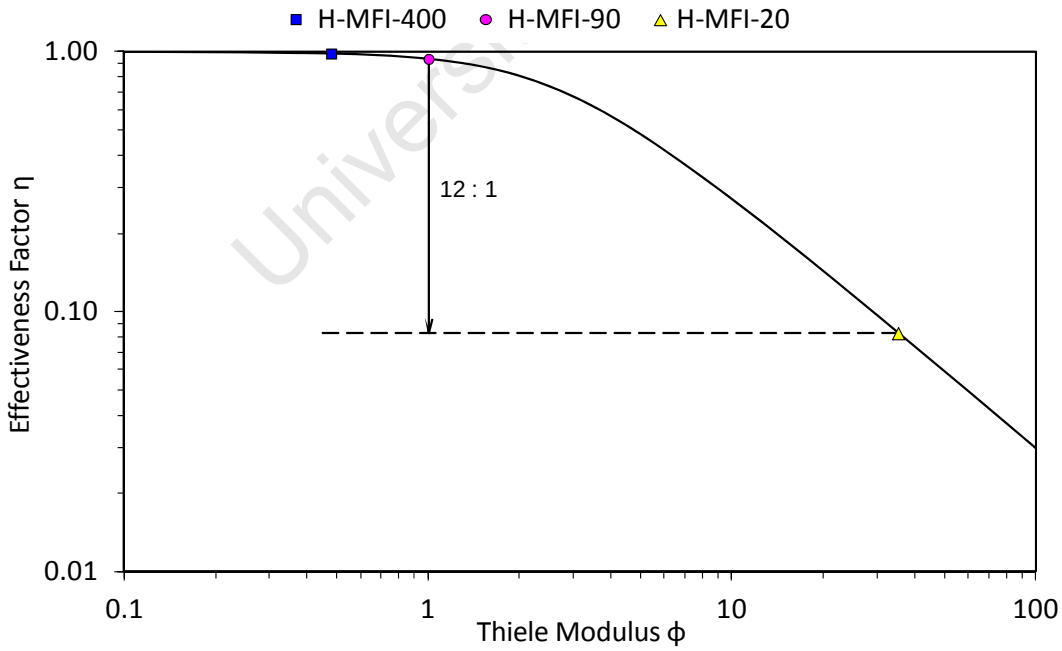

Figure 6-3: Effectiveness factor η as a function of the Thiele Modulus ϕ for all zeolite catalysts tested in correspondence to their tetrahedrally coordinated aluminium related conversion

6.3 Order of reaction

It was not possible to ascertain an order of reaction with reasonable accuracy, on observation of relevant figures. Orders of reaction are, in the gas phase, typically determined from varying pressures (Fogler, 1999).

It could be presumed that the reaction was most likely first order with respect to isopropanol or propene (formed from isopropanol) owing to the fact that, at low temperature, the *m*-cresol was strongly adsorbed within the zeolite micropore system so that the concentration of *m*-cresol was high and occurred in huge surplus compared to the isopropanol or propene alkylating agent. The concentration of the *m*-cresol in the catalyst pore system was therefore not likely to vary and could be taken to remain constant (see Section 2.1.4.1). The rate of reaction was therefore only dependent on the concentration of the adsorbed isopropanol or propene on the active catalyst sites and the overall reaction could therefore be expected to be first order.

A pressure series (in the gas phase) was carried out (see Sections 5.7.1.5 to 5.7.1.10). The results of the pressure series indicate only a moderate effect of the reaction pressure on *m*-cresol conversion (see Figures 5-37 and 5-38). The overall reaction order that can be estimated from the few data points obtained is < 0.5 and decreases with increasing pressure and conversion. It appears that the approach to the thermodynamic equilibrium (see Section 2.1.6.2) of the *m*-cresol to thymol reaction takes effect already.

6.4 Reaction mechanism

In the alkylation of *m*-cresol with isopropanol, the major products observed in the product spectrum were isopropyl-3-tolyl ether, mono-isopropylated phenols (thymol and position isomers) and diisopropylated phenols. The remainder comprised essentially a small amount of heavy compounds, typically observed at higher reactions temperatures, and unconverted *m*-cresol. The derivation of the proposed reaction mechanism is therefore based on the trends of product yields and corresponding selectivities with conversion of the *m*-cresol feed as well as the influence of reaction parameters such as space velocity, reaction temperature and pressure. Selectivities being > 0 or 0 at 'zero' conversion as derived from the selectivity versus conversion plots, was the major criterion for the identification of primary and secondary products. Yield trends were indicative towards compounds being intermediates.

The proposed mechanism correlates more or less with those postulated by other studies (see Section 2.1.5) but is more detailed. Figure 6-4 shows the major routes in this mechanism, with isopropanol (a) reacting preferentially with the hydroxyl group of the *m*-cresol to form an ether that than converts to the ring isopropylated product, or (b) being dehydrated to propene that preferentially alkylates the ring directly. Finally the ring mono-isopropylated isomers react further in subsequent isopropylation steps.

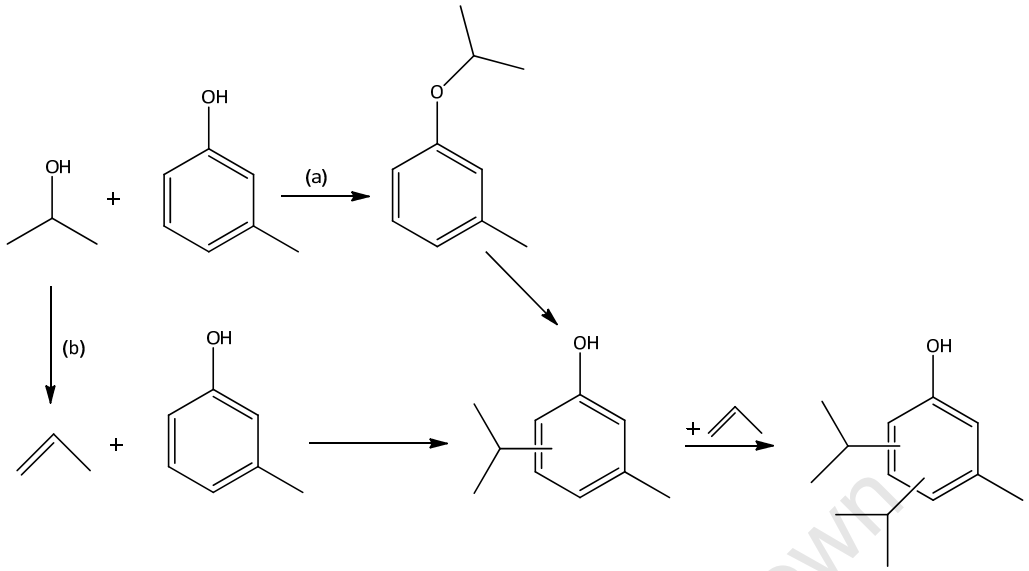

Figure 6-4: Major routes of proposed reaction mechanism (a) Isopropanol condenses with *m*-cresol to form Isopropyl-3-tolyl ether (b) Isopropanol dehydrates to propene

Figure 6-5 shows the detailed mechanism as derived from the results. The individual steps are discussed in Sections 6.4.1 to 6.4.6.

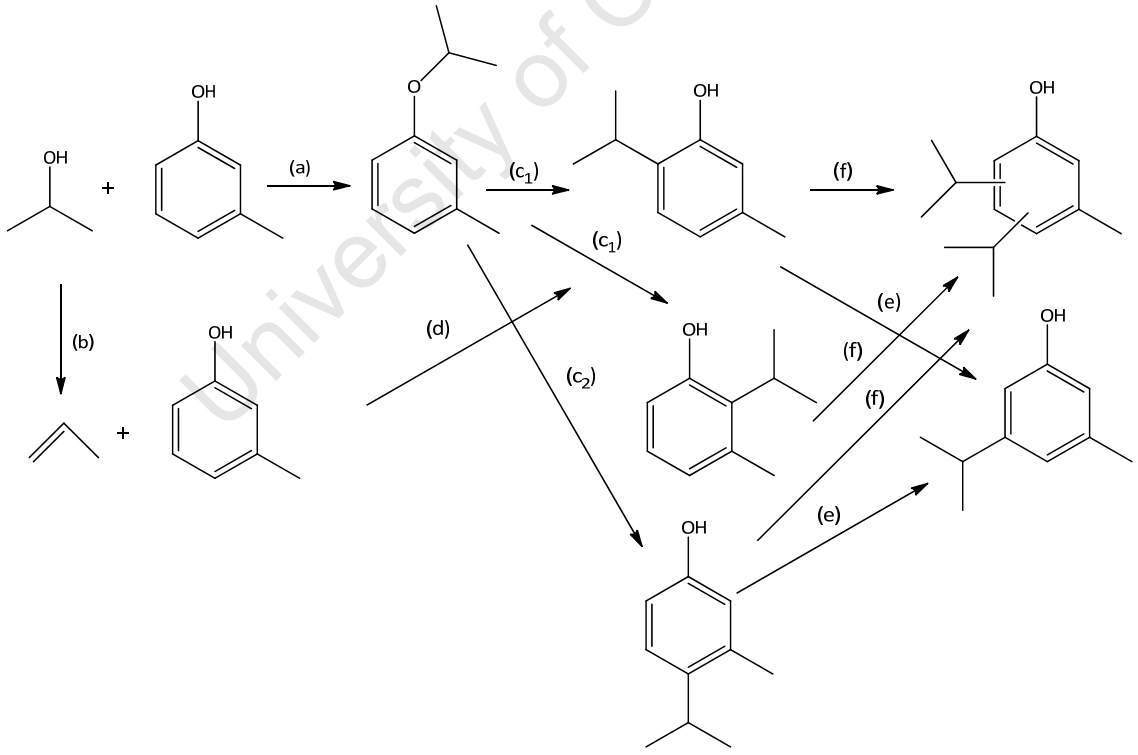

Figure 6-5: Proposed reaction mechanism for isopropylation of *m*-cresol over H-MFI zeolites

Numbering of "routes" in the following sections refers to Figures 6-4 and 6-5.

6.4.1 O-alkylation of *m*-cresol (route (a))

Figure 5-7 and Figure 5-8 show the yield and selectivity toward the O-alkylation product (isopropyl-3-tolyl ether) at 225°C over all catalysts tested. From the figures it maybe inferred that the formation of isopropyl-3-tolyl ether occurs at low conversions (typically < 10%) while at medium to moderately high conversions almost no isopropyl-3-tolyl ether is observed anymore.

On the other hand Figures 5-9 and 5-10 indicate that hardly any or no ring alkylation occurs initially. Selectivity to ring mono-alkylated products tends toward 0 at 'zero' conversion (Figure 5-10) and the yields take a 'dip' toward 'zero' conversion (Figure 5-9), indicating an exponential increase initially as for the secondary products (see Section 5.6.4).

These trends indicate that a rapid alkylation reaction of the hydroxyl group of the *m*-cresol with isopropanol alkylating agent (O-alkylation) occurs as observed, analogously, during methylation of phenol with methanol (see Section 2.1.3.1), resulting in the formation of isopropyl-3-tolyl ether from *m*-cresol (see Section 2.1.3.2.3) as the only primary product. The ether dominates the product spectrum at low conversions (< 10%) and disappears at medium to moderately high conversions due to the parallel, rapid dehydration of the isopropanol (see Section 6.4.2) and the consumption of the initially formed isopropyl-3-tolyl ether in secondary reactions (see Section 6.4.3). The above indicates that the ether only forms by reaction of *m*-cresol with the alcohol but not (or hardly) by reaction with its dehydration product, propene, which is still present at higher conversions. This means also that, at low WHSV, ether formation occurs only in the uppermost layers of the catalyst bed and reacts further in the deeper layers of the catalyst bed as the conversion begins to increase.

6.4.2 Dehydration of alkylating agent (route (b))

Figure 2-10 shows the dehydration reaction of isopropanol to propene. This reaction of the primary alkylating agent is rather rapid (see Section 2.1.3.2.1), is endothermic in nature and runs practically to completion (see Section 2.1.6.1 and Figure 2-13). The temperature profile across the catalyst bed (see Figure 4-5) indicates that this endothermic dehydration occurs right at the beginning of the catalyst bed, i.e., as soon as the feed comes into contact with the uppermost layers of the bed as indicated by the decline in temperature that still occurred despite the high dilution of the upper part of the catalyst bed (see Table 4-4). The subsequent stabilisation of the temperature to the set reaction temperature indicates that the dehydration reaction has gone to completion as the thermodynamic equilibrium suggests (see Section 2.1.6.1 and Figure 2-17). In the tested temperature range of 200-300°C, isopropanol has been reported to completely dehydrate (see Section 2.1.6.1).

To summarize: The rapid dehydration of isopropanol to propene meant that the alkylating agent disappeared and exclusively and selectively condensed with the *m*-cresol to form the

isopropyl-3-tolyl ether as long as it was present in the reaction mixture while the dehydration product propene only alkylated the ring (see Section 5.6.4). Isopropyl-3-tolyl ether and propene are the primary products in the reaction system, whereas all the ring alkylation products are considered secondary products.

Figure 6-4 illustrates the mechanism derived from these observations, namely the alkylation of the hydroxyl group of the *m*-cresol by isopropanol (route (a)) and the parallel dehydration of isopropanol to propene (route (b)) which subsequently alkylates the ring.

It appears that the reaction along route (a) comes to an end as soon as all of the other isopropanol has been dehydrated (route (b)). On the other hand, ring alkylation, subsequent to route (b) is only initiated as a secondary reaction and eventually dominates the reaction system once enough propene has formed.

6.4.3 Internal rearrangement and transalkylation of isopropyl-3-tolyl ether (routes (c))

At low conversions (around 10%), isopropyl-3-tolyl ether selectivities over the H-MFI-20 and H-MFI-400 zeolites were observed to be as high as 30-35% of the total product spectrum (see Figure 5-8) with yields of up to 5 mol% (see Figure 5-7). However, O-alkylation products are, thermodynamically much less stable than C-alkylation products (see Section 2.1.6.5) and indeed show a decline in isopropyl-3-tolyl ether yields at medium to moderately high conversions as shown in Figure 5-7 and Figure 5-8. Isopropyl-3-tolyl ether finally disappeared from the product mixture at medium conversions. A corresponding increase in yield and selectivity of the 2-isopropyl-, 4-isopropyl- and 6-isopropyl- ring mono-isopropylated 3-methyl phenols (in particular, thymol) is observed for all catalysts but the 5-isopropyl-3-methyl-phenol does not form during these early low conversion stages (see Figure 5-14, Figure 5-15, Figure 5-17, Figure 5-18, Figure 5-20 and Figure 5-21).

The disappearance of the isopropyl-3-tolyl ether can be attributed to (i) rapid internal rearrangement of the isopropyl-3-tolyl ether (see Section 2.1.3.1.3) and (ii) the transalkylation with *m*-cresol. *Ortho*-substitution is most likely as a result of the isopropyl group being closest to the *ortho*-positions of the aromatic ring. This results in the formation of thymol and the 2-isopropyl-3-methyl Phenol isomer (routes (C_1)), though thymol is the prevailing product since the 2-position (see aforementioned figures) is severally sterically hindered (see Section 2.1.3.1.1). Transalkylation with *m*-cresol may also form the 4-isopropyl-3-methyl phenol isomer (route C_2) though less likely since the bimolecular transition state of the transalkylation steps is sterically hindered (transition state selectivity) in the pore systems of the medium pore zeolites (see Section 2.1.3.2.1). Hence, selectivity of the 4-isopropyl-3-methyl phenol isomer is rather low.

As mentioned above, no 5-isopropyl-3-methyl phenol forms in this early stage. This isomer is not directly accessible by internal rearrangement of the isopropyl-3-tolyl ether, which only leads to the *ortho*- isopropyl substituted isomers. The 5-isomer can also hardly form by transalkylation with *m*-cresol, like the 4-isomer, since the low reactivity of the 5-position on the phenolic ring (see Section 2.1.3.1.1) adds up to the transition state selectivity which already hinders the formation of substantial amounts of the 4-isomer (see above).

To summarize: The only product from the condensation of isopropanol and *m*-cresol is isopropyl-3-tolyl ether (see Section 6.4.1). This ether reacts further by internal rearrangement or transalkylation with *m*-cresol to form thymol and all of the other mono-ring isopropylated thymol isomers. The selectivities of these products and, correspondingly, rates of formation rank as follows:

Thymol > 2-isopropyl-3-methyl phenol = 2-isopropyl-3-methyl phenol >> 5-isopropyl-3-methyl phenol

The ranking is controlled by and reflects the 'chemical' reactivities of the accepting positions on the ring (*ortho*-, *meta*- or *para*-position, relative to the hydroxyl group) and additionally the steric hindrance imposed at the individual positions.

Thymol and position isomers yields and selectivities (Figures 5-14, 5-15, 5-17, 5-18, 5-20 and 5-21) show coincidentally a 'dip' at < 20% conversion, indicating that they are secondary products, formed *via* isopropyl-3-tolyl ether (routes (A) and (C)) and observable at low conversions.

6.4.4 C-alkylation of *m*-cresol (route (d))

The formation of the ring mono-isopropylated products continues at conversions > 20% when all of the isopropyl-3-tolyl ether (and isopropanol) is converted, with propene as the 'only' alkylating agent and the products as secondary products (see Figures 5-11, 5-14, 5-17 and 5-20). The reaction, involving the direct alkylation by propene or the isopropyl carbenium ion, respectively, onto the aromatic ring of the *m*-cresol molecule (C-alkylation) is comparatively slow. This reaction results, in principle, in the formation of the four isomers thymol, 2-isopropyl-3-methyl phenol, 4-isopropyl-3-methyl phenol and 5-isopropyl-3-methyl phenol isomers, though at different extents.

Figures 5-14, 5-17 and 5-20 show clearly that the yields of 2-isopropyl-3-methyl phenol and 4-isopropyl-3-methyl phenol isomers pass over maxima, simultaneously, indicating that they are consumed by subsequent reactions faster than they form (or do not form at all anymore at medium conversion). With respect to selectivities, these profiles are even sharper (see Figures 5-15, 5-18 and 5-21). The figures also show that thymol formation, in contrast, is still ongoing.

It can be seen from Figures 5-7 and 5-8 that the said maximum and subsequent decline comes with the isopropyl-3-tolyl ether disappearing from the product mixture when conversion increases. The ether has been shown (see Sections 6.4.1 and 6.4.3) to form exclusively from *m*-cresol and isopropanol, not to form any longer once the latter has been consumed (mostly by dehydration to propene, see Section 6.4.2), and subsequently to convert rather rapidly into thymol and the said two isomers, causing the initial increase of their yields. With propene left as the only alkylating agent for the *m*-cresol, the 2-isopropyl-3-methyl phenol and 4-isopropyl-3-methyl phenol isomers no longer form (or hardly form any longer) while thymol formation continues.

From this it can be derived that the percentage of thymol in the fraction of 'thymol and position isomers' i.e. the ring mono-isopropylated products, still increases significantly in the medium to high conversion range, while the percentage of the 2-isopropyl-3-methyl phenol and 4-isopropyl-3-methyl phenol isomers decreases (see Figure 5-13).

To summarize: All of the ring mono-isopropylated compounds are secondary products, be it *via* isopropyl-3-tolyl ether as the intermediate or be it *via* propene. At low conversion, while isopropanol is still present to form the isopropyl-3-tolyl ether, this ether in the major route (routes A and C) form the 2-isopropyl-3-methyl phenol and 4-isopropyl-3-methyl phenol isomers and also thymol. Although this route yields only about 20% of the total ring isopropylated product (see Figures 5-14, 5-17 and 5-20), about half or even less of the resulting ring mono-isopropylated products (the thymol and isomers fraction) is not thymol (see Figure 5-13).

Once the isopropyl-3-tolyl ether has been consumed, the 2-isopropyl-3-methyl phenol and 4-isopropyl-3-methyl phenol isomers no longer (or hardly) form. The remaining alkylating agent, propene, alkylates *m*-cresol almost exclusively in the 6-position, to form thymol (route (d)) but hardly on the other positions on the ring.

6.4.5 Isomerisation of thymol and 4-isopropyl-3-methyl phenol (route (e))

At low conversions, about 20%, hardly any or no formation of the 5-isopropyl-3-methyl isomer occurs (see Figures 5-14 to 5-22). At medium conversion, yields start to increase exponentially, although low yields are observed. However, this is in the same range where the yield of the 4-isopropyl-3-methyl phenol isomer is on the decline, as also shown by Figures 5-14 to 5-22.

It is proposed that, as the conversion increases, isomerisation of these isomers, as well as thymol, *via* a 1,2-methyl shift of the isopropyl group converts them slowly to 5-isopropyl-3-methyl phenol (see Section 2.1.4.3 and Figure 2-15), which is, thermodynamically, the most stable of all the isomers (see Section 2.1.6.3 and Figure 2-22).

The yield and selectivity of the 2-isopropyl-3-methyl phenol isomer also declines (see Figures 5-14 to 5-22) but, naturally, not *via* a 1,2-shift of the isopropyl group but rather by dialkylation (see Section 6.4.6) or transalkylation.

6.4.6 C-alkylation of thymol and position isomers forming diisopropylated phenols (route (f))

Following the slow ring alkylation reaction, the mono-isopropylated isomers (thymol and the position isomers) undergo secondary alkylation with propene to form diisopropylated phenols. Evidence for this phenomenon is provided by the steady increase in the yield and selectivity of the diisopropylated-3-methyl phenols (see Figures 5-23 and 5-24).

While the selectivity of the total position isomers declines at higher conversions (see Figures 5-15, 5-18 and 5-21). It should be noted that at the higher conversion achieved in these experiments the expected decline in the total isomers yield did not yet manifest.

6.5 Effect of reaction parameters

In these series the effects of WHSV, temperature and pressure were studied with respect to determining operating conditions that would optimise catalyst activity and thymol selectivity. Initially, a variation of WHSV and temperature conditions was conducted over all three zeolite samples. Thereafter, upon determination of the optimum WHSV and temperature over the 'best' catalyst viz. the H-MFI-400 zeolite, a pressure series was conducted.

6.5.1 Effect of space velocity and conversion

By manipulation of the feed rate, the effect of varying space velocity was studied for all three zeolite samples. Figure 5-5 shows the effect of variation of space velocity on *m*-cresol conversion over all three zeolite samples obtained at a reaction temperature of 225°C. A reduction in space velocity produced the trivial effect of a corresponding exponential increase in conversion.

At the highest space velocities applied, the trend is as expected, namely an increase in conversion with increasing temperature while the reverse is observed at the lowest space velocities. This counterintuitive behaviour was observed earlier by Nagooroo and Truter (2008) and van der Merwe (2012). It was observed that decreasing space velocity i.e. increasing residence time resulted in increasing yields of diisopropylated and other higher alkylated products. In this way the consumption of the propene became higher than the consumption of the *m*-cresol so that the reaction mixture was depleted of propene and the conversion of *m*-cresol eventually declined with decreasing space velocity. This was particularly obvious at an elevated temperature of 300°C, whereby thermodynamic limitations restricted the reaction system additionally as was observed previously in a study performed by Fletcher et al. (2001b), (see Section 2.1.6.2).

However, this change in conversion had a significant impact on the change in product yields and selectivities (see Section 5.6 and Figures 5-6 to 5-25). The effects of space velocity have been described in great detail in Section 5.4. The trends observed in these figures indicate which ones of the products obtained, are primary, secondary or tertiary products and how

stable they are with respect to further conversion. As discussed in detail in Section 6.4, the proposed reaction network (see Figure 6.5) was developed from these figures.

6.5.2 Effect of temperature

The effect of temperature on catalyst activity and product selectivity was studied extensively over all three zeolite samples in the temperature range 200 - 300°C. Effect of temperature on yields of major products

Figure 5-35 and Figure 5-36 compare the direct influence of temperature on m-cresol conversion, extent of C-mono-isopropylation (total isomers yield), thymol yield and the yields of the most abundant by-products over the catalysts tested.

Figure 5-35 Over all of the zeolites, an increase in temperature caused a corresponding increase in *m*-cresol conversion and thymol yield. Estimating an activation energy is futile taking into consideration all of the complex reaction steps involved in the consumption of the *m*-cresol, significant data scatter and the inconsistencies in trends of which the reasons are subsequently discussed.

Isopropyl-3-tolyl ether was only observed in the product mixtures at temperatures < 250°C (see Figure 5-36). This is consistent with the fact that the activation energy of O-C bond formation is lower than the activation energy of C-C bond formation and therefore ring alkylation is favoured at higher temperatures (see Section 2.1.3.1.2). Isopropyl-3-tolyl ether is therefore the kinetically preferred product under milder reaction conditions (as long as Isopropanol is present). With increasing temperature, yield and selectivity of thymol increase (as long as the space velocity is high enough to suppress over-alkylation and isomerisation).

Figures 6-6 and 6-7 show the effect of temperature on thymol selectivities at constant conversion. Zeolites H-MFI-400 and H-MFI-90, whose crystallites and aluminium contents are so small that mass transfer effects hardly play a role (see Section 6.2 and Figure 6-3) show that an increase in temperature results in an increase in thymol selectivity (at constant conversion). This is a direct consequence of the decline in ether formation with increasing temperature. As discussed in Sections 5.4.3 and 5.4.4 the isopropylation of the ring of *m*-cresol with propene yields almost exclusively the thymol isomer, while the route *via* the ether produces the other isomers with significant selectivities.

Higher temperatures (see Figure 5-36) also favoured the formation of diisopropylated compounds by secondary alkylation of thymol and its position isomers, specifically the 2-isopropyl-3-methyl phenol isomer that still has a very reactive *o*-position (6-position), which is consistent with the observed decline in the yield of this species (see Figure 5-36). However, this trend closely follows conversion and may not be real.

Of specific importance is the rapid increase in the formation of the 5-isopropyl-3-methyl phenol isomer (by 1,2-shift of the isopropyl group) with increasing temperature (see Figure 5-36) which is thermodynamically favoured at higher temperatures.

6.5.3 Effect of pressure

At the optimum reaction conditions i.e. 275°C at 0.25$g_{m\text{-cresol}}/g_{cat}$.hr over the H-MFI-400 catalyst, the effect of pressure variation (1.5 – 12 bar (abs)) on *m*-cresol conversion and thymol selectivity and yield was investigated.

An increase in the operating pressure up to 6 bar (abs) showed a moderate increase in *m*-cresol conversion (see Figure 5-38) but even less of an increase in thymol yield (see Figure 5-39 and Figure 5-40). The decline in *m*-cresol conversion and thymol yield at 12 bar (abs) is indicated by a single data point and could be considered reliable.

The reasons for the moderate effect of pressure on *m*-cresol conversion have been discussed in Section 5.3 in context of the reaction order. The effect of pressure on thymol selectivity is also moderate. No pressure effect was expected anyway as the distribution of isomers and the slight decline points toward the formation of more diisopropylated products.

6.6 Effect of SiO_2/Al_2O_3 ratio

6.6.1 Conversion

As discussed in Section 6.2, the low SiO_2/Al_2O_3 ratio in the H-MFI-20 comes with a comparatively large crystallite size. The combination of these two factors imposes strong mass transfer control on the *m*-cresol isopropylation reaction (see Figure 6-3). The specific effect of the SiO_2/Al_2O_3 ratio can, therefore, not be singled out as the sole contributing factor.

6.6.2 Thymol selectivity

Figure 6-6 and Figure 6-7 show the effect of the SiO_2/Al_2O_3 ratio of the H-MFI catalysts tested on thymol selectivity at conversions of 20% and 30% respectively. The SiO_2/Al_2O_3 ratio is expressed in these figures by the content of tetrahedrally coordinated aluminium present in the respective zeolites. Since conversion data were derived from the WHSV series, this allowed for a direct comparison.

Figures 6-8 and 6-9 show thymol selectivity as a function of the fitted Thiele Modulus (see Section 6.2 and Figure 6-3) suggesting that reactions over the small crystallite and low aluminium content zeolites, H-MFI-400 and H-MFI-90, are not or only slightly affected by mass transfer control effects compared to the large crystallite and high aluminium content H-MFI-20 zeolite catalyst.

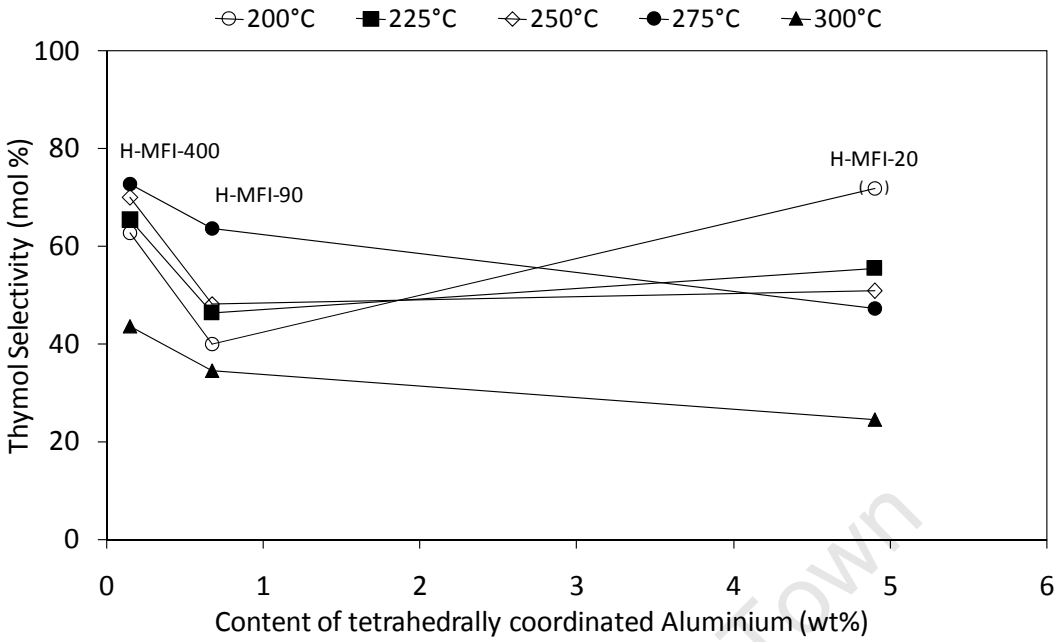

Figure 6-6: Effect of SiO_2/Al_2O_3 ratio (expressed as the content of tetrahedrally coordinated aluminium in the zeolite charged) on thymol selectivity over all catalysts tested at a conversion of 20% for temperature range 200-300°C

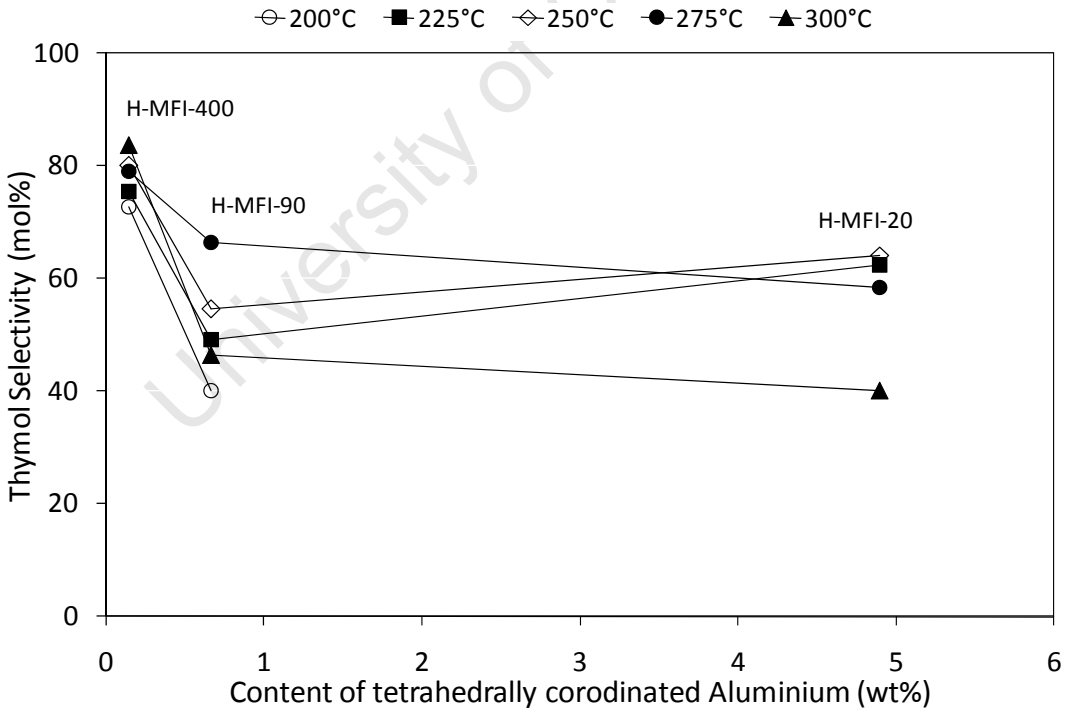

Figure 6-7: Effect of SiO_2/Al_2O_3 ratio (expressed as the content of tetrahedrally coordinated aluminium in the zeolite charged) on thymol selectivity over all catalysts tested at a conversion of 30% for temperature range 200-300°C

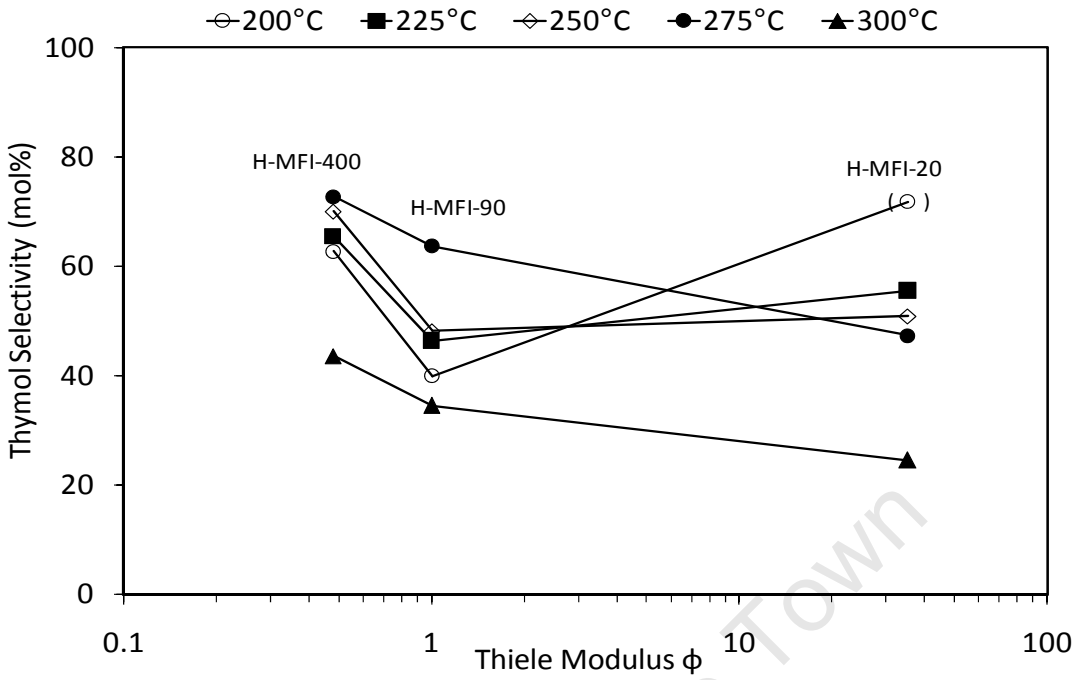

Figure 6-8: Effect of the content of tetrahedrally coordinated aluminium and crystallite size, expressed in terms of the fitted Thiele Modulus (see Section 6.2 and Figure 6-3) on thymol selectivity over all catalysts tested at a conversion of 20% for temperature range 200-300°C

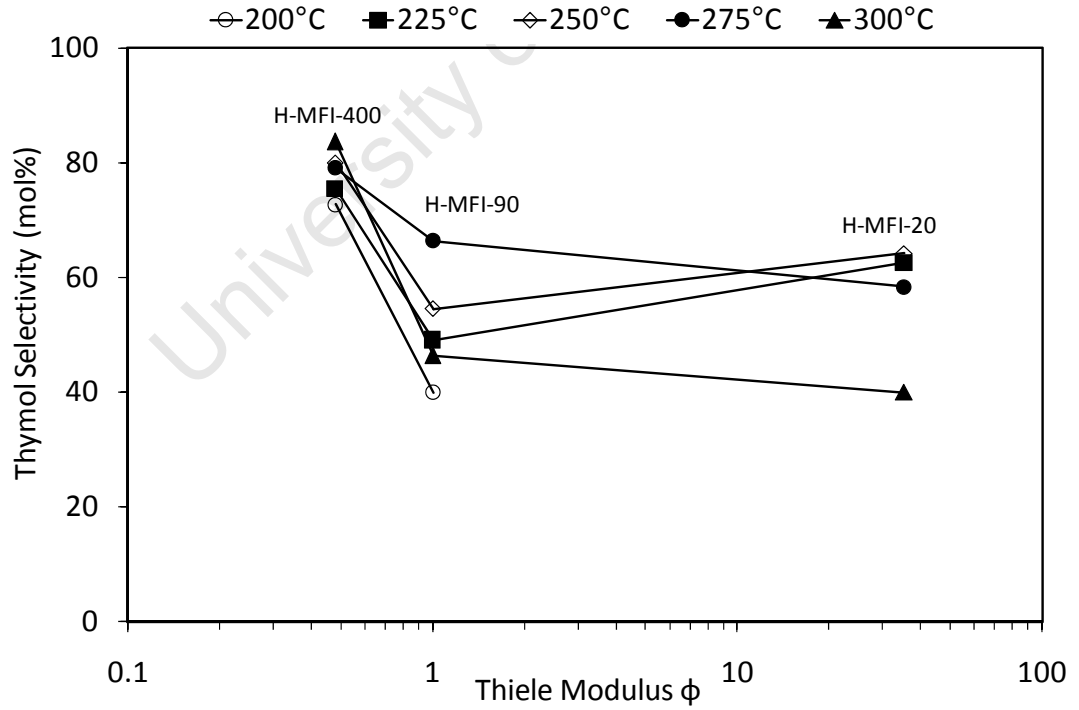

Figure 6-9: Effect of the content of tetrahedrally coordinated aluminium and crystallite size, expressed in terms of the fitted Thiele Modulus (see Section 6.2 and Figure 6-3) on thymol selectivity over all catalysts tested at a conversion of 30% for temperature range 200-300°C

Figures 6-6 to 6-9 reveal the following: Over zeolites H-MFI-400 and H-MFI-90, thymol selectivity increases with increasing temperature (at constant conversion) which reflects the shift in the mechanistic pathways away from the isopropyl-3-tolyl ether route (route (a), (c) in Figure 6-5) to the propene route (route (b), (d) in Figure 6-5) as discussed in Sections 6.4.3, 6.4.4 and 6.5.2. Only at 300°C does thymol selectivity decline again. At this high temperature, additionally affected by the approach to thermodynamic equilibrium conversion, too many undesired side reactions occur.

Over H-MFI-20, however, the effect of temperature on thymol selectivity is reversed. Increasing temperature results in a decline in thymol selectivity. This reflects the mass transfer control imposed on the reaction system by the comparatively large and aluminium-rich H-MFI-20 zeolite crystallites (see Section 6.2 and Figure 6-3). Mass transfer restrictions force intermediates (in this case thymol) to react further. Increased mass transfer restrictions, therefore, reduce intermediate thymol selectivity (see Section 2.2.4.2). At higher temperatures, in a mass-transfer controlled reaction system, the rate constant (k) and, therefore, the Thiele Modulus (*φ)* are higher which results in increased mass transfer control and hence lower intermediate thymol selectivity.

What happens to the thymol?

The distributions of the position isomers as a function of conversion (see Figure 5-16 for H-MFI-20, Figure 5-19 for H-MFI-90 and Figure 5-22 for H-MFI-400) show clearly that over mass transfer controlling H-MFI-20, thymol rapidly isomerises away to the thermodynamically favoured 5-isopropyl-3-methyl phenyl isomer (route (e) in Figure 6-5).

Yields and selectivities of the total position isomers fraction are also lower over the H-MFI-20 zeolite catalyst (see Figures 5-14 and 5-15 for H-MFI-20 and Figures 5-17, 5-18, 5-20 and 5-21 for H-MFI-90 and H-MFI-400). Figure 5-25 indicates that this is due to the formation of 'others' that are mostly higher alkylated compounds. However, Figures 5-23 and 5-24 do not show the presence of diisopropylated compounds, since the latter are too bulky to easily form in the pore system of the H-MFI zeolites.

7 Conclusions

The following conclusions can be drawn from the results obtained:

- H-MFI zeolite catalysts with different SiO_2/Al_2O_3 ratios are active for the isopropylation of *m*-cresol with isopropanol in the gas phase and display little deactivation even over long periods on stream
- The highest selectivity toward the desired product is achieved over the H-MFI zeolite catalyst with the highest SiO_2/Al_2O_3 ratio (i.e. SiO_2/Al_2O_3 ratio of 400), at moderate temperatures (around 275°C) and a WHSV of 0.25 $g_{m\text{-cresol}}/g_{cat}$.hr
- Intermediate isopropyl-3-tolyl ether formation directly from the isopropanol alkylating agent occurs at predominantly low temperatures and the ether is observed in the product mixture at low conversions (high space velocities).
- Internal rearrangement and transalkylation with *m*-cresol of the rather instable isopropyl-3-tolyl ether results in the formation of thymol, 2-isopropyl-3-methyl phenol and 4-isopropyl-3-methyl phenol although with preference (around 50%) of the former.
- Direct ring alkylation occurs *via* rapid initial dehydration of isopropanol to propene and subsequent direct alkylation of the aromatic ring. This route was found to be highly selective towards thymol formation
- Diisopropylated phenol and other higher alkylated products form as consecutive products thus also limiting maximum thymol yield and selectivity
- The 'large' crystallite, high aluminium content H-MFI-20 zeolite catalyst appears to affect mass transfer control on the reaction which reduces thymol selectivity and increases selectivities of thymol isomers (essentially the 5-isopropyl-3-methyl phenol isomer) and higher alkylated products. Since thymol is an intermediate in the reaction sequence, imposing mass transfer control accelerates thymol conversion.

  A possibility maybe the application of very large crystallites of H-MFI zeolites in the micrometer to several ten micrometer range together with measures to deactivate the external surface of the crystallites, as successfully applied by Haag and Olsen (1989) on the disproportionation of toluene.

The *two major conclusions* from this study are therefore the following:

- Thymol selectivity does not increase but declines when imposing mass transfer control on the *m*-cresol isopropylation system, i.e. when employing, other than high SiO_2/Al_2O_3 ratio, nano-sized H-MFI crystallites.
- Based on the results from this work, with respect to thymol selectivity, propene appears to be more efficient an alkylating agent than isopropanol and should, therefore, be used for this purpose.

The *accepted and rejected hypotheses* are the following:

- The results prove hypotheses No. 4 and No. 6 right that mass transfer control determines or influences conversion and selectivity, though not in the sense of hypothesis No. 5, i.e. in favour of thymol, but opposite.
- This means that hypothesis No. 5 is proofed wrong, whereupon mass transfer control increased the primary product selectivity towards thymol, the slimmest of the isomers.
- The results also show that hypotheses No. 4 and No. 6 are not only valid for the 'large' crystallites but likewise for the 'small' crystallites applied, though to a lesser extent.
- The above proves hypotheses No. 1 and No. 2 wrong, since the effect of the SiO_2/Al_2O_3 ratio is not 'direct' but comes in combination with crystal size and reaction temperature according to the Thiele Modulus relation, even for the small crystallites.
- Hypothesis No. 3 is also proved wrong, since in the present context there is no 'optimum' SiO_2/Al_2O_3 ratio, only an optimum, better to say, a maximum allowable Thiele Modulus. This maximum Thiele Modulus must be < 1.
- Finally, hypothesis No. 7 was proved wrong that optimum conditions exist for the reaction at issue. Exactly spoken, there was no need and incentive anymore to test hypothesis No. 7, since it was found that isopropanol is not the alkylating agent of choice.

8 Recommendations

The following areas merit further research for improvement of the reaction:

- Limit further studies to the use of propene as an alkylating agent
- Avoid any mass transfer control in order to preserve the high primary selectivity to thymol
- Study catalysts with comparatively open pore systems and high SiO_2/Al_2O_3 ratios
- Limit 'over-alkylation' by utilising an under stoichiometric feed mixture
- Operate at higher pressure to force back equilibrium limitations.

9 References

Amandi, R., Hyde, J.R., Ross, S.K., Lotz, T.J. and Poliakoff, M. (2005). Continuous reactions in supercritical fluids: a cleaner, more selective synthesis of thymol in supercritical CO_2. *Green Chem*. **7** 288-293.

Appleby, W.G., Gorbson, J.W. and Good, G.M. (1962). Coke formation in catalytic cracking. *Ind. Eng. Chem. Process Des. Develop.* **1** 102.

Ashford, R.D. (1994). Thymol. *Ashford's Dictionary of Industrial Chemicals*. London: Wavelength.

Baerlocher, Ch., Meier, W.M. and Olson, D.H. (2001). *Atlas of Zeolite Framework Types, 5th revised edition.* Amsterdam: Elsevier

Balasubramanian, V.V., Pandurangan, A., Palanichamy, M. and Murugesan, V. (2000). Methylation of phenol over ion-exchanged zeolites. *Ind. J. Chem. Technol.* **7(4)** 149-154

Böhringer, W. (2009a). Personal Communication. Centre for Catalysis Research. University of Cape Town.

Böhringer, W. (2009b). Fuels and Chemicals from Coal and Syngas lecture notes (unpublished). Centre for Catalysis Research. University of Cape Town.

Böhringer, W. (2010). Personal Communication. Centre for Catalysis Research. University of Cape Town.

Botelho, M.G. (2000). *Microbios*. **103** 31.

Biedermann, W., Köller, H. and Wedemeyer, K. (1978). Process for preparing thymol. *US 4 086 283* (assigned to Bayer AG).

Breck, D.W. (1974). *Zeolite Molecular Sieves: Structure, Chemistry and Use*. New York: Wiley. chpt 2, 29-185.

Cabral de Menezes, S.M., Lam, Y.L., Damodaran, K. and Pruski, M. (2006). Modification of H-ZSM-5 zeolites with phosphorus. 1. Identification of aluminium species by ^{27}Al solid-state NMR and characterisation of their catalytic properties. *Microporous and Mesoporous Mater.* **95** 286-295.

Callanan van Steen, L. (1999). Methanol ammination over hydrothermally treated zeolites RHO and mordenite. PhD Thesis. Catalysis Research Unit. University of Cape Town.

Causemann, S. (2010). Personal Communication. Nuclear Magnetic Resonance Unit. Chemistry and Polymer Science Department. University of Stellenbosch

Chaplin, J.A. (2002). The process for preparing (-)-menthol and similar compounds. *WO 2002/036795* (assigned to CSIR).

Chen, N.Y. and Garwood, W.E. (1978). Some catalytic properties of ZSM-5, a new shape selective zeolite. *J. Catal.* **52** 453.

Chen, N.Y., Degnan, T.F. and Smith, C.M. (1994). *Molecular transport and reaction in zeolites*. New York: Wiley. **11** 309.

Choudhary, V.R., Devadas, E., Kinage, A.K., Guisnet, M. (1997). Influence of binder on the acidity and performance of H-gallosilicate (MFI) zeolite in propane aromatization. *Appl. Catal. A: General* **162** 223-233.

Choudhary, V.R., Sivadinarayana, C. and Kshudiram, M. (1999). Influence of catalyst binder on the acidity and activity/selectivity of Ga/H-ZSM-5 zeolite in propane aromatization. *Proc. Indian Acad. Sci. (Chem. Sci.)* **111** 669-676.

Clark, J.H. and Macquarrie, D. J. (1997). Heterogeneous catalysis in liquid phase transformations of importance in the industrial preparation of fine chemicals. *Org. Process Res. De*v. **1** 149.

Csicsery, S.M. (1967). *Chem. Eng. Data*. **12** 118—122.

Csicsery S.M. (1984). *Zeolites*. **4** 202—213.

Csicsery, S.M. (1986). Catalysis by shape selective zeolites – science and technology. *Pure and Appl. Chem.* **58** 841 – 856.

Daubert T.E. and Danner R.P. (1989) Physical and thermodynamic properties of the pure chemicals. New York: Hemisphere.

Dejaifve, P., Auroux, A., Gravelle, P.C., Vedrine, J.C., Gabelica, Z. V. and Derouane, E.G. (1981). Methanol conversion on acidic ZSM-5, offretite, and mordenite zeolites: A comparative study of the formation and stability of coke deposits. *J. Catal.* **70** 123

Derouane, E.G. (1985). Factors affecting the activation of zeolites by coking. *Catalysis by acids and bases,* edited by Imelik, B., Naccache, C., Ben Taarit, Y., Vedrine, J.C., Coudurier, G. and Praliaud, H. *Studies in Surface Science and Catalysis*. Amsterdam: Elsevier Science B.V. **20** 221-240.

Derouane, E.G., Baltusis, L., Dessau, R.M. and Schmitt, K.D. (1985). Quantitation and modification of catalytic sites in ZSM-5. *Studies in Surface Science and Catalysis.* Amsterdam: Elsevier Science B.V. **20** 135-147.

Derouane, E.G. and Gabelica, Z. (1980). A novel effect of shape selectivity: Molecular traffic control in zeolite ZSM-5. *J. Catal.* **65** 486.

Derouane, E.G. and Vedrine, J.C. (1980). On the role of shape selectivity in the catalytic conversion of alcohols and simple hydrocarbons molecules on zeolite ZSM-5. *J. Mol. Catal.* **8** 479-483.

Dirdy, N., Dubreuil, L. and Pinkas, M. (1993). Antibacterial activity of thymol, carvacrol and cinnamaldehyde alone or in combination. *Pharmazie*. **48** 301.

Voges, H.-W. (2003). Isopropyl phenols. Section 1.5.3 of phenol derivatives. *In*: Elvers, B., Hawkins, S. and Russey, W.E. (eds.) *Ullmann's Encyclopaedia of Industrial Chemistry*, Weinheim: Wiley-VCH. 6th ed, Vol. **25** 619-621.

Fletcher, J.V., Böhringer, W. and Fletcher, J.C.Q. (2001a). Zeolite catalysts for thymol synthesis. Phase II Part A (unpublished report). Catalysis Research Unit. University of Cape Town.

Fletcher, J.V., Böhringer, W. and Fletcher, J.C.Q. (2001b). Parameter variation/optimisation - gas phase and mixed phase conversion. Phase II Part B (unpublished report). Catalysis Research Unit. University of Cape Town.

Fletcher, J.V., Böhringer, W. and Fletcher, J.C.Q. (2002). Catalysts for conversion of thymol isomers: Catalyst screening and parameter variation. Phase III Part B (unpublished report). Catalysis Research Unit. University of Cape Town.

Fletcher, J.C.Q. (2009). Personal Communication, Centre for Catalysis Research, University of Cape Town.

Fogler, H.S. (1999). Diffusion and Reaction. *In* N.R. Amundson (ed.), *Elements of Chemical Reaction Engineering.* New Jersey: Prentice Hall. 4th ed, 819-823.

Freude, D., Hunger, M., Pfeifer, H. and Schwieger, W. (1986). ^{1}H MAS NMR studies on the acidity of zeolites. *Chem. Phys. Lett.* **128** 62-66.

Garcia, L., Giannetto, G., Goldwasser, M.R., Guisnet, M. and Magnoux, P. (1996). Phenol alkylation with methanol: effect of sodium content and ammonia selective poisoning of an HY zeolite. *Catal. Lett.* **37** 121.

Grabowska, H. and Wrzyszcz, J. (2001). A method for obtaining thymol by gas phase catalytic alkylation of *m*-cresol over zinc aluminate spinel. *Appl. Catal.* **220** 207-213.

Haag, W.O. and Olsen, D.H. (1984). Structure-selectivity relationship in xylene isomerisation and selective toluene disproportionation. *In:* Whyte Jr., T.E., Dalla Belta, R.A., Derouane, E.G.and Baker, R.T.K. (eds.), *Catalytic Materials: Relationship between structure and reactivity*. ACS Symposium Series. **248** 275-307.

Hwang, S.Y. and Chen, S.S. (2004). Cumene. *In*: Kroschwitz, J.I. (ed.), *Kirk-Othmer Encyclopedia of Chemical Technology,* New York: Wiley 5th ed. Vol. **8** 147-156.

Jacobs, P.A., Mortier W.J. and Uytterhoeven, J.B. (1978). Properties of zeolites in relation to their electronegativity: Acidity, carboniogenic activity and strength of interaction in transition metal complexes. *J. Inorg. Chem.* **40** 1919-1923.

Jacobs, P.A. and Mortier, W.J. (1982). An attempt to rationalize stretching frequencies of lattice hydroxyl groups in hydrogen-zeolites. *Zeolites* **2** 226-230.

Kentgens, A.P.M. (1997). A practical guide to solid-state NMR of half-integer quadrupolar nuclei with some applications to disordered systems. *Geoderma.* **80** 271-306.

Klein, A. and Wedemeyer, K. (1976). Process for the preparation of 5-isopropyl-3-methyl phenol. *US. 3 968 173* (assigned to Bayer AG).

.

Kukard, R., (2008). The effect of zeolite type on the hydrocracking of long n-paraffins. MSc. Thesis. Centre for Catalysis Research. University of Cape Town.

Landau, M.V., Kogan, S.B., Tavor, D., Herskkowitz, M. and Koresh, J.E. (1997). Selectivity in heterogeneous catalytic processes. *Catalysis Today.* **36** 497-510.

Lee, K.-Y., Lee, H.-K. and Ihm, S.-K. (2010). Influence of catalyst binders on the acidity and catalytic performance of HZSM-5 zeolites for methanol-to-propylene (MTP) process: single and binary binder system. *Top. Catal.* **53** 247-253.

Marais, S.F. (2003). Personal communication with Böhringer, W. CSIR Bio/Chemtek, Modderfontain, South Africa.

March, J. and Smith, M.B. (1985). *In: Advanced organic chemistry: Reactions, mechanisms and structure.* New York: Wiley. 3rd ed., chpt 18 499.

Marczewski, M., Perot, G. and Gusinet, M. (1988). Alkylation of aromatics II. Alkylation of phenol with methanol on various zeolites. *In:* Gusinet., M., Barrault, J., Bouchoule, C., Duprez, D., Montassier, C. and Perot, G. (eds.), *Studies in Surface Science and Catalysis.* Amsterdam: Elsevier Science B.V. **41** 273-282.

Marczewski, M., Perot, G. and Guisnet, M. (1996). Alkylation of aromatics. Kinetics of phenol alkylation with methanol. *React. Kin. Catal. Lett.* **57** 21-27.

Martens, J.A., Souverijns, W., van Rhijn, W. and Jacobs, P.A. (1997). Acidity and basicity in zeolites. *In:* G. Ertl, H. Knözinger and J. Weitkamp (eds.) *Handbook of heterogeneous catalysis*. Weinheim: Wiley-VCH. Vol. **1** 324-365.

McCoy, M. (2010). Hot market for a cool chemical. *Chemical & Engineering News*. **88(35)** 15-16.

Meier, W.M. and Olson, D.H. (1978). Atlas of Zeolite Structure Types. Pub. Structure Commission of International Zeolites Association.

Mirth, G., Čejka, J. and Lercher, J.A. (1993). Transport and isomerization of xylenes over H-ZSM-5 zeolites. *J. Catal*. **139** 24-33.

Moon, G. (2003). Alkylation of phenol with methanol over H-ZSM-5, H-Beta, H-Mordenite, H-USY and H-MCM-22. PhD Thesis. Catalysis Research Unit. University of Cape Town.

Möller, K.P., Böhringer, W., Schnitzler, A.E., van Steen, E. and O'Connor, C.T. (1999). The use of a jet loop reactor to study the effect of crystal size and co-feeding of olefins and water on the conversion of methanol over H-ZSM-5. *Microporous and Mesoporous Mater.* **29** 127-144.

Morrison, R.T. and Boyd, R.N. (1987). *In: Organic Chemistry*. 5th ed., Boston: Allyn and Bacon, chpt 14, 499-529.

Motz, J.L., Heinichen, H. and Hölderich, W.F. (1998). Direct hydroxylation of aromatics to their corresponding phenols catalysed by H-[Al]ZSM-5 zeolite. *J. Mol. Catal A.* **136** 175-184.

Nagooroo, S. and Truter, L. (2008). Thymol synthesis by alkylation of *m*-cresol with isopropanol over H-ZSM-5 zeolite catalysts. Final year thesis (unpublished report). Catalysis Research Unit. Department of Chemical Engineering. University of Cape Town.

Namba, S., Kanai, Y., Shoji, H. and Yashima, T. (1984). Separation of *p*-isomers from disubstituted benzenes by means of shape-selective adsorption on mordenite and ZSM-5 zeolites. *Zeolites.* **4** 77-80.

Nagy, J.B., Bodart, P., Hannus, I. and Kiricsi, I. (1998). *In:* Kónya, Z. and Tubak, V. (eds.) *Synthesis, characterization and use of zeolitic microporous materials*. Hungary: DecaGen, chpt 6, 119-131.

Nitta, M., Yamaguchi, K. and Aomura, K. (1974). Alkylation of *m*-cresol with propylene by supported metal sulfates. *Bull. Chem. Soc. Japan*. **47** 2897-2898.

O'Connor, C.T., Moon, G., Böhringer, W. and Fletcher, J.C.Q. (2003). Alkylation of phenol and *m*-cresol over zeolites. *Collect. Czech. Chem. Commun.* **68** 1949-1968.

Olah, G.A. (1963). Friedel-Craft and Related Reactions. *New York: Wiley* 1-4.

Olah, G. A., Krishanamuri, R. and Surya Prakash, G. K. (1991). Friedel-Crafts Alkylation. *In*: *Comprehensive Organic Synthesis*. Oxford: Pergamon Vol. **3** chpt 1.8, 293-339.

Olson, D.H., Kokotailo, G.T., Lawton, S.L. and Meier, W.M. (1981). Crystal structure and structure-related properties of ZSM-5. *J. Phys. Chem.* **85** 2238-2243.

Parton, R.F., Jacobs, J.M., Huybrechts, D.R. and Jacobs, P.A. (1989). Shape-selective catalysis in zeolites with organic substrates containing oxygen. *In*: Zeolites as catalysts, sorbents and detergent builders, edited by Karge, H.G. and Weitkamp, J. *Studies in Surface Science and Catalysis.* **40** 163-192.

Pelrine, B.P. (1978). Synthesis of zeolite ZSM-5. *US 4 100 262* (assigned to Mobil Oil Corp.).

Pierantozzi R. and Nordquist A.F. (1986). Selective O-alkylation of phenol with methanol, *Appl. Catal.* **21** 263-271

Roland, E. and Kleinschmidt, P. (2003). Zeolites. *In:* Bohnet, M., Brinker, J.C. and Cornils, B. (eds.) *Ullmann's Encyclopaedia of Industrial Chemistry.* Weinheim: Wiley-VCH. 6th ed., Vol. **39** 625- 655.

Rollmann, L.D. (1977). Systematics of shape selectivity in common zeolites. *J. Catal.* **47** 113-121.

Rollmann, L. and Walsh, D. (1979). Shape selectivity and carbon formation in zeolites. *J. Catal.* **56** 139–140.

Ruthven, D.M. and Post, M.F.M. (2001). Diffusion in zeolite molecular sieves. *In:* van Bekkum, H., Flanigen, E.M., Jacobs, P.A. and Jansen, J.C. (eds.), *Introduction to Zeolite Science and Practice*, 2nd ed. *Studies in Surface Science and Catalysis.* **137** 525-577.

Santacesaria, E., Grasso, D., Gelosa, D. and Carra, S. (1990a). Catalytic alkylation of phenol with methanol: Factors influencing activities and selectivities. I. Effect of different acid sites evaluated by studying the behaviour of the catalysts: Alumina, nafion-H, silica-alumina and phosphoric acid. *Appl. Catal*. **64** 83-99.

Santacesaria, E., Di Serio, M., Ciambelli, P., Gelosa, D. and Carra, S. (1990b). Catalytic alkylation of phenol with methanol: Factors influencing activities and selectivities. II. Effect of intracrystalline diffusion and shape-selectivity on H-ZSM-5 zeolite. *Appl. Catal.* **64** 101-117.

Sasol (2000). Sasol annual report 2000. Sasol Chemical Industries Ltd., Rosebank, South Africa, **39**, 111.

Selvaraj, M. and Kawi, S. (2008). Comparison of mesoporous and microporous solid acid catalysts for highly selective synthesis of thymol by vapor phase isopropylation of *m*-cresol. *Micropor. Mesopor. Mater.* **109** 458-469.

Shapiro, S. (1996). The inhibitory action of fatty acids on oral bacteria. *Oral Microbiol. Immun.* **11** 350.

Smith, M.E. (1993). Application of ^{27}Al NMR techniques to structure determination in solids. *Appl. Magn. Reson.* **4** 1.

Stull, D.R., Westrum, E.R. Jr. and Sinke, G.C. (eds.) (1969). *The Chemical Thermodynamics of Organic Compounds.* New York: Wiley.

Sykes, P. (1986). *A Guidebook to mechanism in Organic Chemistry: 6th ed.* Essex: Longman, Burnt, Mill, Harlow, chpt. 6, 130-177.

Szostak, R. (1992). *Handbook of Molecular Sieves*, Van Nostrand Reinhold, New York 464.

Teissedre, P. and Waterhouse, A. L. (2000). Inhibition of oxidation of human low-density lipoproteins by phenolic substances in different essential oil varieties. *J. Agric. Food Chem*. **48** 3801.

Truter, L. (2011). Development of a zeolite washcoating technique for microchannel reactors. Catalysis Research Unit, Department of Chemical Engineering, University of Cape Town.

Valyon, J., Mihalyfi, J., Beyer, H.K. and Jacobs, P.A. (1979). Adsorption properties of ZSM-5 zeolite and $_1$H aluminium-free homologue. *In:* Preprints of the workshop on Adsorption of Hydrocarbons in Zeolites, Berlin: Acad. Sci. of the GRD, CIPC. Vol. **1** 134-147.

van der Merwe, J. (2012). Thymol synthesis by acid catalysed alkylation of *m*-cresol with propyl alcohols. MSc. Thesis (in preparation). Catalysis Research Unit. Department of Chemical Engineering. University of Cape Town.

Velu, S. and Sivasanker, S. (1998). Alkylation of *m*-cresol with methanol and 2-propanol over calcined magnesium-aluminium hydrotalcites. *Res. Chem. Intermed.* **24** 657 - 666.

Venuto, P.B. (1977). Aromatic reactions over molecular sieve catalysts: a mechanistic review. *In* Smith, G.V. (ed.) *Proc. 6th Conf. on Catalysis in Organic Synthesis.* New York: Academic Press 67-93.

Venuto, P.B and Landis, P.S. (1968). Organic Catalysis over crystalline aluminosilicates. *Adv. Catalysis. Relat. Subj.* **18** 259.

Venuto, P.B. (1994). Organic catalysis over zeolites: A perspective on reaction paths within micropores. *Microporous Mesoporous Mater.* **2** 297 - 411.

Umamaheswari, V., Palanichamy, M. and Murugesan, V. (2002). Isopropylation of *m*-cresol over mesoporous Al-MCM-41 molecular sieves. *J. Catal*. **210** 367 - 374.

Wan, J., Wei, Y., Liu, Z., Li, B., Qi, Y., Li, M., Xie, P., Meng, S., He, Y. and Chang, F. (2008). A ZSM-5-based catalyst for efficient production of light olefins and aromatics from fluidized-bed naptha catalytic cracking. *Catal. Lett.* **124** 150-156.

Wang, W., De Cola, P.L., Glaeser, R., Ivanova, I.I., Weitkamp, J. and Hunger, M. (2004). Methylation of phenol by methanol on acidic zeolite H-Y investigated by *in situ* CF MAS NMR spectroscopy. *Catal. Lett.* **94** 119-123.

Weisz, P. and Prater, C. (1954). Interpretation of measurements in experimental catalysis. *Advances in Catalysis.* **6** 143–196.

Weitkamp, J. and Ernst, S. (1994). Catalytic test reactions for probing the pore width of large and super-large pore molecular sieves. *Catalysis Today.* **19** 107-150.

Weitkamp, J., Puppe, L. and Kahl, G.H. (1999). Catalysis and zeolites. Fundamentals and Applications. 142-145

Wheeler, A. (1951). Reaction Rates and Selectivity in Catalyst Pores. *Advances in Catalysis*. **3** 250.

Wimmer, P., Buysch, H.J. and Puppe, L. (1991). Process for the preparation of thymol. *US 5 030 770* (assigned to Bayer AG).

Wu, E.L., Landolt, G.R. and Chester, A.W. (1986). Hydrocarbon adsorption characterisation of some high silica zeolites. *In:* Murakami, Y., Iijima, A. and Ward, J.W. (eds.), *New Developments in Zeolite Science and Technology*, *Studies in Surface Science and Catalysis.* Tokyo: Kodansha **28** 547-554.

Xu, J., Yan, A.-Z., Xu, Q.-H. (1997). Alkylation of phenol with methanol on H-beta zeolite. *React. Kinet. Catal. Lett.* **62** 71.

Yadav, G.D. and Pathre, G.S. (2005). Novel mesoporous solid superacidic catalysts: activity and selectivity in the synthesis of thymol by isopropylation of *m*-cresol with 2-propanol over UDCaT-4,-5 and -6. *J. of Phys. Chem.* **109** 11080-11088.

Yadav, G.D. and Pathre, G.S. (2006). Novel mesoporous solid superacids for selective C-alkylation of *m*-cresol with *tert*-butanol. *Micopor. Mesopor. Mater.* **89** 16-24.

Websites accessed:

Innov-X Systems, Theory behind XRF Spectroscopy, accessed 7 January 2011. http://www.innovx.com/themes/IX/graphics/xrfspectrometry/spectrometry.html

Purdue University: Radiological and Environmental Management, accessed 3 September 2010. http://www.purdue.edu/rem/rs/sem.htm

Schmidt, W. Applications of Zeolites, accessed 12 August 2009: http://www.mpi-muelheim.mpg.de/kofo/institut/arbeitsbereiche/schmidt/zeolites_ef.html

Supelco website, accessed 11 October 2010: http://www.sigmaaldrich.com/catalog/ProductDetail.do?lang=en&N4=24310|SUPELCO&N5=SEARCH_CONCAT_PNO|BRAND_KEY&F=SPEC

Webb, M. Sasol considers Free State, Waterberg sites for new coal-to-liquids plant, accessed 8 January 2011. http://www.engineeringnews.co.za/article/sasol-considers-free-state-waterberg-sites-for-new-coaltoliquids-plant-2007-09-10-1

10 Appendix

10.1 Catalyst loading calculations

Example of H-MFI-90 catalyst loading:

Bulk density of H-MFI-90 catalyst = 1.0625 g/cm^3
Bulk density of SiC packing = 3.2170 g/cm^3
Mass of catalyst weighed in = 5.86 g

Total volume occupied by catalyst = $\frac{Mass\ of\ catalyst}{Density\ of\ catalyst}$ = 5.52 cm^3

Catalyst zone A (Top zone):

Volume of catalyst$_A$ = $\frac{Total\ volume\ occupied\ by\ catalyst}{2}$ = 2.76 cm^3

Mass of catalyst$_A$ = $Density\ of\ catalyst \times Volume\ of\ catalyst_A$ = 2.93 g

Volume of SiC$_A$ = $8 \times Volume\ of\ catalyst_A$ = 22.06 cm^3 (Dilution ratio of 1:8 on a volume basis)

Mass of SiC$_A$ = $Density\ of\ SiC \times Volume\ of\ SiC_A$ = 70.97 g

Catalyst zone B (Bottom zone):

Volume of catalyst$_B$ = $\frac{Total\ volume\ occupied\ by\ catalyst}{2}$ = 2.76 cm^3

Mass of catalyst$_B$ = $Density\ of\ catalyst \times Volume\ of\ catalyst_A$ = 2.93 g

Volume of SiC$_B$ = $Volume\ of\ catalyst_B$ = 2.76 cm^3 (Dilution ratio of 1:1 on a volume basis)

Mass of SiC$_B$ = $Density\ of\ SiC \times Volume\ of\ SiC_B$ = 8.87 g

10.2 Experimental Data

The subsequent tables provide the steady-state data of the experiments conducted. Note all the experimental data reported here have been corrected for feed impurities and take into account the results of the blank run.

Experiment 1 - H-MFI-90

	Operating Parameters				Selectivities (mol %)							
Sample Number	WHSV ($g_{m\text{-}cresol}/g_{cat}.hr$)	Pressure (bar (abs))	Catalyst Bed Temperature (°C)	Conversion (%)	*o* - & *p* -Cresol	Isopropyl-Phenyl Ether	Thymol	2-Isopropyl-3-Methyl Phenol	4-Isopropyl-3-Methyl Phenol	5-Isopropyl-3-Methyl Phenol	Diisopropylated Phenols	"Others"
1	1.014	3	224	14.65	3.05	7.86	45.04	20.37	21.14	1.95	3.93	0.77
2	1.012	3	224	16.34	4.00	6.22	44.47	19.52	22.13	2.09	4.42	0.82
3	1.014	3	225	15.46	2.89	6.71	44.99	20.14	22.03	2.01	4.32	0.80
4	1.013	3	225	14.93	3.11	7.63	44.62	20.28	21.53	1.96	4.09	0.79
5	1.013	3	225	15.37	3.39	7.36	43.70	21.66	20.59	1.88	4.54	0.78
6	0.502	3	224	17.91	2.71	2.98	49.36	16.16	23.21	3.11	3.12	1.72
7	0.503	3	223	17.05	2.66	2.25	49.34	17.48	24.23	2.61	3.30	1.65
8	0.512	3	224	19.19	2.64	2.45	47.90	17.81	24.52	2.71	2.95	2.16
9	0.512	3	225	19.50	2.78	2.94	47.16	17.52	24.15	2.52	3.85	2.15
10	0.505	3	225	19.15	2.58	2.32	46.39	18.17	23.17	2.48	3.69	2.33
11	0.247	3	224	33.02	1.27	2.68	48.88	16.39	19.81	2.25	9.65	0.88
12	0.240	3	224	34.94	1.27	2.17	48.58	15.77	20.51	2.47	10.02	0.92
13	0.242	3	225	32.25	1.31	2.79	48.45	16.59	19.17	2.45	10.15	0.94
14	0.248	3	225	32.17	1.30	2.89	49.17	17.04	18.58	2.23	9.77	0.88
15	0.124	3	225	51.96	0.68	1.09	48.56	11.75	17.82	2.84	17.08	1.35
16	0.124	3	224	51.96	0.68	1.09	48.56	11.75	17.82	2.84	17.08	1.35
17	0.125	3	225	48.55	0.81	1.23	49.49	12.65	17.02	2.72	15.89	1.42
18	0.125	3	225	50.71	0.66	1.24	47.18	11.52	18.08	2.70	18.46	1.34
19	0.062	3	224	76.54	0.24	0.33	46.32	4.43	12.52	4.87	23.09	9.98
20	0.062	3	225	77.74	0.30	0.29	48.33	4.79	11.88	4.71	22.62	7.58
21	0.062	3	225	80.81	0.26	0.23	47.41	5.43	12.49	4.55	25.78	8.65
22	0.062	3	224	77.24	0.27	0.28	48.65	4.81	12.34	4.59	21.67	8.17
23	0.063	3	223	78.26	0.27	0.26	46.92	4.66	11.90	4.55	24.42	8.79
24	0.063	3	199	58.56	0.78	1.27	40.17	14.46	26.16	2.18	14.27	1.58
25	0.062	3	200	54.69	0.87	1.54	43.13	16.24	23.18	2.01	12.78	1.17
26	0.062	3	199	55.64	0.82	1.52	41.83	16.14	23.82	1.96	13.65	1.18
27	0.062	3	200	58.45	0.80	1.53	41.87	15.93	25.73	2.08	13.33	1.12
28	0.062	3	200	54.91	0.87	1.55	43.31	16.59	23.26	1.94	12.33	1.05
29	0.062	3	200	57.46	0.77	1.20	42.67	15.89	24.03	2.02	13.13	1.17
30	0.062	3	200	55.15	0.89	1.36	44.29	16.94	22.31	1.89	11.96	1.26
31	0.253	3	200	22.16	3.03	8.68	41.21	22.30	20.33	1.46	2.97	2.73
32	0.257	3	200	22.07	3.07	8.35	39.31	21.25	21.09	1.50	3.40	2.76
33	0.259	3	200	22.50	3.00	8.66	40.20	21.65	21.53	1.45	3.39	2.79
34	0.254	3	200	20.93	3.38	8.78	41.50	22.65	19.61	1.35	2.95	2.64
35	0.255	3	199	22.20	3.02	8.49	40.79	21.88	21.53	1.47	4.92	2.60

36	0.125	3	249	41.19	1.83	0.75	59.76	9.92	10.24	3.54	11.37	4.25
37	0.123	3	250	45.29	1.18	0.53	59.57	6.04	13.63	4.48	11.03	4.94
38	0.126	3	250	45.26	1.07	0.48	60.09	6.08	13.37	4.35	11.59	4.42
39	0.123	3	249	40.83	1.27	0.52	59.52	6.28	13.15	4.20	11.96	4.60
40	0.124	3	250	41.99	1.21	0.51	63.42	6.06	13.26	4.12	9.29	3.63
41	0.258	3	249	36.75	1.55	0.77	58.64	9.15	16.27	3.40	10.52	1.34
42	0.258	3	250	39.64	1.49	0.73	56.57	9.03	17.33	3.48	11.33	1.55
43	0.250	3	250	39.07	1.33	0.59	56.73	9.13	16.85	3.50	11.35	2.06
44	0.260	3	249	36.59	1.53	0.85	57.41	9.53	16.03	3.26	10.59	2.45
45	0.250	3	249	36.04	1.52	0.79	58.35	10.02	16.14	3.26	10.57	1.02
46	0.259	3	274	44.02	1.20	0.28	66.85	3.30	9.91	5.72	11.21	2.87
47	0.258	3	275	45.50	1.05	0.21	67.47	3.02	10.10	5.99	10.70	2.77
48	0.256	3	275	40.65	1.34	0.30	65.87	3.70	9.91	5.73	11.72	2.90
49	0.252	3	274	46.80	1.01	0.19	67.61	3.12	10.12	5.77	10.63	2.84
50	0.517	3	274	35.67	1.69	0.41	64.47	5.31	12.45	4.37	9.76	3.23
51	0.517	3	274	33.31	1.66	0.46	67.17	5.68	11.36	4.18	8.29	2.99
52	0.513	3	275	33.37	1.62	0.36	67.97	5.69	10.86	4.00	7.96	3.36
53	0.509	3	274	34.42	1.98	0.55	65.14	5.56	11.33	4.38	9.75	2.90
54	0.125	3	299	23.15	7.15	0.19	39.38	2.03	6.48	24.99	12.67	9.70
55	0.124	3	300	26.50	5.85	0.55	41.40	1.82	6.93	23.80	13.17	8.74
56	0.124	3	298	25.13	6.67	0.40	42.33	0.98	7.11	23.71	12.28	8.90
57	0.124	3	300	26.52	5.26	0.27	45.97	1.38	7.14	23.03	11.95	7.27
58	0.125	3	299	28.42	4.71	0.33	44.89	1.40	7.35	23.91	12.17	7.35
59	0.124	3	299	28.99	4.57	0.10	46.14	1.52	7.45	23.46	12.04	6.79
60	0.124	3	300	23.63	5.93	0.17	45.26	2.55	7.15	23.46	11.98	6.04
61	0.246	3	299	33.91	3.12	0.14	50.79	2.09	9.40	17.41	13.06	5.75
62	0.256	3	300	36.24	2.52	0.27	52.31	1.69	9.09	17.44	12.31	6.02
63	0.256	3	300	32.39	3.20	0.22	51.28	1.74	8.90	17.69	12.74	6.08

Experiment 2 - H-MFI-400

	Operating Parameters				Selectivities (mol %)							
Sample Number	WHSV ($g_{m\text{-}cresol}/g_{cat.}hr$)	Pressure (bar (abs))	Catalyst Bed Temperature (°C)	Conversion (%)	*o* - & *p* -Cresol	Isopropyl-Phenyl Ether	Thymol	2-Isopropyl-3-Methyl Phenol	4-Isopropyl-3-Methyl Phenol	5-Isopropyl-3-Methyl Phenol	Diisopropylated Phenols	"Others"
1	1.019	3	225	9.27	7.75	29.20	34.55	20.39	9.37	1.13	3.57	0.52
2	1.015	3	224	8.89	8.16	27.35	35.93	22.35	8.87	1.01	2.34	0.74
3	1.015	3	225	9.44	7.52	31.93	33.73	21.08	8.36	1.10	2.06	0.57
4	1.011	3	225	9.54	7.54	34.43	32.35	20.01	7.75	1.04	2.38	0.77
5	1.013	3	225	9.76	7.29	35.76	30.32	19.52	7.80	0.97	3.90	0.59
6	1.012	3	225	9.51	7.33	34.14	32.66	21.22	7.50	0.89	1.95	0.61
7	0.503	3	223	10.58	6.50	9.82	47.23	26.66	9.67	1.15	3.21	1.43
8	0.512	3	224	10.52	6.66	10.86	46.38	26.39	9.72	1.10	3.83	0.76
9	0.510	3	225	10.06	6.96	11.86	46.52	26.71	8.63	1.15	3.26	0.87
10	0.513	3	225	10.27	6.75	10.60	46.77	27.08	8.94	1.28	3.35	1.07
11	0.255	3	224	13.42	4.92	3.93	54.12	25.66	8.68	1.30	4.94	0.91
12	0.257	3	224	13.29	4.90	3.96	53.54	25.99	8.79	1.26	5.15	0.93
13	0.257	3	225	12.71	5.24	4.90	52.44	26.02	8.82	1.28	5.16	0.86
14	0.258	3	224	13.10	5.02	3.56	55.59	25.81	7.79	1.14	4.50	1.17
15	0.258	3	225	12.52	5.47	3.88	54.24	26.17	7.66	1.34	5.05	0.98
16	0.258	3	225	12.98	5.13	3.75	55.09	26.32	7.62	1.16	4.62	0.93
17	0.257	3	225	13.59	4.86	3.27	54.68	25.64	7.82	1.16	6.00	0.98
18	0.127	3	224	17.98	3.26	1.32	65.72	17.30	6.54	1.59	6.46	1.16
19	0.128	3	224	18.09	3.34	1.14	66.60	17.73	6.13	1.39	5.92	1.06
20	0.127	3	224	18.19	3.23	1.31	65.66	17.52	6.36	1.42	6.64	1.16
21	0.128	3	225	17.19	3.56	1.37	65.45	18.54	6.25	1.53	5.85	0.94
22	0.123	3	225	19.59	3.00	1.15	64.04	17.39	7.24	1.51	7.74	1.00
23	0.124	3	223	17.16	3.44	1.47	65.93	17.96	6.12	1.39	6.16	1.03
24	0.062	3	225	31.26	1.39	0.27	77.68	4.61	5.68	3.06	8.05	1.18
25	0.063	3	225	30.09	1.68	0.48	77.48	5.17	5.29	2.80	7.92	1.17
26	0.063	3	224	30.34	1.58	0.30	77.27	5.27	5.35	2.56	8.43	1.21
27	0.064	3	225	35.03	1.19	0.17	76.11	5.14	5.83	2.60	9.52	1.15
28	0.064	3	225	35.75	1.09	0.14	78.38	5.15	5.39	2.41	8.06	1.07
29	0.064	3	224	28.88	1.69	0.43	76.62	5.76	5.08	2.43	8.66	1.41
30	0.064	3	225	29.66	1.54	0.22	79.57	5.90	4.83	2.32	6.46	1.19
31	0.129	3	199	14.23	4.46	22.90	41.94	27.14	3.63	0.51	2.65	0.99
32	0.128	3	200	14.30	4.42	24.68	40.77	26.48	3.63	0.51	2.76	0.94
33	0.127	3	200	14.02	4.58	22.69	42.34	27.50	3.45	0.41	2.31	0.99
34	0.259	3	198	14.03	4.74	50.28	25.57	18.46	3.15	0.42	1.13	0.53
35	0.259	3	199	13.97	4.53	39.00	32.15	20.80	4.42	0.66	1.90	0.84
36	0.256	3	200	14.01	4.15	47.30	26.75	17.79	3.16	0.46	1.09	0.58
37	0.262	3	200	14.40	4.76	35.26	33.23	23.18	4.45	0.56	2.04	0.71
38	0.253	3	200	14.27	4.45	50.53	20.74	14.47	2.22	0.23	1.00	0.57
39	0.255	3	200	13.54	4.56	50.80	25.24	17.46	2.53	0.30	0.95	0.60
40	0.062	3	199	17.60	3.22	7.86	58.89	23.91	3.25	0.66	4.46	1.18
41	0.062	3	199	18.01	3.04	1.76	63.69	24.98	3.08	0.66	4.86	1.26
42	0.064	3	200	16.76	3.42	1.35	63.25	26.23	2.91	0.70	4.61	1.11
43	0.062	3	200	17.56	3.85	1.31	62.75	25.41	3.06	0.71	5.10	1.23

44	0.508	3	249	17.38	3.39	1.26	69.08	13.40	7.22	1.88	6.09	1.13
45	0.509	3	250	18.14	3.24	1.47	68.05	13.54	7.56	1.94	6.40	1.12
46	0.515	3	248	17.77	3.33	1.23	68.97	14.22	7.00	1.83	5.70	1.10
47	0.512	3	250	17.09	3.48	1.30	68.92	14.46	6.78	1.80	5.75	1.02
48	0.261	3	250	20.92	2.55	0.68	75.71	8.09	6.14	2.39	6.19	1.13
49	0.258	3	249	24.70	2.42	0.50	75.25	6.37	6.56	2.70	7.63	1.00
50	0.257	3	249	23.46	2.37	0.50	76.92	6.47	6.13	2.59	6.45	1.14
51	0.259	3	249	22.60	2.33	0.63	76.27	7.15	6.07	2.47	6.64	1.10
52	0.259	3	250	23.66	2.34	0.57	76.50	7.12	6.01	2.46	6.49	1.04
53	0.256	3	250	22.19	2.33	0.65	76.94	6.65	5.92	2.43	6.61	1.17
54	0.128	3	250	28.45	1.63	0.31	79.14	3.56	6.04	4.09	6.23	1.11
55	0.129	3	250	27.97	1.60	0.22	81.03	3.26	5.52	3.87	5.44	1.89
56	0.127	3	250	27.80	1.61	0.25	80.79	3.25	5.56	3.89	5.63	1.92
57	0.128	3	250	28.87	1.51	0.21	79.76	3.23	5.52	3.95	6.60	2.05
58	1.019	3	274	19.58	3.14	2.30	73.06	8.62	6.36	2.21	6.67	1.25
59	1.014	3	273	19.98	2.89	1.47	72.47	9.43	6.63	2.29	7.22	0.89
60	1.022	3	275	19.73	2.87	1.16	74.28	9.62	6.26	2.09	5.59	1.23
61	1.009	3	275	19.72	2.80	1.29	73.42	10.34	6.38	1.88	6.13	1.11
62	1.014	3	274	18.80	2.98	0.92	74.92	10.86	5.67	1.70	5.23	1.14
63	1.013	3	274	18.63	2.96	1.24	74.78	11.00	5.61	1.71	5.01	1.20
64	1.011	3	275	21.10	2.57	0.98	73.30	10.41	6.33	1.85	6.56	1.07
65	1.017	3	275	19.42	2.81	1.17	74.38	10.81	5.74	1.71	5.53	1.22
66	0.257	3	274	29.01	1.95	0.29	79.89	2.99	6.36	4.71	5.93	1.87
67	0.256	3	275	28.38	1.90	0.29	80.46	2.94	6.22	4.57	5.80	2.02
68	0.256	3	275	28.05	1.57	0.35	80.18	3.11	6.03	4.49	5.28	1.21
69	0.252	3	275	28.36	2.19	0.31	79.08	3.00	5.80	4.25	5.60	1.95
70	0.257	3	274	27.64	1.63	0.33	79.58	3.11	5.75	4.26	5.32	2.26
71	0.500	3	274	24.66	2.26	0.00	79.32	4.97	5.50	2.92	5.34	1.68
72	0.515	3	275	24.62	1.95	0.00	78.40	5.42	5.56	2.49	6.47	1.66
73	0.500	3	274	22.43	2.24	0.00	79.55	5.55	5.27	2.50	5.44	1.56
74	0.511	3	275	24.29	1.96	0.00	78.77	5.57	5.51	2.40	5.82	1.74
75	0.517	3	275	23.47	2.57	0.00	79.31	5.56	5.15	2.26	5.42	1.62
76	0.511	3	274	23.24	2.11	0.00	79.82	5.61	5.07	2.25	5.19	1.81
77	0.513	3	275	23.36	2.03	0.00	79.70	5.87	5.12	2.14	5.41	1.61
78	0.257	3	300	24.12	2.98	0.28	62.03	2.55	7.58	18.37	2.86	5.91
79	0.256	3	299	24.32	2.85	0.13	63.11	1.84	8.20	17.01	3.43	5.91
80	0.276	3	299	24.98	2.77	0.25	62.80	2.10	8.04	16.25	3.48	6.77
81	0.253	3	300	23.71	3.01	0.20	64.29	2.22	7.73	14.97	3.11	7.03
82	1.012	3	300	23.82	2.15	0.44	78.73	3.54	6.17	3.88	3.64	4.08
83	1.017	3	300	26.58	1.89	0.35	77.47	3.31	6.54	4.04	4.49	4.24
84	1.015	3	298	23.99	2.12	0.37	79.78	3.60	5.80	3.54	3.41	3.96
85	1.026	3	299	23.72	2.11	0.47	79.62	3.60	5.92	3.71	3.39	3.83
86	1.015	3	299	24.32	2.06	0.51	78.74	3.44	6.21	3.87	3.82	3.93
87	0.516	3	300	27.48	1.89	0.20	74.06	3.00	7.06	7.23	3.46	5.33
88	0.511	3	300	26.01	2.15	0.28	74.18	2.35	6.86	6.93	4.05	5.57
89	0.511	3	300	27.85	1.86	0.31	73.43	2.87	7.35	7.32	3.98	5.10
90	0.512	3	300	26.64	1.93	0.30	76.01	2.50	7.22	7.08	4.22	3.05

Experiment 3 - H-MFI-20

	Operating Parameters			Selectivities (mol %)								
Sample Number	WHSV ($g_{m\text{-}cresol}/g_{cat}.hr$)	Pressure (bar (abs))	Catalyst Bed Temperature (°C)	Conversion (%)	*o* - & *p* -Cresol	Isopropyl-Phenyl Ether	Thymol	2-Isopropyl-3-Methyl Phenol	4-Isopropyl-3-Methyl Phenol	5-Isopropyl-3-Methyl Phenol	Diisopropylated Phenols	"Others"
1	0.255	3	225	25.58	2.46	0.66	57.97	12.15	11.67	3.34	12.69	1.40
2	0.247	3	223	24.73	2.61	0.84	56.72	11.78	12.02	3.42	13.50	1.52
3	0.259	3	225	26.40	2.30	0.79	56.52	11.73	12.27	3.40	14.00	1.26
4	0.252	3	225	26.35	2.34	0.70	57.13	11.76	12.22	3.45	13.31	1.37
5	0.254	3	224	26.13	2.35	0.78	57.16	12.11	11.94	3.43	13.09	1.43
6	0.064	3	224	28.02	2.08	0.23	67.88	3.99	9.41	6.69	9.10	2.75
7	0.064	3	225	34.04	1.66	0.20	61.70	4.01	11.00	6.92	13.78	2.49
8	0.064	3	224	26.63	2.28	0.33	64.29	4.73	9.75	6.24	12.46	2.17
9	0.064	3	224	28.45	2.02	0.25	64.73	4.64	10.38	6.35	11.43	2.31
10	0.064	3	225	32.61	1.77	0.19	61.06	5.02	10.82	6.47	13.04	3.48
11	0.064	3	223	31.05	1.82	0.19	64.76	5.02	10.94	6.31	10.66	2.24
12	0.064	3	226	29.38	2.02	0.26	62.91	5.20	11.22	6.18	12.09	2.16
13	0.064	3	225	29.50	1.96	0.24	62.20	5.30	11.27	5.92	12.73	2.41
14	0.128	3	225	24.20	2.65	0.62	57.12	11.07	12.95	3.81	11.93	2.34
15	0.128	3	225	24.75	2.53	0.55	57.46	10.68	13.73	3.88	12.01	1.58
16	0.127	3	223	23.65	2.72	0.58	54.50	11.41	13.71	3.79	13.40	2.43
17	0.506	3	225	15.79	4.36	7.49	46.13	19.47	15.01	2.05	7.95	1.34
18	0.499	3	225	20.60	3.22	4.40	45.38	18.35	18.02	2.32	7.00	4.22
19	0.504	3	224	16.26	4.23	9.31	43.70	19.53	16.74	1.92	5.06	3.21
20	0.503	3	224	20.40	3.26	6.55	44.38	18.99	19.49	2.17	4.76	3.34
21	0.502	3	225	18.22	3.92	7.02	44.82	20.15	17.54	1.96	4.48	3.41
22	1.058	3	224	11.73	6.03	37.34	28.99	16.12	12.51	1.12	1.36	1.64
23	1.014	3	224	12.16	5.78	38.88	27.59	15.83	13.40	1.08	1.13	1.25
24	1.010	3	225	12.97	5.38	35.92	28.72	16.46	14.25	1.03	1.55	1.31
25	0.011	3	200	18.30	3.02	0.53	73.32	1.98	8.60	9.55	4.23	2.05
26	0.011	3	200	18.27	3.22	0.06	73.62	2.06	8.92	8.94	4.46	2.00
27	0.011	3	198	17.79	3.17	0.05	74.00	2.15	8.79	9.11	4.17	1.92
28	0.011	3	200	21.09	2.71	0.00	71.02	2.44	10.64	8.45	5.78	1.79
29	0.011	3	199	19.90	2.87	0.00	71.28	2.40	10.84	8.37	5.51	1.75
30	0.064	3	200	13.10	5.33	1.92	54.08	18.71	14.01	2.15	7.04	1.35
31	0.063	3	200	12.21	6.28	2.93	52.18	18.63	13.96	2.52	6.69	1.72
32	0.064	3	199	11.13	6.45	3.17	51.97	20.06	13.72	1.95	7.16	0.90
33	0.064	3	198	12.49	5.51	2.99	49.50	19.52	15.28	2.55	7.02	2.43
34	0.063	3	200	12.18	4.79	2.11	54.07	18.34	15.18	2.44	7.27	0.72
35	0.063	3	200	12.12	5.05	2.11	52.33	18.77	15.70	2.55	7.02	1.43
36	0.064	3	200	13.00	4.58	1.88	52.05	18.74	16.60	2.44	7.48	0.84

37	1.017	3	249	19.58	3.01	3.38	52.36	17.72	15.07	2.42	7.51	1.60
38	1.018	3	250	20.04	2.85	3.81	49.94	18.03	16.88	2.31	8.28	0.89
39	1.020	3	248	20.70	2.78	3.55	49.89	17.78	16.73	2.19	8.62	1.35
40	1.017	3	250	20.74	2.71	3.15	51.21	18.21	16.64	2.20	7.66	1.12
41	1.014	3	250	21.72	2.57	3.58	49.89	18.13	17.40	2.18	8.14	0.87
42	0.123	3	249	31.49	1.88	0.12	68.06	2.90	9.77	8.21	8.65	2.32
43	0.123	3	250	31.73	1.85	0.13	66.33	2.90	10.27	8.28	9.62	2.53
44	0.123	3	250	31.81	1.85	0.10	67.61	2.98	10.08	8.05	8.91	2.32
45	0.124	3	249	31.34	1.88	0.11	67.81	3.10	10.11	7.81	8.81	2.29
46	0.505	3	250	25.80	2.91	0.77	58.88	10.88	13.60	3.71	9.86	1.71
47	0.505	3	250	25.00	2.54	0.77	60.02	11.78	13.51	3.33	9.18	1.28
48	0.505	3	249	24.96	2.91	0.83	59.04	11.75	13.59	3.36	9.51	1.42
49	0.505	3	250	26.11	2.37	0.80	58.50	11.14	14.45	3.46	9.71	1.87
50	0.064	3	250	19.24	3.19	0.26	67.53	4.13	11.49	7.13	6.64	2.76
51	0.064	3	249	19.54	3.53	0.23	65.07	4.31	11.81	6.71	8.14	2.71
52	0.064	3	250	17.87	3.89	0.24	67.78	4.88	10.44	6.15	5.79	3.82
53	0.064	3	250	18.89	3.15	0.17	68.04	4.60	11.62	6.63	5.88	2.62
54	0.496	3	275	39.24	1.79	0.13	58.53	2.20	9.89	11.98	9.58	7.42
55	0.502	3	275	38.49	1.89	0.08	59.84	2.13	9.44	11.64	8.77	7.79
56	0.503	3	274	37.16	1.78	0.15	62.42	2.77	9.92	9.22	9.31	6.06
57	0.503	3	274	40.91	1.45	0.16	58.27	3.14	11.48	9.05	12.97	4.95
58	0.502	3	275	37.78	1.60	0.20	60.85	3.42	10.74	8.38	11.58	4.82
59	0.502	3	276	35.91	1.77	0.20	63.47	3.61	10.30	8.01	9.59	4.70
60	0.064	3	273	21.06	8.50	0.43	42.94	1.48	6.29	22.69	3.70	16.81
61	0.064	3	275	20.10	8.59	0.35	44.58	1.44	6.21	21.41	3.52	16.88
62	0.064	3	275	20.87	8.64	0.35	44.64	1.37	6.31	21.31	3.61	16.64
63	0.064	3	275	20.51	7.60	0.31	47.27	1.20	6.57	20.55	3.61	15.82
64	0.066	3	275	19.45	8.33	0.29	47.88	1.03	6.17	19.43	3.79	16.16
65	0.254	3	274	26.27	2.65	0.32	68.04	3.70	9.42	8.08	6.78	3.29
66	0.253	3	275	26.03	2.67	0.43	67.55	3.68	9.50	8.07	6.90	3.51
67	0.254	3	276	26.79	2.51	0.38	66.73	3.63	10.04	8.33	7.36	3.26
68	0.252	3	274	25.69	2.63	0.37	67.27	3.71	9.99	8.16	7.12	3.08
69	1.036	3	275	28.80	2.18	0.62	60.68	8.52	13.54	4.76	10.00	1.79
70	1.015	3	275	30.23	2.04	0.54	60.29	8.36	13.72	4.78	10.39	1.86
71	1.008	3	274	28.16	2.26	0.70	60.68	8.35	13.21	4.76	10.37	1.80
72	1.012	3	274	30.81	2.24	0.54	58.70	8.15	13.61	5.08	11.56	2.07
73	0.506	3	299	34.78	2.61	0.22	54.05	1.62	8.24	21.19	5.24	8.54
74	0.505	3	300	36.15	2.53	0.10	53.47	1.38	8.20	22.07	4.99	8.91
75	0.507	3	300	36.23	2.60	0.08	55.92	1.58	8.48	19.20	5.40	8.39
76	0.507	3	298	34.79	2.45	0.09	56.31	1.49	8.55	19.20	5.49	8.14
77	0.508	3	300	35.81	2.32	0.07	55.84	1.86	8.64	19.13	5.65	8.15
78	0.250	3	300	30.97	3.18	0.10	52.11	2.64	8.50	23.40	5.14	6.85
79	0.252	3	301	30.82	3.73	0.06	49.28	2.34	7.82	26.38	3.99	8.35
80	0.255	3	299	30.00	3.87	0.08	50.87	2.05	7.73	25.67	3.35	8.38
81	0.255	3	300	30.17	3.81	0.09	52.90	1.93	7.71	24.01	3.56	7.98
82	0.128	3	300	30.98	4.74	0.06	39.74	1.70	7.56	33.78	3.65	10.71
83	0.128	3	299	31.09	4.70	0.21	39.56	1.99	7.29	32.74	3.87	11.57
84	0.127	3	299	28.11	5.43	0.27	40.34	0.99	7.32	31.78	5.14	9.49
85	0.128	3	300	30.91	4.27	0.18	42.13	0.96	7.79	31.88	4.01	9.60
86	0.128	3	298	30.95	4.19	0.19	43.88	1.00	7.62	31.69	3.19	9.04
87	0.064	3	300	27.72	7.85	0.32	28.86	1.24	6.13	41.11	2.78	11.59
88	0.064	3	301	23.72	8.79	0.32	32.53	1.23	5.84	36.58	2.31	12.44
89	0.064	3	300	24.73	8.02	0.25	33.25	0.68	6.43	37.17	3.27	11.21
90	0.064	3	300	24.91	7.89	0.32	32.90	0.79	6.73	37.15	3.27	11.13
91	1.015	3	298	41.75	1.16	0.15	54.26	3.18	14.51	9.58	15.43	3.01
92	1.020	3	299	43.21	1.10	0.15	58.03	3.31	13.91	9.90	11.85	3.12
93	1.011	3	300	40.06	1.44	0.16	59.05	3.37	13.11	9.90	11.04	3.25

Experiment 4 - H-MFI-400 (Pressure Series)

	Operating Parameters				Selectivities (mol %)							
Sample Number	WHSV ($g_{m\text{-}cresol}/g_{cat}.hr$)	Pressure (bar (abs))	Catalyst Bed Temperature (°C)	Conversion (%)	*o* - & *p*-Cresol	Isopropyl-Phenyl Ether	Thymol	2-Isopropyl-3-Methyl Phenol	4-Isopropyl-3-Methyl Phenol	5-Isopropyl-3-Methyl Phenol	Diisopropylated Phenols	"Others"
1	0.255	3	275	30.19	1.71	0.30	71.28	3.17	7.58	4.27	6.07	5.26
2	0.256	3	274	30.42	1.52	0.32	72.83	3.03	7.30	3.99	5.72	4.90
3	0.255	3	275	30.54	1.34	0.23	71.98	3.09	7.85	4.03	6.94	4.28
4	0.255	3	275	30.89	1.63	0.28	73.41	3.44	7.09	3.75	6.17	3.81
5	0.257	3	274	30.97	1.43	0.27	73.62	3.45	7.10	3.67	6.14	4.00
6	0.506	3	273	26.81	1.64	0.49	68.67	8.92	8.84	1.96	7.72	1.53
7	0.504	3	274	25.38	1.77	0.57	69.34	9.12	8.41	1.88	7.21	1.44
8	0.504	3	275	24.92	1.73	0.49	70.33	9.08	8.17	1.85	6.57	1.55
9	0.505	3	275	26.15	1.66	0.64	68.84	8.57	8.54	1.94	7.91	1.50
10	0.255	6	274	32.31	1.37	0.46	69.78	5.41	8.57	3.45	8.71	2.05
11	0.255	6	274	35.61	1.13	0.41	68.95	5.07	9.01	3.60	9.58	2.06
12	0.255	6	275	34.70	1.18	0.44	67.30	4.92	8.86	3.46	11.53	2.05
13	0.255	6	276	34.53	1.19	0.45	68.90	5.29	8.99	3.35	9.81	1.86
14	0.504	6	275	24.77	2.19	1.33	62.73	11.54	10.25	2.28	8.04	1.43
15	0.508	6	275	23.92	2.00	1.30	61.76	12.09	10.56	2.13	8.56	1.39
16	0.510	6	275	22.42	2.28	1.58	61.31	12.36	10.22	2.10	8.26	1.54
17	0.503	6	274	24.82	1.94	1.26	62.42	11.96	10.45	2.20	8.19	1.34
18	0.506	6	275	22.73	2.14	1.32	62.90	12.54	9.86	2.01	7.51	1.39
19	0.500	6	275	23.66	2.04	1.39	62.01	12.44	10.20	2.07	8.16	1.42
20	0.503	6	276	28.85	1.53	0.88	57.69	10.98	11.51	2.26	8.24	1.72
21	0.501	6	275	31.08	2.55	0.89	60.87	11.25	11.69	2.44	8.64	1.42
22	0.507	6	275	27.61	1.61	0.91	62.61	11.69	10.96	2.18	8.60	1.25
23	0.503	12	273	24.78	2.07	1.94	54.94	16.41	12.31	1.99	8.66	1.35
24	0.504	12	274	25.46	1.97	2.18	54.85	15.83	13.14	2.11	8.43	1.25
25	0.506	12	275	25.83	2.03	2.26	54.03	15.78	13.70	2.18	8.70	1.07
26	0.504	12	275	25.82	2.68	2.21	53.81	15.71	13.53	2.13	8.53	1.18
27	0.504	1.5	274	17.06	2.88	0.82	74.88	7.08	6.11	1.79	4.19	1.82
28	0.519	1.5	274	18.18	2.61	0.75	75.09	6.61	6.49	1.83	4.53	1.70
29	0.508	1.5	275	18.14	2.62	0.86	74.36	6.96	6.39	1.73	4.76	1.96
30	0.507	1.5	275	18.14	2.62	0.76	75.54	6.84	5.87	1.70	4.25	2.09
31	0.510	1.5	274	19.30	2.55	1.04	71.03	9.39	6.97	1.74	5.48	1.44